The University Of Sheffield.

DEVELOPING BLF1 AS A NOVEL IMMUNOTOXIN FOR CANCER TREATMENT

By:

Shaymaa Abdulzahra Majed

A thesis submitted in partial fulfilment of the requirements for the degree
of
Doctor of Philosophy

The University of Sheffield

Department of Molecular biology and biotechnology

December 2017

Summary

One approach to enhancing the natural properties of antibodies is by conjugating them to toxins, especially where tumours have developed resistance to previous therapeutic regimes. Despite considerable research on immunotoxins, to date only diphtheria toxin has been approved for clinical use. One problem is that even with antibody targeting, there is a risk of damage to normal cells through inappropriate uptake of toxins. A novel small toxin, Burkholderia Lethal Factor 1 or BLF1, which we recently identified, is selective for rapidly dividing cells and is usually only active if it is deliberately introduced into the cytoplasm. These features give BLF1 significant advantages over previous toxins that have been investigated. BLF1 acts specifically to inhibit the initiation of translation mediated by intiation factor eIF4A. Rapidly dividing cells such as cancer cells are particularly dependent on eIF4A mediated translation.

In this study, we further investigated the activity of BLF1 across different cellular models and the role of macropinocytosis in uptake of BLF1 by some cell types that are directly sensitive to the toxin. We demonstrated that high rates of macropinocytosis correlated strongly with direct sensitivity to BLF1 and that BLF1 is primarily active against rapidly dividing cells, consistent with the known role of elF4A.

We also developed model systems for assessing the potential of BLF1 for development as an immunotoxin using antibodies directed against the tetraspanin proteins CD9 and CD63. CD63 in particular was selected as a model antigen because it is rapidly internalised on antibody binding, which is an important feature of immunotoxins. These non-covalently linked BLF1 immunoconjugates were useful for assessing antigen targeting and internalisation; however, it was not really possible to demonstrate significant specific effects on cell growth. This may have been due to

inefficient uptake of the toxin, problems associated with intracellular trafficking (e.g. poor endosomal escape) or instability of the conjugates.

This thesis also describes the successful production of chemically cross-linked BLF1/anti-CD63 and BLF1/anti-CD9 immunotoxins (IMT) that demonstrated targeting and significant effects on the growth of human cancer cell lines. Further investigations revealed that targeted BLF1 IMT could be co-administered with saponin, which may work synergistically to enhance their potency as a combinatorial therapy. Determination of intracellular trafficking of BLF1 IMT suggests that different internalization routing may be involved in the uptake of IMT for a specific cell type or targeting antigen.

Acknowledgment

Firstly, I would like to express my deepest sense of gratitude to my supervisor Dr. Lynda Partridge for all the help and support she given me throughout my PhD. Study. Her guidance helped me in all the time of research and writing of this thesis.

I also show my sincere gratitude to my co-supervisor Dr Guillaume Hautbergue from the Sheffield Institute for Translational Neuroscience (SITraN), University of Sheffield for his guidance and immense knowledge.

Besides my supervisors, I would like to thank my advisors Dr Ewald H Hettema and Dr Julie E Gray, for their insightful advice and encouragement.

My sincere thanks also go to Professor David Rice and Svetlana Sedelnikova, for providing me with BLF1 antibodies, purified BLF1 and assisted me with purification of chemically linked conjugate.

I would thank Professor David Flavell, who provided the saponin.

Great thanks to my colleagues past and present, Dr Atiga, Fawwaz, Tom, Jenny John, Jehan, Ibrahim, Ahmed, Rachel, Muslim, Callum and Anesu for all help, support and friendship.

I express my deep sense of gratitude to Baghdad College of pharmacy and the Ministry of Higher Education in Iraq for giving me the opportunity to undertake this study.

My deepest gratitude to my husband Odai for his full support, encouragement and patience throughout my study. Special thanks for my beautiful daughters Aya and Amenah and my son Ameer for their big love.

Lists of content

Lists of figures

Lists of tables

Lists of abbreviations

Ab	Antibody
ADC	Antibody drug conjugate
ADCC	Antibody-dependent cell-mediated cytotoxicity
ADP	Adenosine diphosphate
ALL	Acute lymphoblastic leukaemia
AML	Acute myeloid leukaemia
ANOVA	Analysis of variance
Anti-MSLN	Anti- mesothelin
AP	Adaptor protein
BLF1	Burkholderia lethal factor 1
BSA	Bovine serum albumin
CD	Cluster of differentiation
CDC	Complement-dependent cytotoxicity
CDRs	Complementary determining regions
CR	Complete response
CTCL	Cutaneous T-cell lymphoma
Da	Daltons
DMEM	Dulbecco's modified Eagle's medium
DNA	Deoxyribonucleic acid
DT	Diphtheria toxin
EC2	Extracellular domain 2
eEFs	eukaroyotic elongation factors

EF2	Elongation factor 2
eIF4A	Eukaryotic initiation factor 4A
ELISA	Enzyme-linked immunosorbent assay
ER	Endoplasmic reticulum
Fab	Fragment antigen binding
FACS	Fluorescence activated cell sorting
Fc	Fragment crystallisable
FCS	Foetal calf serum
FDA	Food and drug administration
FITC	Fluorescein isothyocyanate
FV	Variable fragment
g	Gravitational force
GFP	Green fluorescent protein
GMCSF	Granulocyte-macrophage colony-stimulating factor
GTP	Guanosine triphosphate
HBSS	Hank's balanced salt solution
HER-2	Human epidermal growth factor receptor 2
His	Histidine
HRP	Horseradish peroxidase
Ig	Immunoglobulin
IMT	Immunotoxin
IL2	Interleukin 2
IPTG	Isopropyl β-D-1-thiogalactopyranoside
IRES	Internal ribosomal entry sites
LAMP1	Lysosome associated membrane protein 1
LB	Lysogeny Broth
LH	Left hand
LR	Lysosomal resistant
mA	milli ampere
MAb	Monoclonal antibody
2-ME	2- Mercaptoethanol
MFI	Median fluorescence intensity
MMAE	Monomethyl auristatin E
MTD	Maximum tolerance dose
MW	Molecular weight
NAD	Nicotinamide adenine dinucleotide
NHL	Non Hodgkin lymphoma
NK cells	Natural killer cells
OD	Optical density
PBS	Phosphate-buffered saline
PE	Pseudomonas exotoxin
PE38	Truncated form of Pseudomonas exotoxin
PFA	Paraformaldehyde
PIC	Pre-initiation complex
PR	Partial response
RBL	Rat basophilic leukaemia
RFI	Relative fluorescence intensity
RH	Right hand

RIMs	Recombinant immunotoxins
RIPs	Ribosomal inactivating proteins
RNA	Ribonucleic acid
RT	Room temperature
SDS-PAGE	Sodium dodecyl sulfate polyacrylamide gel electrophoresis
SRB	Sulforhodamine B
TBS	Tris buffered saline
TCA	Trichloracetic acid
TGFβ	Transforming growth factor β
TGN	Trans-Golgi network
TMB	3, 3', 5, 5'-Tetramethylbenzidine
V	Volts
VLS	Vascular leak syndrome
WGA	Wheat germ agglutinin

1 Chapter 1: General introduction

1.1 Antibody targeted therapy:

Cancer is one of the leading causes of death. The clinical use of chemotherapeutic agents is limited by their nonspecific effects on normal tissues, causing systemic toxicity. Since the majority of chemotherapeutic drugs have a low molar mass (<1000 g/mol) they rapidly diffuse into tumour cells and normal tissues causing undesirable side effects. These side effects restrict the use of potent drugs even if they are effective for patients. In addition, chemotherapeutic drugs sometimes need to pass barriers of different pH levels, which results in either activation or inactivation and they are often cleared prematurely before being able to exert their cytotoxic effects. Another major pitfall of conventional chemotherapeutics is the development of drug resistance that has effects on the biological availability to the targeted cell structure (Janthur et al., 2012). However, a vast number of cell surface antigens were identified over the past 20 years that have selective expression or are over-expressed on the surface of malignant cells, along with the development of specific monoclonal antibodies (mAb) targeting specific antigens (Teicher and Chari, 2011). Apart from targeting antigens involved in cancer cell proliferation and survival, the advent of mAb can furthermore stimulate or block immunological pathways that are essential in cancer immune surveillance (Ricart and Tolcher, 2007, La-Beck et al., 2015). Although highly selective and less toxic, intact monoclonal antibodies display a modest anticancer activity by themselves. The killing potency of monoclonal antibodies is greatly improved by coupling with cytotoxic drugs (antibody drug conjugates (ADC)), toxins (immunotoxins) and radionuclides (Ravel et al., 1992, Chari, 2008, Diamantis and Banerji, 2016).

The modern era of targeted therapy for cancer came to light with the discovery of mAb by Kohler and Milstein. This opened the door for a large scale production of mAb (Kohler and Milstein, 1975). Until 2014, close to 47 mAb were approved for human therapy and over 200 mAb are currently in clinical trials for treatment of various solid and haematological malignancies (Ecker et al., 2015).

1.1.1 Design principles:

1.1.1.1 Antibody characteristic features:

Antibodies (Ab) are Y- shaped protein structures produced by cells of the B- lymphocyte lineage, composed of two large heavy chains and two smaller light chains, stabilized with disulphide bonds. Each chain is composed of variable (V) and constant (C) domains based on variability in the amino acid sequence. The light chain is composed of one constant (C_L) and one variable region (V_L). In contrast heavy chain is composed of one variable (V_H) domain and several constant domains (C_H1, C_H2, C_H3, etc) based on the class of the antibody. The main functional domains are the relatively constant Fc region, which interacts with cellular Fc receptors and complement and the Fab region, which contains the antigen binding site (**Fig**.1.1.1). The smallest part that maintains the antigen binding affinity is the variable fragment (Fv), which in recombinant form is commonly stabilized with a 15-amino acid peptide linker. The variable domain of both heavy and light chains is composed of hypervariable loops, known as complementarity determining regions (CDRs) that determine the antibody specificity to bind antigen (Holliger and Hudson, 2005, Olafsen and Wu, 2010). There are five different classes of antibodies: IgG, IgM, IgA, IgD, IgE classified according to the differences in the amino acid sequences in the constant region of their heavy chains. The IgG antibodies have heavy chains named γ-chains; IgM have μ-chains; IgA have α-chains; IgE have ε-chains; and IgD have δ-chains. Based on small differences in the constant region of the heavy chain, antibody classes are further divided into subclasses, for instance subclasses of IgGs are IgG1, IgG2, IgG3 and IgG4 in humans. There are also two light chain types, κ and λ, which will be of the same type in any particular antibody molecule (Schroeder and Cavacini, 2010).

As mentioned above, the development of hybridoma techniques, that involve immunizing mice with a target antigen and then fusing mouse lymphocytes with myeloma cell line cells (Kohler and Milstein, 1975), is used to generate murine monoclonal antibodies. However, as human anti- mouse antibody (HAMA) responses develop in patients treated with murine antibodies, chimeric monoclonal antibodies were generated using genetic engineering technology, where the mouse variable region (V) of both heavy and light chains are combined with the constant region (C) of the heavy and the light chains from human antibodies. Although these chimeric monoclonal antibodies exhibited reduced

immunogenicity, however, the HAMA responses developed in patients were still considerable (Buss et al., 2012). In the next leap forward, humanized monoclonal antibodies were generated from grafting of only the complementary determining regions (CDRs) of a mouse antibody onto human variable regions. With the advent of phage display technology, this was taken further toward generation of fully human antibodies by which genes encoding for the Fab or Fv fragments of human antibodies are expressed in bacteriophage, and subsequently selected and expressed in *E.coli* (Reichert et al., 2005). In addition to phage display, fully human antibodies are also generated after immunizing transgenic mouse strains that express human variable domains. The transgenic mice have impaired endogenous murine Ig machinery; therefore only human antibodies are expressed (**Fig**.1.1.2). The immunogenic potential is significantly reduced with both humanized and fully human antibodies that have similar properties to human endogenous IgGs (reviewed by (Buss et al., 2012)).

In general, naked antibody molecules are rarely potent cytotoxic agents, therefore they can be linked to cytotoxic drugs, toxins, or radionuclides to enhance their anti-cancer activity (Terwisscha van Scheltinga et al., 2017, Froysnes et al., 2017, Blakkisrud et al., 2017). The optimal characteristics for efficacious and safe antibody-based therapy are high affinity to the target antigen, internalization following binding, non-immunogenicity and limited normal tissue expression of the target antigen. Moreover, the isotype of the mAb is another key point to consider in Ab-based therapy design as it will affect whether the targeted therapy has the potential to kill cells via antibody-dependent cytotoxicity (ADCC) and/or complement dependent cytotoxicity (CDC) in addition to the killing induced by cytotoxic agents or toxin (reviewed by (Phillips, 2013)).

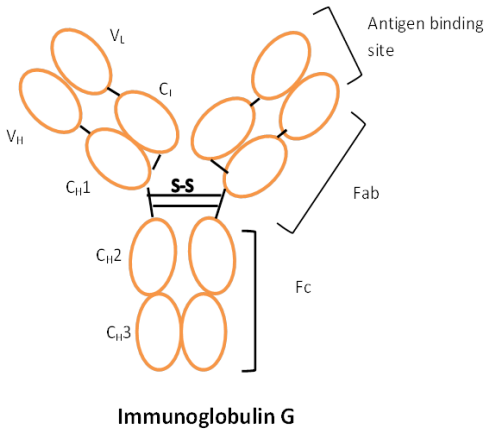

Figure 1.1.1: Antibody structure:
Fc and Fab fragments of an antibody molecule (immunoglobulin G).

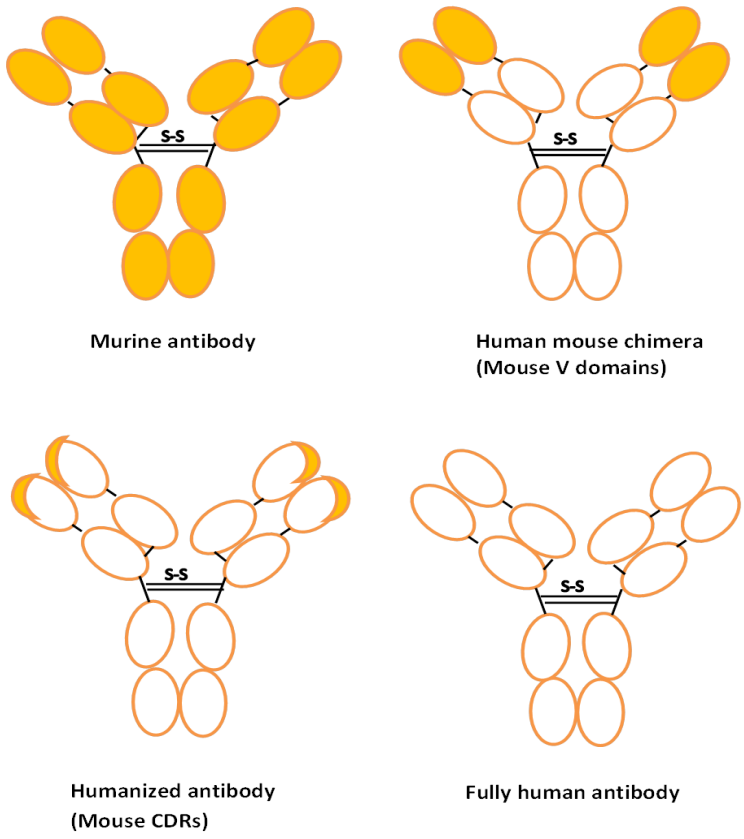

Figure 1.1.2: Types of monoclonal antibodies generated:
Murine antibody (entirely of murine origin), chimeric antibody (murine variable region combined with human constant region), humanized antibody (human antibodies with murine CDR region grafted onto the human variable region), fully human antibody (entirely of human origin).

1.1.1.2 Antigens:

In general, cancer cells do not express unique antigens as this would lead to rapid elimination by the immune system. However, cancer cells occasionally express normal cell surface antigens at higher copy numbers on tumour cells compared to their healthy normal cellular counterparts (Sievers and Senter, 2013).Therefore for a targeted delivery system, the target antigens need to be highly expressed on the surface of tumour tissue with limited distribution on normal tissue (Alewine et al., 2015). Selecting a rapidly internalised antigen is an advantage when generating a targeted toxin therapy, as this will affect efficient delivery of the toxin into the cells (Kuo et al., 2009). Furthermore, it is important to notice that the basis for selection of both the target antigen and the design of the targeted delivery system is the nature of intracellular trafficking of the antigen. Targets that are efficiently trafficked to lysosomes are suitable for ADCs that require lysosomal cleavage or degradation of mAb to liberate the active drug; on the other hand this may be a big issue for protein immunotoxins as the toxin would be subjected to degradation (reviewed by (Phillips, 2013)).

1.1.1.3 Linkers:

A key parameter in the design of Ab based therapy is selecting the right linker to bind the active component to the mAb (Kitson et al., 2013). Basically, the linkers utilized in immunotoxins do not differ from those used in ADCs (Mathew and Verma, 2009). Incorporation of the right linker will influence the efficacy and the release of the biologically active component of the immunoconjugate in targeted cells. The correct linker reduces unwanted effects, such as the formation of aggregates in the blood circulation (Kitson et al., 2013) and premature detachment of the toxin payload from the targeting moiety that leads to non-specific uptake into healthy cells (Dosio et al., 2011). Chemical linkers commonly used to form ADCs can be broadly classified as cleavable linkers that release the active agent under certain intracellular environments and non-cleavable linkers (Ghetie and Vitetta, 2001).

- The acid labile hydrazone linker: enables selective hydrolysis in acidic endosomes and lysosomes following the internalization of ADCs and it is relatively stable at physiological pH

(pH 7.3-7.5); however they have been associated with high nonspecific release of the active constituent in the circulation in preclinical studies (Safavy et al., 2003).

- The disulfide- based linkers: are susceptible to reduction in the endosomes following the internalization of the immunoconjugate, as increasing reducing conditions breaks the bond and releases the toxin (Carlsson et al., 1978). Subsequently, linkers are reduced with high or low efficiency, according to the level of steric hindrance at the carbon atoms adjacent to the disulfide linkage; optimized disulfide linkers are associated with high plasma stability and efficient release of the cytotoxic agent in targeted cells (reviewed by (Ducry, 2013)).

- **The dipeptide linkers**: are predominantly cleaved by specific proteases in the lysosomes, such as citruline-valine linkers, expressing greater stability in the plasma (Sanderson et al., 2005).

In contrast, the **thioether linkers** are considered non-cleavable. In this case, the degradation of the mAb backbone in the lysosome liberates the drug which remains attached to the linker via lysine or cysteine residue of the mAb. These charged moieties are not able to cross membranes as efficiently as ADC conjugated to cleavable linkers. Thereby, the diffusion of metabolites enhances killing of the neighbouring cells, a concept known as the “bystander effect” (Zhou et al., 2012, Kupchan et al., 1972).

Similar to ADC, toxins linked to antibodies through peptide bonds require proteolytic cleavage to release the toxin. Toxins linked chemically via disulfide bonds to antibodies require reduction. Acid labile linkers release the toxin in endosomes or lysosomes (reviewed by (Wayne et al., 2014a)). Thioether linker is appropriate if the ligand is attached to a non translocated part of the bacterial toxin (such as the binding domain) (FitzGerald et al., 1990).

1.1.2 Antibody drug conjugates (ADCs):

ADCs are typically designed to selectively deliver a highly potent cytotoxic drug to antigen expressing cells. The clinical activity and tolerability of ADCs relies on three components: antibody, a cytotoxic drug, and a linker that attaches both (Sievers and Senter, 2013). The mechanism of ADC action underlying cell intoxication involves the binding of monoclonal antibody to the tumor associated antigen or interaction with various cell receptors. The generated ADC-receptor complex is internalized by receptor mediated endocytosis, and

trafficking of the complex to endosomes/ lysosomes. Next the linker is destabilized, due to the low pH in the lysosome, or break down of the antibody backbone by intralysosomal proteases, thus releasing the active drug inside the targeted cancer cell (Flygare et al., 2013). The released cytotoxic drug can interfere with various intracellular pathways, leading to cell death (Sievers and Senter, 2013).

1.1.2.1 Development of antibody drug conjugates:

The early approach was to enhance the anti-tumour action of clinically approved anticancer drugs, such as methotrexate and doxorubicin, by attaching them to murine or chimeric monoclonal antibodies (Shefet-Carasso and Benhar, 2015). Repeated studies, however, have shown that these early ADC had several drawbacks due to insufficient potency of the delivered drug, limited number of drug molecules delivered to the target cell, and the development of immune response preventing repeated cycles of treatment (Teicher and Chari, 2011).

Improvements in all aspects of the early ADC was carried out by replacing the murine monoclonal antibody with humanized or fully human monoclonal antibody, in addition to using highly potent cytotoxic agents that were 100-1000 fold more toxic than the previously used chemical agents. The most frequently used cytotoxic drugs for conjugation to the monoclonal antibodies are tubulin inhibitors (maytansinoid, auristatins) and DNA minor groove binders (calicheamicin, duocarmycins)(Bouchard et al., 2014). For the most part these potent cytotoxic agents were very toxic and lacked a safe therapeutic index as a free drug. An effective ADC should, however, deliver a highly potent cytotoxic agent to antigen-bearing tumour cells whilst minimizing their systemic toxicities (reviewed by (Phillips, 2013).

1.1.2.2 Optimization of ADCs:

As mentioned above, a key issue for developing a successful ADC is the exact link between the cytotoxic drug and the antibody, as this has a massive effect on circulating half-life and safety of the conjugate; thus linkers must be stable in the blood stream to prevent the premature release of the active constituent, while efficiently labile to deliver the cytotoxic drug inside the target cell (Flygare et al., 2013, Shefet-Carasso and Benhar, 2015).

The creation of less heterogeneously loaded ADCs, formed through a site specific interaction to two or more of the eight available sulfhydryl groups of a cysteine residue on

the antibody, liberated after a mild reduction of the interchain disulfide bonds is desirable. To further create more homogeneous ADCs, incorporation of cysteine residues in the antibody backbone to enable thiol conjugation at these specific sites has been investigated (Zhou and Rossi, 2014). In addition, the ratio of drugs to mAb and drug position has an influence on ADCs aggregation, antigen binding, and clearance from the blood stream, potency and tolerability. The potency of ADCs can be reduced by under-conjugation, however the loading of too many drug per mAb can result in decreased plasma half-life, reduced tolerability, and less affinity to the antigen (Senter, 2009, Hamblett et al., 2004). The optimal number of drug moiety per Ab for most recent ADCs is likely to be about four (Senter, 2009).

ADCs may also be improved by employment of new highly potent cytotoxic agents; these are the DNA- alkylating agents duocarmycins and pyrrolobenzodiazepine dimers and RNA polymerase inhibitor amanitin (Beck et al., 2011, Moldenhauer et al., 2012).

1.1.2.3 Advanced ADCs in preclinical and clinical trials:

Ab-based therapeutics are of growing interest in oncology treatment, over 70% of novel ADCs being investigated have entered clinical trial as a treatment for a wide range of solid and haematological tumors. Recently two ADCs, Brentuximab vedotin (Adcetris®) and Adotrastuzumab emtansine (Kadcyla®), were approved for clinical application by both US food and drug administration (FDA) and the European medicine agency(EMA)(Zhou and Rossi, 2014).

Gemtuzumab ozogamicin (mylotarg), an anti CD-33 Ab conjugated to calicheamicin through an acid-labile hydrazone linker, received accelerated approval by the FDA in 2000 for the treatment of acute myelocytic leukaemia (AML) in CD33 positive patients (over 60 years age)(Bross et al., 2001). Based on clear evidence of blast decrease in patient bone marrow, the developer, Pfizer withdrew the product from the markets in 2010 as it failed to demonstrate a relative clinical benefit (Petersdorf et al., 2013). The failure was related to unstable linker that led to premature release of cytotoxic payload and subsequent non selective targeting (ten Cate et al., 2009).

Brentuximab vedotin (Adcetris®) is an ADC that is composed of a human/mouse chimeric IgG1 anti CD-30 mAb, conjugated to the cytotoxic agent auristatin MMAE (Senter and Sievers, 2012). The antibody is covalently linked to an average of four MMAE molecules per

mAb via a protease- cleavable dipeptide linker. Following binding of the ADC to the CD30 antigen, it undergoes rapid internalization and proteolytic cleavage in the lysosome, leading to the release of the active component inside targeted cells (Katz et al., 2011). Brentuximab vedotin has been granted accelerated approval by the FDA for the treatment of Hodgkin's lymphoma and anaplastic large cell lymphoma. In normal physiological conditions, CD30 expression is limited to activated B and T lymphocytes and NK cells, in addition low levels of CD30 expression is noticed in monocyte and eosinophils, making it a good target for Ab-based therapy (reviewed by (Ducry, 2013)).

T-DM1 (trastuzumab emtansine), is an ADC comprised of humanized trasuzumab mAb (anti HER-2) conjugated to DM1 via a non-cleavable thioether linker, for the treatment of HER-2 positive refractory/relapsed metastatic breast cancer. Breast cancer accounts for 28% of all new cases of cancer in women, and 15-25% of these recent cases have overexpression of HER-2 (Kovtun et al., 2006). It was demonstrated that cytotoxic drug release from the ADC occurs as a result of mAb degradation in lysosomes. In addition to the commercially available ADCs discussed above, Table 1.1 represents ADCs currently in clinical trials (Kitson et al., 2013).

Candidate & (Target Antigen)	ANTIBODY-DRUG CONJUGATE [MAb] – [Linker] – [Drug]	Oncology Indication	Developer
Phase III of Clinical Development			
Inotuzumab ozogamicin (CD22)	[Hz IgG4] – [Hydrazone] – [Calicheamicin]	NHL	Pfizer
Gemtuzumab ozogamicin (CD33)	[Hz IgG4] – [Hydrazone] – [Calicheamicin]	Relapsed AML	Pfizer
Phase II of Clinical Development			
Lorvotuzumab mertansine (CD56)	[Hz IgG1] – [SPP] – [Maytansine DM1]	Solid Tumours, MM	ImmunoGen
Glembatumumab vedotin (GPNMB)	[Hu IgG2] – [Valine-Citrulline] –[Auristatin MMAE]	Breast Cancer, Melanoma	Celldex Therapeutics
SAR-3419 (CD19)	[Hz IgG1] – [SPDB] – [Maytansine DM4]	NHL	Sanofi
PSMA ADC (PSMA)	[Hu IgG1] – [Valine-Citrulline] – [Auristatin MMAE]	Prostate Cancer	Progenics
RG7593/DCDT2980S (CD22)	[Hz IgG1] – [Valine-Citrulline] –[Auristatin MMAE]	NHL	Genentech Roche
RG-7596 (CD79b)	[Hz IgG1] – [Valine-Citrulline] – [Auristatin MMAE]	NHL	Genentech Roche
BT-062 (CD138)	[Ch IgG4] – [SPDB] – [Maytansine DM4]	MM	Biotest
Phase I of Clinical Development			
SGN-75 (CD70)	[Hz IgG1] – [Maleimidocaproyl] – [Auristatin MMAF]	NHL, RCC	Seattle Genetics
BAY 79-4620 (CA-IX)	[Hu IgG1] – [Valine-Citrulline] – [Auristatin MMAE]	Solid Tumours	Bayer
Milatuzumab-doxorubicin (CD74)	[Hz IgG1] – [Hydrazone] – [Doxorubicin]	MM	Immunomedics
AGS-5ME (SLC44A4)	[Hu IgG2] – [Valine-Citrulline] – [Auristatin MMAE]	Pancreatic, Prostate Cancer	Astellas
BAY 94-9343 (Mesothelin)	[Hu IgG1] – [SPDB] – [Maytansine DM4]	Solid Tumours	Bayer
ASG-22ME (Nectin-4)	[Hu IgG1] – [Valine-Citrulline] – [Auristatin MMAE]	Soild Tumours	Astellas

Abbreviations - Ch: chimeric; Hz: humanized; Hu: fully human; MMAE: monomethyl auristatin E; MMAF: monomethyl auristatin F; NHL: non-Hodgkin's Lymphoma; PSMA: Prostate-Specific Membrane Antigen; RCC: Renal Cell Carcinoma; GPMNB: Glycoprotein NMB; AML: Acute Myeloid Leukaemia; MM: Multiple Myeloma; CRC: Colorectal Carcinoma.

Table 1.1.1: ADCs currently in clinical trials.
(Kitson et al., 2013). Reproduced with permission.

1.1.3 Immunotoxins:

Immunotoxins are highly potent protein agents, basically composed of an antibody, cytokine, or growth factor linked to a toxin, targeting a specific antigen that is over expressed or selectively expressed on the surface of malignant cells (Gilabert-Oriol et al., 2014). Upon binding to its cell surface receptor, the complex is internalized into the antigen expressing cell, usually through the clathrin-coated pathway, translocation of the enzymatic fragment to the cytosol, and finally cell cycle arrest by apoptosis (Ho et al., 2007). Mostly, immunotoxins are designed to kill cancer cells as part of novel treatment approaches. Additional applications of immunotoxins include immune regulation and the treatment of viral or parasitic diseases (Antignani and Fitzgerald, 2013) (**Fig**.1.1.3).

1.1.3.1 Development of immunotoxin design:

1.1.3.1.1 Chemically conjugated immunotoxin:

The first generation of immunotoxins were made by chemically binding the intact toxin to full length antibody via bifunctional cross-linking agents. These immunotoxins had several undesirable side effects when given to humans due to the presence of cell binding domains (Ia) of multi subunit toxins resulting in “off- target “ toxicities that limited their use clinically (Choudhary et al., 2011, Vitetta and Thorpe, 1991).(**Fig**.1.1.3)(Antignani and Fitzgerald, 2013).

Second generation immunotoxins were produced by eliminating the cell binding domain of multi component toxins (**Fig**.1.1.3) (Antignani and Fitzgerald, 2013). The resulting modified toxin fragment was chemically coupled to an antibody (Choudhary et al., 2011, Vitetta and Thorpe, 1991), thus increasing the amount of targeted toxin that could be safely given to experimental animals and humans; however issues of heterogeneity persisted, with low stability and poor tumor penetration (Shan et al., 2013). Moreover, some immunotoxins still bound weakly to normal cells and resulted in an undesirable side effect called vascular leak syndrome (VLS). VLS is caused by damage to endothelial cells and results in leakage of fluid from the circulation into the tissues, edema, a fall in serum proteins, hypotension, and finally vascular collapse (Vitetta, 2000).

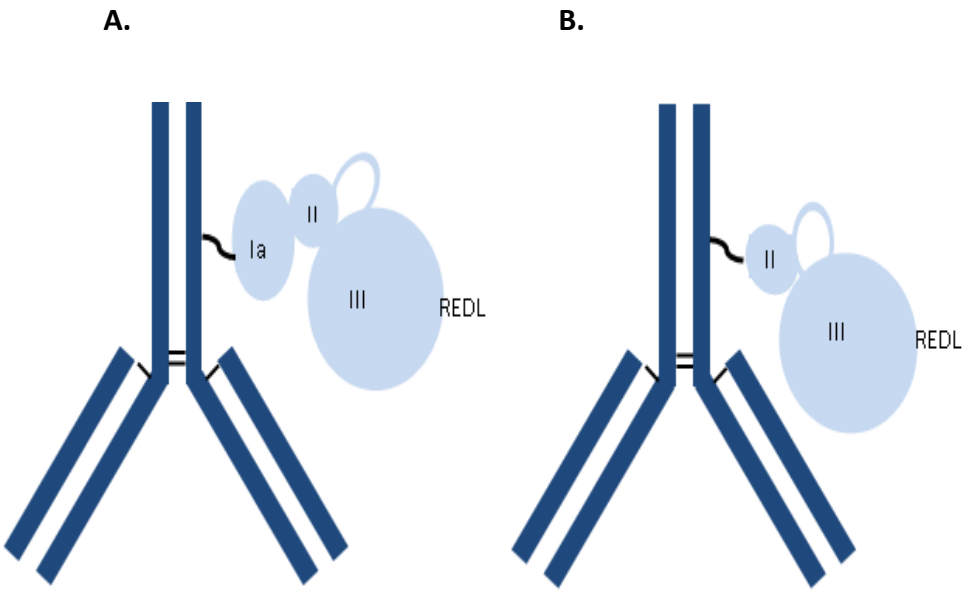

Figure 1.1.3 : First generation immunotoxin (A) and second generation immunotoxin (B) based on Pseudomonas exotoxin were **Ia**: binding domain of a toxin**, II**: translocation domain of a toxin**, III:** enzymatic active domain of a toxin**,** and **REDL:** endoplasmic reticulum retention signal at the C-terminus of the protein**,** Adapted from (Antignani and Fitzgerald, 2013).

1.1.3.1.2 Recombinant immunotoxins:

The next leap forward was produced using molecular DNA technology and involved fusion of the genes encoding the modified toxins that possess the active domain only with genes encoding the variable fragment of an antibody. The generated recombinant immunotoxins (RIMs) are cleaved by intracellular enzymes (Weldon et al., 2015). Two formats of recombinant antibodies have been evaluated in preclinical trials, scFv is produced by expressing the V_H and V_L, joined by a peptide linker in recombinant form. These smaller recombinant immunotoxins exhibit improved penetration to solid tumours; nevertheless they are rapidly cleared from the circulation and in addition express low binding affinity to tumour antigens. This issue could be overcome by either linking two scFv with a single peptide bond to form bivalent scFv, or by construction of a bivalent scFv diabody , through preventing the dimerization of the V_H and V_L domains using a short peptide linker in a single scFv, while using a long linker between both scFvs to force dimerization (**Fig**.1.1.4) (Olafsen and Wu, 2010). The RIMs are produced by different expression systems including bacteria, yeast and mammalian cell lines. Bacteria are the most adequate expression system as they are able to produce protein in large volumes and are resistant to the toxic action of the toxin (Shan et al., 2013). However, there are often problems with the complex protein

folding required for RIMs formation as the bacteria are prokaryotic. Furthermore, *ex vivo* modifications are necessary which limits yields (Yin et al., 2007). Mammalian cell lines such as CHO cells and HEK293 cells are able to generate complex protein structures; however, the relatively high cost and complicated technology limit their use for large scale production (Yin et al., 2007). Furthermore, these cell lines are susceptible to the cytotoxic action of the toxin. Yeast expression system such as *Pichia pastoris* are relatively cheaper and give higher yields of targeted toxin, but again are susceptible to the killing action of the toxin (Cregg et al., 2000).

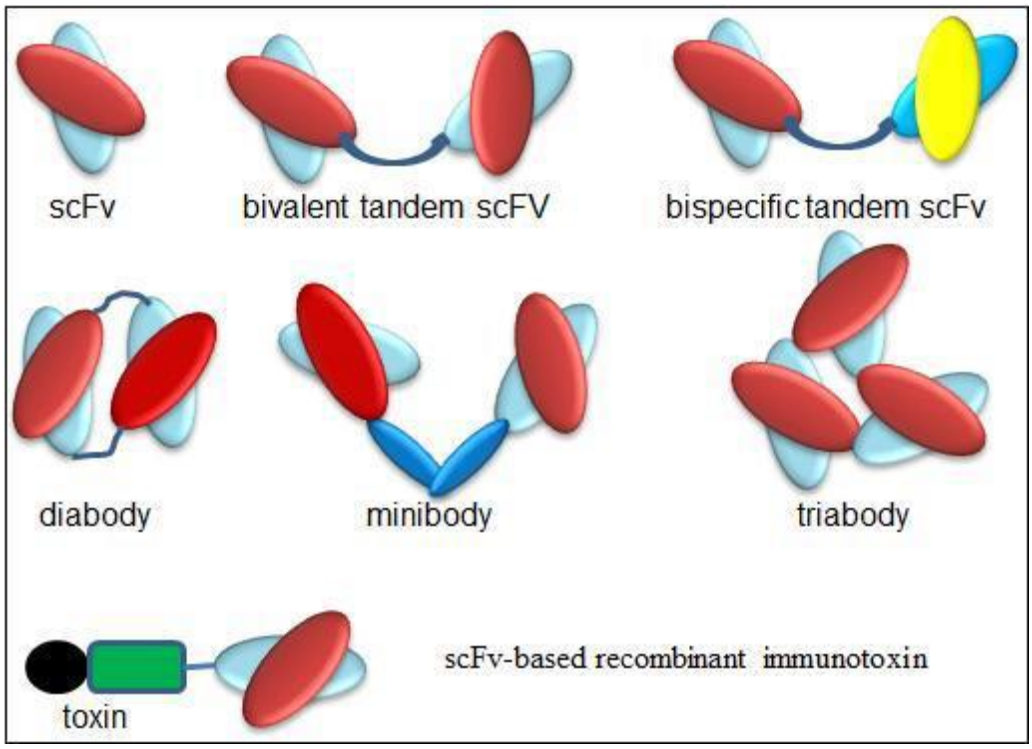

Figure 1.1.4: Cartoon structures of variuos formats of recombinant antibody fragments. **scFv:** The smallest engineered fragment of antibodies (25-30 kDa), **bivalent tandem scFv:** designed by linking two scFv with a peptide linker, **bivalent scFv diabody**: engineered by preventing dimerization of the V_H and V_L domains from one scFv via a short peptide linker, **triabody:** other format of antibodies with increased molecular size**, bisepecific tandem scFv:** engineered by linking two different scFv antibodies
(Shan et al., 2013). Reproduced with permission.

1.1.3.2 Protein toxin characteristic features:

The protein toxins that have entered clinical trials are derived from the plant toxin ricin and bacterial toxins (diphtheria toxin (DT) and pseudomonas exotoxin (PE). Basically, the toxin is

composed of several discrete domains with different functions (Pastan et al., 2006, Adkins et al., 2012), including an active enzyme domain that must enter the cytosol to kill cells, a cell-binding domain that has to be removed or blocked before coupling with an antibody, and finally a translocation domain that functions to transport the active toxin domain to the cell cytosol (Zhan et al., 1994).

The inhibition of protein synthesis via a variety of plant and bacterial toxins were investigated for cancer therapy. However the active enzyme domain of these toxins is toxic to both healthy and transformed cells (Alewine et al., 2015).

1.1.3.2.1 Plant based immunotoxins:

Plant toxins can be classified into type I and type II ribosomal inactivating proteins (RIPs), which exhibit N-glycosidase activity and specifically remove an adenine residue of the 28S rRNA in the 60S large ribosomal subunit (Schrot et al., 2015), thereby damaging ribosomes in an irreversible manner (Stirpe and Battelli, 2006). RIPs are more likely to act as a defence mechanism in plants, as their expression is up-regulated following viral infection and contamination with microorganisms (Iglesias et al., 2005). Type I RIPs include gelonin, saporin, and bouganin that possess the activity (enzymatic) domain in a single chain form (Bolognesi et al., 2000, Stirpe, 2004), while Type II RIPs consist of a double- chain structure, with the cell recognition domain (chain B) linked via a disulfide to the activity fragment (chain A). Type III RIPs have also been suggested, which are pro-enzymes that become active only after the removal of a short peptide fragment (Gilabert-Oriol et al., 2014). In addition, the type I RIP saporin 6 has been reported to induce apoptosis via the mitochondrial cascade prior to the onset of protein synthesis inhibition (Brigotti et al., 2002), and the type II RIP ricin has also been shown to cause early nuclear DNA damage with or after inhibition of protein synthesis (Brigotti et al., 2002). Therefore it has been suggested that RIPs may induce apoptosis through different mechanisms, of which inhibition of protein synthesis is crucial, but not the sole factor for inducing apoptosis (Das et al., 2012). Type II RIPs such as ricin are able to bind to sugars on the cell surface by their B chain (lectin subunit); however binding to the cell surface is not enough to be potent, as there are number of RIPs that are considered to be non-toxic such as ricinus agglutinin. Ricin shows approximately 2868- fold higher potency than ricinus agglutinin in treated cells. This finding has been suggested to be due to insufficient ability of ricinus agglutinin toxin to

translocate into cytosol (Stirpe and Battelli, 2006). However, Nigrin b is another non-toxic type II RIP which has been reported to internalise as efficiently as ricin (Battelli et al., 1997). This highlights the importance of intracellular trafficking following binding for inducing cell killing. Studies on ricin revealed that following binding, the toxin is internalized by both clathrin-dependent and independent endocytosis and that about 5% localises with the trans-Golgi network, followed by backward transport to the ER through the Golgi apparatus (Sandvig and van Deurs, 1996). The ricin toxin in the lumen of the ER is thought to be cleaved and then exported to the cytosol for degradation (**Fig.**1.1.5) (Roberts and Lord, 2004). Type II RIPs used in the construction of immunotoxins include ricin and abrin (Vitetta and Thorpe, 1991, Stirpe, 2004, Frankel et al., 2002). As the B chain of intact ricin binds to most mammalian cells, improvement of selectivity of ricin immunotoxin has taken place by blocking the galactose binding site of the B chain; therefore cell binding occurs essentially through the mAb or mAb fragment of the immunotoxin. Although potent and antigen selective in vitro, ricin A chain immunotoxins are rapidly cleared in the liver and spleen due to uptake by reticuloendothelial cells. Chemical deglycosylation leads to decreased liver toxicity and improved efficacy (Thorpe et al., 1988, Blakey et al., 1987).

The mechanism of uptake of type I RIPs remains obscure, however studies with saporin toxin revealed that the internalisation mechanism is independent of the Golgi apparatus, and speculated to follow a diverse pathway to ricin (Vago et al., 2005). It has also been suggested that saporin is able to enter cells via binding to α2-macroglobulin receptors (Cavallaro et al., 1995).

1.1.3.2.2 Bacterial based immunotoxins:

1.1.3.2.2.1 Pseudomonas exotoxin A (PE):

Secreted by Pseudomonas *aeruginosa* bacterium is a single chain protein of 638 amino acids, that is processed by removal of 25 residues before secretion as a native toxin of 613 residues. The native PE toxin is composed of 3 functional domains, domain Ia is the recognition domain that binds to receptor related proteins. Domain Ib is still of unknown function. Domain II is responsible for toxin translocation into the cytosol. Domain III is the activity or the enzymatic domain that triggers the transfer of ADP-ribose moiety from NAD^+ to elongation factor 2 (EF2), and consequently causes cell cycle arrest and death (Dosio et al., 2014). Therefore, PE binds to the receptor related protein, and internalizes by receptor

mediated endocytosis. Within the endocytic pathway, PE is cleaved by the endoprotease furin that separates the polypeptide chain between domains I and II, but a disulfide bond preserves the linkage between the two domains with a covalent linkage. PE within the endocytic pathway can either follow a trafficking route to the Golgi or final degradation in the lysosome. PE in the Golgi encounters KDEL receptors that recognize a REDL (Arg-Glu-Asp-Leu) sequence in its C terminus and transports PE to the ER via a retrograde manner. Once in the lumen of the ER, the disulfide bond linking the two domains is reduced and therefore separated. The enzymatic domain is subsequently translocated into the cytosol and ultimately halts protein synthesis (**Fig**.1.1.5) (Weldon and Pastan, 2011).Recently, the development of recombinant immunotoxins have focused on the production of smaller and less immunogenic versions of the original PE40/38 molecule (Weldon et al., 2009, Zhou et al., 2012). Through eliminating most of domain II of PE, a smaller molecule was produced that possesses cytotoxic activity with the benefit of removal of one major and several minor immunogenic epitopes. The elimination of domain II also removed many lysosomal cleavage sites and produced a molecule that was termed “LR” for lysosomal resistant (Weldon et al., 2009). Thus the LR version of PE-derived immunotoxins exhibits three new features: it is smaller, less immunogenic and more resistant to cleavage by lysosomal enzymes (Cruz-Migoni et al., 2011, Zhou et al., 2012).

1.1.3.2.2.2 Diphtheria toxin-based IMTs:

DT is a single chain protein of 535 amino acids (58 kDa) secreted by *C. diphtheriae* (De Zoysa et al., 2005), basically composed of a receptor binding domain at the C terminus that binds to the surface receptors on the target cell, a translocation domain consisting of nine helices that enables the toxin to cross the cell membrane and reach the cytosol and an activity domain A at the N terminus (Pastan et al., 2006) that has ADP-ribosylation activity, thereby halting protein synthesis and subsequently killing the cell (Zovickian et al., 1987, Sandvig and Olsnes, 1981). Normally, DT binds to heparin binding epidermal growth factor (EGF)-like precursor on target cells (Naglich et al., 1992). After binding, the DT is internalized by receptor mediated endocytosis into the endosomes, where acidic conditions induce a partial unfolding of the translocation domain, making it more hydrophobic, which triggers the toxin penetration through the endosomal membrane via pore formation (Zhao and London, 2005). Upon entry into the cytosol, the A domain catalyses the transfer of adenine

dinucleotide (NAD^+) to the unique diphthamide residue on eEF2 (Li et al., 2013). This inactivates eEF2, inhibiting ribosome translocation during elongation, and blocking protein synthesis (**Fig.**1.1.5). Recombinant DT is made by replacing the cell-binding domain with a ligand that binds to a growth factor receptor or the Fv fragment of an antibody (Siegall, 1994). These truncated forms of DTs are unable to enter a cell without selective uptake of their carrier ligand by a receptor (Naglich et al., 1992, Boquet et al., 1977).

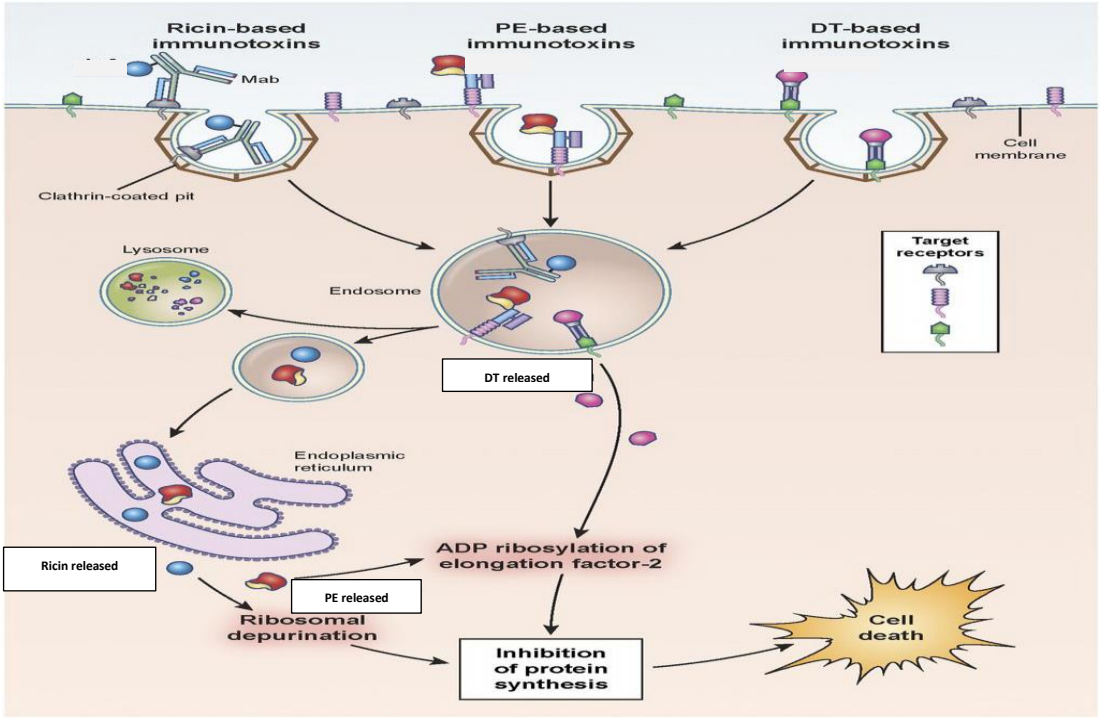

Figure 1.1.5: Modified immunotoxin endocytosis and trafficking within mammalian cells. Ricin and Pseudomonas toxins are trafficked out of the endoplasmic reticulum to the cytosol where they inactivate protein synthesis. Diphtheria-based toxins are trafficked to endosomes where the toxin translocate directly to the cytosol to cause cell death.
(Wayne et al., 2014b). Reproduced with permission.

1.1.3.3 Strategies for future development of IMTs:

To date, most success in immunotoxin therapy has been achieved in targeting leukemic cells in blood, as several factors restrict the entry of immunotoxins to solid tumour mass, including the poor uptake of toxin and inability of cancer patients to receive repeated cycles of treatment without the formation of neutralizing antibodies. The strategies to improve the clinical responses of IT depend on targeting new antigens on the surface of malignant cells, the administration of IMT combinations that target different tumour markers,

identification and elimination of immunodominant domains from the B and T cell epitopes and also the production of less immunogenic IMT, based on human or humanized toxins and antibodies (Pamela A. Trail auth., 2013). Importantly, cancer remedies usually require combination treatments, therefore future development of successful immunotoxins relies on discovering the best enhancing agents for co-administration (Antignani et al., 2016).

The immunotoxin toxicity depends on several biochemical properties, including antigen binding, internalization rate, intracellular processing and intrinsic potency of toxin (Hexham et al., 2001). As mentioned in the examples given above, some toxins, for instance diphtheria toxin, once they have entered the cells, are found in early endosomes that can be later recycled or translocated directly to the cytosol. Other toxins, for instance ricin and cholera toxin, follow a distinct pathway: the retrograde route from early endosomes to the endoplasmic reticulum, via the Golgi apparatus (**Fig.**1.1.6) (Lord and Roberts, 1998, Sandvig and van Deurs, 2000). Thus the critical step in cytotoxic efficiency is the ability to deliver the toxin to the cytosol. Subsequent trafficking characteristics, release and endosomal escape are related to intrinsic toxin features (Hexham et al., 2001). Accordingly some of the work presented in this thesis focuses on the study of the effect of intracellular trafficking on immunotoxin cytotoxicity.

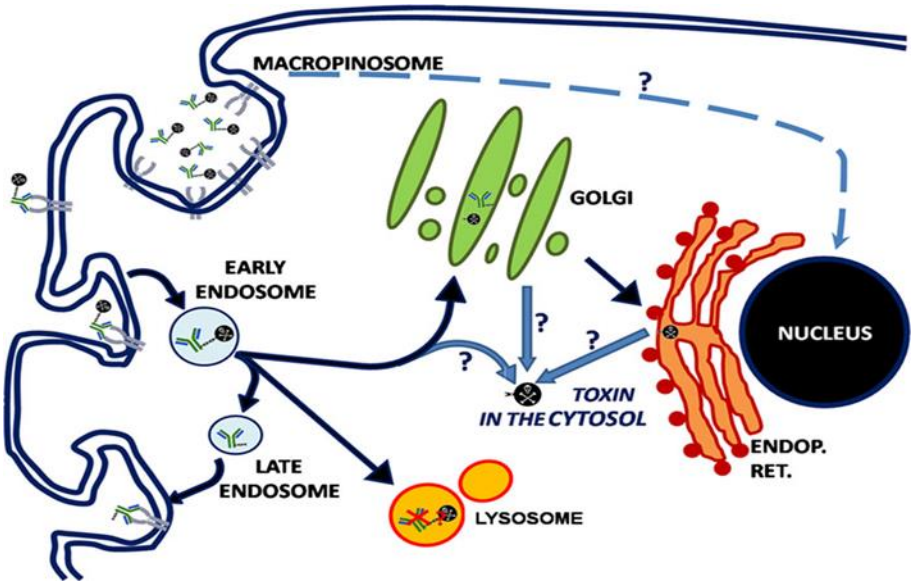

Figure 1.1.6: Intracellular pathways of immunotoxin:

Scheme demonstrating the different Intracellular transport pathways of immunotoxin to release its toxin into the cytosol. (adapted from (Tome-Amat et al., 2015)).

1.1.3.3.1 Efficiency enhancers:

The toxic component of the majority of protein based targeted therapies must enter the cell cytosol to mediate its killing effect. Although more than 500 toxins have been identified in the past decades, no antibody targeted toxin therapy has yet been approved by authorities for treating cancer (Fuchs et al., 2016). In general, plant toxin type I RIPs such as pokeweed, saporin, are considered to have lower cytotoxicity than the type II RIPs. This is not related to the lower enzymatic activity of RIPs but due to the lack of a binding domain (B-chain), leading to inefficient cellular internalization (Puri et al., 2012). Therefore, this type of plant toxin has been extensively used as fusion proteins by coupling the toxins either chemically or recombinantly to ligand to facilitate their cellular internalization (Kreitman, 2006). Since targeted toxins exert their anti-tumoral efficacy only in the cytosol, it is a vital prerequisite for their efficacy that they are able to escape from the endosomal network into the cytosol. Several strategies have been employed to enhance the permeability of endosomal membranes including the use of calcium channel blockers, cell penetrating peptides, organic molecules and other light induced technique (Fuchs et al., 2016)s. To improve the cytosolic delivery of targeted BLF1 conjugates in this thesis, the following enhancers were used:

1.1.3.3.2 Saponin:

It has been demonstrated that triterpenoidal saponins specifically mediate the release of saporin out of the intracellular compartments into the cytosol without affecting the integrity of the plasma membrane (Weng et al., 2012). The synergistic enhancement properties of triterpenoidal saponins were initially observed with type 1 RIP plant toxin agrostin (Hebestreit and Melzig, 2003). Later to this finding, the augmentation of cytotoxic effects by saponins was studied for targeted toxins. The first recombinant immunotoxin investigated consisted of a plant toxin moiety (saporin) and epidermal growth factor as a ligand, where enhanced cytotoxicity of up to 385,000 fold was noted (Heisler et al., 2005). The applicability of combination therapy with a targeted toxin consisting of saporin, EGF and saponin was first conducted *in vivo* experimentation in mice. The therapy resulted in a

94% tumor volume reduction even when using a 50-fold lower targeted toxin concentration (Bachran et al., 2009).

1.1.3.3.3 Bafilomycin A1:

Bafilomycin A1 is a specific inhibitor of vacuolar ATPase (Bowman et al., 1988) causing an elevation of the endosomal and lysosomal pH. Endosomal and lysosomal acidification is required for the transport of endocytosed material and therefore bafilomycin A1 affects the intracellular trafficking of endocytosed material. An inhibitor of vacuolar ATPase blocks the transport at different steps in the endocytotic pathway (Bayer et al., 1998). Transport could be either blocked from early endosomes to late endosomes or from late endosomes to lysosomes followed by translocation to the cytosol (Hebestreit et al., 2006). Meanwhile, one of the major problems affecting the immunotoxin efficiency is the degradation of the targeted toxin by lysosomal enzymes, so that substantial amounts of toxin cannot reach the cytosol to inhibit protein synthesis. Bafilomycin A1 inhibits acidification of the lysosomal compartment and thereby protects the toxin from degradation by lysosomal proteases, in addition to blocking cellular trafficking to the lysosome so that more of the toxin will be released to the cytosol (Yoshimori et al., 1991, Ohkuma et al., 1993). Bafilomycin A has been previously employed to reverse the resistance to gelonin immunotoxin activity, where cytotoxicity of the immunotoxin is limited by accumulation and subsequent degradation within the acidified lysosomal compartment (McGrath et al., 2003).

1.1.3.3.4 Brefeldin A:

Brefeldin A is a fungal metabolite that blocks Golgi apparatus function and its use is concomitant with a redistribution of Golgi proteins back to the trans-Golgi network (Lippincott-Schwartz et al., 1991). The block of Golgi function is possibly necessary for the processing of some toxins during the intoxication process or might inhibit the processing of certain cell components required for interaction with the toxin (Hudson and Grillo, 1991). The intoxication by the plant toxin ricin was impaired in brefeldin A treated cells (Yoshida et al., 1991) and ricin was localised in the trans-Golgi network upon brefeldin A treatment (Sandvig et al., 1991). This indicates that ricin toxin follows a route to the Golgi apparatus, where it is processed by Golgi enzymes or interacts with ricin receptors (Youle and Colombatti, 1987). However, a second distinct effect of brefeldin A was observed in enhancing the cytotoxicity of two ricin A based immunotoxins, and this was assumed to be

due to the hydrophobic nature of the brefeldin A molecule, which would be expected to intercalate into cellular membranes and alter Golgi membrane permeability (Hudson and Grillo, 1991). Here it was considered that treatment of cancer cells with a combined therapy of BLF1 immunotoxin with Brefeldin A might potentiate the anti-tumour effect if it followed a pathway through the Golgi as observed with ricin.

1.1.3.4 Advanced immunotoxins in preclinical and clinical trial:

Denileukin diftitox (Ontak) was the first immunotoxin approved by the FDA in 2001 for persistent or relapsed cutaneous T cell lymphoma. The immunotoxin combines the enzymatic and translocation domains of DT with the recombinant human IL-2 (Alewine et al., 2015). The IL2 domain targets IL2 receptors, which are highly expressed in a wide range of malignancies such as CTCL, adult T-cell leukemia, Hodgkins disease and other B and T- cell lymphoma and leukaemias (FitzGerald et al., 2011). A phase III trial testing of denileukin diftitox in 71 patients with CTCL showed a 30% overall response rate and 10% complete response (Olsen et al., 2001). However, its use in practice was infrequent due to its poor stability, VLS, hypoalbuminemia, visual colour disruption, and hypersensitivity reactions (McCann et al., 2012)

There are currently a number of targeted toxins in clinical trials for a range of different cancers. SS1P is a recombinant immunotoxin which consists of anti-mesothelin antibody (anti-MSLN) linked to a truncated version of PE (PE38) (Hassan et al., 2002). MSLN is a cell surface glycoprotein that is normally expressed in mesothelial cells that line the pleura, pericardium and peritoneum. However, it is robustly expressed in many solid tumours including mesothelioma, pancreatic adenocarcinoma, and lung adenocarcinoma and triple-negative-type breast cancer; these properties making it a highly attractive antigen for the development of safe targeted therapy (Hassan et al., 2004). A phase I trial testing of SS1P in 24 patients with chemo resistant solid tumors expressing mesothelin showed a modest clinical response (Kreitman et al., 2009a). Next, the use of SS1P in combination with standard pemetrexed and cisplatin was investigated in 24 patients diagnosed with advanced malignant pleural mesothelioma. 77% of the patients who received the MTD showed a partial response (Hassan et al., 2014). This compares favourably to a phase III study that showed a 41% response rate in patients with malignant mesothelioma treated with cisplatin and pemetrexed alone (Vogelzang et al., 2003). SS1P is currently being investigated in

combination with pentostatin and cyclophosphamide in a phase II study. These drugs suppress the immune system, thereby reducing the immunogenicity of SS1P in patients with mesothelin-positive cancers (Xie et al., 2017). Furthermore, the immunotoxin RG7787 that consists of a humanized Fv fragment against mesothelin linked to a modified PE fragment has been shown to decrease tumor size in xenograft lung models expressing mesothelin (Hassan et al., 2016).

Some progress has been achieved with immunotoxins targeting malignant brain tumours. In a phase I study, the intracerebral microinfusion of TP-38 immunotoxin was investigated in 15 patients with malignant brain tumors. This targeted toxin, which is composed of TGF-α, a ligand for epithelial growth factor receptor (EGFR) combined to PE38, resulted in two partial responses and one complete response (Sampson et al., 2003). The limited effectiveness is thought to be related to the inefficient delivery of the toxin to the tumour site, in addition to the heterogeneity of receptor expressed on the target cells (Alewine et al., 2015). An approach to address this issue is by the use of bi-specific antibodies with different antigenic target specificities (Chandramohan et al., 2012). Recently completed and on-going clinical trials using immunotoxins are shown in table 1.1.2.

Target/payload	Disease	Immunotoxin	Clinical responses	Side-effects	Phase	Refs
IL-2 conjugated to *diphtheria* exotoxin	CTCL, T-cell non-Hodgkin lymphoma (NHL) and melanoma	Denileukin difititox (Ontak) DAB389IL2 (DD)	10% CR and 34% PR in patients with CTCL;6 CR, 7 PR in 27 patients with refractory /relapsed T-cell NHL; 16.7% PR in stage IV melanoma patients	VLS and allergic reactions	Phase III, Phase II	(Dang et al., 2007, Prince et al., 2010, Telang et al., 2011)
Humanized anti-mesothelin Fab fused to (PE).	advanced mesothelioma	LMB-100	Not yet reported	Not yet reported	ongoing Phase I	2016 Trail identifier NCT02798536
bispecific (scFV) of anti-CD19 and CD22 fused to (DT)	relapsed/refractory B-cell lymphoma or leukemia	DT2219	2 CRs in 25 patients	weight gain, low albumin, transaminitis, and fever	phase I	(Bachanova et al., 2015)
Antibodies against CD19(HD37-dgRTA) and CD22 (RFB4-dgRTA) fused to deglycosylated ricin A chain (dgRTA)	refractory or relapsed B-lineage-ALL	Combotox	1 PRs s in 17 treated patients	VLS	Phase I	(Schindler et al., 2011)
GMCSF fused to DT	AML	GMCSFR	1 CR and 2 PRs in 31 treated patients	Liver toxicity	phase I	(Frankel et al., 2002)
anti-CD22 fused to PE38	Hairy cell leukaemia	BL22	17CR, 4 PR in 36 treated patients	hemolytic uremic syndrome	phase I	(Kreitman et al., 2009b)
Antibodies against wild-type epidermal growth factor receptor (EGFRwt) and mutant EGFR variant III fused to Pseudomonas exotoxin A	glioblastomas	D2C7-IT	Not yet reported	Not yet reported	phase I/II	(Chandramohan et al., 2017) Trail identifier NCT02303678
Antibodies against CD25 (anti-Tac) fused to PE38	Adult T-cell leukaemia (ATL)	LMB-2	6CRs, 2PR in 17 patients treated with 6 cycles of LMB-2 and one cycle with fludarabine and cyclophosphamide	Fever, Transaminases elevations, VLS	Phase II	(Kreitman et al., 2016)
Antibodies against Lewis Y antigen fused to PE40	Advanced solid tumors	SGN-10 or BR96 sFv-PE40	No CR or PR in 46 patients with Lewis Y positive metastatic carcinoma	nausea, vomiting and diarrhoea	Phase I	(Posey et al., 2002)

Table 1.1.2: Immunotoxins used in clinical trials.

1.1.4 Protein synthesis:

Protein synthesis, or translation, is a complex, highly regulated process by which messenger RNA (mRNA) is translated into protein that is vital for the function and survival of almost every cell in the body. Protein synthesis is the most energy consuming process in the cell and is necessary for metabolism, DNA replication and molecule transportation, as well as reactions to environmental stimuli (Buttgereit and Brand, 1995). The first step in protein translation is the transcription of DNA into mRNA that leaves the nucleus and travels to the cytoplasm. The translation machinery of mRNA resides on the ribosome in the cytoplasm or across the endoplasmic reticulum (ER). Translation can be subdivided into three phases; initiation, elongation, and termination (Merrick, 1992). Translational initiation is the most regulated stage of translation and requires a complex apparatus, including the ribosome, RNAs along with various protein factors. Three different types of RNAs are involved in translation process: mRNA which carries the genetic code to be translated to protein, transfer RNA (tRNA) which recognise the AUG start codon of the mRNA via its anticodon loop and recruits the corresponding amino acid to the ribosome, and ribosomal RNA (rRNA) which with other proteins, combine to form the ribosome (Merrick, 1992). The ribosome is the protein manufacturing unit of all living cells and is composed of two subunits: a large and a small subunit (40S and 60S in eukaryotes and 30S and 50S in prokaryotes) named according to the rate of sedimentation (Doudna and Rath, 2002). The small subunit is responsible for the assembly of the pre-initiation complex (PIC) 43s, controls codon-anti-codon base pairing, and decoding of genetic information carried on mRNA. The large subunit catalyses the peptide bond formation of the growing peptide chain. A ribosome also consists of 3 binding sites for tRNA called A, P and E. The A- site binds to aminoacyl-tRNA (tRNA holding a new amino acid that is presented to mRNA being translated), the P-site is occupied by tRNA carrying the growing peptide chain (peptidyl site), and the E- site (exit site) the final place that empty tRNA occupies before leaving the ribosome (Doudna and Rath, 2002).

Translation initiation is regulated by the cap-binding protein complex eukaryotic initiation factor 4F (eIF4F) (Sonenberg and Hinnebusch, 2009) (**Fig.** 1.1.7). During the initiation stage of translation, the 43s (PIC) is assembled, containing the 40s ribosomal unit, intiator tRNA (Met-tRNAi) , and different eukaryotic initiating factors (eIF1, eIF1A, eIF3) (Jackson et al., 2010). The mRNA is then recruited to the 43s PIC by the aid of eIF4F complex that is

composed of three major components: eIF4E, eIF4A, and eIF4G. The mRNA cap-proximal region is unwound in an ATP dependent manner. This complex enters the P-site of the 40s ribosomal subunit to scan for the start codon (AUG) on mRNA that is complementary to the anticodon of Met-tRNAi. Recognition of the start codon triggers the arrest of scanning and hydrolysis of GTP and other eIFs. The large subunit 60s then joins to form an elongation-competent 80s , triggered by the ribosome dependent GTPase eIF5B; the complex is then ready to accept the next complementary aminoacyl-tRNA (Lomakin and Steitz, 2013). During translation elongation phase, one amino acid is added at time to the growing polypeptide chain complementary to the codon found in mRNA. The eukaryotic elongation factor eEF1A triggers the recruitment of aminoacyl-tRNA to the A-site of the ribosome next to the initiator tRNA or peptidyl-tRNA in GTP-dependent manner (Merrick, 1992). The peptidyl transferase activity of the large ribosome subunit catalyses the peptide bond formation of the incoming amino acids (Doudna and Rath, 2002). This reaction leaves an empty tRNA in the P-site and the new peptidyl-tRNA in the A site of the ribosome. In the next step, the ribosome shifts 3 base pairs (or 1 codon) along the mRNA, facilitated by eEF2 in a GTP-dependent manner. Consequently, deacylated tRNA is moved from the P-site to the E site and peptidyl-tRNA is shifted to the P-site. The next codon on mRNA is available to bind with new aminoacyl- tRNA in the A-site. These reactions are repeated until the full polypeptide is generated and the stop codon is reached (Merrick, 1992).The consuming of at least four high energy bonds for each amino acid added to the growing peptide chain makes the elongation a great energy consuming step (Browne and Proud, 2002). The translation process terminates when one of the three stop codons, UAA, UAG, or UGA, enters the A-site of the ribosome as there is no aminoacyl-tRNA complementary to these sequence. Instead, these codons are recognised by GTP-bound eukaryotic release factor (eRF), which bind to the P-site, catalysing the release of the polypeptide chain followed by hydrolysis of GTP to GDP and dissociation of ribosome into large and small subunits (Merrick, 1992). At this stage the ribosomal recycling takes place where the ribosomal subunit dissociates, mRNA and deacylated tRNA are released for another round of translation.

Regulation of translation is incredibly important in the cell, as it provides faster responses to environmental cues than the upstream components of gene expression (Bhat et al., 2015). The role of translation regulation in controlling gene expression is highlighted by the low

concordance between steady state mRNA levels and the cellular proteome (Vogel and Marcotte, 2012). Deregulation of the translation process is considered a hallmark of cancer and contributes to altered proliferation, survival, angiogenesis and altered immune response (Bhat et al., 2015).

1.1.4.1 Factors regulating translation:

Translation control of mRNA expression permits the rapid response to low cellular concentration of the encoded protein during stress, nutrient insufficiency, development, division, aging and disease (Sonenberg and Hinnebusch, 2009). Translation initiation is the rate limiting step of protein biosynthesis. It involves multiple eukaryotic initiator factors (eIFs) which are regulated by kinases and inhibitors summarised in Table 1.1.3. In contrast, elongation involves only two eukaroyotic elongation factors (eEFs), eEF1 and eEF2. In addition, translation termination depends on one factor, eukaryotic release factors that recognise the stop codons, thereby releasing the completed polypeptide chain and dissembling the ribosome (Jackson et al., 2010).

Core initiation factor	Function
eIF1	Prevents premature assembly of 40a and 60s ribosomal subunit, stimulate attachment of eIF2-GTP-Met-tRNAi to 40s ribosomal unit, promote binding of 43s (PIC) to mRNA and subsequent scanning for the start codon, prevents premature eIF2-GTP hydrolysis by eIF5 before start codon recognition.
eIF1A	Cooperates with eIF1 in stimulating eIF2-GTP-Met-tRNAi binding to 40s subunit, and ribosomal scanning.
eIF2	Mediates recruitment of Met-tRNAi by forming eIF2-GTP-Met-tRNAi ternary complex that binds to 40s ribosomal unit.
eIF3	Prevents premature assembly of 40s and 60s ribosomal subunit, enhances eIF2-GTP-Met-tRNAi binding to 40s subunit, promotes binding of 43s (PIC) to mRNA and subsequent scanning for the start codon.
eIF4A	ATP dependent RNA helicase activity that promotes unwinding of mRNA secondary structure.
eIF4B	Enhances the RNA helicase activity of eIF4A
eIF4E	Binds to the 5´ cap structure of mRNA.
eIF4G	Scaffold protein that is a component of eIF4F, and enhance RNA helicase activity of eIF4A.
eIF4F	A cap binding complex, made up of eIF4E, eIF4G and eIF4A, promotes its binding with 43s complex by unwinding the 5´ cap region of mRNA.
eIF4H	Homologous to eIF4B fragment and enhances the helicase activity of eIF4A.
eIF5	A GTPase-activiting protein that stimulates the hydrolysis of eIF2-bond GTP upon recognition of the start codon.
eIF5B	A ribosome dependent GTPase that stimulates ribosomal unit joining.

Table 1.1.3: Roles of initiation factors in translation initiation. Adapted from (Jackson et al., 2010).

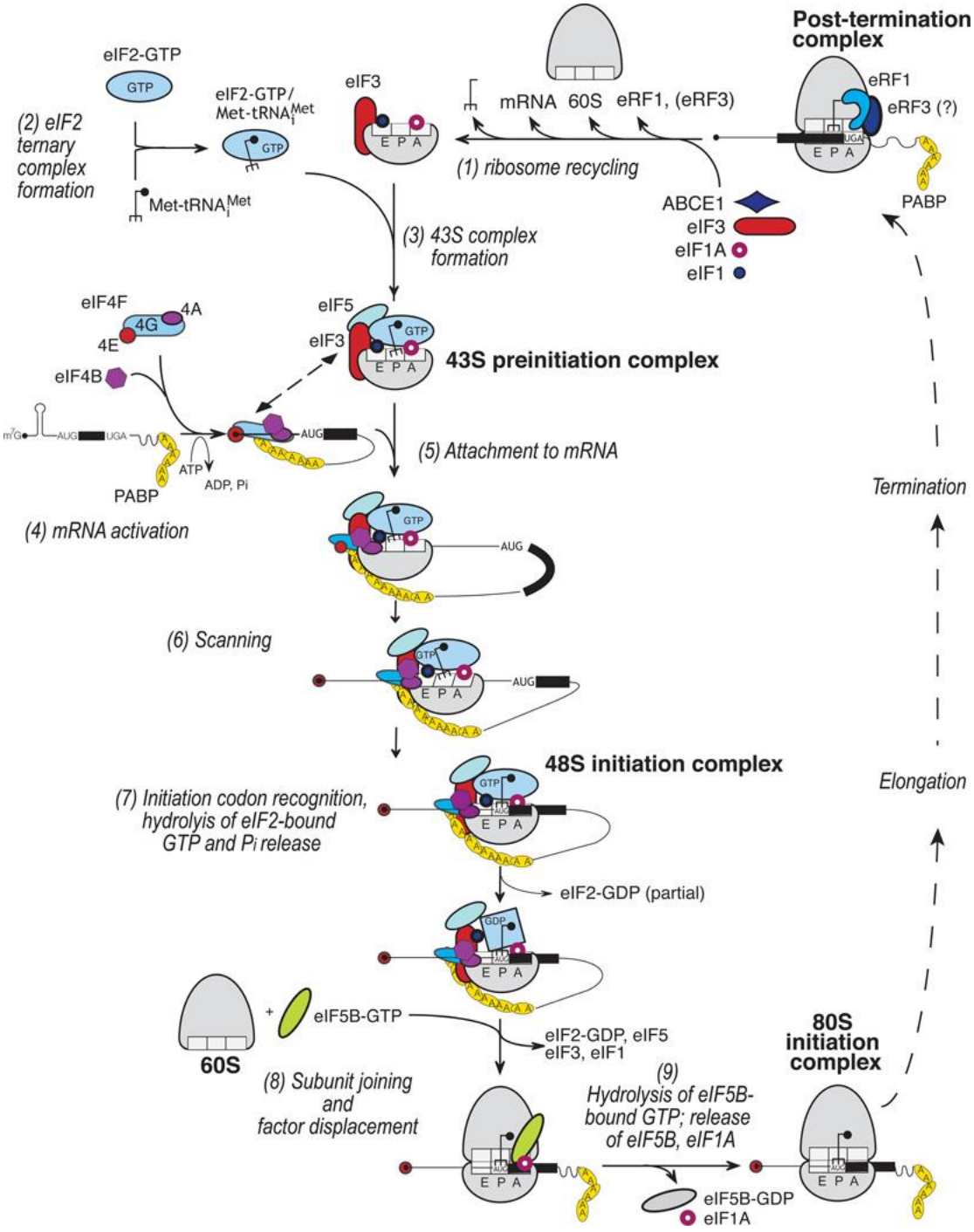

Figure 1.1.7: Pathway of translation initiation:

Stage (1) Ribosomal recycling takes place to yield separated 40S and 60S ribosomal subunits. **Stage (2)** Formation of the ternary complex (eIF2.GTP/Met-tRNA). **Stage (3)** the assembly of 43s (PIC). **Stage (4)** eIF4A resolves secondary structures within the 5' UTR of the mRNA in ATP-dependent manner. **Stage (5)** Attachment of the 43S complex to mRNA. **Stage (6)** mRNA is scanned for the AUG sequence. **Stages (7)** start codon recognition. **Stage (8)** joining of the 60S subunit and hydrolysis of GTP and other eIFs. **Stage (9)** release of eIF1A and eIF5B.GTP from assembled elongation competent 80S ribosomes. During the

translation elongation stage, the EF1 delivers the next complementary tRNA to the 80S ribosomal complex. Following the hydrolysis of eEF1-bound GTP, the tRNA carrying the new amino acid is placed in the A-site next to tRNAi eEF1. A peptide bond is then formed between the incoming amino acids. The ribosome is then shifted 3 base pair with the aid of eEF2 along mRNA, trans-locating the tRNAi to the E-site and tRNA to the P-site. These reactions are repeated until the full polypeptide is formed or the stop codon is reached. The (eRF) binds to the P-site, releasing the polypeptide chain and dissociation of ribosome into large and small subunits (Jackson et al., 2010).Reproduced with permission.

1.1.4.2 Inhibition of the eIF4F complex as a therapy in cancer:

As mentioned previously, protein synthesis is an important cellular process that is regulated by signalling networks in response to a variety of stimuli. Any defect in the protein synthesis pathway can result in cell apoptosis or disease. In cancer, up-regulated signalling pathways lead to uncontrolled growth and survival by influencing the translation pathway. Translational alterations can up-regulate the rate of protein synthesis leading to translation of specific mRNAs necessary for cancer progression and survival (Grzmil and Hemmings, 2012). Thus, shortage of oxygen, insufficient nutrition, or DNA damage producing therapy suppresses the cap-dependent translation and down regulates the overall protein synthesis, mainly by inhibition of ternary complex assembly by eIF4F and eIF2 (Spriggs et al., 2010). Consequently, inhibition of cap-dependent protein translation triggers the translation of mRNA in a cap-independent manner using secondary RNA structures recognised as internal ribosomal entry sites (IRES). The highly structured (IRES) recruits the 40s ribosome subunit and other eIFs directly to the start codons or the 5´ UTR on mRNA and skips the scanning process for the cap. Interestingly, these mRNAs with more structured/GC-rich 5’ UTRs encode oncogenic proteins that support the development, progression, and survival of cancer cells, such as c-MYC, lymphoid enhancer factor (LEF)-1, VEGF, hypoxia-inducible factor (HIF)-1a, XIAP, and BCL2 a (Spriggs et al., 2010).

Importantly, tumor cells with elevated levels of BCL2 and other oncogenic proteins tend to be refractory to conventional chemo and radiotherapy and trigger aggressive metastasis (Davids and Letai, 2012). Many studies have revealed that targeting the translation initiation complex of eIF4F provides a promising target for overcoming drug resistance. Several compounds have been investigated to target translation initiation, either by interfering with eIF4E:eIF4G interaction or with eIF4A activity, mostly, involving eIF4A

activity (Malina et al., 2012). Agents that block a specific signalling network that the cancer cells rely on have also been developed.

Studies have reported that eIF4A is overexpressed in a group of cancers including hepatocellular carcinoma and melanoma (Eberle et al., 1997). Inhibition of eIF4A has received considerable attention in cancer therapy for disrupting the eIF4F complex. As mentioned earlier eIF4A is a DEAD-box RNA helicase that is necessary for unwinding the secondary structure of the 5' UTR mRNA in ATP-dependent manner (Rogers et al., 2002). Silvestrol, pateamine A (PatA) and hippuristanol have been identified as inhibitors of eIF4A. Hippuristanol is a natural product derived from the coral *Isis hippuris,* which appears to function by binding to the C-terminal domain of eIF4A and antagonizing its interaction with RNA. However, it was not found to inhibit other RNA helicases outside of the eIF4A family. Suppressing eIF4A activity by hippuristanol has shown efficacy in Eμ-Myc lymphoma cells, causing increased sensitivity to DNA damaging agents such as doxorubicin in mice (Cencic et al., 2013). However, the use of hippuristanol in vivo has been restricted due to low potency and solubility (Chu and Pelletier, 2015). Further work is on-going to develop analogues more effective for clinical use (Ravindar et al., 2011).

Silvestrol, a rocaglate isolated from Aglaia foveolata, is a potent and selective inhibitor of translation initiation, acts by interfering with the recruitment of mRNA to the eIF4F initiation complex leading to inhibition of pro-survival and pro-growth proteins synthesis necessary for cancer cells survival (Bordeleau et al., 2008). Inhibition of eIF4A with silvestrol had a powerful effect on breast and prostate cancer xenograft models (Cencic et al., 2009). Silvestrol also prolonged the survival time of tumor bearing mice and had a synergistic effect with other therapeutic agents including rapamycin (Kogure et al., 2013). Silvestrol has also been shown to be highly effective against a range of models for leukaemia, lymphoma and solid tumors (Lucas et al., 2009, Alachkar et al., 2013, Wolfe et al., 2014).

1.1.5 BLF1 toxin:

BLF1 is a protein toxin isolated from *Burkholderia pseudomallei*, a bacterium that is endemic in parts of south-east Asia and northern Australia and causative agent of the disease melioidosis (Currie, 2015, Wiersinga et al., 2006). Infected individuals present with symptoms including severe pneumonia, septicaemia, fever, skin and organ abscesses that is very similar to the symptoms seen in tuberculosis and malaria infection. There is a mortality

rate of 50% following primary infection in North East Thailand, but there can be a long latent period between exposure and signs of infection in some individuals. This has led to the infection being described as “the Vietnamese time bomb”, as many American soldiers were exposed to this pathogen during the war in Vietnam (Currie, 2015, Wiersinga et al., 2006).

In 2010, the first lethal toxin from *B.Pseudomallei* was discovered following proteome analysis of *B.Pseudomallei* and the non-pathogenic *Burkholderia thailandensis* strain that pointed out the expression of 14 hypothetical proteins of unknown function in the pathogenic strain (Cruz-Migoni et al., 2011). The structure of Burkholdria lethal factor one (BLF1) toxin was determined using X-ray crystallography. Although showing little sequence homology, the crystal structure clarified that BLF1 is structurally related to the C-terminal domain of the cytotoxic necrotising factor 1 (CNF1) produced by some pathogenic strains of *Escherichia coli*. Crucially, the positions of cysteine and histidine residues in the active sites were conserved between the two proteins (**Fig**.1.1.8). CNF1 is known to act by deamidating glutamine residues in Rho GTPases and so disrupting actin cytoskeleton assembly (Flatau et al., 1997). Intraperitoneal administration of recombinant BLF1 killed mice and was also toxic to macrophage cell lines in culture, confirming its activity as a toxin. Affinity chromatography using recombinant BLF1 identified eukaryotic initiation factor 4 A (eIF4A) as a major protein interacting with BLF1 in lysates from human cells. It was subsequently shown that BLF1 extensively inhibits protein synthesis by deamidation of Gln^{339} of eIF4A, with subsequent inhibition of the RNA helicase activity required for melting mRNA secondary structures during initiation of translation (Cruz-Migoni et al., 2011). It thus results in destabilization of one or more steps that control mRNA translation that have been associated with alteration in the cell cycle and /or regulation of cell growth; however it does not change the ATPase activity of eIF4.

It has been suggested that BLF1 has potential as an anticancer treatment if targeted to tumour cells (Hautbergue and Wilson, 2012). Importantly, BLF1, unlike other toxins such as ricin or diphtheria toxin mentioned previously, has no receptor to bind to the surface of mammalian cells and so is unlikely to be taken up non-specifically. The exception is for macrophage cells lines, which seem to take it up via macropinocytosis (Cruz-Migoni et al., 2011). Thus, for a significant toxic effect of BLF1 on other cell lines, it has to be introduced

into the cytoplasm using agents such as Endoporter™ or by transfection with the gene encoding the toxin. Normally, Burkholderia is intracellular, thus it is probably not necessary for the BLF1 toxin to bind to the cell surface during infection. Hence BLF1 is considered as a potential candidate toxin for immunotoxin design.

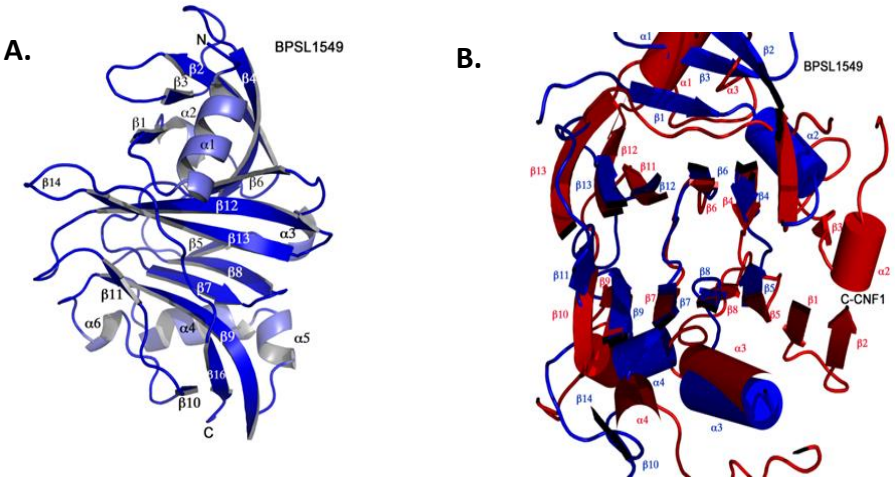

Figure 1.1.8: Analysis of BLF1 structure:
(A) Cartoon representing of the structure of BLF1 with the β strands and α helices numbered. **(B)** Cartoon demonstrating the similarities between BLF1 (blue) and CNF-1 (red), strands and helices numbered as in (A). (Cruz-Migoni et al., 2011). Reproduced with permission.

1.1.6 Cancer target antigens:

1.1.6.1 Using CD63 as model cancer antigen:

CD63 is a member of the tetraspanin superfamily (Hemler, 2005), involved in regulation of membrane protein trafficking, leukocyte recruitment and adhesion processes (Yanez-Mo et al., 2009). CD63 expression is present within the endosomal system and at the cell surface. The major site of CD63 in most cells is in the late endosomes and lysosomes and therefore it is referred to as a lysosomal membrane protein (Pols and Klumperman, 2009). Importantly, the small pool of CD63 present on the cell surface reflects CD63 passing over the cell surface on its way to late endosomes and lysosomes. A proportion of cell surface associated CD63 is endocytosed via clathrin coated vesicles due to the presence of the GYEVM lysosomal targeting motif at the CD63 C-terminal domain (Rous et al., 2002, Janvier and Bonifacino, 2005, Hunziker and Geuze, 1996). This motif interacts with adaptor proteins AP-

2 and AP-3 to allow the trafficking of cell surface proteins such as the H, K-ATPase β-subunit into intracellular compartments such as the lysosome (Duffield et al., 2003). CD63 has also been suggested as a target antigen for use in treatment of melanoma (Hotta et al., 1988) and for targeting tumour infiltrating macrophages due to the high internalization rate of CD63:anti-CD63 complexes (Audran et al., 1995). A Canadian company, Arius, also issued a patent in 2006 for an anti-CD63 antibody (Patent WO 2005092377 A9 "Cytotoxicity mediation of cells evidencing surface expression of CD63"). However, CD63 was first reported on early stage melanoma cells (Hotta et al., 1988), and during later malignant progression CD63 levels was reduced, suggesting a negative correlation between the level of CD63 and invasiveness (Jang and Lee, 2003). This negative correlation is also observed in other tumour types such as ovarian cancer tissues, thus lower expression levels are found to correlate with tumour metastasis (Zhijun et al., 2007). In lung adenocarcinoma, low CD63 expression correlates with poor prognosis (Kwon et al., 2007). Similarly, in breast- and colon cancers a negative relation between CD63 and cancer invasiveness and metastasis is present (Sauer et al., 2003, Sordat et al., 2002). These findings, together with its wide expression (Pols and Klumperman, 2009), suggest that it may not be a good tumour target. Nevertheless, CD63 may be useful as a model cancer antigen for investigating the potential of BLF1-based immunotoxin, as described in section 1.6.

1.1.6.2 CD9 as a cancer antigen:

The tetraspanin CD9 is another possible therapeutic target as it is reported to have multiple roles during cancer development that, when deregulated, were found to correlate with metastasis and poor prognosis. This negative correlation was observed in many cancer types such as ovarian cancer, prostate cancer, and distant metastasis of gastric cancer (Furuya et al., 2005, Wang et al., 2007, Murayama et al., 2015). However, CD9 expression levels were significantly higher in patients with gastric cancer without distant metastasis, thus, the low levels of CD9 in solid tumor correlated with poor prognosis. In contrast, CD9 was found to act as a tumor suppressor in melanoma and lymphoma (Yoon et al., 2010). CD9 is present ubiquitously on the surface of different types of cells including a wide range of malignant cells, in addition to normal cells (Murayama et al., 2015). Although CD9 does not have an internalization motif as CD63, it has been suggested that it probably relies on associated partners that have a functional internalization motif to promote internalization

(reviewed by (Rana and Zoller, 2011)). A recent study revealed that treatment with anti-CD9 antibody had anti-proliferative effect in mice bearing human gastric cancer cells as CD9 ligation induces apoptosis through the activation of JNK, p38 MAPK, Caspase-3 and P46 Shc pathways (Murayama et al., 2015).

1.1.7 Aims:

1. Our overall aim was to investigate the potential of BLF1 toxin as an immunotoxin, by coupling it with antibodies that would target it to cancer cells and induce its uptake. CD63 is a model antigen that could be targeted with BLF1 conjugated to anti-CD63 monoclonal antibody. CD63 is rapidly internalized from the cell surface on antibody binding as it has a lysosomal targeting/internalization motif at its C-terminus; antigen internalization is an important property for ADC and immunotoxins. In addition, hybridomas secreting monoclonal antibodies to CD63 were available "in house", therefore large amounts of monoclonal antibody could be produced for conjugating to the toxin. Another initial aim was to make use of stable cell lines transfected with the human CD63 that were available in the lab, so the effects of the immunotoxin could be monitored on cells expressing different amounts of CD63 on the surface. This would be useful in determining the levels of surface target antigen required for efficient killing. Cells stably transfected with mutated version of CD63 (with altered internalization motifs) were also available, so we hoped to investigate how important this was for killing. Furthermore, targeting the related CD9 antigen would be interesting as it does not have an internalization motif, but tends to be expressed at higher levels on the cell surface than CD63. Also, hybridomas secreting monoclonal antibody to CD9 were available "in house".

2. A secondary aim was to investigate the relative sensitivity of different cell types to BLF1 in the absence of agents that directly transport the toxin into cells. This is important as this could potentially cause side effects if it is taken up by some cells *in vivo* in a non-targeted way. BLF1 had previously been shown to be directly toxic to the mouse macrophage cell line J774, but not to other cell lines, although relatively few had been investigated (Cruz-Migoni et al., 2011). The direct effect of BLF1 on J774 cells was assumed to be due to non-specific uptake by macropinocytosis, but this had not been demonstrated. It was therefore of

interest to examine the mechanism of uptake of BLF1 by these cells and others of the mononuclear phagocyte lineages.

3. Alongside immunotoxin development, it was also of interest to determine if BLF1 alone shows preferential cytotoxicity towards certain cell types e.g. those particularly dependent on EIF4A, such as rapidly dividing cancer cells. We intended to use a recently developed system based on an agent previously used for transfection (Lipofectamine™) to enhance the delivery of BLF1 toxin to the cytosol of cell lines that do not normally take up toxin.

4. Finally, since intracellular trafficking is an important aspect to consider in developing immunotoxins, we aimed to determine the intracellular localisation of BLF1 following uptake.

2 Chapter 2: Materials and methods

2.1 Materials:

Unless stated otherwise, chemical and general reagents were supplied from Bio Rad, Sigma, Fisher Scientific and SLS, and were analytical grade or equivalent.

2.1.1 General buffers and reagent:

The water used to prepare solutions and buffers was ultra-pure water generated using the Neptune (Purite) System (Scientific Laboratory Supplies Limited). Sterilization was by autoclaving instruments and solutions which are of autoclavable material. The sterilization of heat sensitive solutions was by filtration using 0.2 micron pore size filters.

2.1.1.1 Buffers and solutions:

All general buffers and solutions used are mentioned in the table below.

Table 2.1.1: General buffers and solutions used.

Type of buffer or solution	Preparation
Anhydrous sodium carbonate(0.2 M)	2.12 g Na_2CO_3, dissolved in 100 ml dH_2O
Immunoblotting buffer (10x)	30.3 g Tris, 144 g glycine, made up to 1 L with dH_2O
Immunoblotting buffer (1x)	100 ml 10x blotting buffer, 200 ml methanol, made up to 1 L with dH_2O
Immunoblotting blocking buffer	5 g semi-skimmed milk powder, made up to 100 ml 1x TBST buffer
Carbonate-bicarbonate buffer (100 mM)	3.03 g Na_2CO_3, 6 g $NaHCO_3$ made up to 1 L with dH_2O, pH adjusted to 9.6 with HCl
Cell dissociation solution (CDS)	This solution was purchased from Sigma (C5914) as 1x solution , 4 mls was used for a T75 flask
Coomassie blue stain	500 ml absolute methanol, 2.5 g Coomassie Brilliant Blue R-250 (BioRad), 100 ml acetic acid made up to 1 L with dH2O
Coomassie de-stain	300 ml methanol, 100 ml acetic acid, made up to 1 L with dH_2O
FACS buffer (B/B/N)	0.1% sodium azide , 0.2% bovine serum albumin (BSA) dissolved in HBSS, stored at 4^oC
HBSS (Hanks buffered saline solution)	1x HBSS with/without Ca^{2+} and Mg^{2+}, purchased from Lonza
Hoechst staining	Hoechst dye was purchased from Life Technologies. Stock

solution	solution was prepared in dH_2O at 10 mg/ml, stored in aliquots at -20°C
Internalization buffer	1 g of BSA in 500 ml of HBSS containing Ca^{2+} and Mg^{2+}
4% paraformaldehyde solution	4 g of paraformaldehyde was dissolved in 50 ml dH_2O adding 1 ml of 1 M NaOH and heating the mixture in water bath for 60 minutes at 60C°. After cooling, 10 ml of 10 x PBS was added, the pH was adjusted to 7.4 and dH_2O was added up to 100 ml. After mixing, the solution was filtered and stored at 4C°
PBS (phosphate buffered saline) 10x	80 g NaCl, 2 g KCl, 11.5 g Na_2HPO_4, 2 g KH_2PO_4. Made up to 1 L with dH_2O
PBST buffer	100 ml of 10 x PBS, 0.5 ml of Tween 20, made up to 1 L with dH_2O
Propidium iodide 1mg/ml solution (Sigma)	1:1000 diluted in 1x PBS
SDS-PAGE running buffer (5x)	15 g Tris-base, 72 g glycine, 5 g SDS, made up to 1 L with dH_2O
SDS-PAGE stacking gel buffer (4x)	30.3 g Tris-base, 2 g SDS, pH adjusted to 6.8 and made up to 500 ml with dH_2O, stored at 4°C
SDS-PAGE separating gel buffer (4x)	90.85 g Tris-base, 2 g SDS, pH adjusted to 8.8 and made up to 500 ml in water stored at 4°C
Sodium bicarbonate buffer(1 M)	0.84 mg $NaHCO_3$, made up to 10 ml with dH_2O, pH adjusted to 8.3 with NaOH
Sodium hydrogen carbonate (0.2 M)	1.68 g $NaHCO_3$, dissolved in 100 ml dH_2O
10x TBS (Tris buffered saline)	24.2 g Tris, 87.66 g NaCl pH adjusted to 7.6 with HCl made up to 1 L with dH_2O
1x TBST (Tris buffered saline with Tween 20)	100 ml 10x TBS, 250 µl Tween 20, made up to 1 L with dH_2O
1x trypsin –EDTA solution	10x solution provided by Sigma (59418C) diluted 1:10 in HBSS (without Ca^2 and Mg^{2+})
Vectashield mountant with DAPI	For nuclei staining provided by vector Laboratories (H-1200)

2.1.1.2 Electrophoresis gel materials:

Table 2.1.2: Electrophoresis gel components.

Gel	Composition
SDS-PAGE separating gel (15%)	2.5 ml water, 5 ml 30% acrylamide, 2.5 ml separating buffer (4x), 50 µl 10% ammonium persulphate (made up in water) 10 µl TEMED
SDS-PAGE stacking gel (5%)	5.8 ml water, 1.7 ml 30% acrylamide, 2.5 µl stacking buffer (4x), 50 µl 10% ammonium persulphate (made up in water) 20 µl TEMED

2.1.1.3 Sulforhodamine B (SRB) assay buffers and solutions:

Table 2.1.3: Reagent and solutions for the SRB assay.

Reagent	Preparation
50% Trichloroacetic acid solution (TCA)	50 g trichoracetic acid was dissolved in 80 ml water, the final volume was adjusted to 100 ml and stored at 4°C
80% Trichloroacetic acid solution (TCA)	80 g trichoroacetic acid was dissolved in 80 ml water, the final volume was adjusted to 100 ml and stored at 4°C
0.4% w/v SRB solution	0.4 g of sulforhodamine B salt (Sigma, cat. no S9012) was dissolved in 100 ml of 1% acetic acid solution
Unbuffered Tris-base (10mM)	1.21 g Tris-base was dissolved in 95 ml water and pH adjusted to 10.5, final volume 100 ml

2.1.1.4 Chemical cross linking buffers and reagent:

Table 2.1.4: Reagents and solutions for chemical cross linking.

Reagent	Preparation
EDTA (0.5 M)	18.6 g EDTA was dissolved in 90 ml dH_2O,and pH adjusted to 7.0 with HCl, final volume 1 L
Sodium phosphate dibasic (400 mM)	1.36 g Na_2HPO_4 was dissolved in 20 ml dH_2O
Sodium phosphate monobasic (400 mM)	960 mg NaH_2PO_4 was dissolved in 20 ml dH_2O
Sodium phosphate buffer 400 mM (pH7.5)	16.2 ml of 400 mM Na_2HPO_4 3.8 ml of NaH_2PO_4, pH was adjusted to 7.5, and stored at 4C°
Sodium chloride (3 M)	3.5 g NaCl was dissolved in 20 ml dH_2O
Sodium azide 2%	400 mg NaN_3 was dissolved in 20 ml dH_2O
Phosphate buffered saline with EDTA (PBS-EDTA)	10 ml sodium phosphate buffer 400 mM, 2 ml NaCl (3 M), 400 µl EDTA (0.1 M), 400 µl 2% NaN_3 made up to 40 ml with dH_2O
SPDP (20 mM) Hetero bifunctional cross linker from Life Technologies (Cat. No. 21857)	20 mM SPDP was freshly prepared by dissolving 2 mg in 320 µl DMSO

2.1.1.5 Plasmids:

Vectors containing genes coding for different versions of the BLF1 toxin were produced in commercially available pET vectors (Novagen) by Dr Guillaume Hautbergue, essentially as described in (Rust et al., 2015). All plasmids used and their characteristics are described in Table 2.1.5.

Table 2.1.5: plasmids used.

Plasmid symbol	Vector, selectable marker	Characteristics
6His-BLF1	pET14b (ampicillin)	Encodes BLF1 with a 6 histidine vector-encoded tag at the N-terminus (Rust et al., 2015).
6His-mCherry-BLF1	pET14b (ampicillin)	Encodes mCherry labelled BLF1 with 6 histidine vector-encoded tag at the N-terminus (Rust et al., 2015).
6His-mCherry-BLF1 (C94S)	pET14b (ampicillin)	As above, but encoding inactive mCherry labelled (C94S mutated) BLF1 (Rust et al., 2015).
Cys2-6His-BLF1	pET24b (kanamycin)	Encodes BLF1 modified to contain a cysteine residues in position 2 after the ATG at the N-terminus (unpublished).

2.1.2 Immunological reagents:

2.1.2.1 Primary and secondary antibodies:

All primary monoclonal antibodies and secondary polyclonal antibodies used for immunofluorescence studies, non-covalent linkage, and Western blots are mentioned in Tables 2.1.6 and 2.1.7 respectively.

Table 2.1.6: Primary antibodies.

Antibody	Target	Target species	Conc. (µg/ml) or dilution	Source
Isotype control (IgG1κ, hybridoma clone JC-1)*	Phosphonamidate hapten	NA	10	In house (Muranova et al., 2004)
Isotype control ($IgG2b,_k$)	Trinitrophenol+KLH	NA	10	BioLegend
Mouse anti – human CD9	CD9	Human	10	Prof. Peter Andrews University of Sheffield

(hybridoma clone 602.29)*				(Andrews et al., 1981)
Mouse anti-human CD63 (hybridoma clone H5C6)*	CD63	Human	10	Developmental Studies Hybridoma Bank (Azorsa et al., 1991)
Rat anti-BLF1	BLF1	*Burkholdea pseudomallei*	1:64000 dilution	Prepared by Bioserv UK and provided by Professor David Rice, University of Sheffield
Mouse anti-His Cat. No.372900	Histidine	NA	40	Invitrogen®

* hybridomas grown and antibody purified from supernatants by protein-G affinity chromatography by Bioserv UK.

Table 2.1.7: Secondary antibodies.

Antibody	Target antigen	label	Dilution	Source	Cat. No.
Goat anti-mouse IgG	Mouse IgG Fab fragment	FITC	1:250	Sigma	F 4018
Rabbit anti-rat IgG	Rat IgG	FITC	1:350	Sigma	F9387
Rabbit anti-mouse IgG	Mouse IgG	HRP	1:5000	Sigma	A9044
Goat anti-rat HRP	Rat	HRP	1:5000	abcam®	Ab97057
goat anti-mouse $F(ab')_2$ fragment	IgG, Fc-specific	none	20 µg/ml	Sigma	M0659

2.1.2.2 Intracellular staining markers:

Table 2.1.8: Markers used for intracellular staining.

Marker	Target	Concentration or Dilution	Source	Catalogue Number
Lamp1 Alexa fluor 647	CD107a (late endosomal marker)	1:250	BioLegend	328611
PHrodo ™ Red Dextran	Endosomes, lysosomes	20 µg/ml	Life technologies	P10361
Lysotracker™green DND-26	Lysosomes	1:20000	Life technnologies	L7526
Transferrin-FITC	CD71	1:250	BioLegend	13163042
Wheat germ agglutinin, alexa fluor 488	Golgi	5 µg/ml	Life technologies	W112611

2.1.3 Reagents for bacteriological work:

Table 2.1.9: Bacteriological reagents.

Reagent	Preparation
Ampicillin	A stock solution was made at 100 mg/ml in dH_2O and then was sterilized by filtration and stored at -20C^o until use.
Chloramphenicol	Stock solution was made at 34 mg/ml in 2-propanol and then was sterilized by filtration and stored at -20 C^o until use.
Kanamycin	A stock solution was made at 50 mg/ml in dH_2O and then was sterilized by filtration and stored at -20 C° until use.
LB Broth (Lysogeny Broth)	10 g tryptone, 5 g yeast extract, 10 g NaCl. Dissolved in 1 L purified H_2O and pH adjusted to 7, then autoclaved.
LB Agar	10 g tryptone, 5 g yeast extract, 10 g NaCl, 15 g bacteriological agar. Dissolved in 1 L purified H_2O, pH adjusted to 7, then autoclaved.
TB	12 g tryptone, 24 g yeast extract, 2.3 g KH_2PO_4, 12.5 g K_2HPO_4, 4 ml glycerol. Dissolved in 1 L purified H_2O, pH adjusted to 7, and autoclaved

2.1.4 Reagents for BLF1 protein purification:

Table 2.1.10: Purification reagents.

Reagent	Preparation
Protease inhibitor cocktail tablet, EDTA free (Sigma, Cat. No. S8830)	One tablet dissolved in 100 ml dH_2O, and stored at 4C^o
PMSF (0.1 M) phenylmethylsulfonylfluoride protease inhibitor (Sigma)	174 mg of PMSF dissolved in 10 ml isopropanol and stored at -20C^o
Bacterial lysis buffer	50 mM Tris, 1 M NaCl pH8, 0.5% triton x100
Nickel column washing buffer	50 mM Tris, 1 M NaCl, 5 mM imidazole
Nickel column elution buffer	20 mM Tris, 200 mM NaCl, 200 mM imidazole

2.1.5 Mammalian cell culture:

2.1.5.1 Cell lines:

Mouse macrophage cell line:

J774.2 cell line: is a mouse BALB/c monocyte/macrophage cell line, recloned from J774.1 original ascites and solid tumour (Ralph and Nakoinz, 1977b). These cells were obtained from ECACC (the European Collection of Cell Cultures).

KO-CD9 and WT-CD9 cell line: The CD9 -/- macrophage cell line and corresponding wild type CD9 +/+ macrophage cell lines were kind gifts from Dr Gabriela Dveksler (Dept. Pathology, Uniformed Services University of the Health Sciences, Bethesda, Maryland, USA; (Ha et al., 2005).

RAW264.7 cell line: a mouse macrophage cell line, was originally established from a Balb/c mouse by Abelson leukaemia virus transformation (Ralph and Nakoinz, 1977a). These cells were obtained from Dr Peter Grabowski (Medical School, University of Sheffield), obtained from the American Type Culture Collection (ATCC).

Rat basophilic cell line

RBL2H3 (WT) and RBL2H3 (CD63): The rat basophlic leukemia (RBL) line is a high-secreting clone derived from the earlier RBL cell line (Barsumian et al., 1981). The WT cells were a kind gift from Dr Birgit Helm (University of Sheffield). RBL2H3 cells stably transfected with human CD63 were generated “in house” as described previously (Smith et al., 1995).

Human cell line

A549 cell line: it is a human epithelial cell line obtained from 58 year’s old Caucasian male with carcinoma (Giard et al., 1973). The cell line was obtained from ECACC.

HaCaT cell line: is a human keratinocyte cell line obtained by transformed keratinocytes obtained from histologically normal skin (Boukamp et al., 1988). The HaCaT cells were kindly provided by Professor Sheila MacNeil, Univeristy of Sheffield.

HEK293 cell line: this cell line was derived by transformation of cultures of normal human embryonic kidney cells with adenovirus DNA (Graham et al., 1977). The HEK293 cells were obtained from ECACC.

HeLa cell line: this is a human epithelial cell line, obtained from the cervix of 31 years adult black female with adenocarcinoma(Scherer et al., 1953) The Hela cells were obtained from ECACC.

HL-60 cell line: this is a cell line derived from peripheral blood leukocytes obtained by leukopheresis of a 36 age Caucasian female with acute promyelocytic leukemia (Collins et al., 1977). The HL60 cells were originally kindly provided by Dr Jim Gallagher, University of Sheffield.

MES-SA/DX-5 cell line: chemo resistance uterine sarcoma cell line was a kind gift from Dr. Helen Colley, University of Sheffield.

MeWo cell line: melanoma cell line was derived from human melanoma (Grose and Brunel, 1978) and kindly provided by J. Marshall, ICRF, London UK.

THP1 cell line: is a human monocytic cell line derived from a patient with acute monocytic leukemia (Tsuchiya et al., 1982). This cell line was obtained from ECACC.

U937 cell line: this is a human monocytic cell line derived from a patient with histiocytic lymphoma (Sundstrom and Nilsson, 1976). The U937 cells were originally kindly provided by Dr Jim Gallagher, University of Sheffield.

2.1.5.2 Cell line media:

All media for mammalian cell culture were purchased as 1x solutions from the manufacturer as shown in Table 2.1.11. Heat inactivated foetal calf serum was purchased in batches from Biowest or Sigma after testing its ability to support growth of cell lines.

Table 2.1.11: Cell line media.

Cell line type	Media	Source of media
A549	DMEM+Glucose 4.5 g/L+10% FCS	Gibco
HaCat	DMEM+Glutamax+10% FCS	Gibco
HEK293	DMEM +Glucose 1 g/L+10% FCS	Gibco
Hela	EMEM+10% FCS	Lonza
HL-60	RPMI1640+25 mM HEPES+10% FCS	Gibco
J774	DMEM+Glucose 4.5 g/L+10% FCS	Gibco
KO-CD9	DMEM+Glucose 4.5 g/L+10% FCS	Gibco
MES-SA/DX-5	McCoy's 5A +10% FCS	Gibco
MeWo	DMEM+Glucose 4.5 g/L+10% FCS	Gibco
RAW264.7	DMEM+Glutamax+10% FCS	Gibco
RBL2H3 (transfected)	As for RBL2H2 WT + 400 mg/l G418	Gibco
RBL2H3(WT)	DMEM+Glucose 4.5 g/L+10% FCS	Gibco
THP1	RPMI1640+2ME+10% FCS	Gibco
U937	RPMI1640+25 mM HEPES+10% FCS	Gibco
WT-CD9	DMEM+Glucose 4.5 g/L+10% FCS	Gibco

2ME: 2-Mercaptoethanol, 50 ml FCS, and 500ul of 10^{-2}M stock solution of 2-ME were added to 450 ml of RPMI 1640 media.

2.1.5.3 Additional solutions and reagents used with mammalian cells:

All additional solutions and reagents used with cultured mammalian cells are mentioned in the Table 2.1.12 unless otherwise stated, these reagents were sterile-filtered (0.2µm filters) before use.

Table 2.1.12: Solution and reagent used in cell culture.

Reagent	Preparation	Source
Amiloride hydrochloride hydrate powder	Stock solution was prepared in purified water at 50 mg/ml, stored in aliquots at -20^{o}C	Sigma (Cat. No. A7410)
Bafilomycin A_1	Stock solution was prepared in DMSO at 0.1 mg/ml, stored in aliquots at -20^{o}C	Sigma (Cat. No. B1793)
Brefeldin A	Stock solution was prepared in DMSO at 10 mg/ml, stored in aliquots at -20^{o}C	Sigma (Cat. No. B7651)
Dimethyl sulfoxide (DMSO)	DMSO was purchased from Sigma as 1x solution	Sigma (Cat. No. D2650)
Freezing mixture	90% FCS, 10% DMSO, stored at 4C^{o} or in aliquots at -20^{o}C	
G418	Stock solution was prepared in purified water at 250 mg/ml and stored in aliquots at -20^{o}C	Gibco
Lipofectamine 3000 reagent	The reagent was diluted in opti-MEM medium at 0.15 µl/5 µl, and mixed 1:1 with diluted protein in opti-MEM medium plus 2 µl/100 µl of P3000 (neutral co-lipid reagent)	Invitrogen
Saponin (adjuvant)	Stock solution was prepared in cell media at 2 mg/ml and stored at 4^{o}C	Sigma (Cat. No. 47036)
Saponin (is a complex mixture of triterpenoid saponins from *Gyosophila paniculata L*)	Stock solution was prepared in cell media at 1.2 mg/ml and stored at 4^{o}C	A kind gift from Dr David Flavell (Southampton General Hospital), prepared as described in (Weng et al., 2010)
Phorbol 12-myristate 13-acetate (PMA)	Stock solution was prepared in DMSO at 50-100 µg/ml, and stored at -20^{o}C	Sigma

2.1.6 Burkholderia lethal factor 1 (BLF1) toxin:

Recombinant versions of BLF1 were prepared and purified in collaboration with Dr Guillaume Hautbergue or obtained from Dr Svetlana Sedelnikova. The toxin was essentially expressed and purified as described (Cruz-Migoni et al., 2011) and in detail in section 2.2.10.

2.1.7 Routine laboratory instruments and equipment:

Commonly used instruments and equipment are listed in Table 2.1.13

Table 2.1.13: Common laboratory instruments and equipment used.

Instruments or equipment	Provider
Autoclave	Rodwell
Bench top cooling lab. centrifuge	Sigma (3K15)
Flow cytometer	Becton Dickinson (BD) FACS Calibur or LSR II (BD)
Image analysis system	ChemiDoc™ MP system
Incubators (CO_2)	Galaxy R (Scientific Laboratory Supplies)
Laminar flow cabinets	Medical Air Technologies (MAT) Class II
Fast liquid chromatography system	AKTA (GE-Healthcare)
Liquid nitrogen dewars (35 HC)	Statebourne BIO36
Micropipettes	Gilson
Microscopes	Nikon A1 Confocal inverted system with EM-CCD Camera. Nikon Eclipse 400 UV light with digital camera DXM1200 Nikon inverted light microscope. Olympus inverted microscope.
NanoDrop R Spectrophotometer ND-1000	Labtech international
Plate reader (96 well)	Lab-tec. (LT-4500)
SDS-PAGE and Western blotting equipment	Biorad Mini PROTEAN Tetra
Spectrophotometer	WPI

2.1.8 Glassware and plastic ware used:

Most of the glassware and the plastic ware used mentioned in Table 2.1.14.

Table 2.1.14: Glassware and plastic ware used.

Type of glassware and plastic ware	Provider
Non-sterile pipette tips (1ml, 200µl, 20µl)	Starlab
Tissue culture flasks (T25, T75)	Greiner
Plastic cell scraper	Sarstedt
96 well plate	Costar (3595)
Round bottom FACS tubes (12x75mm)	Elkay
Lab-Tek II chamber slides	Nalgene Nunc International

FluoroDish™	World Precision Instruments, Inc.20110401
Pasteur pipettes	Mexcel
Spectrophotometer cuvettes	Sarstedt

2.1.9 Software:

- Graph pad 6 Prism statistical analysis software was used for data and graphs analysis
- Microsoft office Excel 2010 was used for recording data in spreadsheets and for preliminary data analysis
- The BD CellQuest™ Pro software was used for acquisition of flow cytometry data.
- FlowJo software was used for flow cytometry data analysis.
- NIS-Elements (Nikon) confocal software was used for capturing confocal images.
- Image J and Fiji software: were used for analysis of microscopy images of cells.

2.2 Methods:

2.2.1 Cell culture methods:

2.2.1.1 Growth conditions:

RAW 264.7, MeWo and J774.2 cell line were cultured in a humidifed atmosphere of 8% CO_2 at 37°C, while THP1, HL-60, A549, KO-CD9, WT-CD9, Hela, MES-SA/DX-5, HEK293 and HaCaT cell lines were incubated in 5% CO_2. Cells were harvested and sub cultured depending on the type of cell line.

2.2.1.2 Cell harvesting and subculture:

Cells were harvested and subcultured depending on cell type.

For all mouse macrophage cell lines harvesting was performed by first replacing the old media with 10 ml fresh media, then using a plastic scraper to harvest the cells and then subculturing 1:10 with fresh media in a screw capped tissue culture flask.

For all human adherent cell lines (HEK293, A549, HeLa, HaCaT, MeWo and MES-SA/DX-5) growing in T75 flasks, the media was removed and the cells were washed once with 10 ml HBSS (without Ca^{2+} and Mg^{2+}). Then, the cells were harvested either by an enzymatic method using 2 ml trypsin-EDTA or 4 ml cell dissociation solution dependent on the

subsequent use. When using trypsin-EDTA, the flask was placed in the incubator at 37°C for 5-20 minutes. After detachment of all of the cells, the enzyme was inactivated by adding 8ml of fresh media containing 10% FCS, and then the cells were centrifuged for 5 minutes at 200 g. When using cell dissociation solution the flask was incubated for 10-15 minutes in the incubator to allow cell detachment. The cell suspension was transferred to a universal tube and 8 ml of complete media was added before centrifugation at 200 g for 5 minutes. The media was discarded and the cell pellet was re suspended with fresh media and subcultured into culture flasks or tissue culture plates after cell counting depending on experimental requirements.

For cells growing in suspension (THP1, HL60, and U937 cell lines) the cells were subcultured in fresh medium, typically at a ratio of 1:6 depending on cell growth. Cells were harvested by centrifugation for 5 minutes at 200 g.

2.2.1.3 Cell counting and viability measurement:

Cell counting was performed using an improved Neubauer haemocytometer. Viability was assessed by trypan blue exclusion after incubation of 100 µl of cell suspension with 400 µl of trypan blue (Sigma) for 3 min.

2.2.1.4 Cell freezing:

Cell freezing was carried out when the cells reached medium log phase. Cells were harvested as described above then centrifuged at 200 g for 5 minutes and re-suspended with 1 ml freezing solution (10% DMSO and 90%FCS) to approximately 3-10 $x10^6$ cells/ml. Then, the mixture was transferred to cryovials, with all manipulations performed on ice to avoid the toxic effect of DMSO). The vials were transferred to a freezing plug (Jencons) for 90 minutes to allow gradual freezing of the cells in the nitrogen vapour phase of a liquid nitrogen dewar. Finally, the vials were transferred to liquid nitrogen.

2.2.1.5 Cell thawing:

Following removing of the cells vial from liquid nitrogen, the vial was agitated in water bath at 37°C or under running warm water until almost thawed. The cell vial was wiped with a tissue soaked in 70% ethanol and the contents transferred into a sterile universal tube placed in ice. 9 ml of pre-warmed medium without FCS was added gradually. The cell suspension was centrifuged at 200 g for 5 minutes, then the cell pellet re-suspended with

fresh medium containing 10% FCS and transferred to tissue culture flask and cultured at 37°C.

2.2.2 SRB assay:

The sulforhodamine B (SRB) assay is a colorimetric assay that was used to determine the cellular protein content after treatment with BLF1 toxin or immunoconjugates. The assay was primarily developed for testing anticancer drugs. Absorbance was measured at 570 nm. Reading observed in the absence of any treatment was considered as 100% after normalisation to a blank control (cell- free medium with SRB reagent).

2.2.2.1 Cell preparation:

Semi-adherent mouse macrophage cell lines (2.1.5.1) were harvested as described in 2.2.1.2, counted and seeded at 6,250 cells per well in 96 well culture plates and incubated 3-4 hours to allow the cells to attach before the experiment.

Adherent human cell lines (2.1.5.1) were harvested as described in 2.2.1.2, counted and seeded at the required density (6,250 or 5000 cells per well) into flat-bottomed 96 well plates and incubated for 3-4 hours or overnight to allow cell attachment prior to the experiment.

Suspension cells (2.1.5.1) were harvested as described in 2.2.1.2, counted and seeded at 6,250 cells per well into flat-bottomed 96 well plates and then incubated for 4 hr to allow the cells settle to the bottom of the wells.

Stimulation of THP1 and J774.2 with phorbol myristate acetate (PMA): These cells grow in suspension as mentioned in section 2.1.5.1. 2 µl of 100 µg/ml stock of PMA was added to 10 ml of cell suspension ($0.187X10^6$ cell/ml in culture medium), and then 100 µl of this was seeded per well into flat-bottomed 96-well plates. The cells were cultured for 48 hours to induce differentiation into macrophages and then used in the experiment. Some wells containing cells without PMA were always included as a control.

2.2.2.2 Standard curve of absorbance (at 570nm) *vs.* cell number:

Cell number optimization for the various cell lines was first performed to determine the optimal initial cell number per well for the subsequent cytotoxicity assays. The cells were harvested as usual; however non-enzymatic cell dissociation solution was used for the

adherent cell lines instead of trypsin-EDTA. After harvesting, the cells were re-suspended to $2x10^4$ cells/ml with fresh medium. 100 µl of cell suspension was transferred per well into 96-well flat bottomed microtitre plates in quadruplicate then serial dilutions to a total volume of 100 µl were made in medium across the plate. Wells containing 100 µl of medium (no cells) were included to account for background. The cells were allowed to adhere or settle (non-adherent cells) for 3-4 hours. Then the cells were fixed by layering 50 µl of cold 50% TCA on the top of the medium (for non-adherent cells 80% TCA was used) and after 5 minutes at room temperature, the plates were incubated at 4C° for 1 hour. The plates were washed 5 times using tap water to remove the TCA, growth medium etc, by flicking the plates over the sink to remove the liquid. The plates were left to air dry, then stained by adding 100 µl of 0.4% sulforhodamine B sodium salt solution and incubated for 30 minutes. The SRB stain was removed by flicking the plates and rinsing the wells with 1% acetic acid four times and then the plates were allowed to air dry completely. The bound dye was solubilized by adding 50 µl of 10 mM unbuffered tris base for 5 minutes and agitated using a gyratory shaker, then the OD was measured at 570 nm using a plate reader. Finally a standard curve of cell number vs OD was plotted using GraphPad Prism 6 for Windows version 6.07.

2.2.2.3 Measrunig the effect of BLF1 on cell growth:

Cells were harvested as described above, counted and diluted to $0.0625x10^6$ cells/ml in medium (or $0.187x10^6$ cells/ml for cell suspension with PMA), and then 100 µl of cells was plated per well in 96 well plates. The cells were allowed to adhere for 3-4 hrs. For toxin treatment 10 µl of the medium was replaced with 10 µl of toxin (0.001-5 µM). Assays were performed in quadruplicate. For assays involving Lipofectamine, Lipofectamine reagent and p3000 reagents were added simultaneously with toxin. The cells were cultured for 72 hours and the impact on cell growth was monitored using an inverted microscope. Next the cells were fixed with TCA, stained as above (2.2.3) and optical density determined at 570 nm using a plate reader.

2.2.2.4 Measuring the effect of antibody/BLF1 conjugates on cell growth:

Cells were harvested as mentioned in 2.2.2.1, counted and diluted to $0.05x10^6$ cells/ml in medium and then 100 µl was pipeted into 96-well plates. After 24 hr of cell proliferation, 10 µl of medium was replaced with 10 µl of antibody/BLF1 conjugate at an appropriate range

of final concentrations. Assays were performed in quadruplicate. For assays involving toxicity enhancers (brefeldin A, bafilomycin A, saponin, lipofectamine), these reagent were added simultaneously with the conjugate. After 1 hr treatment the cells were washed 2X with HBSS buffer and re-suspended with pre- warmed media. The cells were allowed to proliferate for a further 72 hr. Next the cells were fixed with TCA, and the SRB assay was carried out as described above (2.2.3).

2.2.3 BLF1 toxin preparation:

2.2.3.1 Preparation of unconjugated BLF1:

The purified recombinant 6His-BLF1 toxin (typically supplied at a concentration of 21 mg/ml) was diluted 1:5 with HBSS, filter-sterilised and then working dilutions were prepared in medium or 1xPBS (typically 50 µM, 10 µM, 5 µM, 1 µM. 0.5 µM and 0.1 µM, 0.05 µM).

2.2.3.2 Preparation of BLF1/antibody-coated bead model conjugates:

Initially, 20 µg of mouse anti-6His antibody was mixed with 10 µg 6His-BLF1 in a total volume of 500 µl (1x PBS+ 0.1% Triton x100) for 30 minutes at room temperature on a rotary mixer. 20 µg of targeting antibody (anti-CD63 or anti-CD9) or the isotype control was then added to the previous mixture. To assemble the beads with both the toxin and the targeting antibody, 10 µl of anti-mouse IgG-coated magnetic beads (Cat No. MMXA-10-10) from Spherotech were washed with 400 µl 1x PBS+ 0.1% Triton x100, and the supernatant was discarded by placing the tube on a magnetic separator (life tech. Cat. No.12321D). The beads were re-suspended with the mixture of anti-6His/BLF1 toxin and targeting antibody or isotype control for 1 hour on a rotary mixer. The assembled beads was washed twice with 400 µl of 1x PBS by using the magnetic separator and re-suspended in 500 µl 1x PBS. A range of concentrations (neat, 1/10, 1/100, 1/1000) of the assembled bead model conjugates was tested in the SRB assay as described above.

2.2.3.3 Preparation of secondary antibody-linked BLF1/antibody model conjugates:

100 µl of anti-His antibody at 80 µg/ml was mixed with 100 µl of 6His-BLF1 (160 µg/ml) for 30 minutes on a rotary mixer. Subsequently 100 µl of this solution was added to 100µl of targeting antibody (anti-CD63 or anti-CD9 at 80 µg/ml) or isotype control together with 200

µl of goat anti-mouse IgG (Fc specific) antibody (40 µg/m).The mixtures were incubated for 1 hr on a rotary mixer. A range of concentrations (neat, 1/10, 1/100, 1/1000) of the assembled conjugates were tested in the SRB assay as described above.

2.2.3.4 Preparation of chemically cross-linked BLF1 immunotoxin:

2.2.3.4.1 Chemical conjugation of BLF1 to monoclonal antibodies:

Chemical cross-linking of modified BLF1-6His with cysteine to targeting monoclonal antibodies was achieved using the heterobifunctional cross-linker *N*-succinimidyl-3-(2-pyridyldithio) propionate (SPDP, Pierce/Thermo Scientific), essentially according to manufacturer's instructions. Reagents and buffers used are described in Table 2.1.4. In brief, typically 2-3 mg of monoclonal antibody (anti-CD63 or anti-CD9) in PBS-EDTA buffer was modified with 20 mM SPDP for 1 hr at 25 °C and excess non-reacted SPDP reagent was removed using a G-25 desalting column equilibrated with PBS-EDTA. SPDP-modified antibody was then mixed with the modified BLF1Cys2-6His BLF1 at a molar ratio of 1:10 and incubated for 18 hr at 25 °C. The resulting immunotoxin concentration was measured by Bradford assay using Quick start ^{TM} Bradford protein assay kit from Bio-Rad assay before purification by gel filtration. Finally, a range of concentrations of the immunotoxin (purified by gel filtration or non-purified) was tested in the SRB as described above.

2.2.3.4.2 Chemical conjugation of un-modified mCherry BLF1 to monoclonal antibodies:

In some cases, BLF1 without the cysteine modification was chemically cross-linked to targeting antibodies, again using SPDP. In these cases, both BLF1 and antibody proteins were modified separately with 20 mM SPDP for 1 hr at 25 °C and excess SPDP reagent was removed using a G-25 desalting column equilibrated with PBS-EDTA. The modified antibodies were chemically reduced by incubating with 150 mM dithiothreitol (DTT) for 30 min at 25 °C and thereafter DTT was removed using a G-25- desalting column (GE Healthcare). SPDP-modified antibody and BLF1 (at a molar ratio of 1:10) were incubated for 18 hr at 25 °C. These conjugates were not further purified, but a range of concentrations was tested in the SRB assay as described above.

2.2.3.5 Purification of targeted antibody/BLF1 conjugate by gel filtration:

The un-purified conjugates prepared as described in 2.2.3.4.1 was concentrated by filtration using Vivaspin MWCO 100 kDa devices (GE Healthcare) and applied to a 10x300 mm Superdex 200GL column equilibrated with PBS-EDTA buffer. The conjugate was eluted with 20 ml PBS-EDTA (flow rate 0.5 ml/min) and fractions of 0.35 ml were collected. Determination of the protein concentration was performed by Bradford assay (Biorad) on eluted fractions after gel filtration. Fractions that contained protein were analyzed by Nu-PAGE 4-12% BT Novex under non-reducing conditions. 2 µg of protein sample and 3 -5µL of standard protein marker (All Blue Precision Plus, Biorad, 161-0373) were loaded onto the gel. Samples were electrophoresed at 170 V for approximately 60-90 minutes. Gels were either unstained (for Western blotting) or stained with a solution of 0.1% (w/v) Coomassie Blue R-250 (AppliChem) in 40% (v/v) methanol and 10% (v/v) acetic acid, destained in a solution of 30% (v/v) and 10% (v/v) acetic acid. The yield of purified conjugate was generally 2.9 mg, starting from 4mg. Furthermore, the purity of combined fractions was analysed by Western blotting as described below with primary polyclonal antibody against BLF1 (Table 2.1.6) followed by goat anti-rat IgG-HRP (Table 2.1.7).

2.2.3.6 Western blotting:

Western blotting of unstained gels was carried out in a Mini Trans Blot Cell (Biorad) containing blotting buffer (Table2.1.1) and a cooling unit to prevent over-heating. The transfer cassette was set up using a foam pad followed by blotting paper, the gel, a nitrocellulose membrane pre-wetted in methanol, blotting paper and finally a second foam pad. All components were immersed in blotting buffer before assembly. The transfer was run at a constant current of 250 mA for 60 min and transfer efficiency was assessed by transfer of the protein ladder onto the membrane. After protein transfer the membrane was incubated overnight at 4°C in blocking solution before adding the antigen specific antibodies (for dilutions, see table 2.1.6). The membrane was incubated with the primary antibody for 60 minutes at room temperature or overnight at 4 °C. The membrane was washed (3x 5 minutes) in PBS-T to remove unbound antibody and was then incubated in secondary antibody (for dilutions, see table 2.1.7), diluted in blocking solution, for 30 minutes at room temperature. After a further 3x 5 minute washes, bound secondary

antibody was detected by enhanced chemiluminescence using chemiDoc MP system (Bio-Rad).

2.2.4 Determination of antibody/conjugate binding by flow cytometry:

Binding of targeting antibodies, unconjugated BLF1 or BLF1 conjugates to various cell lines was assessed by flow cytometry and FACS analysis.

2.2.4.1 Indirect immunofluorescence in tubes:

This experiment was performed using live cells with high viability (>90%) at 4°C to avoid capping, internalisation and shedding of the antigen. Cells were harvested appropriately (using cell dissociation solution for adherent cells) and washed twice with cold buffer (BBN). The harvested cells were re-suspended to $0.5x10^6$ cells/ml with BBN and 1 ml aliquots were placed in FACS tubes. Next, the tubes were centrifuged at 400 g for 2 min. The supernatant was removed using a Pasteur pipette attached to a suction pump. The pellet was re-suspended with 25 µl of primary antibody, mixed by vortexing and incubated for 1 hr on ice. Then, 1 ml of cold BBN was added to each tube, and centrifuged at 400 g for 2 min., this was repeated twice. The supernatant was discarded and 25 µl of secondary labelled antibody (FITC-labelled Abs) was added and incubated for 45 minutes in the dark on ice. Next the cells were washed twice as described before. The cell pellet was re-suspended with 300µl BBN and stored on ice until analysis. For assessing binding of BLF1 conjugates, essentially the same process was used, except cells were incubated first with conjugate, then with primary antibody to BLF1 or targeting antibody, followed by a final incubation with appropriate FITC-labelled antibody. Flow cytometry was carried out using the LSRII machine (Becton Dickinson) using the Flow Cytometry Facility at the Medical School, University of Sheffield. Data analysis was carried out using Flow Jo software.

2.2.4.2 Direct immunofluorescence in tubes:

The cells were harvested and washed as described above and dilutions of labelled protein was made in BBN and stored on ice. Cell pellets were resuspended with 25 µl of the labelled protein and incubated for 45 minutes in the dark on ice. The cells were then washed twice as described before, and resuspended with 300 µl BBN and analysed on LSRII machine (Becton Dickinson).

2.2.5 Assessment of antibody-induced antigen internalisation:

The efficiency of cell surface antigen internalisation induced by targeting antibodies or BLF1 conjugates was assessed by flow cyotmetry. Cells were harvested appropriately and suspended in internalisation buffer (HBSS, 0.2% BSA, no azide) at $10x10^6$ cells/ml. 50 µl of this suspension was placed in each FACS tube, and 25 µl of primary antibody or antibody toxin conjugate was added and the cells incubated for 30 minutes at 4°C. The tubes were then washed with 1 ml of internalisation buffer, and cell pellets were re-suspended in 100 µL internalisation buffer. Control samples were incubated on ice, whilst test samples (including appropriate isotype or BLF1 alone controls) were incubated in a water bath at 37°C, for 15 or 45 minutes then immediately transferred to ice and quenched with 2 ml ice-cold B/B/N. 2 ml of ice-cold B/B/N was also added to control samples after also 45 minutes. All samples were centrifuged and washed, then incubated with 50 µl secondary (FITC labelled) antibody for 30 minutes in the dark at 4°C. The cells were then washed again with 1 ml B/B/N and subsequently fixed with 0.3 ml 2% PFA, or suspended in 0.3 ml B/B/N and kept on ice. Fluorescence was determined using a LSRII flow cytometer, with analysis using FlowJo V10 software. The percentage of antibody or BLF1 conjugate-induced internalisation at each time point was determined using the following calculation, where MFI is median fluorescence intensity: [(MFI (t = 0) – MFI (t = x))/MFI (t = 0)) x 100].

2.2.6 Internalization analysis of antibody-toxin conjugate:

A549, RBL2H3 and MeWo cells (2 ml of $5x10^4$ cells/ml) were seeded overnight on a glass bottom FluoroDish™ (see table 2.1.14). After 24 hr the cells were treated with an appropriate dilution of antibody-mCherryBLF1conjugate (model immunoconjugate conjugate and IMT) or isotype control for 1 hr. The cells were washed with HBSS three times and re-suspended with 2 ml of complete medium and incubated for 24 hr. Next the cells were washed with HBSS 3 times and re-suspended with 1ml phenol red free medium containing Hoechst stain and incubated for 10 minutes at room temperature as described above before visualization using confocal microscope.

2.2.7 Determination of antibody/conjugate binding by fluorescence microscopy:

Binding of BLF1 conjugates to various cell lines was assessed by fluorescence microscopy.

2.2.7.1 Immunofluorescence of cells grown on coverslips:

A sterile 12 mm diameter glass coverslip was placed in the bottom of a sterile 24 well plate. Cells were harvested and cultured on the top of coverslip at a density of $1x10^5$ /well overnight. The following day the supernatant was removed and the cells washed once by adding and removing 1 ml HBSS. Next, the cells were fixed with 2% PFA for 15 minute at 37^oc. The cells were then washed three times with 1XPBS and incubated with 150 µl of an appropriate dilution of conjugate for 1 hour at RT in the dark. The unbound conjugate was removed by washing 3 times with 1x PBS. Next, 150 µl of appropriate dilution of primary antibody to BLF1 was added and incubated for 45 minutes in humid dark condition. After washing an appropriate dilution of FITC-labelled antibody was added and incubated for 45 minutes in humid dark condition. After washing (as described above) the coverslips were carefully removed from the 24 well plates with a needle. Cover slips were affixed to microscope slides using Vectashield with DAPI mountant (VectorLabs) and sealed with nail varnish to prevent slides drying out. The slides were examined using fluorescent microscope or confocal microscope.

2.2.7.2 Immunofluorescence of cells grown on chamber slides:

Cells were harvested and re-suspended in medium at a density of $7x10^4$ cells/ml. Then 0.5 ml of cell suspension was dispensed into each chamber of Lab-Tek™ slide and incubated overnight. The following day the supernatant was removed from each well and washed once by adding and removing 1 ml HBSS. Next, the cells were fixed and permeabilised by adding 0.5ml of acetone to each chamber for 5 minutes. The cells were washed by topping all chambers with 1xPBS, then flicking to remove the PBS. A second wash was carried out by placing the slide in a tank containing fresh PBS for 10 minutes with stirring. The slide was then removed from the tank and incubated with 100µl of appropriate dilution of conjugate in humid dark condition at RT for 1 hr. Next, the slide chambers were rinsed with PBS twice, and a third wash performed by placing the slide chamber in a tank containing PBS with stirring for 15 minutes. The slide chambers were then incubated with 100 µl of FITC conjugated antibody for 30 minutes in a dark humid condition. The slide chambers were washed as previously, and the plastic chambers were then separated from the slide following the manufacturer's instructions. The slide was left to air dry in dark place before adding a small drop of mountant to each slide section. Next, a large coverslip was placed on

the slide and sealed with nail vanish and stored at 4C^{o} until examined using fluorescent microscope.

2.2.8 Measurement of cell uptake of fluorescent molecules:

2.2.8.1 Uptake of mCherry- labelled BLF1 measured by flow cytometry:

Uptake of mCherry- labelled BLF1 (wild type or the C94S mutant) by J774.2 cells was assessed. After harvesting, 2 ml of cells at 0.25x10^{6} cells/ml were seeded in 6 well culture plates and incubated overnight. Next day the media was replaced with 2 ml of medium containing 100 µg/ml mCherry BLF1 and incubated for 1, 6, 12 or 24 hours. After washing 3 times with 1 ml ice cold HBSS, the cells were resuspended with fresh media and harvested by scraping. Next the cells were centrifuged at 200 g for 5 minutes and re-suspended with 300 µl BBN and stored on ice until analysis using a LSRII flow cytometer (Becton Dickinson) and FlowJo software.

2.2.8.2 Uptake of FITC-labelled dextran:

Cells were appropriately harvested and 2 ml at 0.25x10^{6} cells/ml were seeded in 6 well culture plates and incubated overnight. Next day the media was replaced with 2 ml medium containing 100 µg/ml FITC labelled dextran 70 kDa (Life technologies) and incubated for 1 hr at 37°C or on ice (control). After washing with 1 ml cold HBSS cells were harvested by scraping or trypsin treatment and analysed using a LSRII flow cytometer (Becton Dickinson) and FlowJo software.

2.2.8.3 Uptake and intracellular trafficking of Alexafluor 488 labelled BLF1 in the presence/absence of toxicity enhancers:

This experiment was performed to identify the intracellular compartment, in which the unconjugated BLF1 accumulate after internalization. The toxin was chemically labelled with Alexa fluor 488 as described in 2.2.10. MeWo cells were harvested and seeded on a glass bottom FluoroDish™ (see table 2.1.14) (2 ml at 5x10^{4} cells/ml) and cultured at 37°C overnight. Next day, growth media was removed and replaced with medium containing Alexfluor 488 labelled BLF1 (1 µM) with or without 2 µg/ml of saponin for 1 hr. Next the cells were washed 3 times with HBSS and incubated for a further 3 hr. Cells were washed 3 times with HBSS then incubated with phenol red-free media containing 30 µg/ml of pHrodo® Red Dextran (10,000MW)(life technologies, cat. no.P10361) and incubated for 30

min at 37 °C. The cells were then washed 3 times with HBSS, re-suspended with phenol red-free complete medium containing Hoechst stain (1:2000) (life technologies, cat. no.H3570) to counter-stain the nucleus and kept at room temperature for 5-10 min. The immunofluorescence was visualised by confocal microscopy.

2.2.8.4 Investigation of intracellular trafficking of antibody/BLF1 conjugates:

Trafficking of mCherryBLF1 conjugates to various cell lines was assessed by confocal microscopy.

2.2.8.4.1 Immunofluorescence of cells grown on coverslips:

A549 and MeWo cells were seeded on glass coverslips placed in 24-well plates at $1x10^5$cell /well and cultured at 37°C overnight. Next day cells were treated with antibody-toxin conjugate (model conjugate and IMT) at (0.5 µM corresponds to BLF1 in IMT, and 0.2 µM corresponds to BLF1 in model conjugate). At appropriate time points cells were washed 3 times with HBSS, fixed and permeabilized with acetone (0.5 ml/well) for 5 minutes in humid conditions. Cells were then washed 3 times with 1x PBS and incubated with an appropriate concentration of labelled intracellular marker in B/B/N (Table 2.1.4) for 1 hr at RT in the dark. Next cells were washed 3 times with PBS. The coverslips were removed and mounted onto microscopy slides using Vectashield with DAPI and sealed as described in 2.2.6.2 before visualisation by confocal microscope.

2.2.8.4.2 Immunofluorescence of cells grown on a glass bottom FluoroDish™:

A549 and MeWo cells were seeded on a glass bottom FluoroDish™ at (2 ml of $5x10^4$ cells/ml) and cultured at 37°C overnight. Next day, cells were treated with antibody-toxin conjugate (anti-CD63 or anti-CD9 IMT) at 1:100 dilution (corresponds to 0.5 µM BLF1 in IMT) for 1 hr. The cells were then washed with HBSS three times and re-suspended with 2 ml of complete medium and incubated for 3 hr. Next the cells were washed with HBSS 3 times and re-suspended with 1 ml phenol red free medium containing appropriate concentration of labelled intracellular marker (Table 2.1.4) for 30 min at 37°C. Next cells were washed with HBSS 3 times and re-suspended with 1 ml phenol red free medium containing Hoechst stain and incubated for 5-10 minutes at room temperature as described above before visualization using confocal microscope.

2.2.9 Determination of binding specificity of non-chemically crosslinked antibody/ BLF1 conjugate by enzyme linked immunosorbent assay:

A 96-well, flat bottomed immunoassay plate was coated with an appropriate dilution of CD63 or CD9 antigen in 0.05 M carbonate/bicarbonate buffer or just buffer as a control (Table2.1.1); plate was wrapped with cling-film and incubated overnight at 4 °C. Excess unbound protein was discarded and the plate was washed twice with PBS-Tween and dried by tapping the plate on a paper towel. 150 µl of blocking buffer (PBS-Tween+1% milk powder; Table 2.1.1) was added to each well and incubated for 2 hr at room temperature. The blocking buffer was then removed by flicking the plate over the sink, washing twice with PBS-Tween and dried by tapping on a paper towel. 50 µl of a series of dilutions of non-chemically bond antibody/BLF1 conjugate in blocking buffer were added to each well and incubated for 1 hr at room temperature. The plate was washed and dried as previously. 50 µl of an appropriate dilution of primary antibody to BLF1 in blocking buffer was added to each well and incubated for 1 hr at room temperature. The plate was washed and dried as previously. 50 µl of anti-rat horseradish peroxidase-conjugated secondary antibody appropriately diluted in blocking buffer was added to each well and incubated for 1 hr at room temperature. Next the plate was washed twice with PBS-Tween and twice with dH_2O after which 50 µl of TMB substrate (Sigma) was added to each well. The colour was allowed to develop for 15 minutes before the reaction was stopped by addition of 50 µl of 2 M H_2SO_4., The absorbance was measured by a plate reader a 450 nm.

2.2.10 Alexa488 Protein labelling:

Alexa488 dye was used to label BLF1, and (CD63, CD9) antibody for fluorescence analysis. Labelling was performed essentially according to manufacturer's guidelines. In brief, Alexa488 dye from Life technologies was dissolved in 100 µl of DMSO to give a 10 mg/ml stock dye which was stored in aliquots at -20C°. The amount of Alexa488, $NaHCO_3$ and Tris-HCl to be used for labelling were calculated based on the number of moles of protein to be labelled, with a molar excess of 20 used (as suggested by the manufacturer). A minimum of 200 µg of recombinant protein was added to a 0.5 ml Eppendorf wrapped with foil and appropriate volumes of Alexa488 and NaHCO3 were added and incubated for 2 hours at 4 °C on a rotary mixer. Meanwhile, PD-SpinTrap G-25 columns (GE healthcare) were prepared by removing storage buffer and washing the column 5 times with 300 µl volumes of PBS.

After the 2 hours incubation free succinyl groups were quenched by adding Tris-HCl and incubating for 20 minutes at room temperature. Samples were then added to the prepared desalting columns, which were centrifuged at 800 g for 2 minutes and the flow through containing labelled protein was collected. The OD280 and OD494 of the resulting labelled protein were read on a Nanodrop (see table 2.1.13) and used to determine the degree of labelling using the following equation.

$$DOL = \frac{OD494X\ MW}{71000X\ \text{protein concentration (M)}}$$

DOL: degree of labelling

OD494: absorbance at maximum wavelength of the dye

Protein concentration: concentration determined by Nano drop (OD280)

71000: molar extinction coefficient of the dye.

2.2.11 Bacterial BLF1 protein expression and purification:

2.2.11.1 Transformation of *E. coli* BL21 (DE3) competent cells:

The BLF1 plasmid was transformed in *E.coli* BL21 (DE3) - RP cells (see table 2.1.5) for overexpression. Aliquots of competent cells (100 µl) were defrosted on ice for 2 minutes. 2 µl of BLF1 expression plasmid (100 ng/µl stock) was added to the cells, mixed and incubated for 10 minutes on ice. The DNA was transformed into *E.coli* by heat shock for 5 minutes in a water bath at 37 °C. The cells were then incubated on ice for 2 minutes, 1 ml LB medium was added and the cells were incubated for 1 hour at 37 °C with shaking. The cells were then centrifuged for 1 min at 7000 rpm (4,700 g). The supernatant was poured off and the pellet was re-suspended in the remaining medium. 25-100 µl of the culture was plated on LB agar supplemented with appropriate antibiotics (table 2.1.9) and incubated overnight at 37 °C. A streak of colonies were picked and inoculated into a flask containing 4 ml of TB medium and cultured for 6 hours at 37°C on a shaking tray at 200 rev min^{-1}.Two flasks each containing 750 ml of TB medium were pre-warmed at 37°C to be ready for inoculation. 1.5 ml of the culture was added to each flask containing 750 ml of TB medium and 750 µl of chloramphenicol (34 mg ml^{-1} stock) and 750 µl kanamycin (50 mg ml^{-1} stock; for pET24b-BLF1) or ampicillin (100 mg ml^{-1} stock; for pET14b-BLF1) and grown at 37°C until OD_{600} of 0.7

was achieved; at this point 300 µl of 1 mM IPTG was added to induce expression. The culture was allowed to grow for additional 1 hr at 37°C and incubated overnight at room temperature with shaking. The cells were then harvested by centrifugation at 6000 rpm (6,371 g) in a JA10 rotor (*Beckman*) for 10 min at 4°C, the supernatant was decanted and the bacterial pellets were frozen at -20°C until lysis and purification.

2.2.11.2 Cell lysis by sonication:

The bacterial cell pellets collected previously (2.1.5.1) were thawed on ice and re-suspended with lysis buffer (50 mM TRIS pH8.0, 1 M NaCl, 0.5% Triton X-100) supplemented with PMSF and protease inhibitor cocktail and disrupted by sonication at 100% (Sonicator *Soniprep*) for 30 second rounds (5 rounds in total). The cell debris was removed by centrifugation at 24,000 g for 20min at 4°C. The supernatant was collected for downstream purification.

2.2.11.3 Affinity purification of 6His tagged BLF1:

An appropriate volume of cobalt beads (Clontech Laboratories, Inc. Cat. No. 635507) (1 ml of beads for every 10 grams of bacterial pellet) was transferred to a 50 ml falcon tube, allowed to settle, and the head volume containing ethanol was discarded. The beads were re-suspended with 10 bed volumes of milliQ water, allowed to settle again and the head volume discarded; this washing was repeated twice. Washed cobalt beads were re-suspended with 10 ml lysis buffer (table2.1.10) and loaded into a 15 ml gravity flow column (*Biorad*) then the cell lysate was added and allowed to flow through. The protein bound to the cobalt beads was washed twice with 10 ml washing buffer (table2.1.10), after which the beads were incubated for 5 min with 3 ml of elution buffer (table2.1.10) this was repeated 3 times. The 3 fractions of eluted protein were concentrated to 5 ml using ultrafiltration on a 10 MWCO membrane in an *Amicon* device (*Millipore*). The concentrated protein was then subjected to gel filtration using a Superdex 200 column equilibrated with 1x PBS. The peak fraction corresponding to monomeric BLF1 was concentrated by ultrafiltration on Amicon as previously described. The purity of BLF1 was estimated to be greater than 95% as shown by SDS-PAGE. The concentration of pure BLF1 protein is quantified by measuring the absorbance at 280 nm. Approximately 35-50 mg pure BLF1 fusion proteins obtained from 1.5 L cultures.

2.2.11.4 Sodium Dodecyl Sulphate-Polyacrylamide Gel Electrophoresis (SDS PAGE):

SDS-PAGE was carried out using the Mini- PROTEAN Tetra cell system as instructed by the manufacturer (Biorad). 15% separating gels and 5% stacking gels were prepared as described in Table 2.1.3. The protein samples were mixed with the loading buffer (4x reducing for Coomassie staining) and were boiled for 5 minutes at 95°C. 12 µl of protein sample and 3 µL-5 µl of standard protein marker (All Blue Precision Plus, Biorad, 161-0373) were loaded into the gel. Samples were electrophoresed at 170 V for approximately 60-90 minutes.

2.2.11.5 Coomassie staining and de-staining:

Once SDS-PAGE gel had been run (2.2.11.4) the resolving gel was carefully removed from the glass plates, transferred to a container and stained with Coomassie brilliant blue stain (Table 2.1.1) overnight with gentle agitation. Once stained, the gel was briefly washed with dH_2O and transferred to de-stain (Table 2.1.1) for 4 hours or until background was clear.

3 Chapter 3: investigation of uptake, intracellular transport, and cytostatic/cytotoxic action of BLF1 toxin

3.1 Introduction:

Burkholderia lethal factor1 (BLF1) is produced as a virulence factor by the pathogenic bacterium *Burkholderia Pseudomalle*i, that is the causative agent of melioidosis. This toxin is typically very potent as previously described (1.1.5); a dose of 100 µg of recombinant BLF1 introduced into Balb/c mice by the intraperitoneal route was lethal by day 14 (Cruz-Migoni et al., 2011). BLF1 does not appear to enter mammalian cells by binding to cell surface receptors; this was assumed to be because the BLF1 producing pathogen *B.pseudomallei* is usually intracellular (Willcocks et al., 2016) and no effect was observed on mouse 3T3 fibroblast cells unless the toxin was introduced deliberately into the cytoplasm using agents such as Endoporter. However, a significant effect of BLF1 was observed on the mouse macrophage cell line J774.2 even in the absence of agents that allow its transduction into the cytoplasm (Cruz-Migoni et al., 2011). The cytotostatic/cytotxicity observed here was assumed to be due to the high rate of macropinocytosis in the macrophage cell line, although this had not been formally demonstrated. Macrophages function as antigen presenting cells and must rely on apparently non-specific mechanisms to capture antigen leading to antigen presentation and T-cell activation (Norbury et al., 1995, Sallusto et al., 1995). Since high rates of BLF1 uptake by macrophages may cause toxicity, as observed in Balb/c mice, it was of interest to investigate this further, since it might affect the potential therapeutic application of the toxin.

3.1.1 Enhancing the intracellular delivery of BLF1:

Effective intracellular delivery of different biologically active compounds is one of the key barriers to drug delivery. Various pharmaceutical agents, including protein, antibodies, and enzymes need to be delivered directly to the cytoplasm, bypassing the endocytic pathway, to avoid lysosomal degradation and exert their therapeutic action (Torchilin, 2006). Multiple methods have been developed to bring various drug macromolecules and drug-loaded pharmaceutical cargo directly into the cytoplasm. These include biochemical techniques, such as cell penetrating peptides, and physical techniques, such as microinjection. However, these techniques are often associated with cytotoxicity, low efficiency, and are not

convenient (Torchilin, 2006, Erazo-Oliveras et al., 2014). Previous studies have demonstrated that botulinum-derived proteases can be efficiently delivered into neuroendocrine cells using certain DNA transfection reagent, inducing cytotoxic effects in neuroendocrine tumour cells (Arsenault et al., 2014). In this chapter, the newly available DNA transfection reagent lipofectamine 3000 (LF3000) was tested to find its efficiency to deliver BLF1 toxin into a range of cell lines. This would also allow determination of the BLF1 sensitivity of cell lines that did not take up the toxin by macopinocytois. LF3000 has been shown to be able to deliver saporin toxin into neuroblastoma N2a cells, and was more efficient and less toxic than LTX (Rust et al., 2015).

3.1.2 Investigating the uptake mechanism of BLF1:

Macropinocytosis is a distinct endocytic uptake mechanism that accompanies cell membrane ruffling to generate large intracellular vesicles of irregular size and shape called macropinosomes (Swanson and Watts, 1995, Lim and Gleeson, 2011). This mode of fluid-phase endocytosis is up-regulated in several conditions, for example to uptake nutrition requirements of Dictyostelium amoeba under axenic conditions or support massive uptake of soluble antigens by immature dendritic cell (Amyere et al., 2002). Macropinocytosis has also been reported as a mechanism some viruses and bacteria use to invade host cells, such as adenovirus (Kalin et al., 2010) and *Salmonella typhimurium* bacteria (Alpuche-Aranda et al., 1994). Alternatively, a transient increase in macropinocytotic activity (5–10 min) has also been observed after stimulation of cells with growth factors or phorbol esters (Amyere et al., 2002). In cancer, this form of fluid-phase uptake is also induced by oncogenes such as *Ras* and *Src*, and is an essential nutrient delivery pathway that cancer cells rely on to drive their growth and proliferation. The albumin present in the extracellular fluid is internalized through macropinosomes and targeted to lysosomes for proteolytic degradation, yielding their constituent amino acids that support the metabolic and biosynthetic needs of cancer cells (Commisso et al., 2014).

Flow cytometry techniques have been developed for measuring macropinocytosis, usually using fluorescein-labelled dextran. This technique was initially developed to investigate chemotactic peptide induced macropinocytosis by human polymorphonuclear leukocytes (Davis et al., 1986). In another example, macropinocytosis in 6 sublines of the Dunning R-

3327 rat prostatic adenocarcinoma models representing high and low metastatic potential was assessed by flow cytometry by measuring uptake of fluorescein (FITC)-labelled dextran (70 kDa). The association of membrane ruffling with macropinocytosis suggested its correlation with the metastatic potential of cancer cells (Mohler and Sharief, 1993). Interestingly, the lung cancer cell line A549 was shown to macropinocytose 3x faster than normal lung epithelial cells (Srinivasan et al., 2013). In addition, fluorescein-labelled dextran has been widely used to measure macropinocytosis in many cell lines and primary cells. For example, the rate of endocytosis of FITC- dextran, (40 kDa) was quantified via flow cytometry (Autenrieth and Autenrieth, 2009). Therefore it was of interest here to investigate the rate of uptake of FITC- dextran by different cell lines to see if this correlated with their sensitivity to BLF1, particularly cancer cells lines with lower rate of macropinocytosis.

The plasma membrane ruffling that leads to macropinocytosis is uniquely sensitive to inhibitors of Na^+/H^+ exchange. Therefore, the macropinocytic inhibitor amiloride was used to address the role of macropinocytosis in the uptake of FITC- labelled dextran (Koivusalo et al., 2010).

3.2 Aims:

The aims of the work described in this chapter were:

- To investigate the sensitivity of other macrophage and human cancer cell lines to BLF1.
- To investigate the effect of the transfection reagent lipofectamine 3000 on delivery of BLF1 into the cytosol of different cell lines, including dividing/non-dividing cells.
- To investigate the role of macropinocytosis in uptake of BLF1 by correlating sensitivity with rates of macropinocytosis as measured using fluorescent dextrans and flow cytomery.
- To investigate the uptake of BLF1 by cells using fluorescent (mCherry) tagged BLF1 assessed using flow cytometry.

3.3 Results:

3.3.1 Expression and affinity purification of 6His-BLF1, 6His-mCherry BLF1, and mutant inactive C94S fusions:

As described in 2.1.8 vectors encoding BLF1 (wild type), mCherry tagged BLF1 and the mCherry tagged C94S mutant, which is enzymatically inactive, were generated by Dr Guillaume Hautbergue, SITraN, University of Sheffield. In all cases, the constructs were designed so that BLF1 was expressed with an N-terminal 6His tag to facilitate purification. These forms of BLF1 were expressed in *E.*coli to provide protein for use in later functional studies and conjugation processes to generate immunotoxins (Chapters 4, 5). The relevant vectors were used to transform BL21 cells and after induction with IPTG, cultures were harvested and bacteria lysed as described in 2.2.11.1 and 2.2.11.2. The 6His- tagged forms of BLF1 were purified from the lysates by affinity chromatography on cobalt beads as described in 2.2.11.3. After concentration, the fractions eluted from the cobalt beads were further purified by gel filtration using a Superdex 200 column and concentrated if needed by ultrafiltration under nitrogen gas using an Amicon device (*Millipore*). Samples from each steps of the purification procedure were run on SDS PAGE gels and subsequently stained with Coomassie blue (**Fig**.3.3.1). The His-tagged wild type BLF1 is predicted to have a molecular weight of approximately 24 kDa.The higher molecular weight band observed here after affinity purification (lane 4) at ~ 50 kDa is thought to represent dimers of BLF1 protein. BLF1 (shown in lane 5) is the protein after gel filtration with bands being detected at the expected molecular weight as indicated by the red arrow. The mCherry tagged BLF1 and the mCherry tagged C94S mutant is predicted to have a molecular weight of approximately 53 kDa. The mCherry tagged proteins after gel filtration (lanes 9 and 13) were detectected at the expected molecular weight at 53 kDa . However, a lower band was also detected after affinity purification and gel filtration for the mCherry tagged protein (lane 8,9,12,13) and is thought to represent cleavage product of the 6His-mCherry-BLF1 (likely 6His-GFP). Peaks corresponding to the monomeric BLF1 fusion proteins were collected from the S200 gel filtration step. The concentration of purified BLF1 was quantified by measuring the absorption at 280 nm as described in 2.2.11.3.

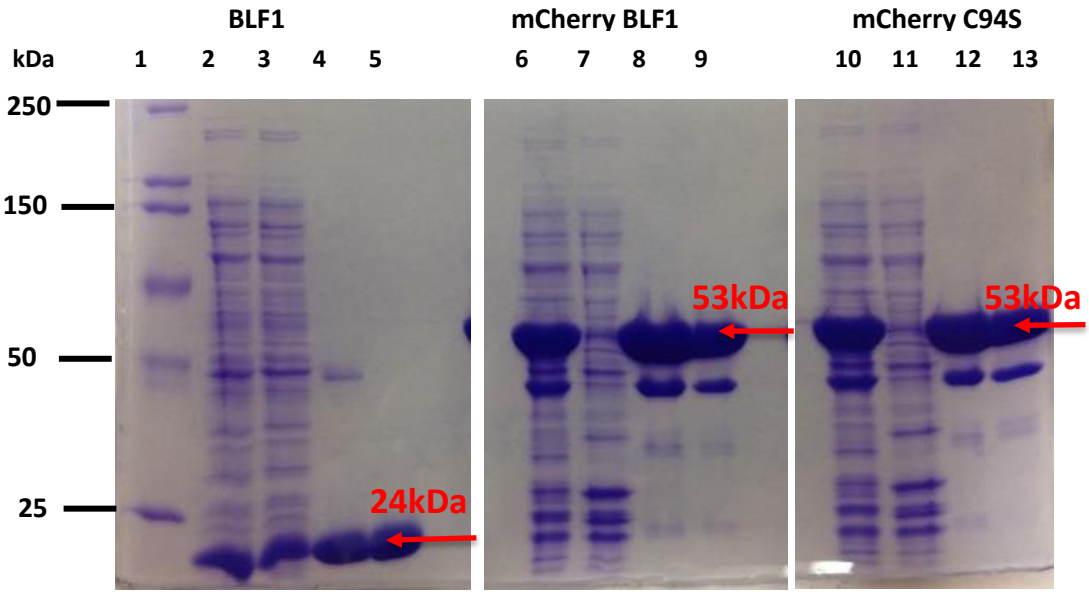

Figure 3.3.1: SDS-PAGE analysis of BLF1-6His purification from bacterial cell lysates: Lysates were prepared from *E. coli* cells transformed to express BLF1 (untagged WT, mCherry tagged WT or mCherry tagged C94S (mutant) as described in 2.2.11. Fractions collected after each purification steps were analysed by 15% SDS-PAGE stained with Coomassie blue. Lane1, protein marker (labelled in kDa); lane 2, 6, 10, cell free extract; lane 3, 7, 11, flow –through; lane 4, 8, 12 elution after Cobalt column purification; lane 5, 9, 13 sample after gel filtration on Superdex 200 (peak corresponding to monomeric protein fusions).

3.3.2 Cell line models used for studying the cytostatic/cytotoxic effects of BLF1:

Previous studies have shown that BLF1 is directly cytostatic/cytotoxic at low doses to the mouse macrophage cell line, J774.2. It was therefore of interest to compare the effect of the toxin on other macrophage and human cancer cell lines. The effect of BLF1 toxin on different cell lines was examined after growing the cells in the absence and presence of various concentrations of the toxin for 72 hours using the sulforhodamine B (SRB) assay (2.2.2), which measures cellular protein as an estimate of cell number (Skehan et al., 1990). The SRB assay is sensitive and inexpensive and has been widely used in the pharmaceutical industry to assess the effects of anti-cancer drugs. Although originally described as a cytotoxicity assay (Skehan et al., 1990), the test actually assesses cell number and therefore does not distinguish between anti-proliferative and cytotoxic effects. However, since anti-proliferative effects are also desirable (and sometimes preferable) properties of anti-cancer treatments, this assay was routinely used throughout this thesis.

3.3.2.1 Standard curve for cell number vs absorption:

To investigate the effect of BLF1 toxin on different cell lines, we needed firstly to determine the optimal cell number for each cell line to be used in the SRB assay. Therefore, a known number of cells at different densities were plotted against the colorimetric absorbance at 570 nm (**Fig**.3.3.2). The concentration of cells optimal to be used for the SRB assay was $0.05x10^6$ - $0.0625x10^6$ cells/ml. This was determined to take into account that the untreated control cells would divide and increase in number (and therefore absorption) after 72 hr in culture.

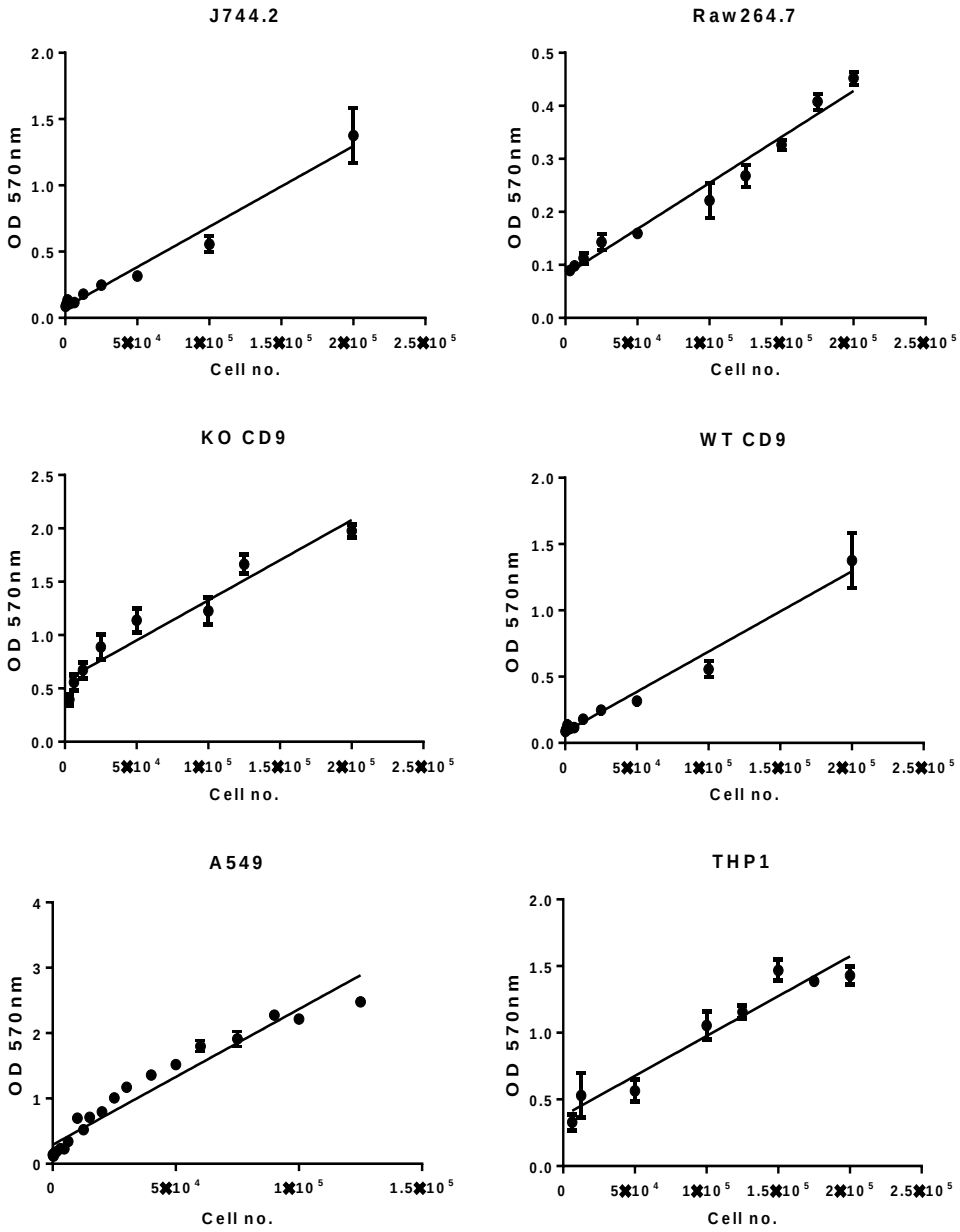

Figure 3.3.2: Calibration curve:
Known cell numbers were plated and their corresponding optical density values at 570nm determined following SRB procedure. Lines of regression for J774.2, RAW, KO CD9, WT CD9, A549, and THPI has equations y = 6.082 × $10^{-6}x$ + 0.0796, y =1.735x10^{-6} x +0.08101, y =7.5x10^{-6} x +0.5741, y =6.058x10^{-6} x +0.08278, y =2.076x10^{-5} x +0.2908 and y =5.97x10^{-6} x +0.377 respectively.

3.3.2.2 Effect of BLF1 on mouse macrophage cell line growth:

3.3.2.2.1 Effect of BLF1 on J774.2 and RAW264.7 mouse macrophage cell line growth:

A time course of the effect of BLF1 was investigated on the J774.2 cell line (Ralph and Nakoinz, 1975). Cells were cultured in the presence or absence of different concentrations of BLF1 toxin. After 24, 48, 72 hr cells were fixed and cell growth was assessed using SRB assay as described in (2.2.2.3). The SRB assay revealed that the effect of toxin increases with time and incubation for 72 hr is the optimum length of time for BLF1 to exert its effects (**Fig**.3.3.3) and significant cytostatic/cytotoxic effects were evident at concentrations down to 0.5 µm compared to the control (no toxin) (**Fig**.3.3.4). This is very similar to previous observations (Cruz-Migoni et al., 2011).

The RAW264.7 cell line is also a long-established macrophage cell line (Ralph and Nakoinz, 1975). Incubation of RAW cells in the absence or presence of various concentrations of BLF1 for 72 hr showed that it had a similar sensititivity to BLF1 toxin (**Fig**.3.3.4). This suggests a similar uptake mechanism for both cell lines.

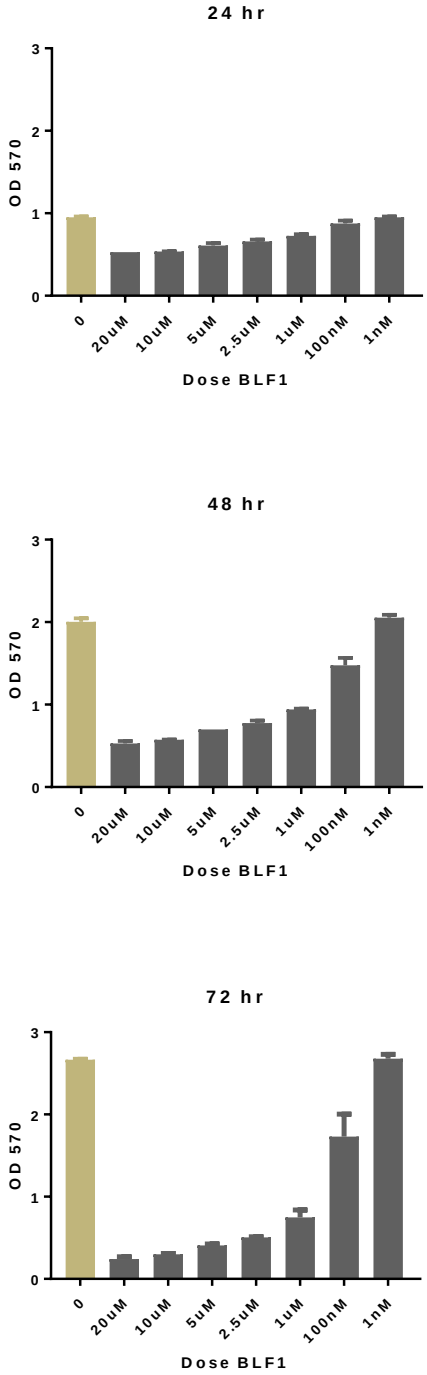

Figure 3.3.3: Time course of the effect of BLF1 on mouse macrophage cell line J774.2 cell growth:

6250 cells/well were cultured in 96 well plates in the presence/ absence of various concentrations of BLF1 toxin. After 24, 48 or 72 hrs cells were fixed and cell growth assessed using the SRB assay as described in (2.2.2.3), where OD at 570nM gives a measure of

cellular growth. Two independent experiments were performed in quadruplicate (values are mean ± SEM).

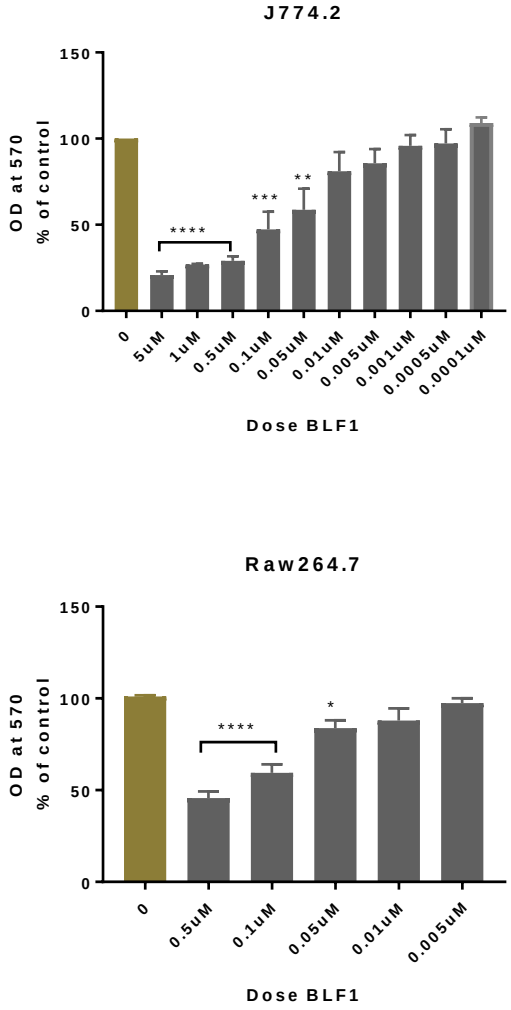

Figure 3.3.4: Effect of BLF1 on mouse macrophage J774.2 and RAW264.7 cell line growth: J774.2 and RAW264.7 cells (6250 cells/well) were cultured in 96 well plates in the presence or absence of various concentrations of BLF1 toxin. After 72 hours cells were fixed and cell growth assessed using the SRB assay, where OD at 570 nm gives a measure of cellular growth. Three independent experiments were performed in quadruplicate, with values shown as mean ± SEM. The significance of difference between treated and untreated cells was determined by one way ANOVA with Dunnett's multiple comparisons test where **** is significantly different at $p<0.0001$, *** is significantly different at $p<0.001$ and * is significantly different at $p< 0.05$.

3.3.2.2.2 Effect of BLF1 toxin on the cellular growth of KO and WT-CD9 cells:

It was of interest to investigate the BLF1 effect on additional mouse macrophage cell lines. Macrophage cell lines derived from the bone marrows of mice which had been subject to knockout of the *CD9* tetraspanin gene and the corresponding wild type mouse were available in the laboratory (Ha et al., 2005) and so were investigated. Cells were cultured in presence or absence of different concentrations of BLF1 for 72 hr. SRB assay revealed that the toxin had a significant effects on the growth of both cell lines (**Fig**.3.3.5,3.3.6). Interestingly, the macrophages derived from CD9 KO mice seemed to be slightly less sensitive to BLF1, showing no significant effects at 0.1 µM and 0.05 µM concentrations, in contrast to those from WT mice.

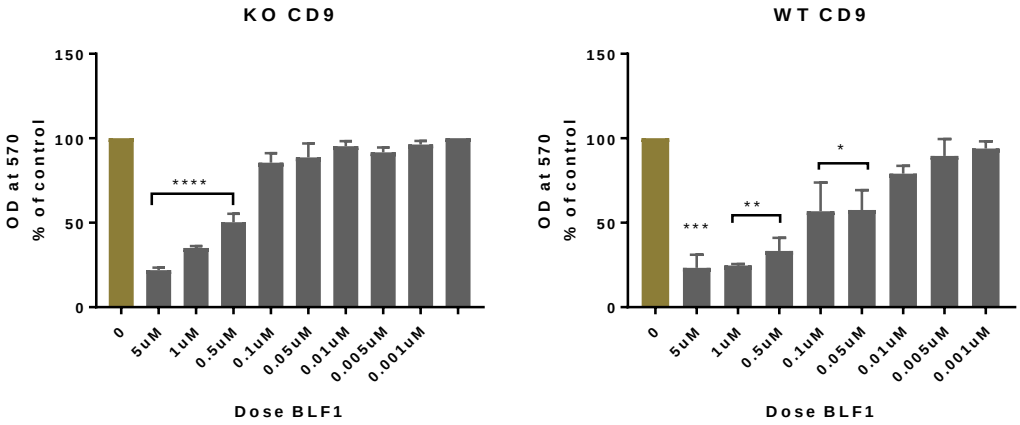

Figure 3.3.5: Effect of BLF1 on mouse macrophage cell lines derived from WT and CD9 KO mice:

Cells were cultured in the presence or absence of various concentration of BLF1 toxin for 72 hours and cell growth assessed using the SRB as described in **Fig**.3.3.4.Three independent experiments were performed in quadruplicate, with values shown as mean ± SEM. The significance of difference between treated and untreated cells was determined as described in **Fig**.3.3.4.

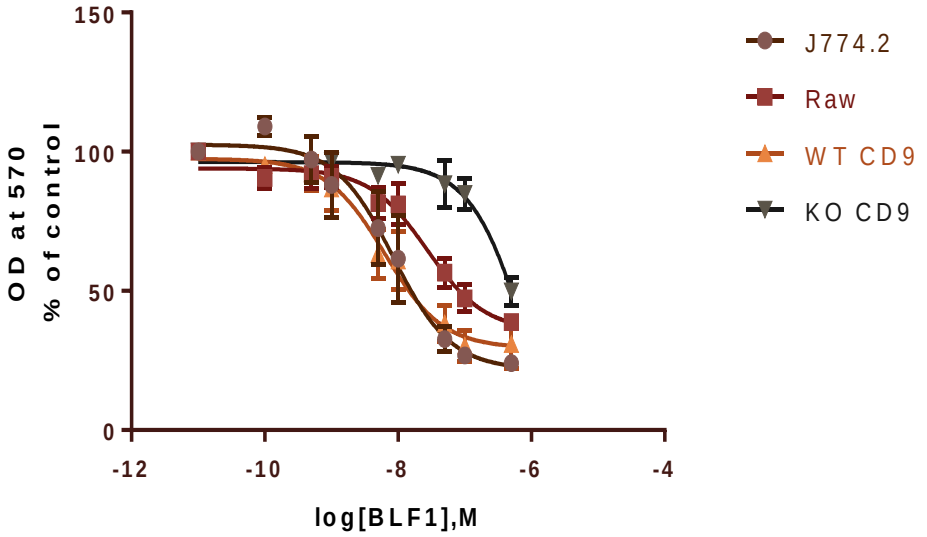

Cell line	Log IC_{50}	IC_{50} (µM)
J774.2	-8.072	0.008
RAW	-7.564	0.027
WT CD9	-8.202	0.006
KO CD9	-5.992	1.018

Figure 3.3.6: Effect of BLF1 on the sensitivity of various mouse macrophages cell lines: Cells were cultured in the presence or absence of various concentration of BLF1 toxin for 72 hours and cell growth assessed using the SRB assay as described in **Fig**.3.3.4. IC_{50} values indicate the concentration of BLF1 needed to inhibit 50% of cellular growth. Three independent experiments were performed in quadruplicate, with values shown as mean ± SEM.

3.3.2.3 Effect of BLF1 on human cancer cell line growth:

3.3.2.3.1 Effect of BLF1 on human monocyte cell line growth:

Since BLF1 was shown to have a potent effect on mouse macrophage cell lines, it was of interest to investigate its effects on human mononuclear phagocyte cell lines. The effect of BLF1 was investigated on the THP1 monocyte cell line (Tsuchiya et al., 1980) and on the U937 monocyte cell line (Sundstrom and Nilsson, 1976). The effect of BLF1 was also examined on the promyelocytic cell line HL60 (thought to represent an earlier myeloid precursor (pre-monocyte/granulocyte)(Collins et al., 1977) using the SRB assay as described above. No significant effects on cell growth were observed at any concentrations for any of these three cell lines (**Fig.**3.3.7).

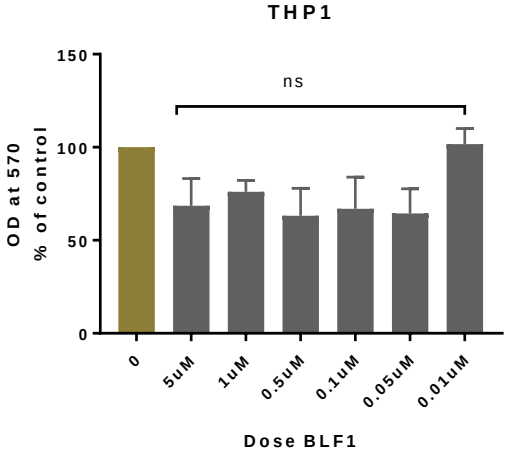

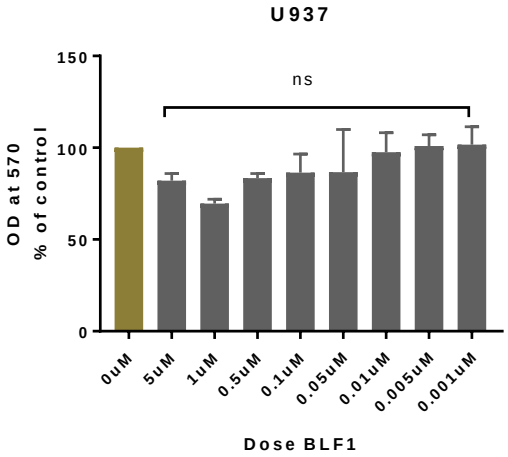

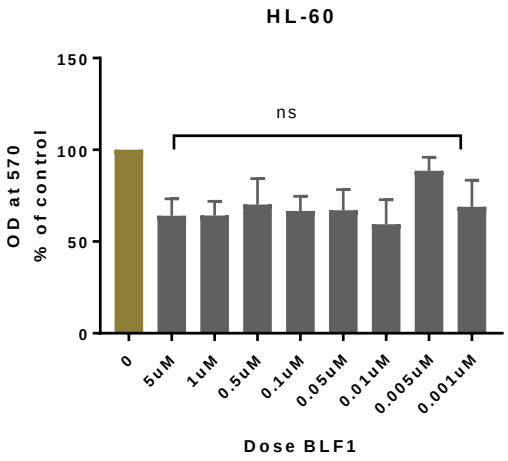

Figure 3.3.7: Effect of BLF1 on THP1, U937 and HL-60 human cell line:
Cells were cultured in the presence/ absence of BLF1 toxin for 72 hr and cellular growth was assessed using the SRB assay as described in (2.2.2.3) except that cells were fixed with 80% TCA as recommended for suspension cells. Three independent experiments were performed in quadruplicate with values shown as mean ± SEM and the significance of difference between treated and untreated cells was determined as described in **Fig.**3.3.4.

3.3.2.3.2 Effect of BLF1 toxin on stimulated THP1 with PMA:

THP1 and U937 cells represent an earlier mononuclear phagocyte differentiation stage (monocyte) than the mouse macrophage cell lines that were sensitive to BLF1. It was postulated that the cells with a less mature phenotype might be less active in macropinocytosis and so unable to take up the BLF1 toxin. However, it is widely reported that these cell lines can be induced to differentiate to a more macrophage-like phenotype in response to stimulation with agents such as phorbol esters (Tsuchiya et al., 1982). THP1 cells were therefore treated with phorbol ester for 48 hr before being treated with BLF1, as described in 2.2.2.1. There was a visible morphological change in PMA-treated cells, which became strongly adherent, consistent with differentiation (**Fig**.3.3.8A). However, the toxin had no significant effect on this human monocytic cell line growth after 72 hours of incubation with the toxin (**Fig.**3.3.8B).

A.

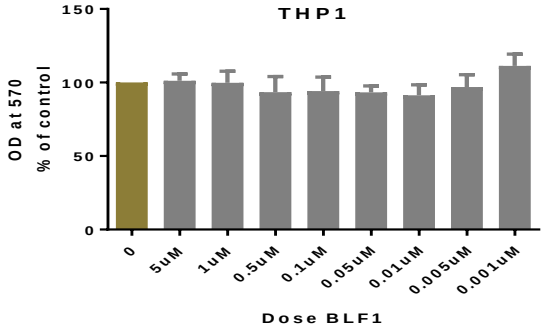

B.

Non-stimulated PMA **Stimulated PMA**

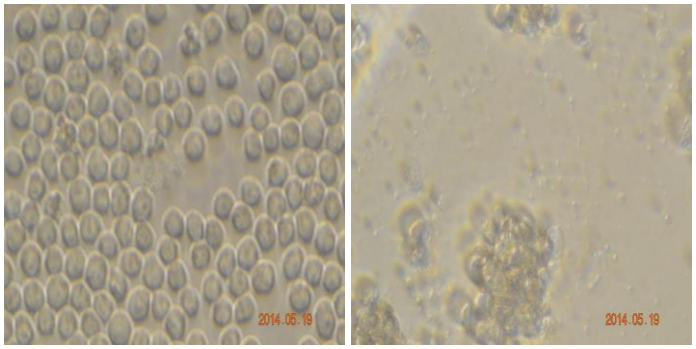

Figure 3.3.8: Effect of BLF1 on THP1 cells with PMA:
(**A**) THP1 cells were cultured in the presence or absence of PMA (20 ng/ml) for 2 days. The cells were then cultured in the presence/absence of different concentrations of BLF1 toxin for a further 72 hours, before assessing cell growth using the SRB assay as described previously. Three independent experiments were performed in quadruplicate, with values shown as mean± SEM and the significance of difference between treated and untreated cells was determined as described in Fig.3.4. (**B**) Light microscopy images of human THP1 cells cultured in the presence or absence 20 ng/ml of PMA for 48 hr. Images were captured with a Nikon inverted microscope using the 60x objective.

It was surmised that the lack of an effect of BLF1 on the PMA-treated THP1 cells might be because although the cells were more macrophage-like, they had stopped dividing after stimulation with PMA, and BLF1 preferentially affects dividing cells. To try to investigate this, the BLF1-sensitive J774.2 mouse macrophage cell line was also treated with PMA in an effort to stop them dividing. J774.2 cells were therefore also treated with phorbol ester for

48 hr before being treated with BLF1. The PMA-treated cells became strongly adherent, consistent with differentiation, and stopped dividing (**Fig**.3.3.9B). Interestingly, the toxin had no significant effect on J774.2 cells that had been treated with phorbol ester after 72 hours of incubation (**Fig**.3.3.9). This suggests that BLF1 predominantly affects dividing cells.

A.

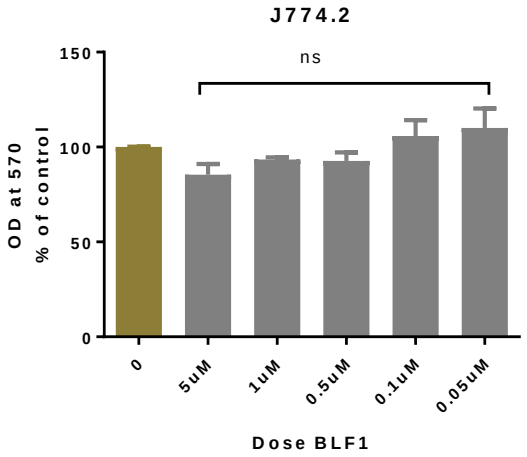

B.

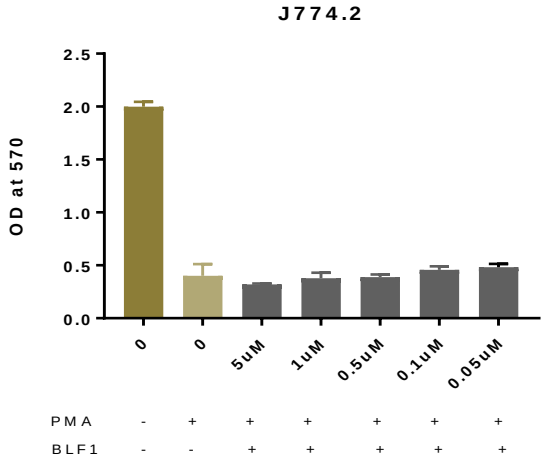

Figure 3.3.9: Effect of BLF1 on J774.2 cells stimulated with PMA:
J774.2 cells were cultured in the presence or absence of PMA (20 ng/ml) for 2 days. The cells were then cultured in the presence/absence of different concentrations of BLF1 toxin for a further 72 hours, before assessing cellular growth using the SRB assay as described previously. **A**. Normalized data to cells treated with PMA only. **B**. Raw data before normalization, which includes controls where cells were not treated with PMA. Two independent experiments were performed in quadruplicate, with values shown as mean ±

SEM and the significance of difference between treated and untreated cells was determined as described in **Fig**.3.3.4.

3.3.2.3.3 Effect of BLF1 toxin on human epithelial cancer cell line:

As mentioned previously in (3.1.2) macropinocytosis activity is induced in cancer, so it was of interest to investigate the effect of BLF1 on human cancer cell lines. The human epithelial cell lines A549 (a human alveolar epithelial cell line derived from lung carcinoma (Giard et al., 1973)) and HeLa (the well-known human epithelial cell line derived from cervical cancer (Scherer et al., 1953)) was also tested. Furthermore, a human cell line derived from malignant melanoma was investigated (MeWo) (Grose and Brunel, 1978). Measurement of cellular growth by the SRB assay indicated that the toxin had only a significant effect on A549 cells at the highest concentration used (4 µM) (**Fig**.3.3.10.A). The MeWo human melanoma cell line appeared to be slightly more sensitive to BLF1 (**Fig.**3.3.10.C) and the HeLa cells seem to be more sensitive than the other two human cancer cell line examined in this study (**Fig**.3.3.10.B).

A.

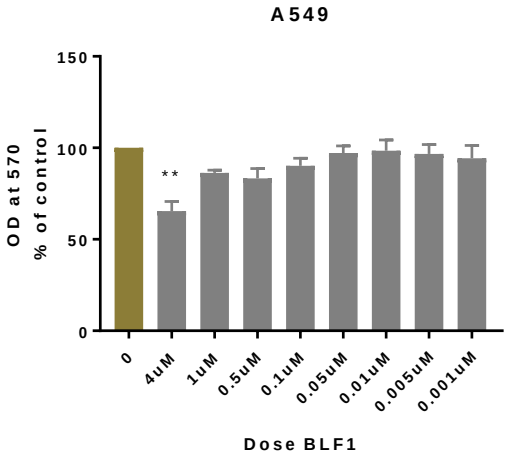

B.

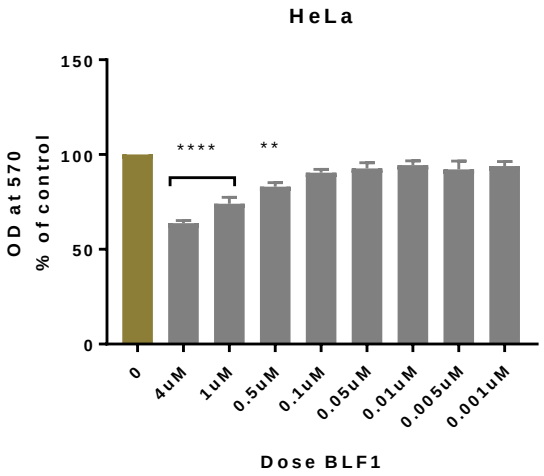

C.

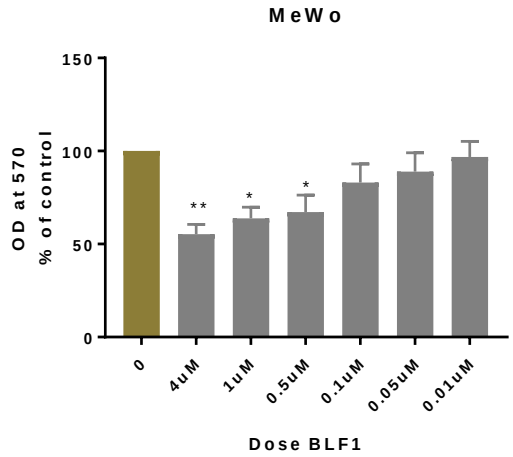

Figure 3.3.10: Effect of BLF1 on A549, HeLa, and MeWo human cancer cell lines:
Cells were cultured in the presence or absence of various concentration of BLF1 toxin for 72 hours and cellular growth was assessed using the SRB as described in **Fig.**3.3.4.Three independent experiments were performed in quadruplicate, with values shown as mean ± SEM. The significance of difference between treated and untreated cells was determined as described in **Fig**.3.3.4.

3.3.2.4 Effect of BLF1 toxin on normal human epithelial cell:

Since the cell lines examined to date were all derived from cancers, which are reported to have higher than usual rates of macropinocytosis (Commisso et al., 2014), it was of interest to study the effects of BLF1 on a non-cancerous cell line (**Fig.** 3.3.11A). The effect of BLF1 on the human embryonic kidney cell line HEK293 (derived from human embryonic kidney cells by transformation with Adenoviral DNA, (Graham et al., 1977)) was therefore investigated. Furthermore, a non-tumour derived cell line; that were spontaneously transformed from human keratinocytes (Boukamp et al., 1988) HaCaT was also investigated. Measurement of cellular growth by the SRB assay indicated that the toxin had only a significant effect on HEK293 cells at the highest concentration used (5 µM). The HaCaT cells line appeared to be more sensitive to BLF1 (**Fig**.3.3.11B).

A.

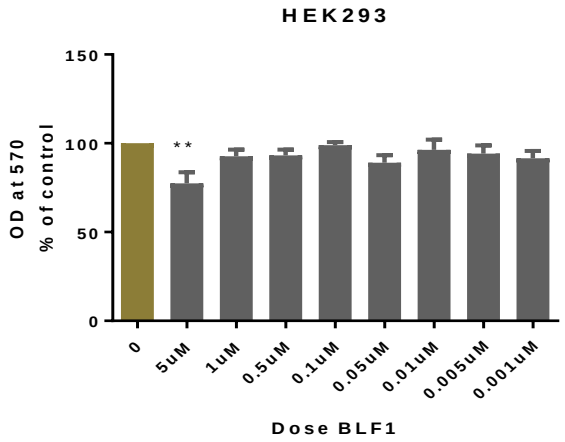

B.

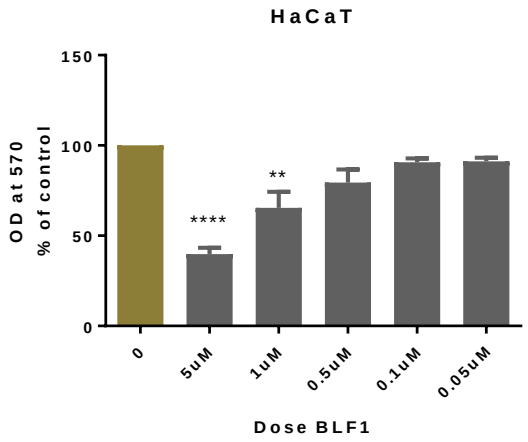

Figure 3.3.11: Effect of BLF1 on the HEK293 and HaCaT normal human cell lines:
Cells were cultured in the presence or absence of various concentration of BLF1 toxin for 72 hours and cellular growth was assessed using the SRB as described in **Fig**.3.3.4. Three independent experiments were performed in quadruplicate, with values shown as mean ± SEM. The significance of difference between treated and untreated cells was determined as described in **Fig.**3.3.4.

3.3.3 Intracellular delivery of BLF1 using new DNA transfection reagent in various cell lines:

As mentioned in 3.1.2, it has been shown that the DNA transfection reagent lipofectamine can deliver toxins into neuroblastoma cells. Here, we tested the recently introduced Lipofectamine 3000 (LF3000) reagent for its capacity to deliver BLF1 into a variety of cell lines. The effect of LF3000 on the cytostatic/cytotoxicity of BLF1 for the mouse macrophage cell lines (J774.2, RAW264.7), human epithelial cancer cell lines (A549, HeLa) and the non-cancer human cell line HEK293 was investigated using the SRB assay. The results showed that a combination of lipofectamine 3000 with BLF1 lead to significant inhibition of cell growth compared to BLF1 alone for most of the tested cell lines (**Fig**.3.3.12). This indicates that the transfection reagent is able to deliver BLF1 into a variety of different cell types. As indicated by the estimated IC_{50} values (**Fig.**3.3.12.B), even in the presence of lipofectamine there was some variation in the sensitivity of the cell lines to BLF1; RAW264.7 cells in particular showed a very marked effect on cellular growth at sub-nanomolar concentrations of BLF1. However, the effect of lipofectamine varied between cell lines, with only slight enhancement of the effect of BLF1 in the presence of LF3000 for the J774.2 cell line. This is

not unexpected, as this cell line has previously been shown to efficiently take up BLF1 and is very active in macropinocytosis. Furthermore we tested the effect of LF3000 on the delivery of FITC-dextran to J774.2 cells that correlates with the sensitivity of these cells to BLF1. As shown in (**Fig**.3.3.13), there was little difference in the uptake of the dextran between cells which had or had not been treated with lipofectamine.

A.

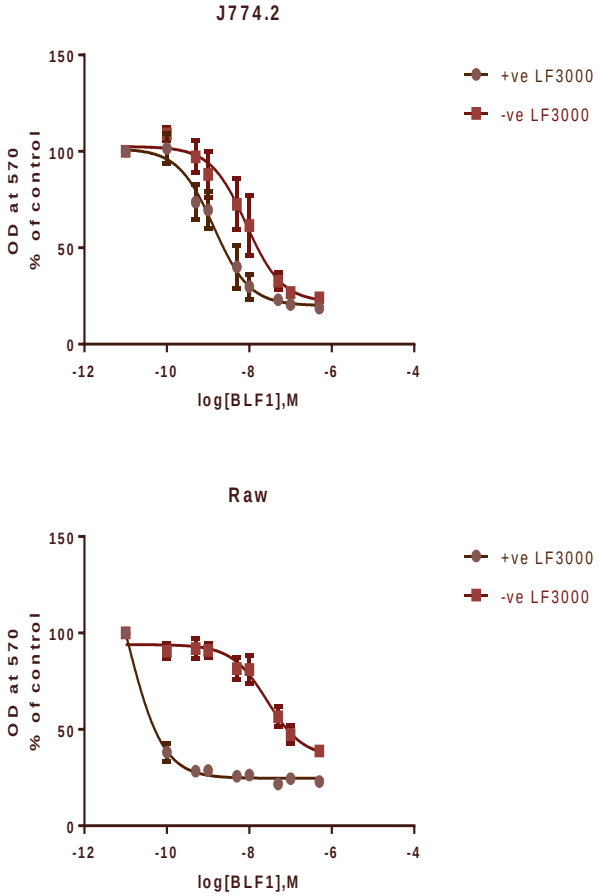

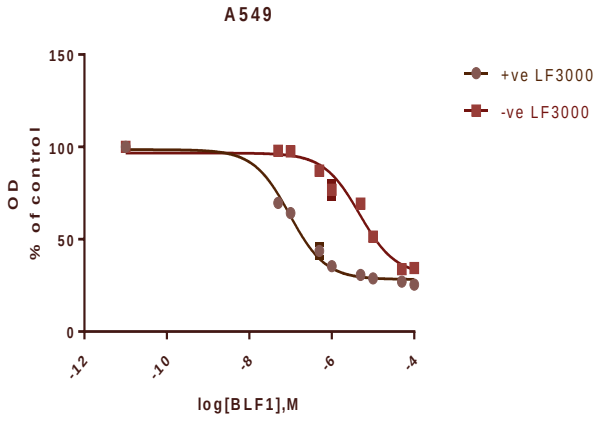
A549
150
100
50
0
OD
% of control
-12
-10
-8
-6
-4
log[BLF1],M
+ve LF3000
-ve LF3000

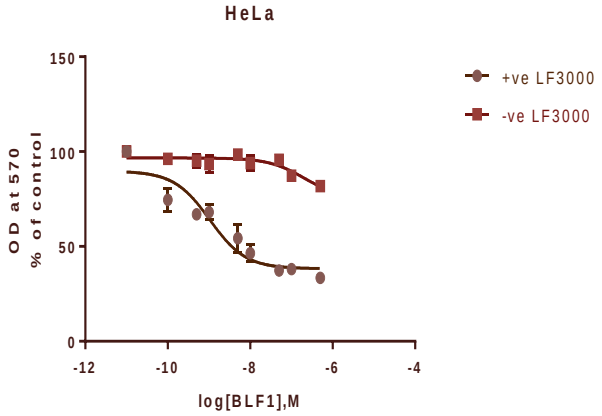
HeLa
150
100
50
0
OD at 570
% of control
-12
-10
-8
-6
-4
log[BLF1],M
+ve LF3000
-ve LF3000

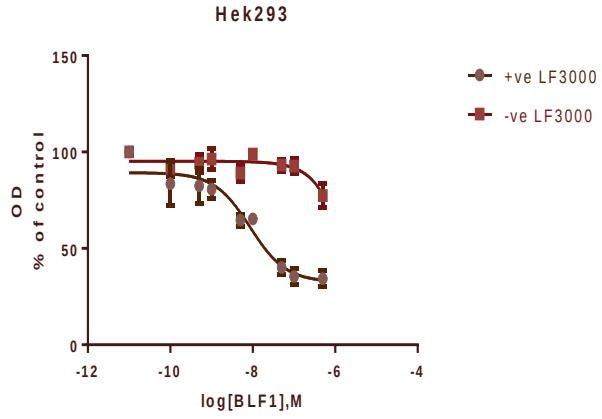
Hek293
150
100
50
0
OD
% of control
-12
-10
-8
-6
-4
log[BLF1],M
+ve LF3000
-ve LF3000

B.

Cell line	IC_{50} with LF3000		IC_{50} without LF3000	
	Log IC_{50}	µM	Log IC_{50}	µM
J774.2	-8.859	$1.3X\ 10^{-3}$	-8.072	$8X\ 10^{-3}$
RAW	-10.97	$1.07X\ 10^{-5}$	-7.564	$2.7X\ 10^{-2}$
A549	-7.022	$9X\ 10^{-2}$	-5.325	4.73
HeLa	-8.979	$1X\ 10^{-3}$	-6.695	$2X\ 10^{-1}$
HEK293	-8.062	$8.6X\ 10^{-3}$	-3.862	$1.3X\ 10^{2}$

Figure 3.3.12: Effect of lipofectamine on the sensitivity of various cell lines to BLF1:
A. Enzyme transduction using LF3000 was performed 4 hr after plating cells as previously described in 96 well plates. BLF1 was pre-incubated for 5 minutes at 20°C in Optimem media with/without the transfection reagents (2.2.2.3) before adding to the cells and culturing for 72 hr. Cellular growth was assessed using the SRB assay as described previously. Three independent experiments were performed in quadruplicate **B**. IC_{50} values indicate the concentration of BLF1 with/ without LF3000 needed to inhibit 50% of cellular growth.

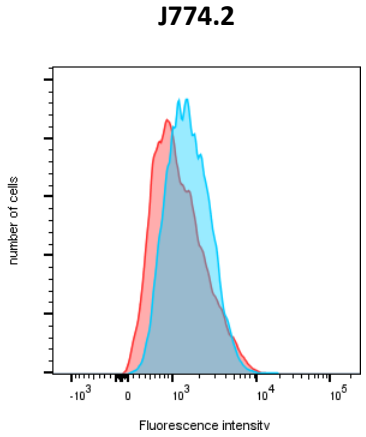

Figure 3.3.13: Flow cytometry analysis of the uptake of FITC-dextran by J774.2 cells in the presence or absence of lipofectamine:
Cells were cultured in 6 well culture plates overnight. FITC- tagged dextran (MW 70 kDa) was pre-incubated for 5 minutes at 20°C in Optimem media with/ without the transfection reagents before adding to the cells for 1 hr at 37°C. Cells were then harvested and analysed by flow cytometry as described previously. The overlay histogram represents the fluorescence intensity of J774.2 cells incubated with FITC-dextran in the presence of LF3000 (blue) or diluent (red).

3.3.4 Comparison of the capacity for macropinocytosis by cells with different sensitivities to BLF1:

3.3.4.1 Measurement of macropinocytosis by uptake of fluorescent dextran:

To investigate the relationship between BLF1 sensitivity and macropinocytosis, we measured the rate of macropinocytosis of different cell lines using fluorescent dextran and flow cytometery (Mohler and Sharief, 1993). In addition to the previous cell lines described, we used a rat basophilic cell line (RBL2H3) transfected with human CD63 antigen, used later as model for testing the cytostatic/cytotoxic effect of BLF1 targeted conjugate. Furthermore, the mouse neuroblastoma cell line (N2a) was also included, as it had been reported that the N2a is 100 times less sensitive than J774.2 cells to BLF1 (Rust et al., 2015). The results revealed that the mouse macrophage J774.2 and RAW cell lines exhibited a much higher uptake of FITC-labelled dextran compared to the other cell lines (**Fig**.3.3.14.A.B). Fluorescence imaging of cells incubated with FITC-labelled dextran confirmed the observation made by flow cytometry (**Fig**.3.3.14.A); there is significant level of uptake of dextran by J774.2 cells at 37°C compared to cells incubated on ice. However the human kidney cell line (HEK293) did not show any uptake compared to cells incubated on ice (**Fig.**3.3.15).

A.

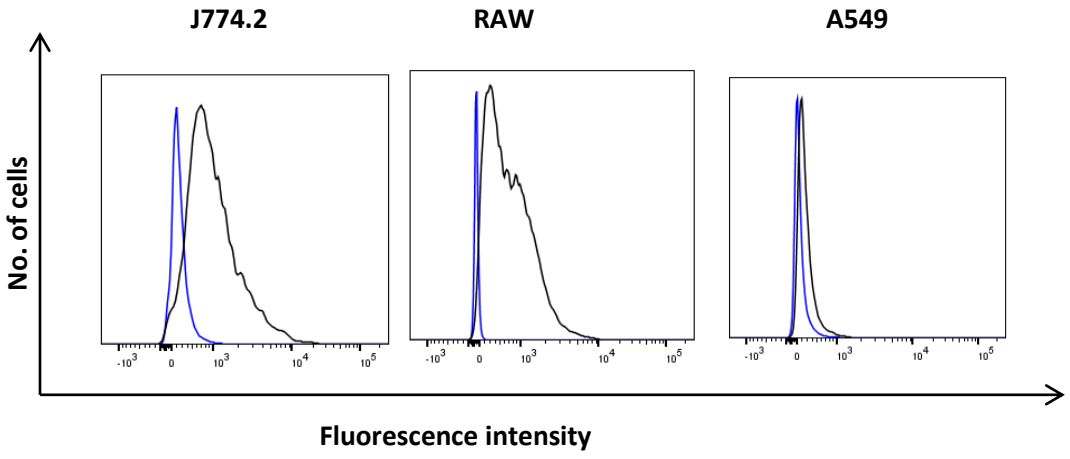

B.

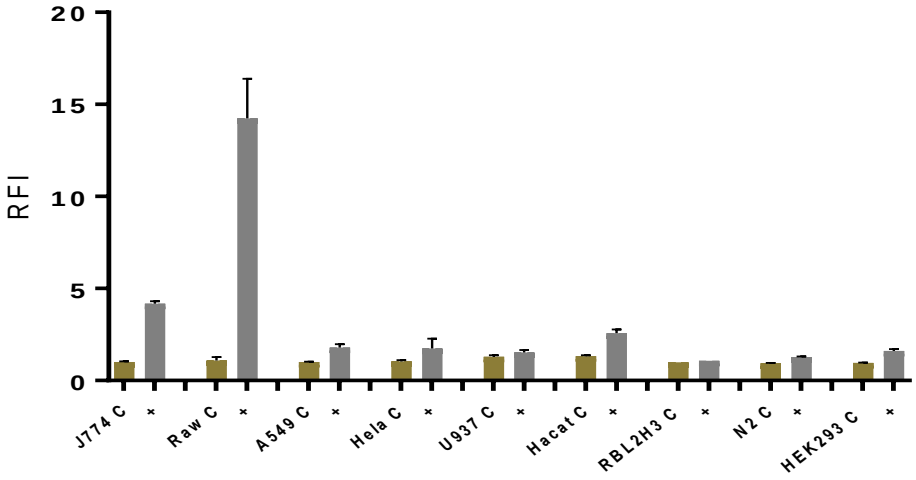

Figure 3.3.14: Flow cytometry analysis of fluorescent dextran uptake by different cell lines:

Cells were cultured in 6 well culture plates overnight and incubated with medium containing FITC- labelled dextran (70 kDa) as described in (2.2.8.2). After 1 hr at 37°C or on ice, cells were harvested and analysed by flow cytometry **A**. The overlay histogram of fluorescence intensities of cells incubated with FITC-dextran at 37°C (black) and on ice (blue) for J774.2, RAW and A549 cells **B**. Relative fluorescence intensity values for different cell lines incubated with FITC-dextran. This was calculated as the ratio of the median fluorescence intensity (MFI) of cells incubated with FITC-labelled dextran: MFI of cells incubated with medium alone. The experiments were performed three times in duplicate. Values represent mean ± SEM.

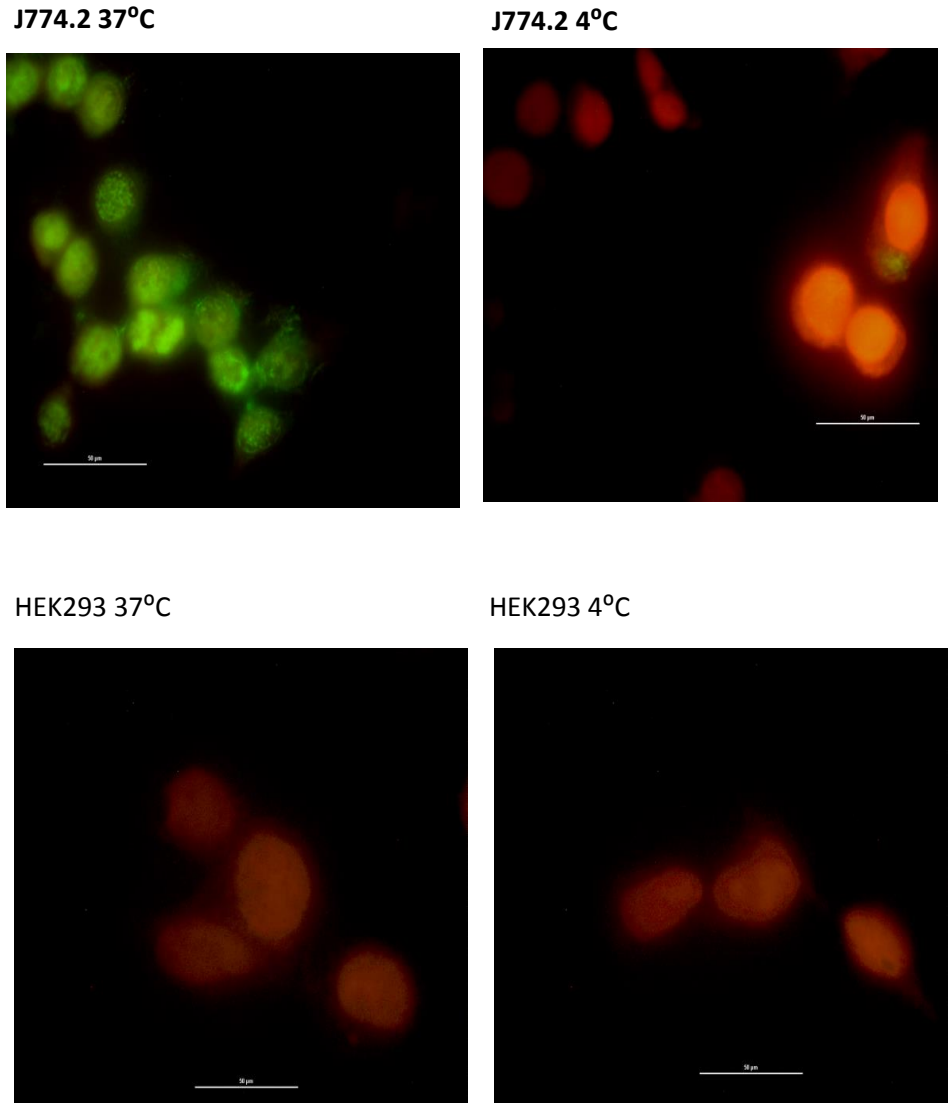

Figure 3.3.15: Fluorescence microscopy images of FITC-dextran uptake by J774.2 and HEK293 cells:
Cells were seeded into 8-well LAB TEK™ chamber slides overnight and incubated with FITC-labelled dextran (70 kDa). After 1 hr at 37°C or on ice, cells were fixed and nuclei were counterstained with propodium iodide (red). Slides were imaged using a Nikon Eclipse E400 Fluorescence microscope (100 x oil objectives) scale bar = 25 µm.

3.3.4.2 Inhibition of macropinocytosis by amiloride:

As described previously (3.1.3) macropinocytosis is uniquely sensitivite to the inhibitor amiloride. To further investigate this mechanism, the uptake of FITC-dextran by mouse macrophage J774.2 cells and human lung cancer A549 cells was assessed in the presence of different concentrations of amiloride. Flow cytometry data demonstrated significant inhibition of FITC-labelled dextran uptake by about 70% in mouse macrophage J774.2 in the presence of 3 mM amiloride (**Fig**.3.3.16.A). The inhibitor was nontoxic for the J774.2 cells at the concentration used as demonstrated by an unchanged scatter profile of the treated cells in flow cytometry (**Fig.**3.3.16.C). In addition, as previously, little uptake of dextran and no inhibitory effect were observed with amiloride in the lung cancer cell line A549 (**Fig.**3.3.16A).

A.

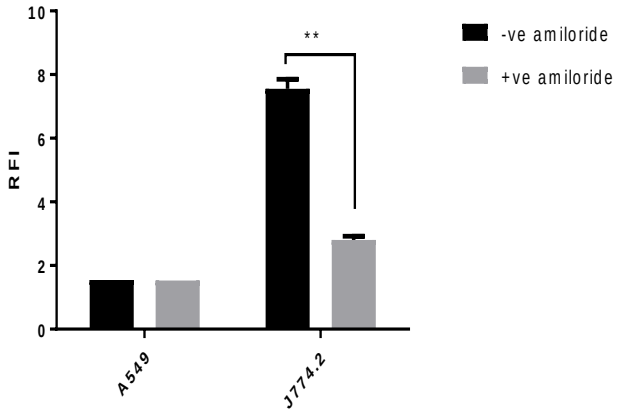

B.

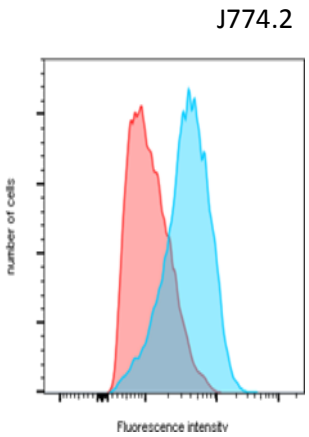

C.

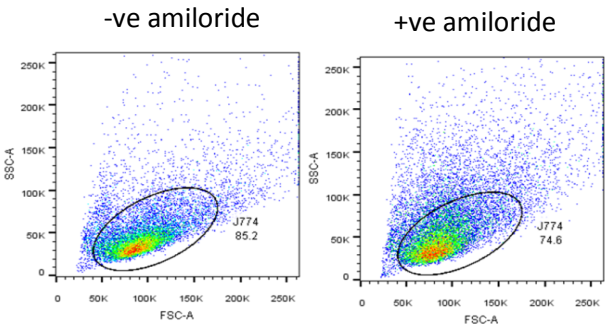

Figure 3.3.16: Effect of amiloride on the uptake of FITC- dextrans:
Cells were cultured in 6 well plate overnight and then treated with 3 mM amiloride or diluent (-ve amiloride) for 30 minutes prior to incubation with FITC labelled dextran for 1 hr as described in 2.2.4. Cells were harvested and analysed by flow cytometry. **A**. Data are expressed as RFI (relative fluorescence intensity) i.e ratio of median fluorescence intensity (MFI) of cells incubated with FITC-labelled dextran to MFI of cells not incubated with dextran). **B**. Overlying histogram of fluorescence intensity of J774.2 cells incubated with FITC-dextran in the presence of 3 mM amiloride (red) or diluent alone (blue). **C.** The dot plot shows the amiloride treated and non-treated J774 cells gated according to forward scatter (FSC) and side scatter (SSC).

3.3.5 Investigation of BLF1 uptake and intracellular transport using mCherry tagged BLF1:

In order to investigate and monitor the uptake and intracellular localisation of BLF1, an mCherry tagged version of BLF1 (described in 3.3.1) was used. In some experiments, a rat antibody specific to BLF1, provided by Professor David Rice, was also used (2.1.2.1).

3.3.5.1 Cytostatic/cytotoxic effect of mCherry tagged BLF1:

Initially, experiments were carried out to determine if tagging the BLF1 toxin with mCherry had any effect on its activity. The effects of wild type and mCherry tagged BLF1 were assessed alongside one another on the mouse macrophage cell lines J774.2 and RAW264 using the SRB assay as previously described. As shown in **Fig**.3.3.17, mCherry BLF1 exhibits the same level of growth inhibition as the untagged protein.

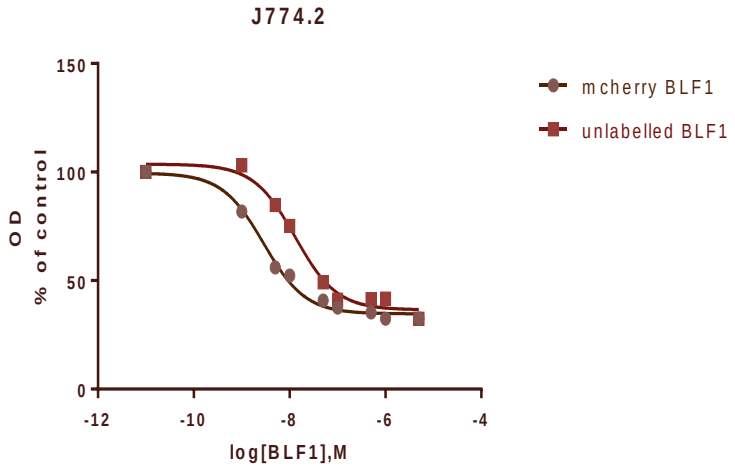

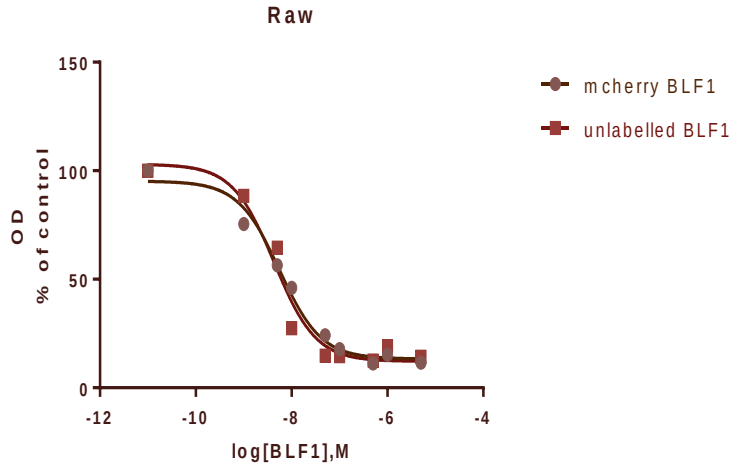

Cell line	mCherry BLF1		BLF1	
	Log IC_{50}	µM	Log IC_{50}	µM
J774.2	-8.542	$2.8X10^{-3}$	-7.883	$1.3X\ 10^{-2}$
RAW	-8.250	$5X\ 10^{-3}$	-8.363	$4X\ 10^{-3}$

Figure 3.3.17: Effect of mCherry-tagged and wild type BLF1 on J774 and RAW264 mouse macrophage cell lines:
Cells were cultured in the presence of wild type or mCherry tagged BLF1 for 72 hr and cellular growth was assessed using the SRB assay as described in **Fig**.3.3.4. Two independent experiments were performed in quadruplicate (mean ± SEM).

3.3.5.2 Investigation of BLF1 cell surface binding:

It was previously reported that BLF1 lacks a cell surface binding domain required for efficient cellular entry (Cruz-Migoni et al., 2011). Since the BLF1 producing pathogen is intracellular, BLF1 does not require a binding domain to reach the host cytoplasm. However, binding of BLF1 to the J774.2 cell line, which efficiently takes up the toxin, had not been directly investigated.

3.3.5.2.1 Flow cytometry analysis of cell surface binding of mCherry tagged BLF1 to J774.2 cells:

This experiment was designed to evaluate the binding of mCherry tagged BLF1 to the surface of J774.2, cells which were shown previously to be sensitive to the tagged toxin (**Fig**.3.3.17). Flow cytometry data confirmed that there is no surface binding of mCherry BLF1 to J774.2 as compared with mCherry protein. (**Fig**.3.3.18). The fluorescence intensity observed for cells incubated with the mCherry proteins is essentially the same as the autofluorescence observed for unstained cells (incubated with buffer alone).

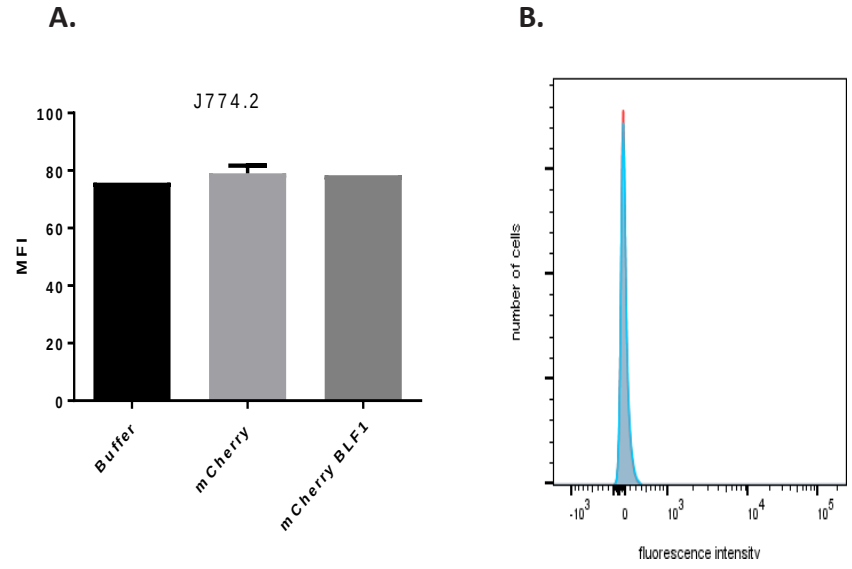

Figure 3.3.18: Binding of mCherry tagged BLF1 to mouse macrophage J774.2 cells:
Cells were incubated on ice for 1 hr with either wash buffer, 5 µM mCherry protein, or 5 µM mCherry tagged BLF1 as described in 2.2.4.2. After washing, stained cells were analysed by flow cytometry using 610/20 filter. **A.** Fluorescence intensity of cells is expressed as MFI. Two independent experiments were performed in duplicate; mean ± SEM. **B**. Overlying histogram of fluorescence intensity of J774.2 cells incubated with mCherry BLF1 (red) and mCherry alone (blue).

3.3.5.2.2 Flow cytometry analysis of cell surface binding of unlabelled BLF1:

In an effort to detect and amplify the signal from any low level binding of BLF1 to cells, the binding of wild type (untagged) BLF1 was assessed using a newly developed BLF1 specific rat antibody and a secondary FITC-labelled antibody as described in (2.2.4.1). Binding to mouse macrophage J774.2 cells (which are sensitive to the toxin) and human lung cancer A549 cells (which are less sensitive to the toxin) was investigated. As shown in **Fig.**3.3.19, there is no evidence of BLF1 binding to a receptor on either of these cell types, since the fluorescence intensities obtained with BLF1 and the rat BLF1 antibody show no difference relative to those obtained with rat serum control or BLF1 and secondary antibody alone.

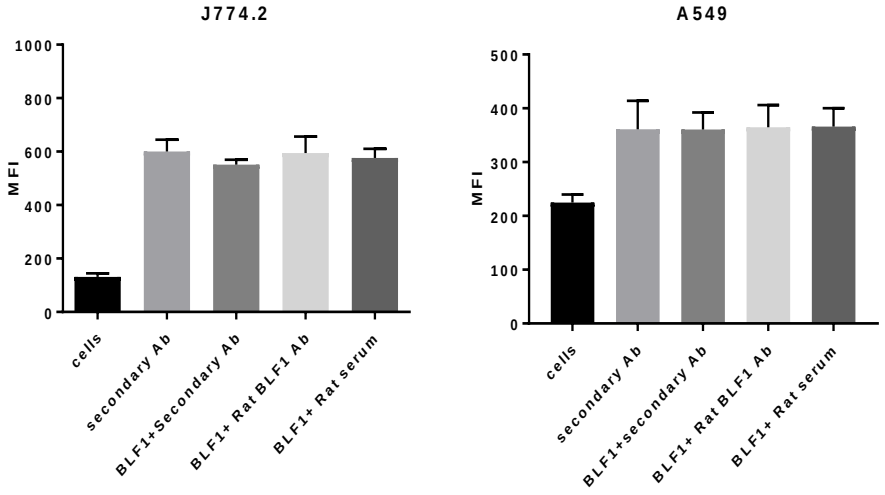

Figure 3.3.19: Binding of untagged BLF1 to mouse macrophage J774.2 and human cancer A549 cells:
Cells were incubated with unlabelled BLF1 (5 µM) on ice, followed by rat anti-BLF1 antibody or rat serum control and secondary anti rat FITC IgG antibody before analysis by flow cytometry as described in 2.2.4.1. A control for cell autofluorescence (cells incubated with wash buffer only) was included. Data are expressed as MFI. The experiment performed three times in duplicate, values represent mean ± SEM.

3.3.5.3 Investigation of BLF1 uptake by flow cytometry:

3.3.5.3.1 Flow cytometry analysis of mCherry tagged BLF1 uptake:

As described in section 3.3.4 mouse macrophage cells (J774.2 and RAW264) exhibit high rates of macropinocytosis of fluorescent dextran compared with human epithelial cancer cell lines (A549, HeLa). This is assumed to explain the greater sensitivity of the macrophage cell lines to BLF1 in the absence of delivery reagents such as lipofectamine. Thus, we measured the rate of uptake of mCherry tagged BLF1 by the J774.2 and A549 cells over a 1 hour period. Initial experiments indicated that the uptake by J774.2 cells was higher than A549 cells; however the fluorescence intensity was low compared to that of FITC-dextran over the same period (**Fig.**3.3.20).

The uptake of mCherry tagged BLF1 and mCherry tagged C94S mutant was therefore investigated over a longer time period. The mCherry tagged C94S mutant was included here since it is enzymically inactive, so should not cause toxicity over the longer time period. Since an estimate of dead cells can be made by flow cytometry based on their scatter profiles, the effect of these proteins on cell viability was also assessed. Analysis by flow cytometry demonstrated that mCherry tagged BLF1 and C94S was present at significant levels by 24 hour (**Fig**.3.3.21.A, B), with most cells staining positively for mCherry. The histogram depicted in **Fig**.3.3.21.C demonstrates that by 24 hours both mCherry BLF1 and mCherry C94S show a 10- fold increase in fluorescence intensity compared to the negative control.

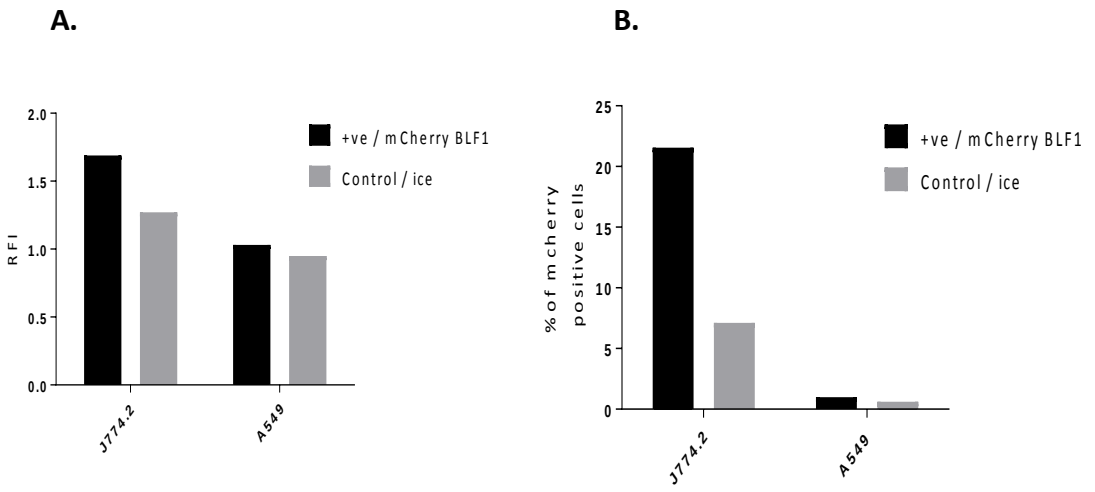

Figure 3.3.20: Flow cytometry analysis of mCherry-BLF1 uptake in J774.2 and A549 cells: J774.2 and A549 were seeded in a 6-well plate and incubated with medium containing 100 µg/ml mCherry-BLF1 for 1 hr at 37°C or on ice (control) as described in 2.2.4.2. After washing, cells were harvested and analysed by flow cytometery as previously described in **Fig.**3.3.18. (**A**) Relative fluorescence intensity (MFI of cells incubated with mCherry-BLF1: MFI of cells incubated in medium). (**B**) Percentage of cells stained with mCherry-BLF1.

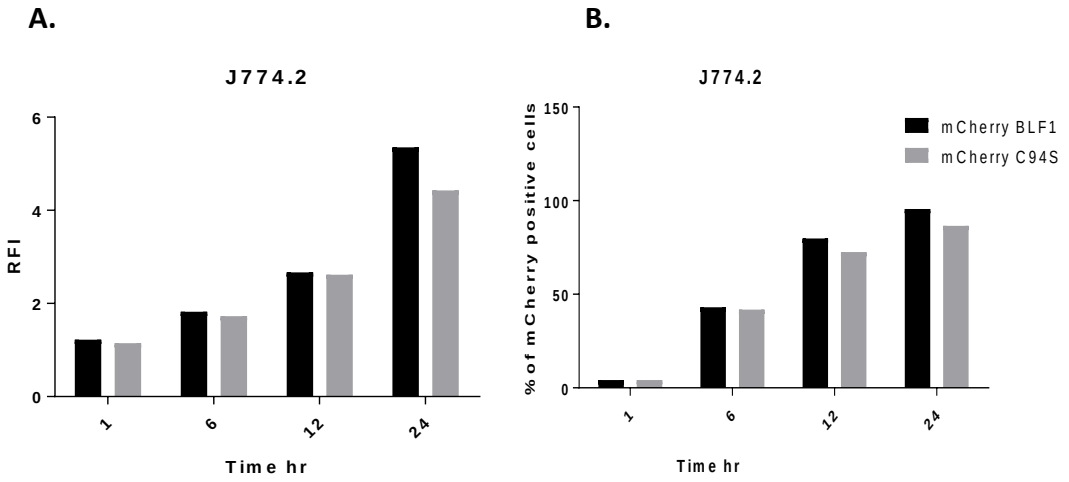

C.

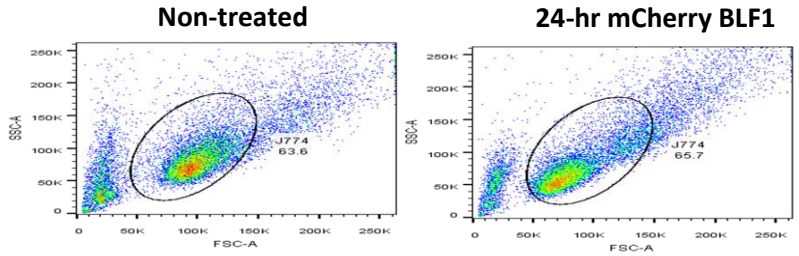

D.

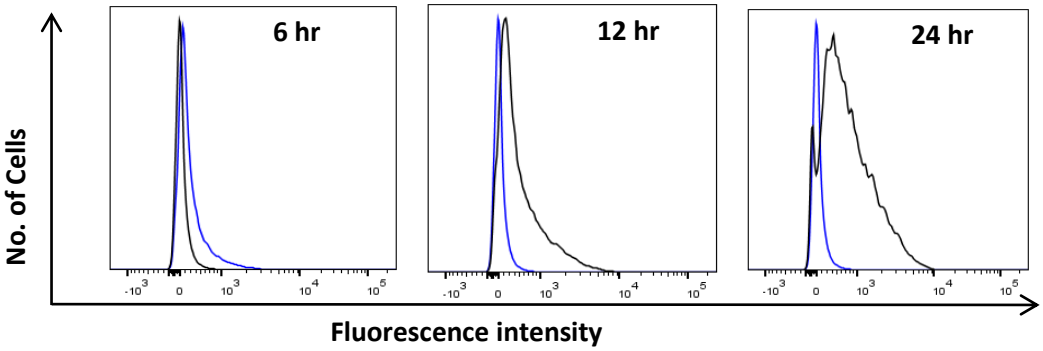

Figure 3.3.21: Flow cytometry analysis of mCherry-BLF1 and mCherry- C94S uptake over 24 hours:

J774.2 cells were seeded in 6 well culture plates and incubated with 100 µg/ml mCherryBLF1 or mCherry-C94S for 1 hour, 6 hours, 12 hours, and 24 hours. After washing, cells were harvested and analysed using flow cytometry as described in **Fig**.3.3.16. (**A**) Relative florescence intensity (MFI of cells incubated with mCherry labelled BLF1: MFI of cells incubated in medium). (**B**) Percentage of cells stained with mCherry. (**C**) The dot plot shows the mCherry BLF1 treated and non-treated J774 cells gated according to forward scatter (FSC) and side scatter (SSC).(**D**) Overlying histogram of fluorescence intensity of cells incubated with mCherry-C94S (black) or diluent (blue).

3.4 Discussion:

Previously it had been shown that BLF1 was only toxic to cells such as mouse 3T3 fibroblasts if deliberately introduced into the cytoplasm using protein delivery agents such as BioPORTER. However, the mouse macrophage cell line J774.2 was sensitive to the toxin in the absence of such agents, presumably due to active uptake of BLF1 by macropinoytosis (Cruz-Migoni et al., 2011). It was therefore of interest to investigate the sensitivity of other cell lines to BLF1, particularly those of mononuclear phagocyte origin, since active macropinocytosis is a feature of antigen presentation (Norbury et al., 1995, Sallusto et al., 1995). In addition, we wished to determine if the effects of BLF1 on different cell types in the absence of protein delivery agents correlated with their capacity for macropinocytosis.

The results here have shown a significant effect of BLF1 on the long-established mouse macrophage cell lines J774.2 and RAW264.7 growth (Ralph and Nakoinz, 1977a)(**Fig**.3.3.3,3.3.4,3.3.6), even at low doses (0.5 µM), confirming previous results. BLF1 had also effective impact on cellular growth of mouse macrophage cell lines established more recently by retroviral transformation of bone marrow derived macrophages (Ha et al., 2005) although with reduced sensitivity observed at 0.5 µM (**Fig**.3.3.5). These cell lines were established from wild type Balb/c mice or mice that had been knocked out for the *CD9* tetraspanin gene and were being used by other laboratory members for research into the function of CD9. It was noted that the CD9 -/-macrophages were slightly less affected by BLF1 than the wild type macrophages. CD9 is a member of the tetraspanin superfamily of proteins, which are known to be involved in membrane trafficking (Charrin et al., 2014). It might be interesting in the future to compare rates of macropinocytosis between these cell lines.

However, BLF1 did not show any effective impact on cellular growth of THP1 and U937 human monocyte cell lines or the human promyelocytic cell line HL60 (**Fig**.3.3.7). In addition, no effect of BLF1 was seen when THP1 cells were treated with phorbol ester to differentiate them to macrophages (**Fig.**3.3.8). However, phorbol ester also inhibits cell division and slows the growth of cells. A similar effect was also observed with J774.2 as they were no longer sensitive to BLF1 after stimulation with PMA and stopped dividing (**Fig**.3.3.9). This suggests that slowly dividing cells are less affected by the inhibition of eIF4A caused by BLF1 toxin. The possibility that PMA reduces macropinocytosis by J774.2 cells is

considered unlikely, as phorbol esters are reported to stimulate macropinocytosis by macrophages (Swanson, 1989). Interestingly, unpublished data from our group has shown that non-dividing primary human monocytes cultured for up to 5 days with BLF1 were also not affected by the toxin (Lynda Partridge, personal communication).

The effect of BLF1 on a variety of human cell lines was also investigated. Some growth arrest effects were observed with high doses of BLF1 (5 μM) with A549 lung cancer and HeLa human epithelial cells and at lower doses of BLF1 (0.5 μM) with the human melanoma cell line, MeWo (**Fig.**3.3.10). In addition, a significant growth arrest was observed in the non-cancer derived HaCat (keratinocyte) cell line which is reported to have a high rate of macropinocytosis and was used in previous studies to show that HPV-16 entered cells by a macropinocytosis –like process (Schelhaas et al., 2012)(**Fig.**3.3.11B). Interestingly, BLF1 showed no efficiency in arresting the cell growth of normal HEK293 epithelial cell line (**Fig.**3.3.11A). This suggests that BLF1 has a wider therapeutic window unlike other toxin that will be of benefit for future immunotherapy development.

For cells that did not take up BLF1 efficiently by macropinocytosis, it was of interest to determine their sensitivity to the toxin once it has been introduced into the cytoplasm. This chapter also highlights the use of an efficient and simple way to deliver BLF1 toxin into different cell types (**Fig**.3.3.12, 3.3.13). A method for delivering botulinum toxin into cell lines using DNA transfection reagents has previously been described by our collaborators (Arsenault et al., 2014) and here we used a more recently developed form of lipofectamine (LF3000) that greatly increased the efficiency of BLF1 delivery by around 100-1000 fold, allowing killing to be observed in nanomolar concentrations (Rust et al., 2015). Lipofection reagents generally rely on positively charged lipids (liposomes) interacting with negatively charged DNA (Felgner et al., 1994). Later formulations also contain a neutral co-lipid that helps promote fusion of the liposome with the plasma membrane (Dalby et al., 2004). The exact mode of action of LF3000 is unclear for proprietary reasons. However, its activity seems to be charge independent, unlike previous formulations, as it can deliver saporin (which is positively charged at neutral pH) into cells (Rust et al., 2015). This suggests it contains neutral co-lipid that could be sufficient for protein delivery.

The possible role of macropinocytosis in the uptake of BLF1 toxin was investigated in a range of cell lines by measuring their ability to take up fluorescent dextran, a commonly

used method of measuring macropinocytosis (Davis et al., 1986) (**Fig**.3.3.14). Flow cytometry data revealed that the mouse macrophage cell lines J774.2 and RAW246.7 internalised dextran much more efficiently than other cell lines studied. Indeed, professional macrophages are known to exhibit not only phagocytosis but also high rates of macropinocytosis (Lim and Gleeson, 2011), which may explain the significant effect of BLF1 on these cells. Notably, however, the human monocytic cell line U937 did not exhibit high rates of macopinocytosis. As mentioned previously, this may have been due to the relatively immature phenotype of these cells. As also mentioned previously, even when U937 cells were stimulated to differentiate with phorbol ester, they were still insensitive to BLF1. It may have been interesting to investigate dextran uptake by these more mature cells; however, on phorbol ester stimulation, the U937 cells became very adherent and formed clumps, making analysis by flow cytometry difficult. Some cancer cells have been reported to show increased levels of macropinocytosis, which may support proliferation (Commisso et al., 2014). This may explain the slight effect of BLF1 alone on A549 and HeLa cells. However, uptake of fluorescent dextran by the A549 and HeLa cells did not appear to be high relative to those cell types that were less sensitive to BLF1 (e.g. HEK293 cells). It should be noted that the uptake of dextran was determined only after 1 hr of incubation, and macropinocytosis activity might be slower in epithelial cells than in macrophages. The non-cancer derived keratinocyte cell line, HaCat, which was relatively sensitive to BLF1, did show some elevation of macropinocytosis relative to the other cell lines.

Furthermore, pre-incubation of J774.2 cells with 3 mM amiloride, a known inhibitor of macropinocytosis (Koivusalo et al., 2010) for 30 minutes lead to significant inhibition of fluorescent dextran uptake (**Fig.**3.3.16), confirming that this was the mechanism of uptake.

Finally, experiments were carried out using a fluorescently tagged version of BLF1 to investigate its uptake directly. Titration experiments in the mouse macrophage cell lines (J774.2 and RAW246.7) demonstrate a similar potency of mCherry tagged BLF1 to the wild type (**Fig.** 3.3.17). Hence the presence of the N-terminal tag and the increase in the size of mCherry tagged BLF1 to 52 kDa had no impact on the toxin efficiency.

Analysis of the binding of mCherry tagged BLF1 to the surface of J774.2 by flow cytometry showed no evidence of interaction with any type of receptor (**Fig**.3.3.18) and this was confirmed for untagged BLF1 using an anti-BLF1 antibody (**Fig**3.3.19). This confirms that

there is no receptor for BLF1 on J774.2 and A549 cells and the uptake of the toxin by these cells is through nonspecific uptake involving macropinocytosis. This finding is consistent with the previous report that the only specific interaction of BLF1 in mammalian cells was with eIF4A, as demonstrated by affinity chromatography and pull-down experiments using BLF1 as the ligand (Cruz-Migoni et al., 2011). However, direct binding of BLF1 to J774.2 and A549 cells had not previously been investigated.

Flow cytometry analysis of mCherry-labelled BLF1 uptake over 1 hr in J774.2 and the human epithelial cell line A549 (**Fig.**3.3.20) demonstrated greater uptake of mCherry BLF1 by J774, consistent with a greater rate of macropinocytosis.

Flow cytometry analysis in the mouse macrophage cell line revealed that mCherry BLF1 accumulated gradually inside cells and was present at detectable levels in almost all J774.2 cells by 24 hr (**Fig**.3.3.21), again indicating a non-specific fluid phase uptake by macropinocytosis. However, detection of the mCherry signal using the lasers available on the flow cyotmeter was relatively inefficient, as indicated by the relatively low fluorescence intensities observed here (**Fig.**3.3.21D). Interestingly, fluorescent microscopy studies carried out in cooperation with Professor Bazbek Davletov's laboratory confirmed that the uptake of mCherry C94S was strongly reduced in J774.2 by pre-incubation with amiloride. Fluorescence microscopy also showed very high levels of co-localization of mCherry-tagged C94S with fluorescent dextran (Rust et al., 2015). It therefore appears very likely that susceptibility of the mouse macrophage cell line to BLF1 is at least in part due to the high rate of macropinocytosis.

In summary, our investigations revealed that the enhanced uptake via macropinocytosis accounts for the increased sensitivity to the action of BLF1 toxin in the macrophage cell lines tested. However, other cells lines are only sensitive at higher concentration of the toxin. In addition, the work suggests that BLF1 is primarily active against rapidly dividing cells, consistent with what is known about the role of eIF4A. Overall, this suggests that BLF1 is suitable for development as a therapeutic agent for cancer.

4 Chapter 4: The functional assessment of model BLF1/antibody conjugates.

4.1 Introduction:

There has been considerable interest in the past few years in the area of drug targeting as it has become clear that minimal interaction with the non- targeted site is required to achieve an optimal pharmacological action of the drug. As stated in Chapter 1, this thesis focuses on the recent approach for cancer treatment which is the immunotoxin. The main toxins currently used for clinical development of targeted toxin therapy are limited to Diphtheria toxin (DT), Pseudomonas exotoxin A (PE), and a numbers of ribosomal inactivating proteins (RIPs) such as ricin, saporin and gelonin despite hundreds of toxins that have been identified over the past three decades (Pastan et al., 2006). All currently used toxin conjugates in clinical trials exhibit off-target toxicity by blocking protein synthesis that causes cell death. The non-specific cytotoxic action causes dose limiting side effect such as hepatotoxicity and vascular leak syndrome (VLS) (Alewine et al., 2015) and was described in Chapter 1. In chapter 3, BLF1 was shown to arrest cell proliferation in a range of cancer cell lines at its highest concentration and the sensitivity to BLF1 increased in the presence of lipofectamine. However, BLF1 showed only a slight effect at the highest concentration on an embryonic kidney cell line and no effect on a non-dividing macrophage cell line. This suggests that BLF1 has a selective cytotoxic activity unlike the previously identified toxins. BLF1 therefore appears to be suitable for development as an immunotoxin, by coupling it chemically to specific monoclonal antibodies. As chemical coupling requires a relatively large amount of the proteins (BLF1 and monoclonal antibodies), some initial studies were carried out using model immunoconjugates, where BLF1 was non-chemically linked to specific monoclonal antibodies. The aim here was to carry our preliminary studies on the parameters important for successful targeting of BLF1 to cancer cells. It was also hoped that these methods might provide a general strategy for screening the suitability of particular antibody: toxin combinations prior to direct chemical cross-linking.

4.1.1 Targeting antigens:

One of the key points for a successful immunotoxin is to choose an appropriate target antigen that monoclonal antibodies bind to with adequate affinity and allow the release of toxin payload following antigen specific binding (Alewine et al., 2015). In this work, the efficiency of anti-CD63 and anti-CD9 antibodies for targeting and delivering BLF1 toxin by non-covalently assembled conjugate was tested. As described in Chapter 1, CD63 is a member of the tetraspanin superfamily that was discovered on the cell surface of blood platelets and in early stage human melanoma cells. Many studies indicated that CD63 is expressed mainly in the intracellular compartment such as endosomes and lysosomes and also present at the cell surface (Rous et al., 2002, Janvier and Bonifacino, 2005, Peden et al., 2004). A key property of the CD63 antigen for its application is its rapid internalization after antibody binding. CD63 has a lysosozomal/internalization domain at its C-terminus that allows it to interact with adaptor protein complexes, promoting internalization by clathrin-mediated endocytosis. Thus, CD63 seems to be an attractive model antigen for efficient toxin delivery. Hybridomas secreting monoclonal antibodies to CD63 were also available in house, therefore relatively large amounts of antibody could be produced for conjugating with the toxin. Interestingly, although CD63 is used here just as a model, the use of AR7BD-33-11A, an anti-CD63 monoclonal antibody (patent AR7BD-33-11A "Characterization of the therapeutic anti-cancer antibody AR7BD-33-11A antigen"), has shown efficacy in preclinical models of human prostate, breast and colon cancer. This antibody was also effective in suppressing tumor in A375 and A2058 melanoma models respectively. AR7BD-33-11A antibody was reported to mediate its anti-cancer effect through ADCC and direct antibody effects that lead to cell death (patent AR7BD-33-11A "Characterization of the therapeutic anti-cancer antibody AR7BD-33-11A antigen").

CD9 is another member of the tetraspanin family, as also described in Chapter 1. Unlike CD63, CD9 does not have a C-terminal lysozomal targeting/internalization motif so would not be expected to internalize rapidly. Targeting this antigen would make an interesting comparison with CD63. In addition, monoclonal antibodies to CD9 were available "in house". Again, although used here as a model antigen, previous studies have shown that CD9 expression was up-regulated in chemo resistant small cell lung cancer and it was identified as an important prognostic marker in adenocarcinoma of the lung (Higashiyama

et al., 1997). Moreover, high levels of CD9 expression were observed in patients with gastric cancer without metastasis; however low levels of CD9 were associated with distant metastasis. It has been therefore suggested that targeting CD9 could be useful to treat malignancies (Murayama et al., 2015). Moreover, the attachment of a cytotoxic payload, such as a toxin, to the anti-CD9 antibody may help to improve the treatment further. Also we have previously generated monoclonal antibody to the CD9 antigen.

4.1.2 Cell line models:

A cell line initially selected for testing immunoconjugates was the rat basophilic leukaemia cell line (RBL2H3), since our research group has generated many stable transfectants of these cells expressing human tetraspanin antigens (Smith et al., 1995, Higginbottom et al., 2000) including wild type and mutated versions of human CD63 that vary in their expression and capacity to internalize. It was hoped that such cell lines would provide a good models for investigating the importance of these properties i.e level of target expression, capacity to internalize in developing immunotoxin. Furthermore, the anti-CD63 antibodies available are specific to human CD63, so untransfected cells provide a good control. The anti-CD63 antibody used here (see table 2.1.6) (Azorsa et al., 1991), had previously been shown to be specific for human CD63, with no cross-reactivity with rat CD63. This cell line was therefore investigated as model for assessing the cytotoxic effect of BLF1 targeted conjugate. The A549 human lung cancer cell line was also selected. This cell line was originally developed by culturing cancerous lung tissue from a 58 years old Caucasian male (Giard et al., 1973). This cell line has been previously used to investigate the anti-tumor efficiency of different immunotoxins (Zhou et al., 2012, Zimmermann et al., 1997, Ho et al., 2007, Borowiec et al., 2016). In addition, previous data in (3.3.2.3.3) A549 cells were sensitive to BLF1 toxin particularly in presence of lipofectamine (3.3.3). The level of cell surface CD63 and CD9 on A549 cells was assessed to determine if these target antigens were suitable for allowing specific delivery of toxin to the tumor cells.

4.1.3 Development of model targeted BLF1 conjugates:

To investigate whether anti-CD63 or anti-CD9 antibodies could promote the targeting of BLF1 toxin, we generated a model conjugate, in which antibody coated magnetic beads were used to couple BLF1 to antigen-specific monoclonal antibodies (CD63 or CD9). In previous proof-of-concept work by a member of our group, conjugates comprised of such

beads together with BLF1, TRAIL (which binds to death receptors on tumour cells) and a targeting antibody to CXCR4 (an internalising chemokine receptor) were shown to induce substantial cell death in in vitro models of pancreatic, liver, breast, cervical cancer and myeloma (Tazzyman et al., 2015).

In parallel, we also investigated a soluble version of a model immunoconjugate, where the toxin and targeting antibodies were linked using a secondary antibody. It was reasoned that this soluble model conjugate might more closely mimic a conventional immunotoxin and be taken up more easily by target cells. This model conjugate is illustrated in Figure 4.3.18. The secondary antibody chosen was in the form of F (ab') 2 fragments, to reduce any possible effects due to Fc receptor binding on target cells. In addition, the secondary antibody was specific to the Fc region of mouse IgG, to prevent interference with antigen binding. As previously this antibody was used to couple BLF1 to antigen-specific monoclonal antibodies (CD63 or CD9). Model conjugates were characterized using antigen positive for human CD63 (RBL transfected with human CD63) and antigen negative RBL cell line (WT). A human cancer epithelial cell line (A549) which is positive for both antigens was also investigated.

Initial *in vitro* studies were performed to examine the binding and the internalization of the model conjugate in the antigen expressing model cell line. Additionally, the toxicity of targeted BLF1 conjugate was investigated in antigen expressing model cell line.

4.2 Aims:

An initial aim was to investigate the expression of the target antigens (CD63 and CD9 on the model cell lines and assess their internalization on antibody binding. Model BLF1-antibody conjugates were then constructed and their ability to target BLF1 specifically to the antigen was assessed. Model conjugates were characterized using RBL2H3 cells transfected with human CD63 and antigen negative RBL2H3 cells (WT). A human cancer epithelial cell line (A549) which is positive for both antigens was also investigated. The next aims were to investigate internalisation of the BLF1 model conjugates by cells and to assess their effects on cell growth.

4.3 Results:

4.3.1 Design and optimization of BLF1/bead-targeting conjugate:

As mentioned above, prior to chemically coupling BLF1 to antibody, attempts were made to determine if BLF1 could be targeted specifically to cancer cells by coupling it to antibodies using non-chemical methods, in this instance commercially available magnetic beads covalently coated with anti-mouse IgG. The protocol is detailed in 2.2.3.2, but in brief, His-tagged BLF1 was first incubated with mouse anti-His before adding the targeting antibody (mouse anti-human CD9, CD63 or isotype control) followed by the anti-mouse IgG coated beads, to generate the conjugate (**Fig**.4.3.1). After separation and washing, the beads were re-suspended in 500 µl PBS and used either neat or at the dilutions indicated.

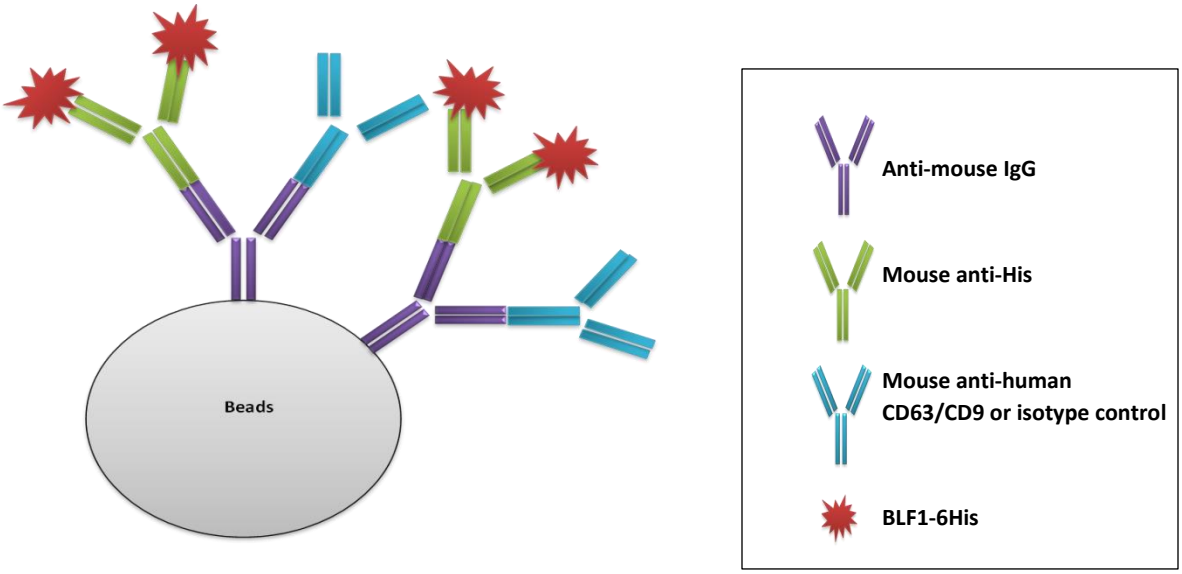

Figure 4.3.1: Diagrammatic representation of BLF1/bead targeting conjugate.

4.3.1.1 Expression of human CD63 on transfected rat basophilic cancer cell line (RBL2H3):

Initially the tetraspanin protein expression levels on the surface of model cancer cell lines was investigated as representative target antigens required for the selective binding of antibody-targeted immunotoxin. As mentioned previously, rat basophilic leukemia cells that had been stably transfected to express human CD63 were available and the anti-CD63 antibody used here is specific for human CD63. Data from flow cytometry confirmed the expression of human CD63 antigen by these cells (**Fig**.4.3.2).

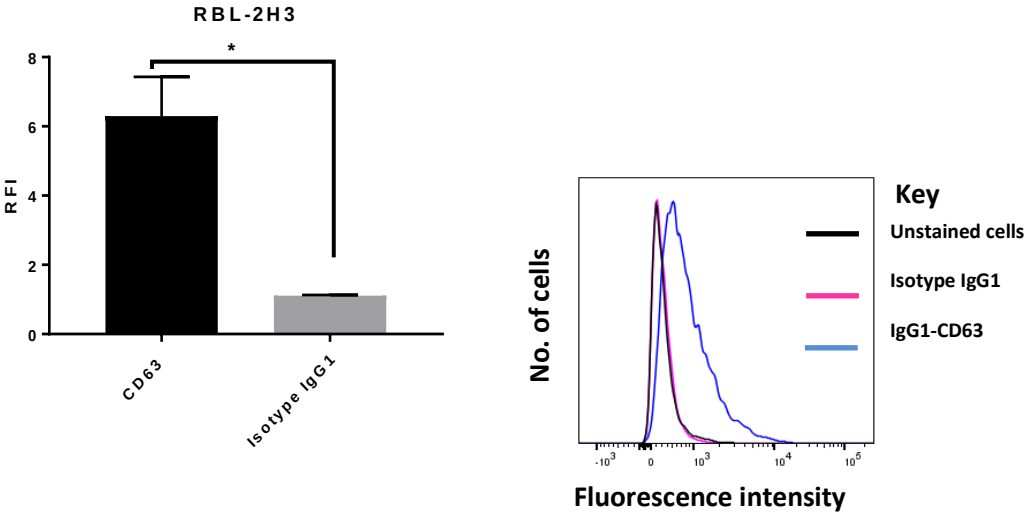

Figure 4.3.2: Surface expression of CD63 protein on rat basophilic leukaemia cells (RBL-2H3) transfected with human CD63:
Cells were incubated with anti-CD63 antibody or isotype control followed by secondary FITC-conjugated anti-mouse IgG antibody before analysis by flow cytometry as described in (2.2.4). **A**. Bar chart represents the relative fluorescent intensity (MFI of anti-CD63, or isotype IgG1: MFI of unstained cells. **B**. Overlay histogram of the fluorescence intensity of anti-CD63 and its isotype in transfected RBL-2H3 cells. Three independent experiments were performed in duplicate, with values shown as mean ± SEM. The significance of difference between anti-CD63 and isotype treated cells was determined by unpaired t- test at $p<0.05$.

4.3.1.2 Functional assessment of BLF1/anti-CD63 bead conjugate:

The resulting BLF1/anti-CD63 beads conjugate were tested for binding specificity for CD63 antigen, cytostaticity/cytotoxicity, and intracellular co-localization.

4.3.1.2.1 Assessment of binding specificity using enzyme linked immunosorbent assay (ELISA):

The binding specificity of the BLF1/anti-CD63 bead conjugate was initially assessed using recombinant protein corresponding to the large extracellular domain (EC2) of CD63 using ELISA. Previous studies by our group have shown that the recombinant EC2 fold correctly, is recognised by conformation-sensitive antibodies and is biologically functional (Parthasarathy et al., 2009). The rat anti-BLF1 antibody, provided by Professor David Rice and described previously in 2.2.4.1, was used to detect the toxin component of the bead conjugate. The results demonstrate that BLF1, as a part of the anti-CD63-toxin bead conjugate, can be targeted specifically to the EC2 domain of CD63 (**Fig**.4.3.3A), whereas there was no detectable signal with the corresponding isotype control-toxin bead conjugate (**Fig**.4.3.3B) or other controls.

A.

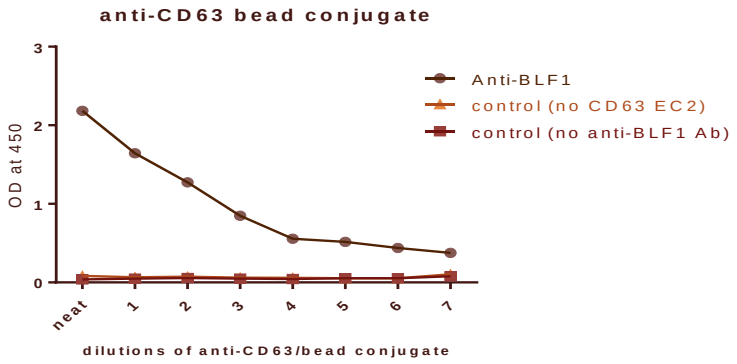

B.

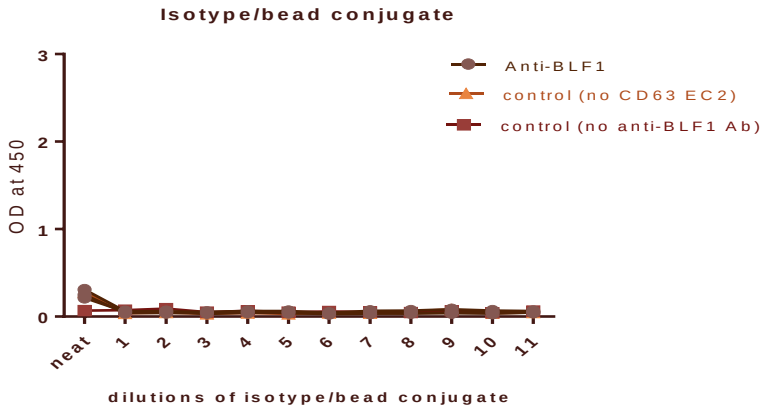

Figure 4.3.3: Assessment of specific binding of the BLF1/anti-CD63 bead conjugate by ELISA:
96-well immunoassay plates were coated with recombinant CD63-EC2 as described in 2.2.9. After blocking, the plates were incubated with neat and doubling dilutions of BLF1/anti-CD63 or BLF1/isotype control bead conjugates (starting with neat conjugate, equivalent to 10 µg/ml of BLF1), washed and incubated with rat anti-BLF1 followed by anti-rat IgG-HRP. The plates were then developed using TMB substrate and read at 450 nm on a plate reader as described in 2.2.9. Controls were wells without EC2 protein coating or without anti-BLF1 antibody. **A.** Binding with BLF1/anti-CD63 bead conjugate **B.** Binding with BLF1/isotype control bead conjugate. Two independent experiments were performed in triplicate.

4.3.1.2.2 Assessment of binding specificity by flow cytometry:

This experiment was performed to assess the cell surface binding of the BLF1/anti-CD63 bead conjugate. RBL2H3 cells stably transfected to express human CD63, as described above and the corresponding wild type cells were used. The rat anti-BLF1 antibody was used to detect the BLF1 part of the bead conjugate. Flow cytometry data demonstrated significant binding of the BLF1 anti-CD63/bead conjugate to the RBL cells transfected with human CD63 compared with the wild type cells (**Fig**.4.3.4). This confirms that the BLF1 anti-CD63/bead conjugate can target BLF1 specifically to cells expressing human CD63.

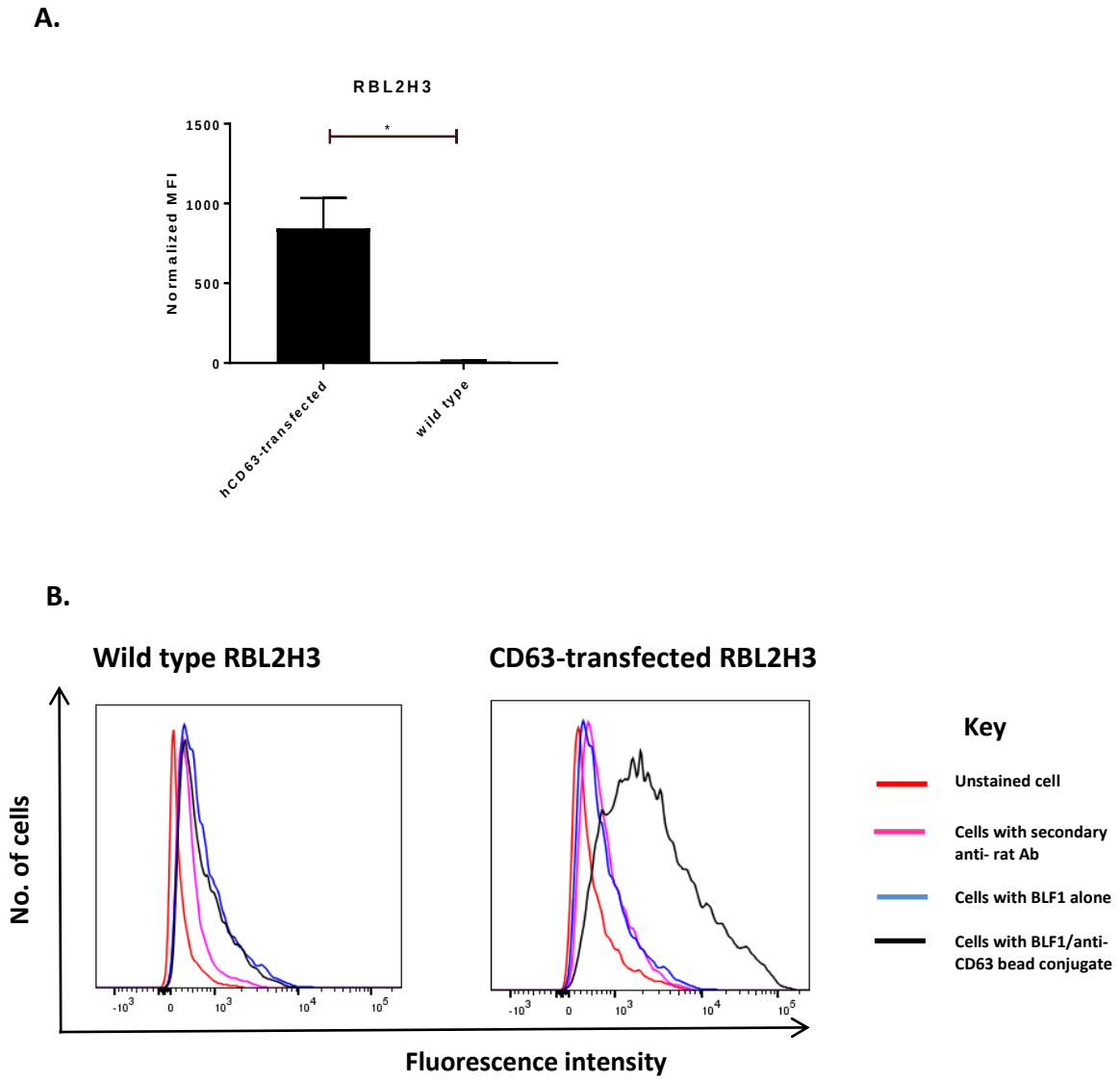

Figure 4.3.4: Assessment of specific cell surface binding of the BLF1/anti-CD63 bead conjugate using flow cytometry:
Cells were incubated with anti-CD63/bead conjugate (1:6 dilution) followed by rat anti-BLF1 then with secondary anti-rat IgG-FITC antibody before analysis by flow cytometry as described in 2.2.4. **A.** Bar charts represent the normalized median fluorescent intensity of killing domain (BLF1 toxin) as a component of BLF1/anti-CD63 bead conjugate in transfected RBL2H3 as compared to WT cells. **B.** Overlay histogram of median fluorescence intensity of BLF1 staining as a component of BLF1/anti-CD63 bead conjugate for both hCD63 transfected RBL2H3 and WT cells. Cells incubated with BLF1 alone or secondary anti-rat antibodies were included as a control. Two independent experiments performed in duplicate, with values shown as mean ± SEM. The significance of difference was determined as described in (**Fig.**4.3.2).

4.3.1.2.3 Investigating the effect of BLF1/anti-CD63 bead conjugate on the growth of hCD63-transfected RBL-2H3 cells:

Having established that the BLF1/anti-CD63 bead conjugate could be targeted specifically to hCD63-transfected RBL2H3 cells, the effect of the conjugate on the growth of these cells was investigated using the SRB assay previously described (2.2.2.4). As additional controls, the effects of beads alone and a conjugate in which the wild type BLF1 was replaced with the inactive mutant version of BLF1 (C94S) were included. After 72 hours there was no significant effect on the growth of the RBL2H3 cells with any of the conjugates tested (**Fig**.4.3.5A). However, the attachment of BLF1/anti-CD63 bead conjugates to the surface of the cells was confirmed by light microscopy.

A.

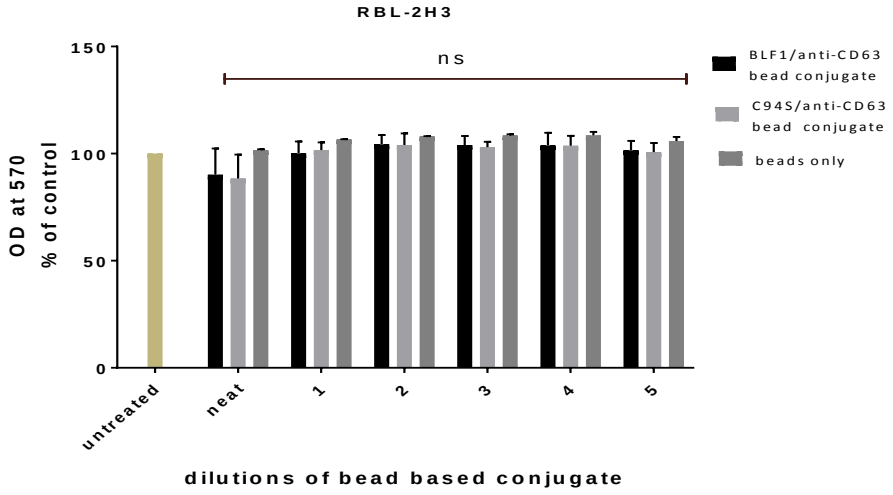

B.

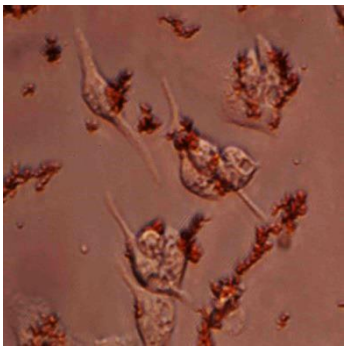

Figure 4.3.5: Effect of BLF1/anti-CD63 bead conjugate on the growth of RBL-2H3 cells transfected with human CD63:

A. Cells were plated into 96-well plates and treated with doubling dilutions of BLF1/anti-CD63bead conjugate (wild type or C94S BLF1) conjugates (starting with neat conjugate, equivalent to 1:10 dilution of conjugates prepared with an initial concentration of 1 µg/ml of BLF1 before purification) or beads alone for 72 hours. The cell growth was then assessed using the SRB assay as described previously (**Fig.**3.3.4, Methods 2.2.4). The experiment was performed three times in quadruplicate with values shown as mean ± SEM. Data were analysed using 2-way ANOVA. **B**. Light microscopy images of the cells cultured in the presence of BLF1/anti-CD63 bead conjugate for 1 hr. Images were captured with Nikon inverted microscope using the 60x objective.

Since the conjugate had no effect on the growth of hCD63-transfected RBL2H3 cells, the effect of BLF1 alone, in the presence or absence of lipofectamine (LF3000) on these cells was investigated using the SRB assay. Surprisingly even in the presence of lipofectamine 3000, BLF1 had no significant effect on cell growth (**Fig**.4.3.6), even at concentrations that showed a strong effect on other cell lines (**Fig.**3.3.6).

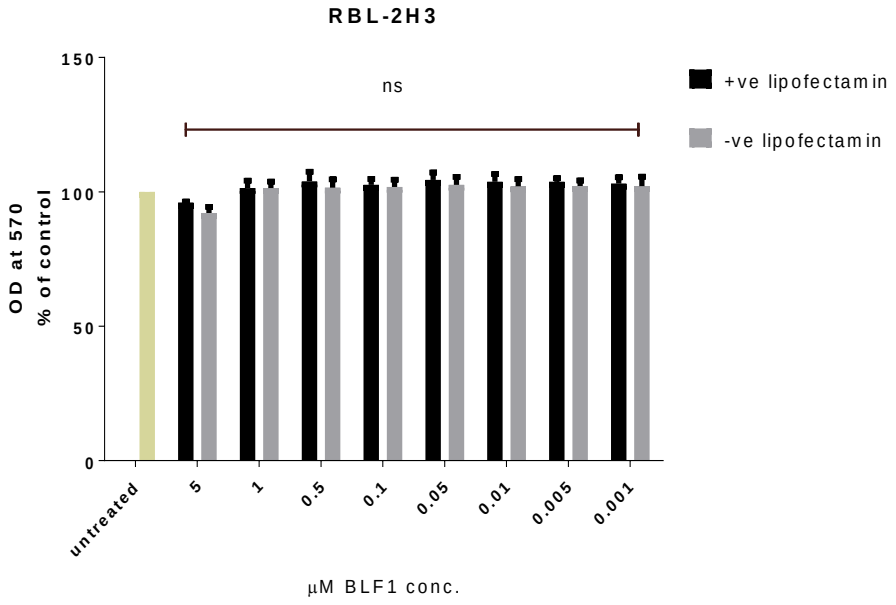

Figure 4.3.6: Effect of BLF1 on hCD63-transfected RBL-2H3 cells:
Cells were cultured in the presence or absence of different concentrations of BLF1 with or without LF3000 for 72 hr, then the cellular growth was assessed using the SRB assay as described previously (**Fig**.3.3.4, Methods 2.2.2.4). Two independent experiments were performed in duplicate with values shown as mean ± SEM. Data were analysed using 2-way ANOVA.

It was then speculated that RBL2H3 cells could survive independently of the activity of eIF4A, the factor inhibited by BLF1. Therefore, the effect of saporin, a different protein toxin

that completely shuts down protein synthesis (Stirpe et al., 1983), was determined in hCD63-transfected RBL-2H3 cells, again in the absence and presence of Lipofectamine reagents (**Fig**.4.3.7). Even at high concentrations of saporin, which have been shown to be highly toxic to mouse neuroblastoma cells (N2a) (Rust et al., 2015), only a very slight effect on the RBL2H3 cells was apparent. It therefore appears that this cell line has an unusual resistance to toxins that affect protein synthesis.

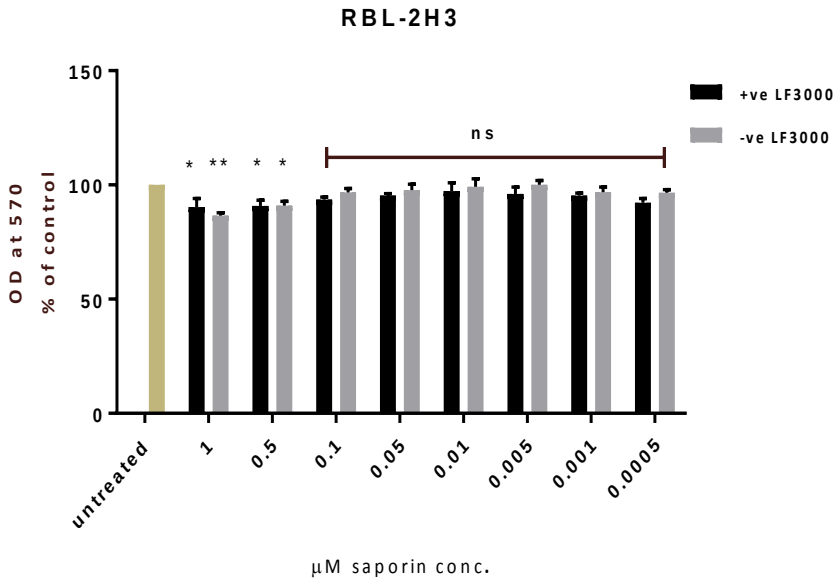

Figure 4.3.7: Effect of saporin on hCD63-transfected RBL-2H3:
Cells were cultured in the presence or absence of different concentrations of saporin, with or without LF3000 for 72 hr then the cell growth was assessed using the SRB assay as described previously (**Fig**.3.3.4, Methods 2.2.2.4).Three independent experiments were performed in quadruplicate, with values shown as mean ± SEM. The significance of difference was determined as described in **Fig**.4.3.6.

As described in Chapter 3, the mouse macrophage cell line J774.2 exhibited unusual sensitivity to BLF1 toxin (**Fig.**3.3.3). To determine if BLF1 conjugated to beads could show any effect on cell growth, the effects of BLF1/bead conjugate (without anti-CD63 antibody, since these cells do not express human CD63) and mutant BLF1 C94S/bead conjugate were determined. The SRB assay data showed that both conjugates significantly affect the growth of mouse macrophage J774.2 cell line at its highest concentration (equivalent to 0.1 µg/ml of BLF1 in the conjugate) in an anti-CD63 independent manner (**Fig.**4.3.8). This confirms

that BLF1 conjugated to beads can affect growth of cells that are sensitive to BLF1, although the effect with the C94S BLF1 mutant was unexpected. However, although enzymatically inactive, the C94S mutant is still able to bind to eIF4A (Cruz-Migoni et al., 2011) and deleterious effects with this have previously been observed at high concentrations (Lynda Partridge, personal communication).

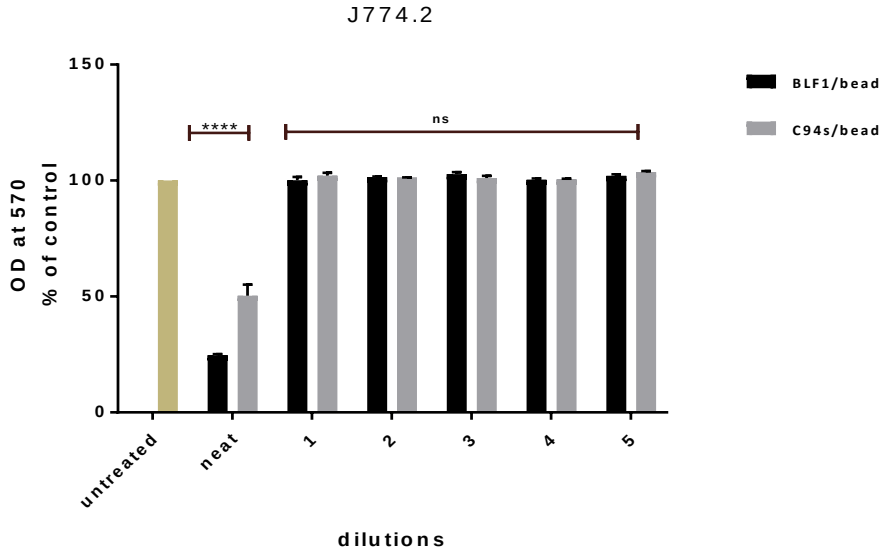

Figure 4.3.8: Effect of BLF1/bead conjugates on the J774.2 cell line
Cells were cultured in the presence or absence of doubling dilutions of wild type BLF1/bead or BLF1 C94S/bead conjugates (starting with neat conjugate, equivalent to 0.1 µg/ml of BLF1) for 72 hours. Then the OD at 570 nm was measured. Two independent experiments were performed in quadruplicate, data shown as mean±SEM and analysed as described previously.

4.3.1.2.4 Expression of CD63 and CD9 on human cancer cell line A549:

The proposed targeting antibodies directed against the CD9 and CD63 tetraspanins were assessed for their binding to A549 cells by indirect fluorescence and flow cyotmetry as described in (2.2.4). The results demonstrated that A549 cells show surface expression of both tetraspanins, although expression of CD9 was higher as indicated by the greater fluorescence intensity (**Fig**.4.3.9). Therefore both tetraspanins could be used as potential immunotoxin targets for this cancer cell line and their relative efficiency compared.

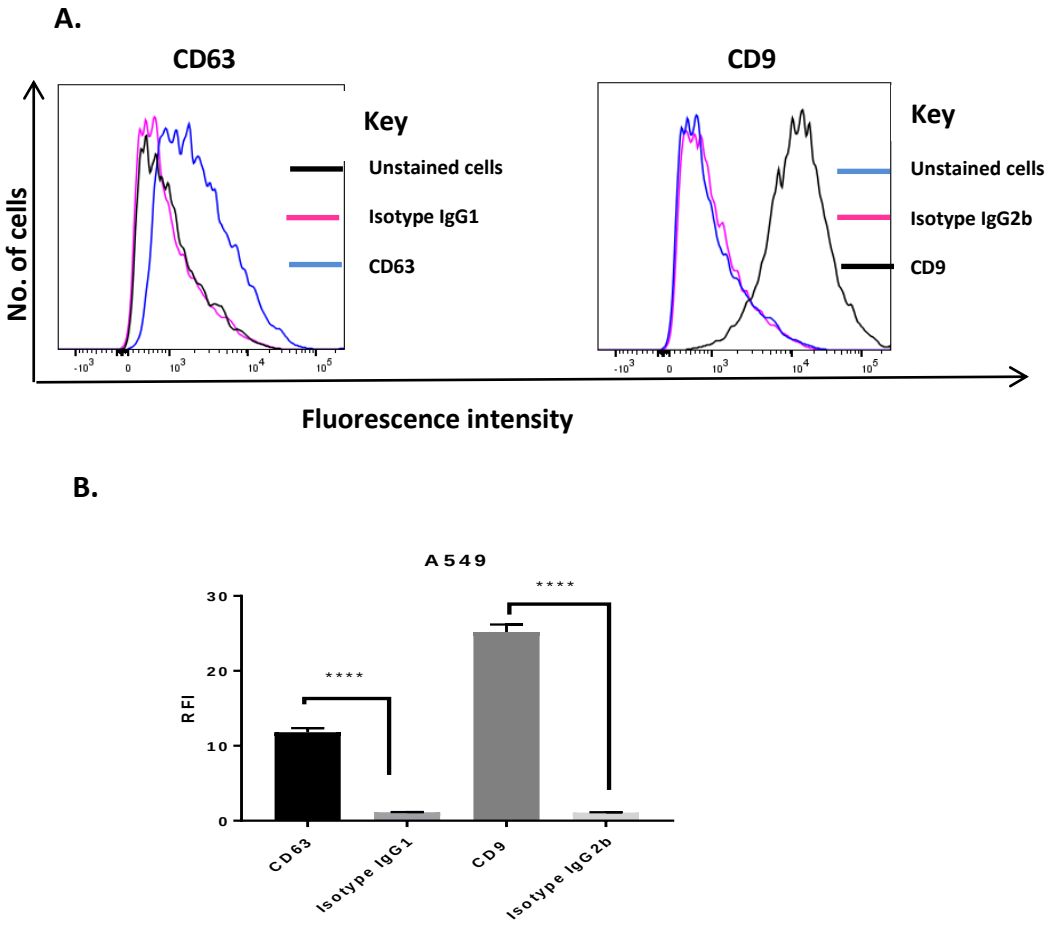

Figure 4.3.9: Surface expression of CD63 and CD9 protein on human lung cancer cell line (A549):
Cells were incubated with monoclonal anti-CD63, anti-CD9 or appropriate isotype controls followed by secondary FITC-conjugated anti-mouse IgG antibody and analysed by flow cytometry as described in (2.2.4). **A**. Overlay histograms of fluorescence intensity of anti-CD63, anti-CD9 and their respective isotype controls in A549. **B.** Bar charts represent the relative fluorescent intensity (median fluorescence intensity (MFI) for anti-CD63, anti-CD9, IgG1 or IgG2b: MFI for unstained cells (control). Three independent experiments were performed in duplicate, with values shown as mean ± SEM. The significance of difference was determined as described in (**Fig**.4.3.2).

4.3.1.2.5 Antibody internalization via target antigen in A549 cells:

As mentioned previously, the basis for creating a successful immunotoxin is that the antibody component is able to specifically bind to the target antigen and internalize, delivering the toxin into the cytoplasm. Although previous work by our group had shown that CD63 is rapidly internalised on antibody binding on a variety of cell lines, the A549 cell

line had not been studied. Flow cytometry was therefore used to assess the extent and rate of antibody internalisation via CD63 and CD9 antigens in A549 cells (**Fig**.4.3.10). In brief, cells were incubated with primary antibody in the cold to allow binding, and then for various time periods at 37°C to allow internalisation, with remaining cell surface primary antibody detected using anti-mouse IgG-FITC. As shown there was a significant (40%) loss of cell surface fluorescence by 15 minutes with the anti-CD63 antibody, with little further loss at the later time points. This indicates rapid internalisation of CD63 following antibody binding, consistent with the known properties of this antigen. By contrast, there was less significant internalization for the CD9 antigen, which lacks an internalization motif, over the time points selected.

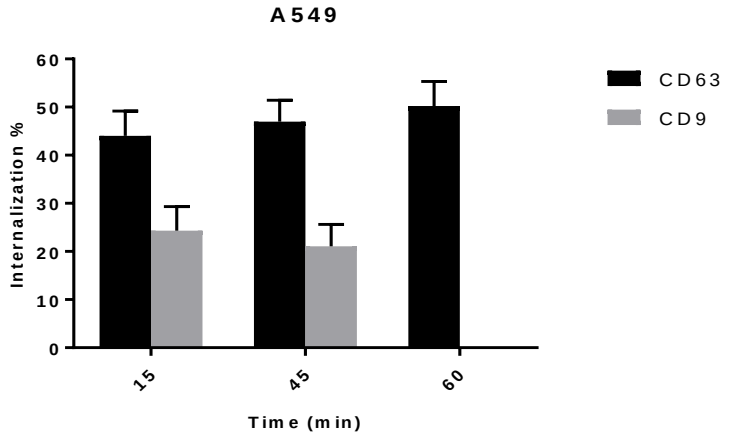

Figure 4.3.10: Antibody-induced internalization of CD63 and CD9 antigen on A549 cell: Cells were incubated with primary antibodies (anti-CD63, anti-CD9 or isotype control) on ice for 30 minute. Samples were then warmed to 37°C for the times indicated, then quenched with ice-cold wash buffer and remaining cell surface primary antibody detected using FITC-conjugated secondary antibody. The controls for no internalization (time zero) were incubated on ice throughout. Samples were then analysed by flow cytometry and the % internalisation of the target antigen at the various time points calculated as described in (2.2.5). Bar chart represents the percentage of CD63 and CD9 antigen internalized. Three independent experiments were performed in duplicate, with values shown as mean ± SEM.

4.3.1.2.6 Assessment of binding of the BLF1/anti-CD63 beads conjugate to A549 cells by flow cytometry:

The experiments described in the previous section showed that the hCD63-transfected RBL2H3 cell line was not suitable for testing the model BLF1 anti-CD63 bead conjugates. Knowing that A549 cells were susceptible to the BLF1 toxin (**Fig.**3.3.10) and expressed CD63

naturally on their surface (**Fig.**4.3.9), the binding of anti-CD63/bead conjugate to these cells was therefore tested by flow cytometry, using the rat anti-BLF1 antibody to detect the BLF1 component. As shown in (**Fig**.4.3.11) there is higher binding of the BLF1-anti-CD63 bead conjugate compared with the BLF1-isotype control bead conjugate. The secondary anti-mouse IgG-FITC was used to detect the monoclonal antibody component of the conjugate. Again higher binding was detected with the anti-CD63 containing conjugate compared to the isotype control conjugate, although surprisingly this was not statistically significant.

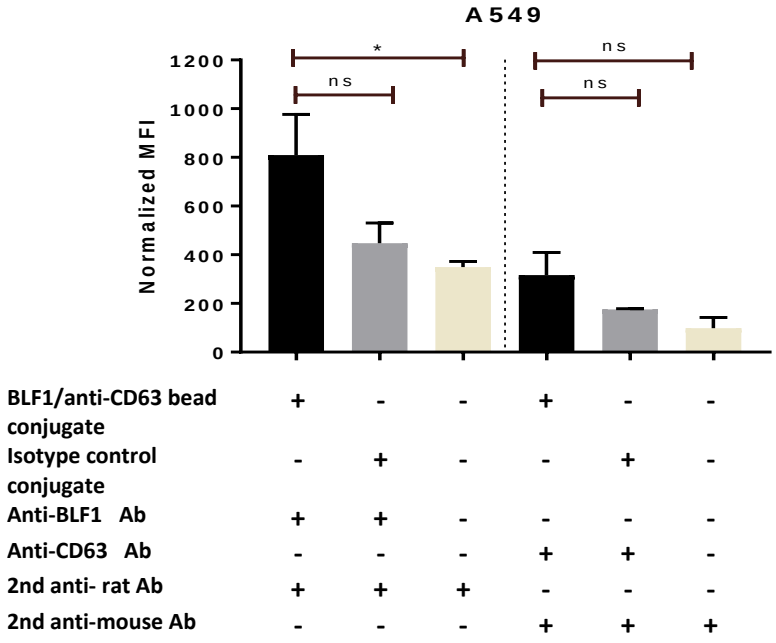

Figure 4.3.11: Assessment of surface binding of BLF1/anti-CD63 bead conjugate to A549 cells by flow cytometry:
Cells were incubated with the BLF1/anti-CD63 bead conjugate or BLF1/isotype control bead conjugate(1:6 dilution), then with rat anti-BLF1 followed by anti-rat IgG-FITC to detect BLF1 (left hand panel) or with anti-mouse IgG-FITC to detect the mouse antibodies (right hand panel). Controls where cells incubated secondary antibody alone. Three independent experiments were performed in duplicate, with values shown as mean± SEM. Data analysed using one way ANOVA with Sidak's multiple comparisons test where * is significantly different at $p<0.05$.

4.3.1.2.7 Assessing the effect of BLF1/anti-CD63 bead conjugate on the growth of A549 cells:

The experiments described above show that the model BLF1/anti-CD63 bead conjugate can target the toxin to the A549 lung cancer cell line. The effect of the conjugate on the growth

of A549 cells was therefore assessed using the SRB assay. The effect of lipofectamine (LF3000) in enhancing delivery of the targeted CD63 bead conjugate was also investigated. After 72 hours there was about a 30% reduction in cellular growth on treatment with 1:10 dilution of neat BLF1/anti-CD63 bead conjugate (which corresponds to conjugates prepared with an initial concentration of 10 µg/ml of BLF1 before purification) and a lower reduction (~12%) with the BLF1/isotype control) compared with untreated cells (**Fig**.4.3.12). Combination of lipofectamine with the BLF1/anti-CD63 bead conjugate significantly improved the effect of the conjugate (**Fig.**4.3.12). However, the isotype bead conjugate in combination with lipofectamine had a similar effect on the tested cells.

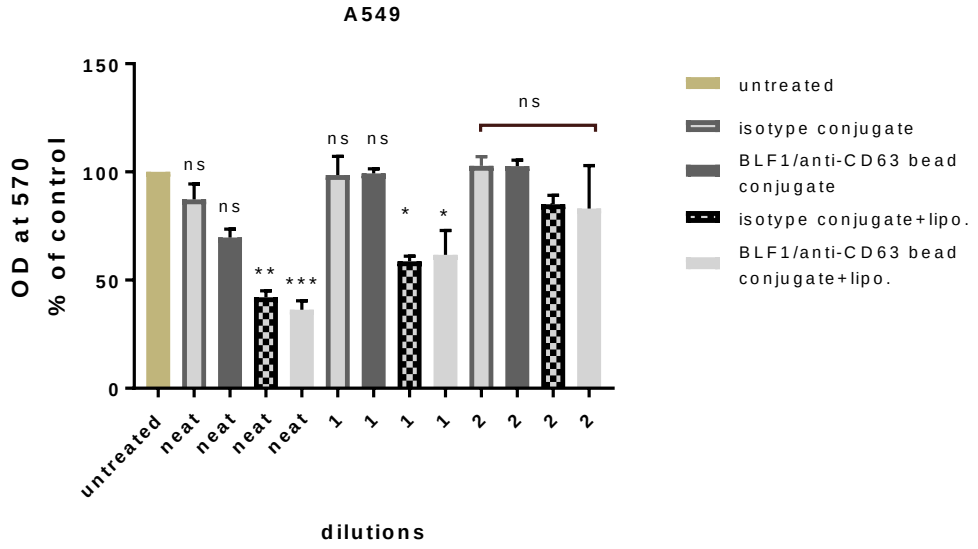

Figure 4.3.12: Effect of BLF1/anti-CD63 bead conjugate on the growth of A549 cells:
Cells were cultured in the presence or absence of doubling dilutions of BLF1/anti-CD63 or BLF1/isotype control/ bead conjugates (starting with 1:10 dilution of neat conjugate corresponding to conjugate prepared with 10 µg/ml BLF1) with or without LF3000 for 72 hours as described in 2.2.2.4.The cellular growth was assessed using the SRB assay as previously described (2.2.2.4). Three independent experiments were performed in quadruplicate with values shown as mean ± SEM. Data were analysed as described in **Fig.**4.3.11.

4.3.1.2.8 Internalization of the BLF1/anti-CD63 bead conjugates by A549 cells:

To try to determine the efficiency of BLF1 targeting and delivery into the cytosol of A549 cells, bead conjugates were prepared using the mCherry-tagged version of the toxin. After incubating the cells with these conjugates for 1 hr, the cells were fixed and stained using anti-mouse IgG-FITC to detect the mouse antibody component of the conjugates and

imaged by confocal microscopy (**Fig.**4.3.13). The images demonstrate that BLF1 can be targeted into A549 cells as a part of the conjugate, in an anti-CD63 dependent manner as observed from the co-localization of the mCherry-BLF1 (red) with the anti-CD63 component (FITC-green) in figure (4.3.13). No staining was observed when mCherry-BLF1 was used with the isotype control conjugate as shown in figure (4.3.13).

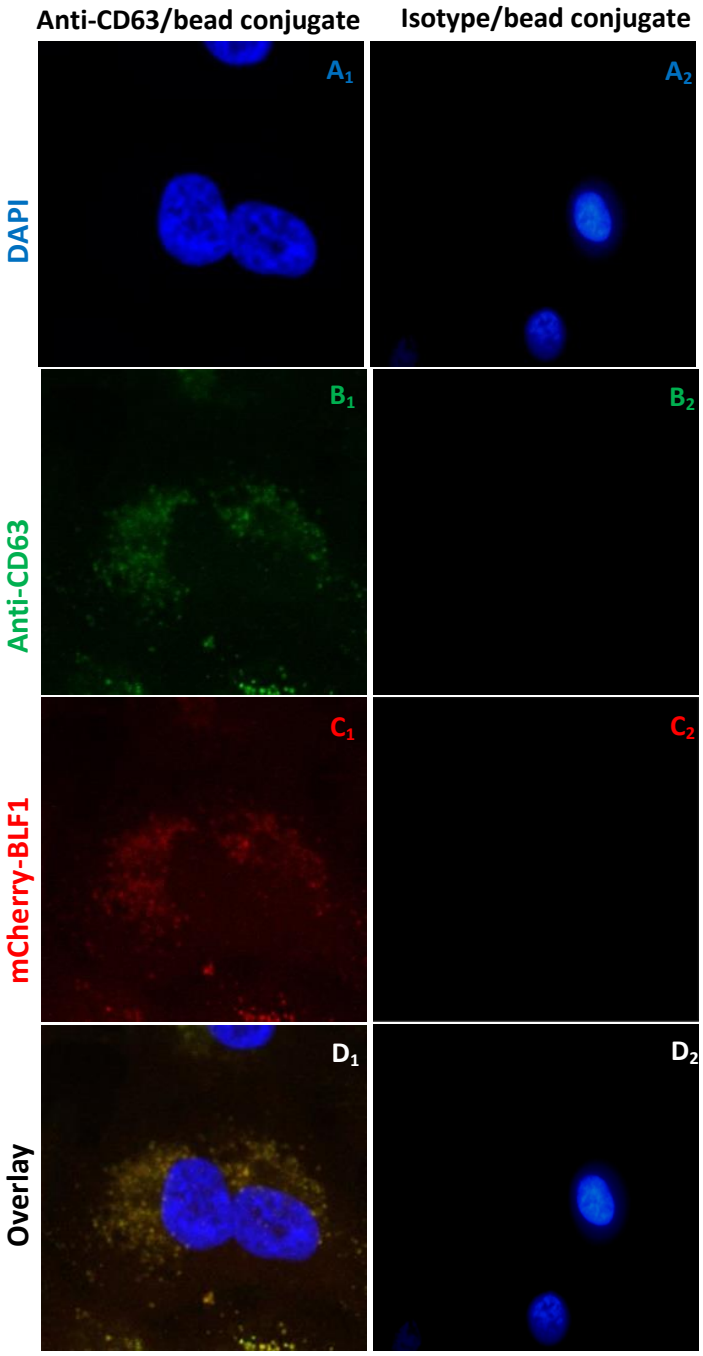

Figure 4.3.13: Internalization of BLF1/anti-CD63 bead conjugates by A549 cells:

Cells were grown overnight on cover slips in 24 well plates, then incubated with medium containing mCherry-BLF1/anti-CD63 bead conjugate or mCherry-BLF1/isotype control bead conjugate at 1:10 dilution (equivalent to 1 µg/ml=0.04 µM BLF1) for 1hr. The cells were then fixed and stained with FITC-labelled anti-mouse IgG and nuclei stained using the DNA stain, DAPI as described in (2.2.8.4.1). Cells were visualised by confocal microscopy using appropriate filters and the 60x oil objective. Two independent experiments were performed. (**A_1, A_2**) DAPI nuclear stain, (**B_1, B_2**) anti-mouse IgG-FITC staining targeting domain represent anti-CD63 and IgG1, (**C_1, C2**) mCherry BLF1, (**D_1, D_2**) combined images.

4.3.1.3 Functional assessment of BLF1/anti-CD9 bead conjugate:

As CD9 antigen expression is higher than CD63 on A549 cells, it was postulated that targeting this antigen might increase the amount of toxin to which the cancer cells are exposed. Although the CD9 antigen shows a slower rate of endocytosis on antibody binding than the CD63 antigen (**Fig.**4.3.10), there is internalization over time. It was therefore deemed of interest to investigate model BLF1 conjugates that target the CD9 antigen.

4.3.1.3.1 Assessment of binding specificity using enzyme linked immunosorbent assay (ELISA):

The binding specificity of the BLF1/anti-CD9 bead conjugate was initially examined by testing its reactivity with recombinant protein corresponding to the large extracellular domain (EC2) of CD9 in ELISA, using the rat anti-BLF1 antibody to detect the toxin as described in 4.3.4.1. Previous studies by our group have shown that the recombinant CD9 EC2 folds correctly and is biologically active (Parthasarathy et al., 2009). The results show that BLF1, as a part of the anti-CD9-toxin conjugate can be targeted to the EC2 domain of CD9, whereas there was no detectable signal with the corresponding isotype control-toxin bead conjugate or other controls (**Fig**.4.3.14A and **Fig**.4.3.14B).

A.

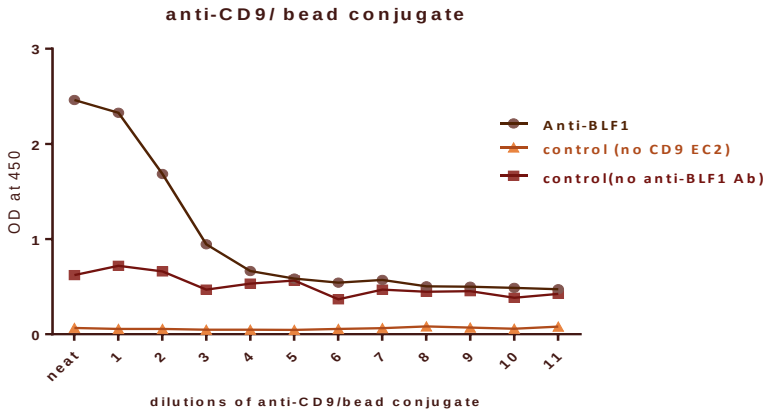

B.

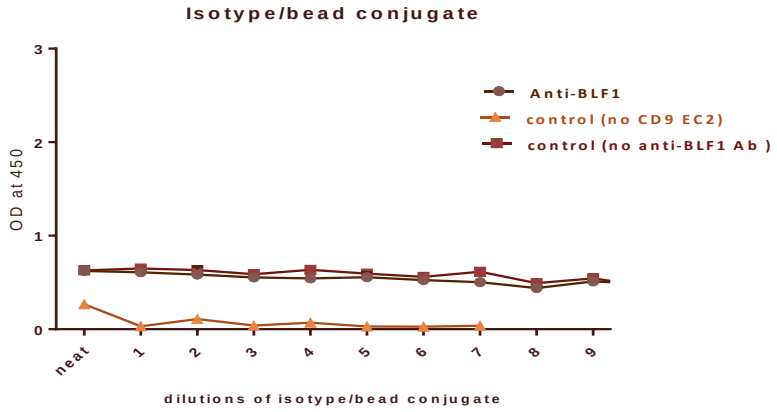

Figure 4.3.14: Assessment of specific binding of the BLF1/anti-CD9 bead conjugate by ELISA:

96-well immunoassay plates were coated with recombinant CD9-EC2 domain as described in 2.2.9. After blocking, the plates were incubated with neat and doubling dilutions of BLF1/anti-CD9 or BLF1/isotype control bead conjugates (starting with neat conjugate, which corresponds to conjugates prepared with an initial concentration of 10 µg/ml of BLF1 before purification), then with rat anti- BLF1 antibody followed by anti-rat IgG-HRP. Substrate was added and the plates were developed and read at 450 nm on a plate reader as described in 2.2.9. Controls were wells without EC2 protein coating or without anti-BLF1 antibody. **A.** Binding with BLF1/anti-CD9 bead conjugate **B.** Binding with BLF1/isotype control bead conjugate. Two independent experiments were performed in triplicate.

4.3.1.3.2 Assessment of binding specificity by flow cytometry:

To assess cell surface binding of the BLF1/anti-CD9 bead conjugate to A549 cells by flow cytometry, the rat anti-BLF1 antibody was used as described previously (4.3.3.6). The secondary anti-mouse IgG-FITC was used to detect the monoclonal antibody component of the conjugate. The data obtained with the anti-BLF1 indicates that binding of the BLF1/anti-CD9 bead conjugate to the A549 cells is greater than the BLF1/isotype control bead conjugate. Significantly higher binding with the anti-mouse IgG-FITC secondary also indicated binding of the anti-CD9 component of the conjugate to the A549 cells, but not the isotype control. Furthermore, BLF1 alone did not show any binding to A549 cells (**Fig**.4.3.15).

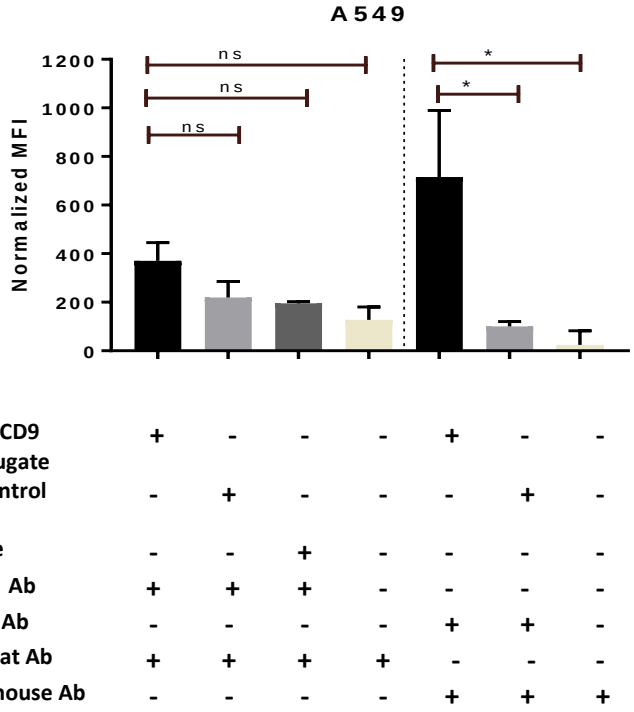

Figure 4.3.15: Assessment of surface binding of BLF1/anti-CD9 bead conjugate to A549 cells by flow cytometry:
Cells were incubated with the BLF1/anti-CD9 bead conjugate or BLF1/isotype control bead conjugate (1:6 dilution), then with rat anti-BLF1 followed by anti-rat IgG-FITC to detect BLF1 (left hand pane) or with anti-mouse IgG-FITC to detect the mouse antibodies (right hand panel).Three independent experiments were performed in duplicate, with values shown as mean ± SEM. Data analysed using one way ANOVA with Sidak's multiple comparisons test where * is significantly different at $p<0.05$.

4.3.1.3.3 Assessing the effect of BLF1/ anti-CD9 bead conjugate on the growth of A549 cells:

The effect of BLF1/anti-CD9 bead conjugates on the growth of A549 cells was tested in the presence or absence of lipofectamine (LF3000) using the SRB assay as described in 4.3.3.7. A significant reduction in A549 cellular growth was observed only in the presence of lipofectamine (**Fig**.4.3.16).

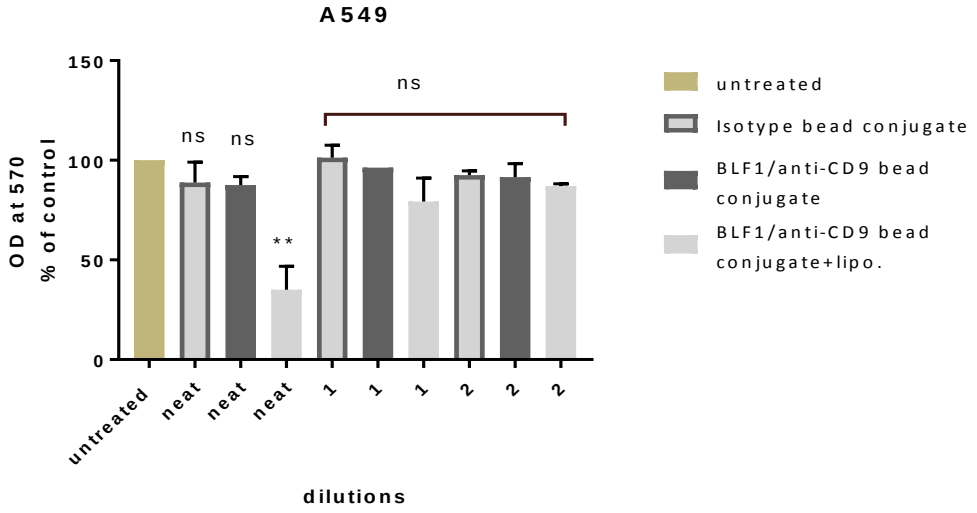

Figure 4.3.16: Effect of BLF1/anti-CD9 bead conjugate on the growth of A549 cells:
Cells were cultured in the presence or absence of doubling dilutions of BLF1/anti-CD9 or BLF1/isotype control bead conjugates (starting with 1:10 dilution of neat conjugate, which corresponds to conjugates prepared with an initial concentration of 10 µg/ml of BLF1 before purification), with or without LF3000 for 72 hours. The cell growth was assessed using the SRB assay as previously described (2.2.2.4). Three independent experiments performed in duplicate, with values shown as mean ± SEM. The significance of difference was determined as described in **Fig**.4.3.11.

4.3.1.3.4 Internalization of BLF1/anti-CD9 bead conjugates by A549 cells:

As described in section 4.3.3.8, the mCherry-tagged version of BLF1 was used to make model conjugates to assess delivery of the toxin into cells as a part of the conjugate. The images demonstrates that BLF1 can be targeted to A549 cells as a part of an antibody-toxin conjugate, in an anti-CD9 dependent manner as observed from the co-localization of mCherry-BLF1 (red) with the anti-CD9 targeting component (FITC-green) in (**Fig**.4.3.17).

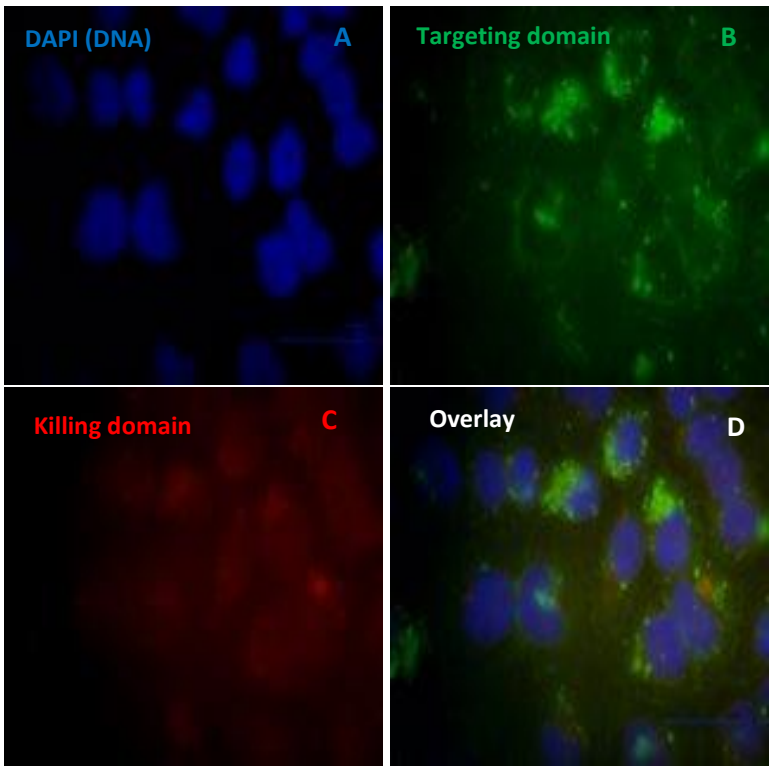

Figure 4.3.17: Internalization of BLF1/anti-CD9 bead conjugates by A549 cells:
Cells were grown overnight on a cover slips in 24 well plates, then incubated with medium containing mCherry-BLF1/anti-CD9 bead conjugate at 1:10 dilution (equivalent to 1 µg/ml=0.04 µM mCherry BLF1) for 24 hour. The cells were then fixed and stained with FITC-labeled anti-mouse IgG and nuclei stained with DAPI as described in 2.2.8.4.1. Cells were visualised by confocal microscope using appropriate filters and the 60x oil objective. (**A**) DAPI nuclear stain. (**B**) Anti-mouse IgG-FITC staining. (**C**) mCherry BLF1. (**D**) Is a combined image.

4.3.2 Design and optimization of novel soluble model conjugate for immunotoxin development:

To facilitate the selection of antibodies capable of efficiently delivering a cytotoxic payload to cancer cells, we developed an additional novel model immunotoxin. This consisted of anti-mouse IgG antibody in the form of the $F(ab')_2$ fragment that was specific for the Fc region of mouse IgG. This secondary antibody was used to non- covalently link the targeting mouse antibody with mouse anti-His antibody holding the toxic payload (BLF1). Furthermore, the anti-mouse IgG (Fc specific) ($F(ab')_2$) antibody fragment does not detect the Fab fragment of mouse IgG, therefore it does not mask the antigen-binding site of the targeting antibody.

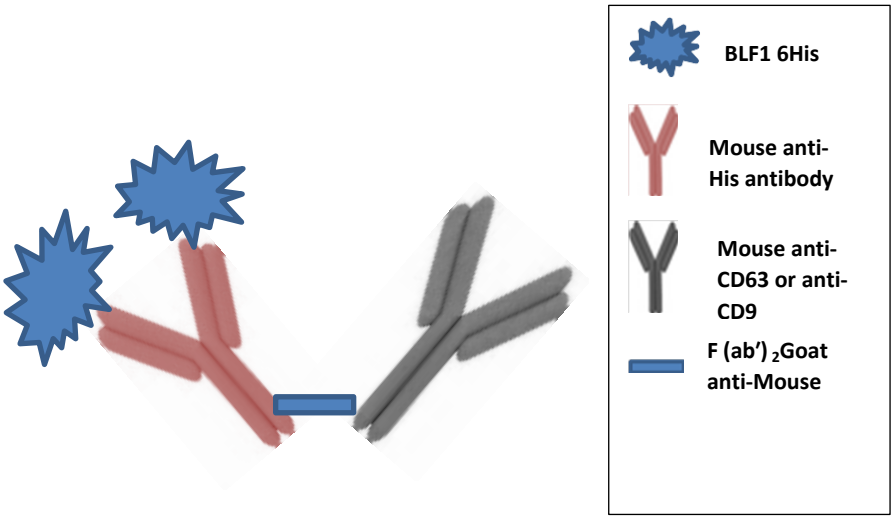

Figure 4.3.18: Diagrammatic representations of the soluble BLF1/antibody model immunoconjugate.

4.3.3 Functional assessment of the BLF1/antibody model immunoconjugate:

The resulting BLF1/anti-CD63 and BLF1/anti-CD9 immunoconjugates were tested for binding specificity for targeted antigen, cytostaticity/cytotoxicity, and intracellular co-localization. The conjugate was designed so that when used to assess impact on cell growth, the final concentration of BLF1 added to the cells was not more than 2 µg/ml (~ 0.08 µM), as described in 2.2.3.2.

4.3.3.1 Assessment of binding specificity using enzyme linked immunosorbent assay (ELISA):

The binding specificity of the soluble model immunoconjugates was examined using the soluble recombinant EC2 domain of CD63 or CD9 as described in 4.3.4.1, using the rat anti-BLF1 antibody to detect the toxin component. As shown in (**Fig**.4.3.19.A_1, B_1) there was significant detection of BLF1 when the anti-CD63 or anti-CD9 model conjugate was used, but no detectable signal with the isotype control conjugate (**Fig**.4.3.19.A_2, B_2). This confirms that the BLF1/anti-CD63 and BLF1/anti-CD9 model immunoconjugates can be targeted

specifically to the EC2 of CD63 and EC2 of CD9 respectively, although the anti-CD63 conjugate shows better binding.

A_1.

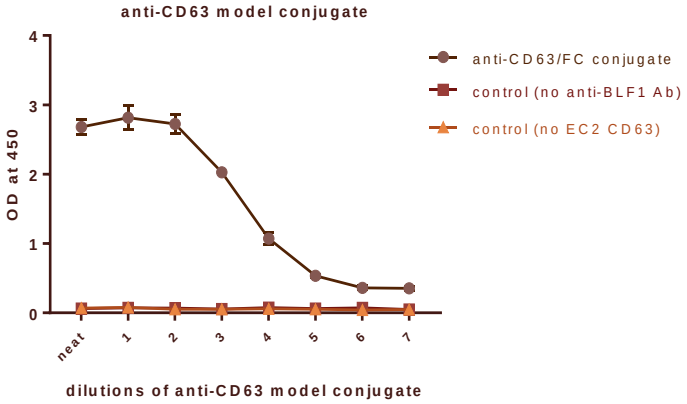

A_2.

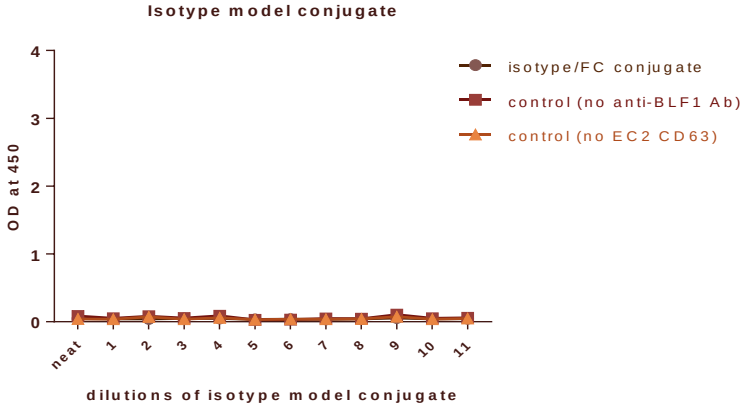

B_1.

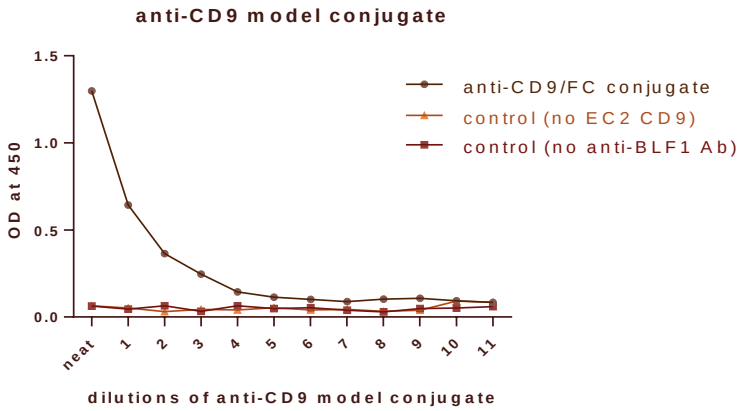

B_2.

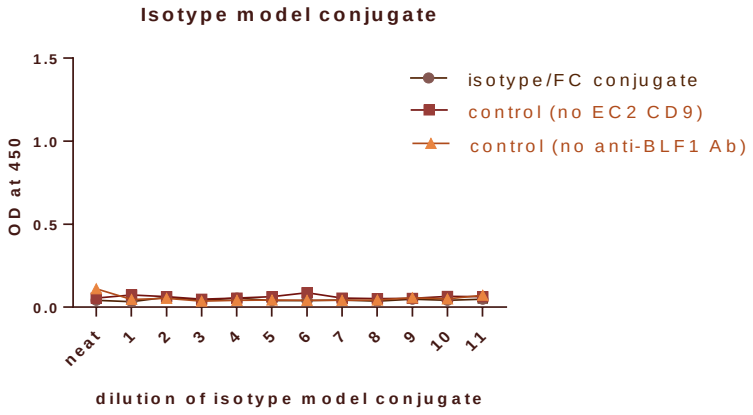

Figure 4.3.19: Assessment of specific binding of the BLF1/antibody model immunoconjugate by ELISA:
96-well immunoassay plates were coated with recombinant CD63-EC2 or CD9-EC2 as described in 2.2.9. After blocking, the plates were incubated with doubling dilutions of BLF1/anti-CD63, BLF1/anti-CD9 or BLF1/isotype control conjugates (starting with neat conjugate, equivalent to conjugates prepared with an initial concentration of 10 µg/ml of BLF1 before purification), washed and incubated with rat anti-BLF1 followed by anti-rat IgG-HRP. The plates were then developed using TMB substrate and read at 450 nm on a plate reader as described in 2.2.9. Controls were wells without EC2 protein coating or without anti-BLF1 antibody. (**A_1**, **A_2**) Binding with BLF1/anti-CD63 or anti-CD9 model conjugate (**B_1**, **B_2**).Binding with BLF1/anti-CD9 or BLF1/isotype control conjugate. Two independent experiments were performed in triplicate.

4.3.3.2 Assessment of binding specificity by flow cytometry:

The cell surface binding of the soluble BLF1 model immunoconjugates was assessed using the RBL-2H3 cell line transfected with human CD63 (see section 4.3.4.2) and the human lung cancer cell line A549 (section 4.3.4.4) as these cell lines express different levels of CD63 on their surface. The data shows that there is significant detection of both the BLF1 component and the mouse antibody component when the target cells are incubated with the BLF1/anti-CD63 immunoconjugate, but not with the corresponding isotype control conjugate (**Fig**.4.3.20.A, B). Moreover, higher binding was observed with the BLF1/anti-CD63 immunoconjugate with the A549 cell line that expresses higher levels of CD63 antigen than RBL2H3 (CD63) cells.

In addition, A549 cell lines also express high levels of CD9 protein on their surface, therefore the BLF1 component and mouse antibody component of BLF1/anti-CD9 immunoconjugate was determined. The data shows that there is significant detection of both components, but not with the corresponding isotype conjugate (**Fig.**4.3.20.C). Moreover, the binding profile of BLF1/anti-CD63 immunoconjugate to A549 cells was higher than the binding of BLF1/anti-CD9 immunoconjugate, in line with the ELISA data (4.3.3.1).

A.

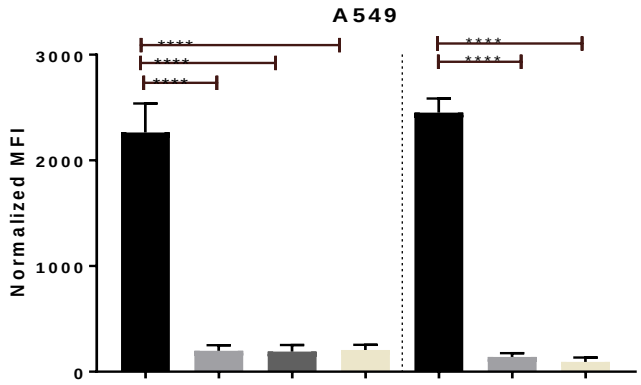

BLF1/anti-CD63 Immunoconjugate	+	-	-	-	+	-	-
Isotype control conjugate	-	+	-	-	-	+	-
BLF1 alone	-	-	+	-	-	-	-
Anti-BLF1 Ab	+	+	+	-	-	-	-
Anti-CD63 Ab	-	-	-	-	+	+	-
2nd anti- rat Ab	+	+	+	+	-	-	-
2nd anti-mouse Ab	-	-	-	-	+	+	+

B.

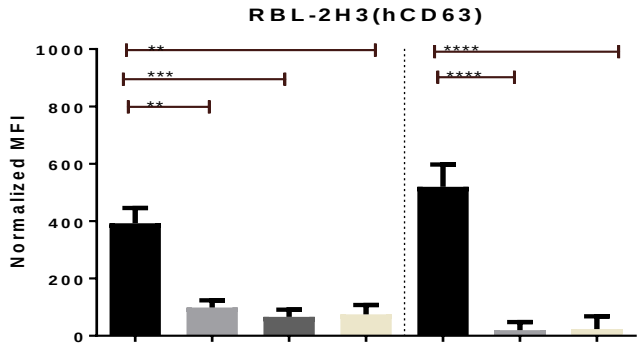

BLF1/anti-CD63 Immunoconjugate	+	-	-	-	+	-	-
Isotype control conjugate	-	+	-	-	-	+	-
BLF1 alone	-	-	+	-	-	-	-
Anti-BLF1 Ab	+	+	+	-	-	-	-
Anti-CD63 Ab	-	-	-	-	+	+	-
2nd anti- rat Ab	+	+	+	+	-	-	-
2nd anti-mouse Ab	-	-	-	-	+	+	+

C.

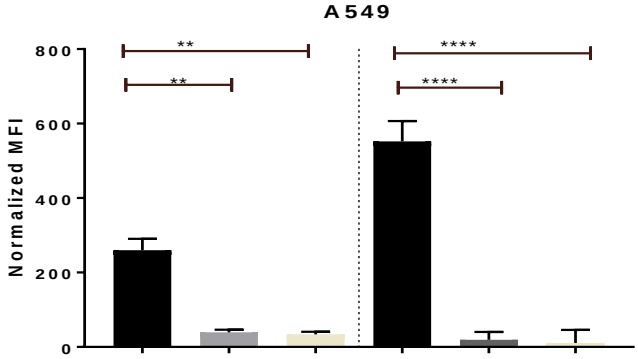

BLF1/anti-CD9 Immunoconjugate	+	-	-	+	-	-
Isotype control conjugate	-	+	-	-	+	-
Anti-BLF1 Ab	+	+	-	-	-	-
Anti-CD9 Ab	-	-	-	+	+	-
2nd anti- rat Ab	+	+	+	-	-	-
2nd anti-mouse Ab	-	-	-	+	+	+

Figure 4.3.20: Assessment of surface binding of BLF1 model immunoconjugate to A549 and RBL2H3 cells by flow cytometry:
Cells were incubated with the BLF1/anti-CD63 immunoconjugate, BLF1/anti-CD9 immunoconjugate, BLF1/isotype control conjugate or BLF1 alone, then with rat anti-BLF1 followed by anti-rat IgG-FITC to detect BLF1 (left hand pane) or with anti-mouse IgG-FITC to detect the mouse antibodies (right hand panel).**A**. Binding of BLF1/anti-CD63 model immunoconjugate with A549. **B.** Binding of BLF1/anti-CD63 model immunoconjugate with RBL2H3 (hCD63).**C**. Binding of BLF1/anti-CD9 model immunoconjugate with A549.Three independent experiments were performed in duplicate, with values shown as mean± SEM. Data analysed using one way ANOVA with Sidak's multiple comparisons test where **** is significantly different at p<0.0001.

4.3.3.3 Visualisation of binding characterization of the soluble BLF1/anti- CD63 immunoconjugate to A549 cells:

To further confirm the results obtained by flow cytometry (**Fig.**4.3.20), binding of the soluble BLF1 immunoconjugate to A549 cells was examined by fluorescence microscopy, using conjugate prepared with mCherry-tagged BLF1. The images concurred with the flow cytometry data, as mCherry-BLF1 is detected on the surface of A549 cells, broadly co-locating with the mouse monoclonal antibody (FITC-green) when the immunoconjugate containing anti-CD63 is used, but not with the isotype control conjugate as shown in figure (4.3.21).

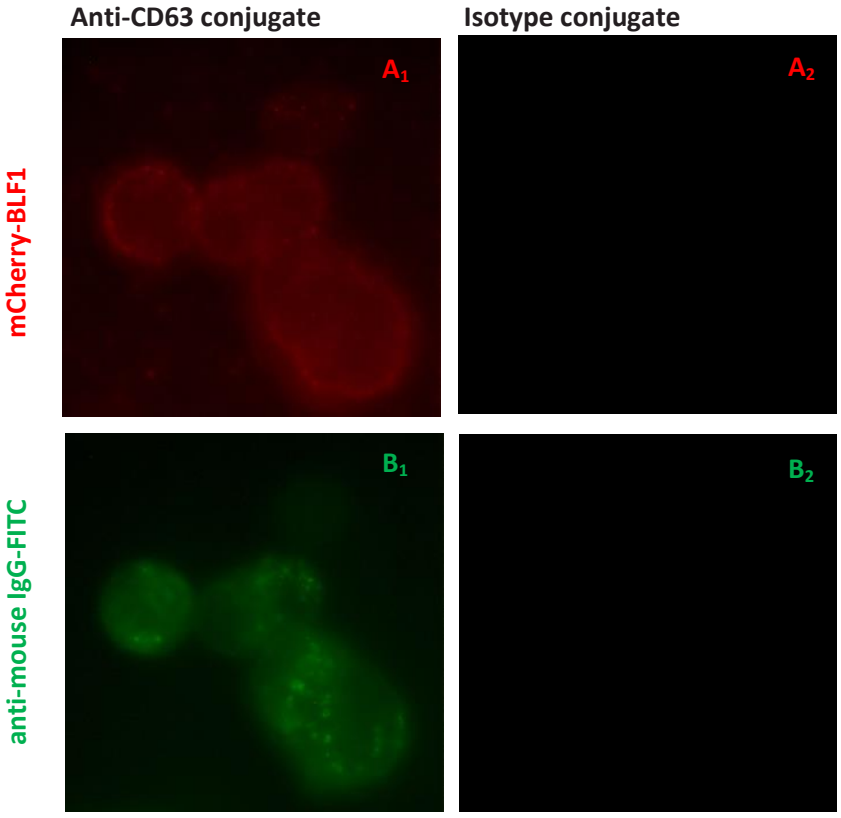

Figure 4.3.21: Binding of model mCherryBLF1/anti-CD63 immunoconjugate to A549 cells:
Cells were seeded into 8-well LabTek™ chamber slides, fixed and incubated with mCherryBLF1 immunoconjgate prepared using anti-CD63 or isotype control mouse antibody as described in (2.2.7.2). Mouse antibody was detected using secondary anti-mouse IgG-FITC antibody (**A_1, A_2**) Detection of mCherry-BLF1 in anti-CD63 or isotype control conjugates, respectively. (**B_1, B_2**) Detection of mouse antibody in anti-CD63 or isotype control conjugates, respectively. Slides were imaged using a Nikon Eclipse E400 fluorescence microscope using appropriate filters (100x oil objective).

4.3.3.4 Internalization of the BLF1/antibody model immunoconjugate by A549 cells:

The capacity of the soluble model BLF1 immunoconjugte to be internalised was determined by flow cytometry, essentially as described previously (section 2.42 and **Fig**.4.3.3). Data from flow cytometry showed that there is a significant loss of detectable fluorescence at the cell surface over time with the samples incubated with the BLF1/anti-CD63 and BLF1/anti-CD9 conjugate at 37^{o}C, compared to samples incubated with their isotype control conjugate (**Fig**.4.3.22). This indicates internalisation of both immunoconjugates following antibody binding to antigen bearing A549 cells.

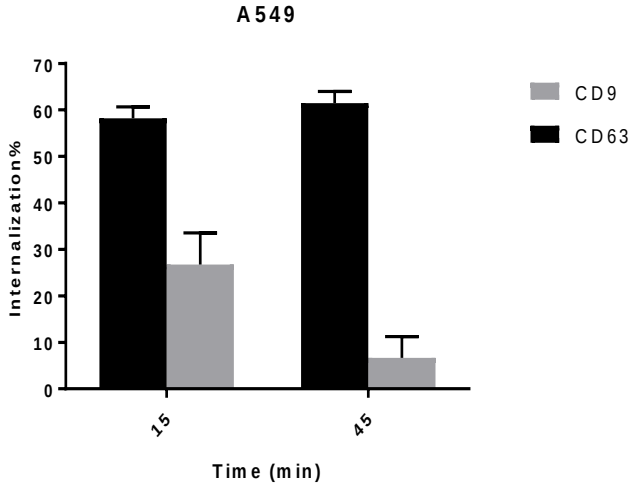

Figure 4.3.22: Internalization of the model BLF1 immunoconjugate by A549 cells:
Cells were incubated with BLF1/anti-CD63, BLF1/anti-CD9 or isotype control conjugates on ice for 30 minute. Samples were then warmed to 37°C for the times indicated, then quenched with ice-cold wash buffer and then with rat anti-BLF1 followed by anti-rat IgG-FITC to detect BLF1.The controls for no internalization (time zero) were incubated on ice throughout. Samples were then analysed by flow cytometry and the % internalisation of the

immunoconjugate at the various time points was calculated as described in (2.2.5). Three independent experiments were performed in duplicate, with values shown as mean ± SEM.

4.3.3.5 Assessing the effect of the BLF1/antibody model immunoconjugate on the growth of A549 cells and augmentation with saponin:

The experiments described above suggest that the model BLF1/anti-CD63 and BLF1/CD9 immunoconjugates can target and deliver the toxin into the A549 lung cancer cell line. The effect of the conjugate on the growth of A549 cells was therefore assessed using the SRB assay. The BLF1/anti-CD63 model immunoconjugate and its isotype control conjugate (starting with neat conjugate, corresponds to conjugates prepared with an initial concentration of 10 µg/ml of BLF1 before purification) appeared to be nontoxic to the cells (**Fig**.4.3.23.A). However, BLF1/anti-CD9 immunoconjugate showed significant impact on cellular growth at a final concentration of 2 µg/ml (equivalent to 0.08 µM BLF1, which had no effect on A549 cells alone as shown in 3.3.3) and had a decreasing effect at higher dilutions. However, in this case the isotype control also exhibited some effect, although this was less than the anti-CD9 immunoconjugate (**Fig**.4.3.23.B).

As described in (1.1.3.3.2) triterpenoidal saponins have been reported to enhance the activity of immunotoxins. The effect of combining the model immunoconjugates with saponin was therefore investigated (**Fig**.4.3.23.C, D). Saponin at a non-cytotoxic concentration of 2 µg/ml resulted in significant inhibition of cell growth with the neat immunoconjugates (equivalent to 1 µg/ml of BLF1 in assembled BLF1/anti-CD63, and 2µg/ml in assembled BLF1/anti-CD9 immunoconjugate) and further clear impact on cellular growth at lower concentration. A synergestic effect was observed using non toxic concentrations of the conjugate (2) in combination with saponin, resulting in about 60% reduction in cell growth. However, the isotype control immunoconjugate appeared to have a significant toxic effect on the cells in combination with saponin (**Fig**.4.3.23.C) suggesting that this effect was non-specific.

A.

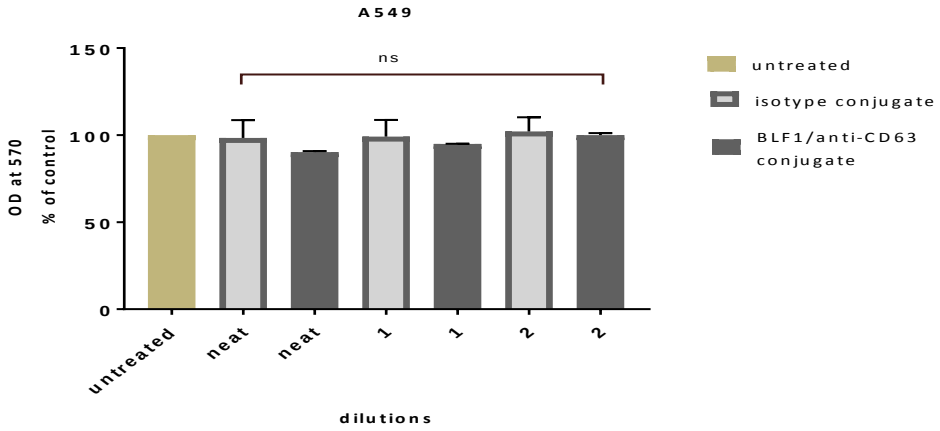
A549
150
100
50
0
OD at 570
% of control
ns
untreated
neat
neat
1
1
2
2
dilutions
untreated
isotype conjugate
BLF1/anti-CD63
conjugate

B.

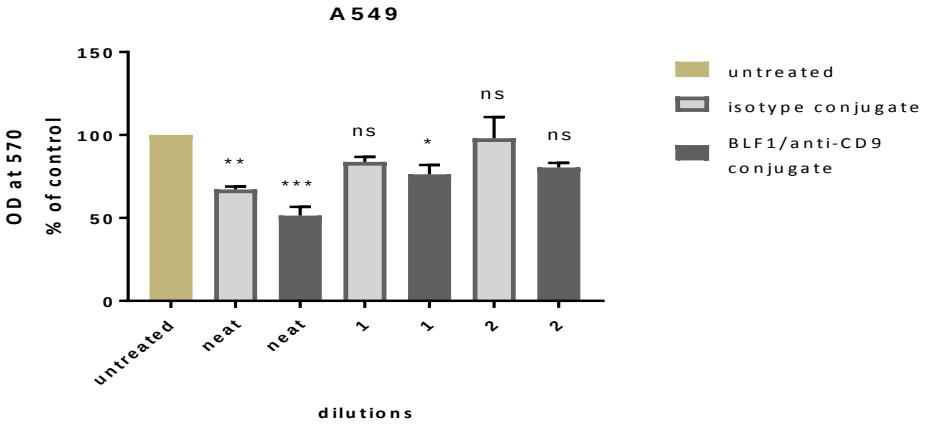
A549
150
100
50
0
OD at 570
% of control
**
***
ns
*
ns
ns
untreated
neat
neat
1
1
2
2
dilutions
untreated
isotype conjugate
BLF1/anti-CD9
conjugate

C.

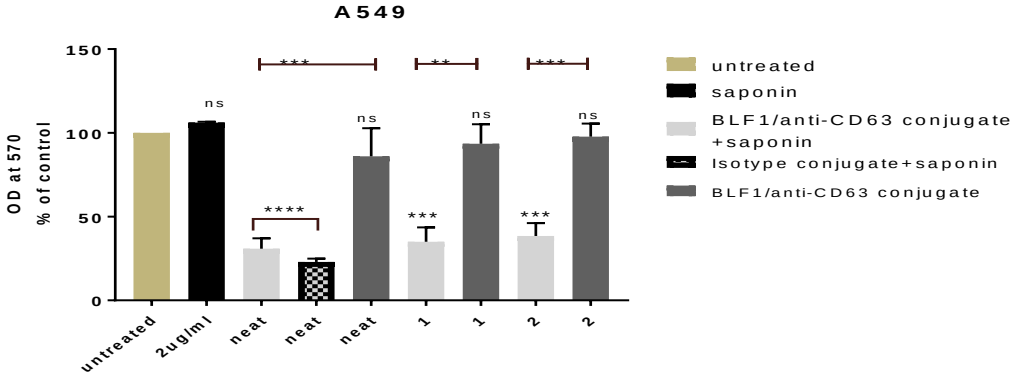
A549
150
100
50
0
OD at 570
% of control
***
**
***
ns
ns
ns
ns
****
***
***
untreated
2ug/ml
neat
neat
neat
1
1
2
2
untreated
saponin
BLF1/anti-CD63 conjugate
+saponin
Isotype conjugate+saponin
BLF1/anti-CD63 conjugate

D.

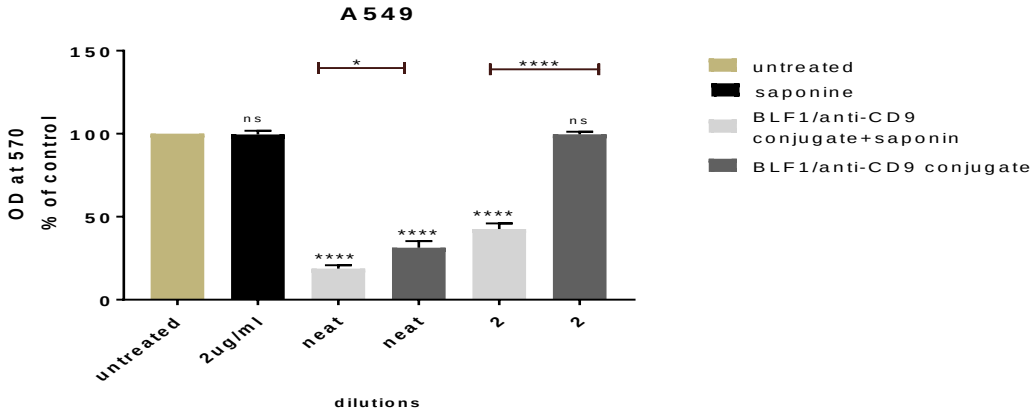

Figure 4.3.23: Effect of model immunoconjugate on the growth of A549 cells:
Cells were cultured in the presence or absence of different concentration of BLF1/anti-CD63, BLF1/anti-CD9 or BLF1/isotype control immunoconjugates with or without saponin for 72 hours as described in 2.2.4. The cell growth was assesed using the SRB assay as previously described (2.2.3).**A.** The effect of BLF1/anti-CD63 model immunoconjugate and its isotype control conjugate on A549. **B**. The effect of BLF1/anti-CD9 and its isotype control conjugate on A549. **C.** The effect of combining BLF1/anti-CD63 model immunoconjugates with saponin on A549. **D.** The effect of combining BLF1/anti-CD9 model immunoconjugates with saponin on A549.Three independent experiments were performed in quadruplicate with values shown as mean± SEM. Data were analysed by one way ANOVA with Dunnett's and Sidak's multiple comparisons tests where **** is significantly different at $p<0.0001$, *** is significantly different at $p<0.001$ and ** is significantly different at $p<0.01$.

4.3.3.6 Intracellular trafficking of BLF1/model immunoconjugate:

The preceding section showed that the immunoconjugates were specifically internalised. Attempts were then made to follow the fate of BLF1 and the targeting antibody at later time points after incubation with the cells.

4.3.3.6.1 Visualization of the internalized soluble BLF1/anti-CD63 immunoconjugate:

Initially, the intracellular localisation of internalized BLF1 after A549 cells had been incubated with BLF1/anti-CD63 model immunoconjugate for 24 hours was investigated, as it was expected that the immunoconjugate would be processed by this time. Since wild type BLF1 might damage the cells, in this case a mCherry-tagged version of the inactive mutant (C94S) was used to construct the conjugates. The images obtained from confocal

microscopy (**Fig**.4.3.24) showed that the BLF1 appeared within large vesicles near the nucleus, with some in smaller vesicles scattered throughout the cytoplasm. No signal for BLF1 was detected when the isotype control conjugate was used.

As described previously in section 4.3.1.2.3, RBL-2H3 cells appeared to be insensitive to BLF1 toxin. However, we also demonstrated that BLF1 could be targeted to RBL-2H3 cells expressing human CD63 by anti-CD63 antibodies (**Fig**.4.3.6). It was therefore of interest to investigate the intracellular localisation of internalised BLF1 by these cells. Interestingly, after incubation of these cells with mCherry BLF1 (C94S)/anti-CD63 conjugate for 24hr, BLF1 appeared to be strongly contained in a few very large vesicles (**Fig**.4.3.24.B), in contrast to the more diffuse pattern observed with A549 cells (**Fig.**4.3.24.A).

A.

BLF1/anti-CD63 immunoconjugate **Isotype immunoconjugates**

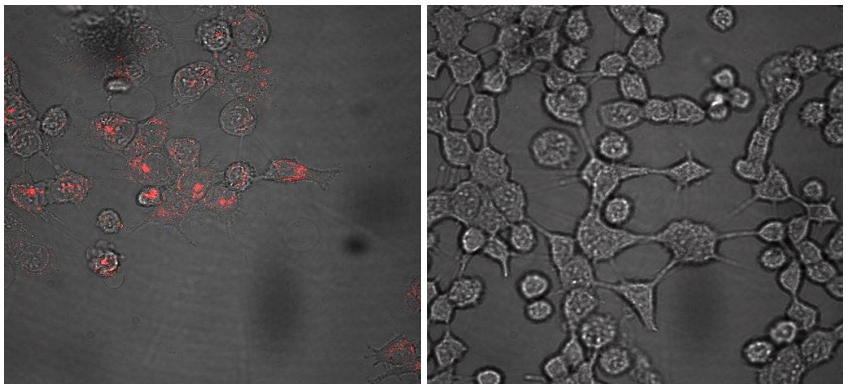

B.

BLF1/anti-CD63 immunoconjugate

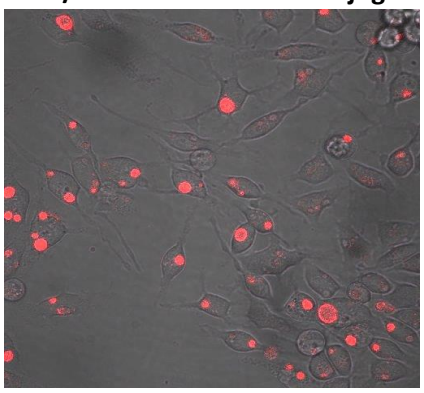

Figure 4.3.24: Intracellular localization of BLF1 24 hours after incubation with model BLF1/anti-CD63 immunoconjugates:

Cells were cultured overnight in glass-bottomed FluoroDish™, and then incubated with mCherry-BLF1 (C94S)/anti-CD63 or mCherry-BLF1 (C94S)/isotype control model immunoconjugates for 24 hr as described in (2.2.6). Slides were imaged using confocal microscopy (60 x oil objectives). **A.** A549 cells treated with anti-CD63 (LH image) or isotype control (RH image) conjugates. **B.** RBL-2H3 cells transfected with human CD63 treated with anti-CD63 conjugate.

To investigate whether the targeting antibody (anti-CD63) and BLF1 are colocalized in A549 cells after internalisation, model conjugates were constructed using mCherry-tagged BLF1 (C94S) and fluorescently labelled (Alexa Fluor 488) anti-CD63. The localisation of the fluorescently labelled components was studied after incubation of the conjugate with A549 cells for 6 and 24 hours. The images obtained from confocal microscopy (**Fig**.4.3.25) indicated colocalization of anti-CD63 with BLF1.

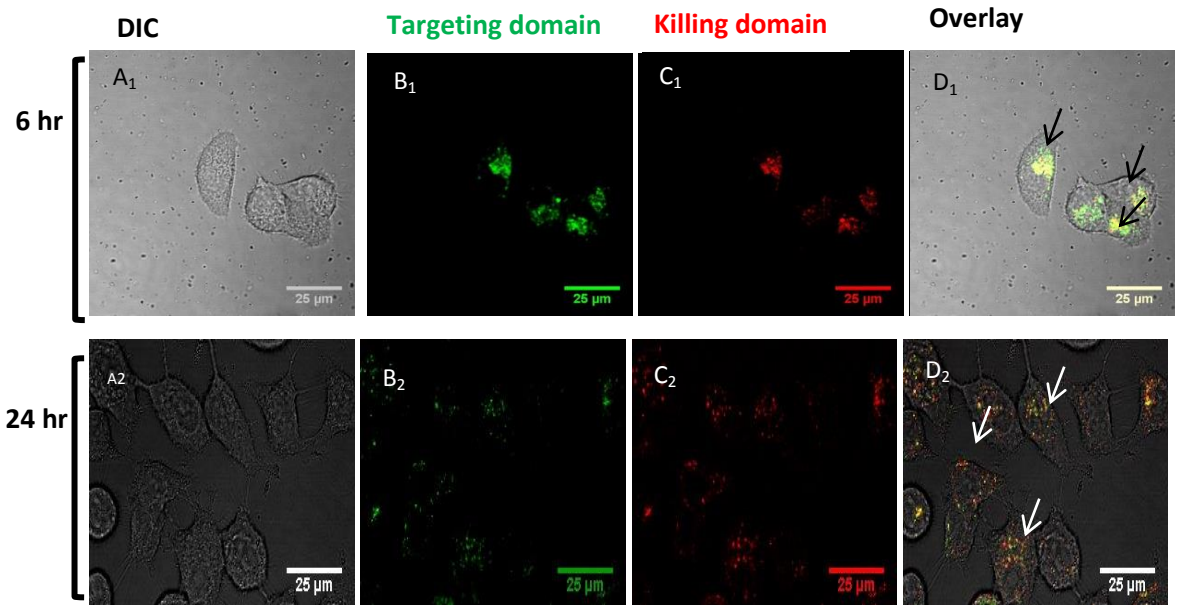

Figure 4.3.25: Immunofluorescence live images of A549 cells incubated up to 24 hours with BLF1/anti-CD63: model immunoconjugate:
Cells were cultured overnight in glass-bottomed FluoroDish™, then incubated with model immunoconjugate constructed using mCherry-BLF1(C94s) and Alexa Fluor 488-labelled anti-CD63 for 6 and 24 hours as described in (2.2.6).(**A1, A2**) grey background of A549 cells. (B_1, B_2) Green fluorescence corresponds to anti-CD63. (**C_1, C_2**). Red fluorescence corresponds to BLF1 (C94s). (**D_1, D_2**) merged images. Slides were imaged by confocal microscopy (60 x oil objectives) using appropriate filters.

To describe the intracellular trafficking pathway in more detail, co-localization of BLF1 with endosomes after incubation of A549 cells with the BLF1/anti-CD63 model immunoconjugate

was investigated. A549 cells were cultured with the conjugate for 1.5 hr and endosomes were labelled using antibodies to transferrin, which is a marker for early endosomes. The results indicated partial colocalization of BLF1/anti-CD63 model immunoconjugate with early endosomes as indicated by arrows (**Fig.**4.3.26).

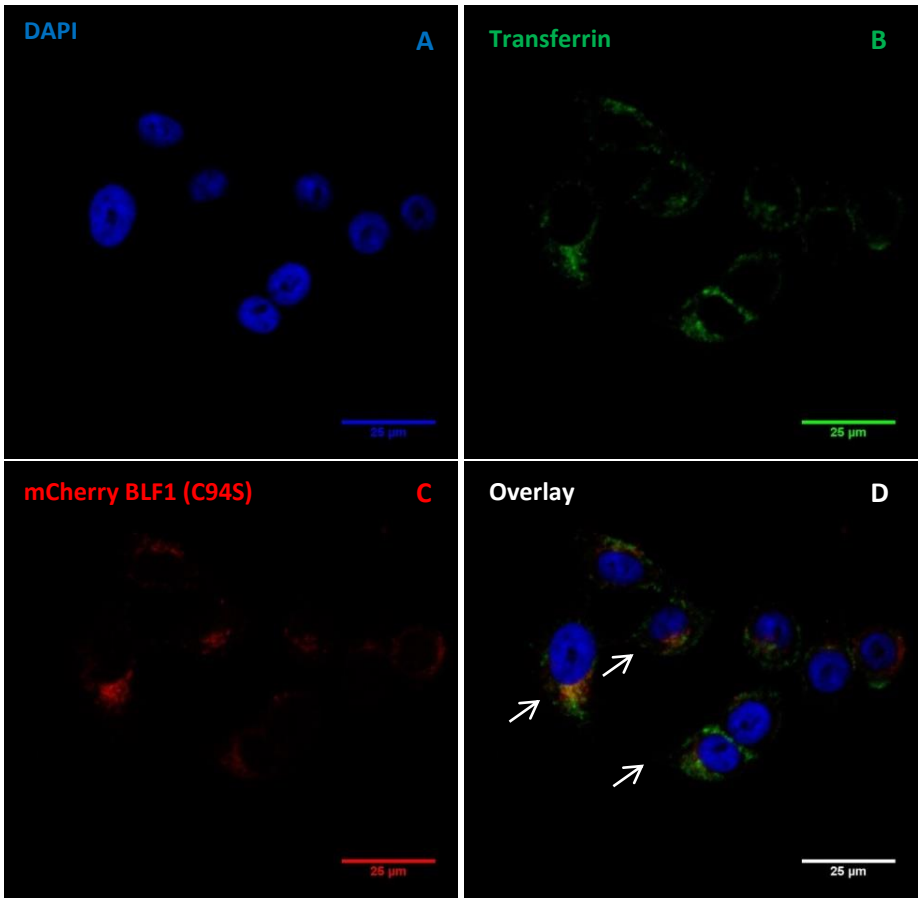

Figure 4.3.26: Immunofluorescence images of A549 cells incubated for 90 minutes with mCherryBLF1 (C94S)/anti-CD63 immunoconjugate:
Cells were cultured overnight on a coverslip placed in 24 well plates and incubated with mCherry-BLF1 (C94S)/anti-CD63 conjugate for 90 minutes. Cells were then fixed and permeabilised and stained with anti-transferrin antibody as described in (2.2.8.4.1) (**A**) Blue fluorescence corresponds to nuclei stained with DAPI. (**B**) Green fluorescence corresponds to the early endosomal marker (transferrin). (**C**) Red fluorescence corresponds to mCherry-BLF1 (**D**) Merged images. Slides were imaged using a Nikon Eclipse E400 Fluorescence microscope (100 x oil objectives) using appropriate filters.

4.3.3.6.2 Visualization of the internalized soluble BLF1/anti- CD9 immunoconjugate by A549:

The internalization of BLF1/anti-CD9 conjugate and its isotype control conjugate was also visualized 24 hr after addition to the cells. For with this purpose, targeting antibody (anti-CD9) was labelled with Alexa Fluor 488 dye as described in (2.2.10) prior to conjugation with inactive mutant mCherry C94S. The images obtained from confocal microscopy (**Fig**.4.3.27) indicated uptake of BLF1 and some co-localization with the targeting antibody. Interestingly, however, a considerable amount of the labelled targeting antibody was present on cell membrane. No signals were detected when the cells were incubated with the isotype control conjugate (**Fig**.4.3.28).

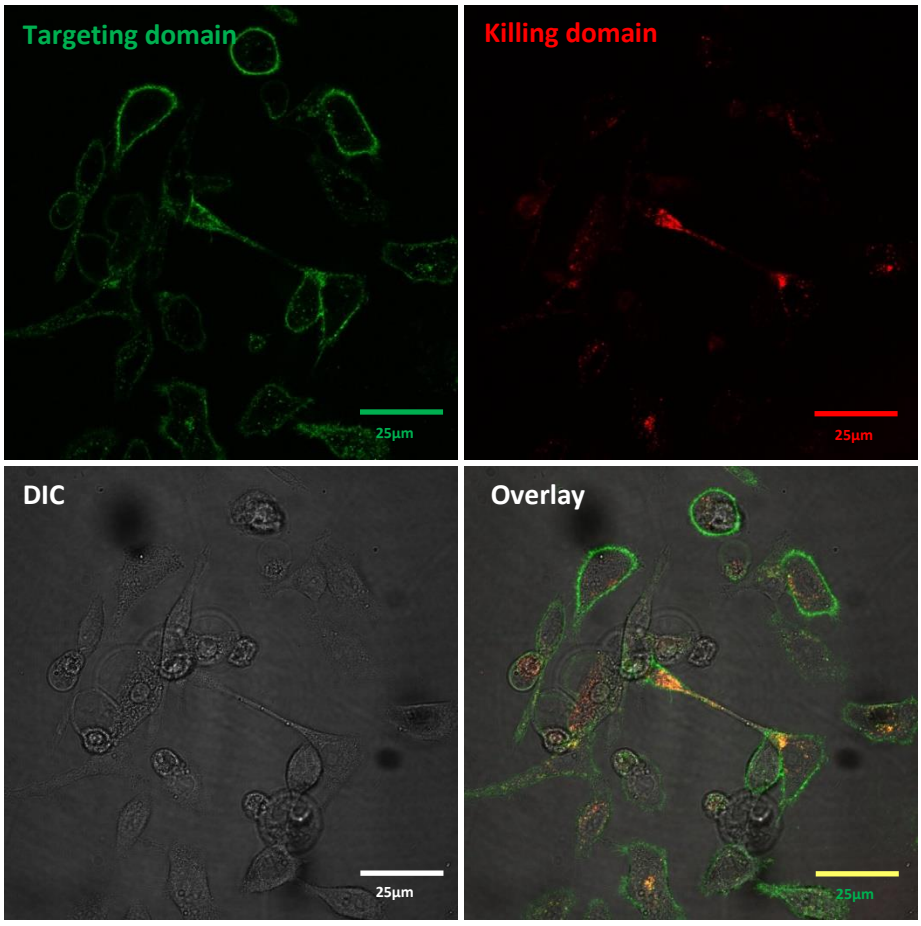

Figure 4.3.27: Immunofluorescence live images of A549 cells incubated for 24 hours with BLF1/anti-CD9 model immunoconjugate :
Cells were cultured overnight in glass-bottomed FluoroDish™, then incubated with model immunoconjugate constructed using mCherry-BLF1 (C94s) and Alexa Fluor 488-labelled

anti-CD9 for 24 hr as described in (2.2.6). Green fluorescence corresponds to anti-CD9. Red fluorescence corresponds to mCherry BLF1 (C94S). Grey corresponds to phase contrast. Slides were imaged by confocal microscopy (60 x oil objectives) using appropriate filters.

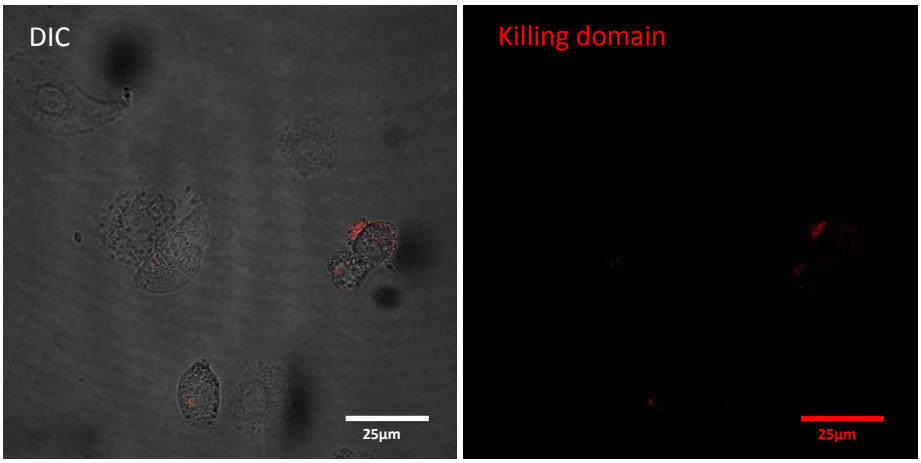

Figure 4.3.28: Immunofluorescence live images of A549 cells incubated for 24 hours with isotype control conjugate:
Cells were cultured overnight in a glass-bottomed FluoroDish™, and then incubated with isotype control conjugate constructed using mCherry-BLF1 (C94s) for 24 hours as described in (2.2.6). Red fluorescence corresponds to mCherry BLF1 (C94S). Grey corresponds to phase contrast. Slides were imaged using confocal microscopy (60 x oil objectives) using appropriate filters.

In order to identify the organelles, in which the accumulation of the BLF1/anti-CD9 immunoconjugate took place after internalization, colocalization with the endosomal marker LAMP1 was investigated (**Fig**.4.3.29). Images from fluorescent microscope revealed that some of the labelled conjugate accumulated in the vesicles that surround the nucleus and colocalized with LAMP1 demonstrating possible accumulation in acidic vesicles such as late endosomes and lysosomes.

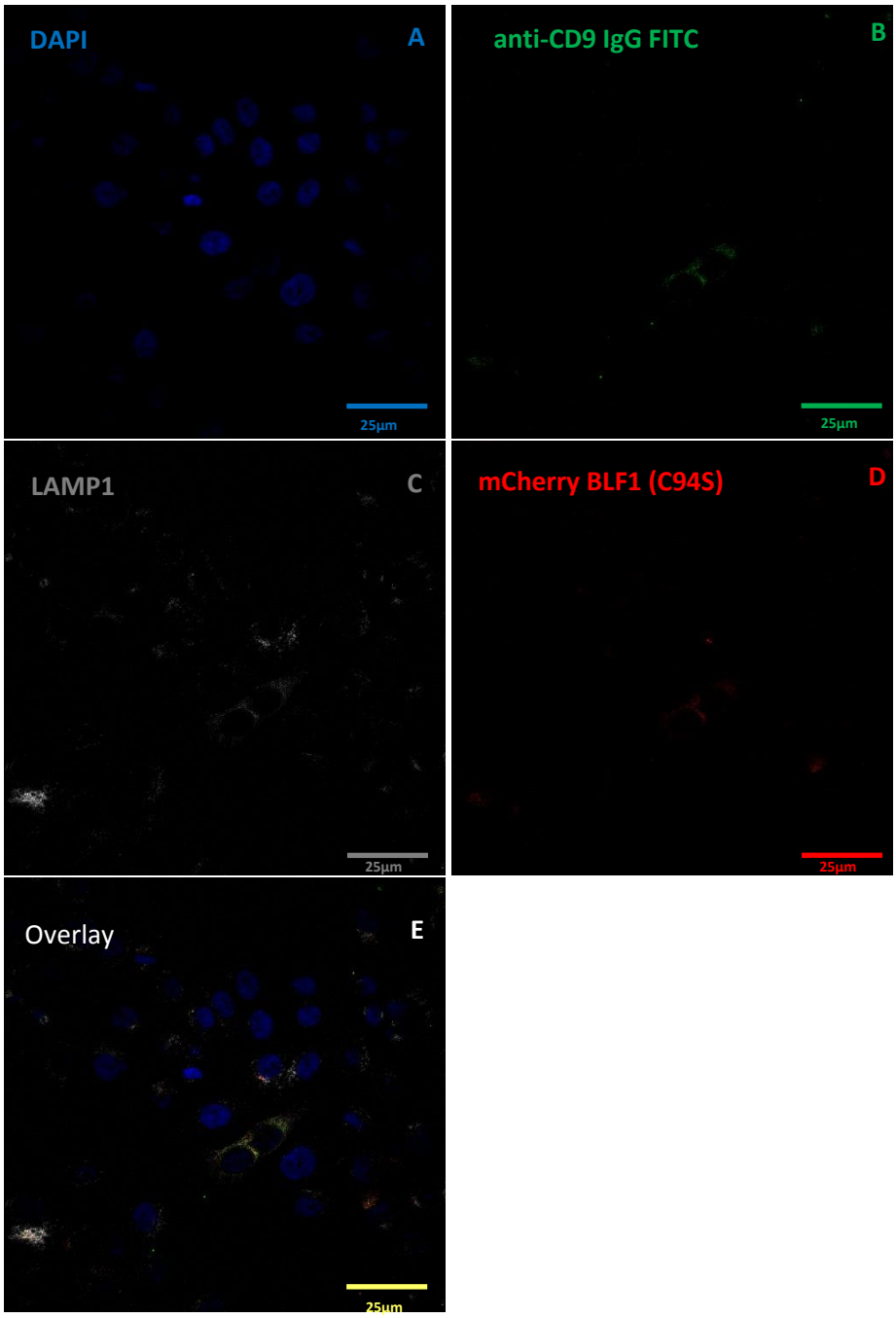

Figure 4.3.29: Confocal images of A549 cells incubated for 2 hours with mCherryBLF1 (C94S)/anti-CD9 immunoconjugate:
Cells were cultured overnight on a coverslip placed in 24 well plates and incubated with mCherry-BLF1 (C94S)/anti-CD9 conjugate for 2 hr. Cells were then fixed and permeabilised and stained with Alexafluor-647 labelled anti human-anti-LAMP1 antibody as described in (2.2.8.4.1).(**A**) Blue fluorescence corresponds to nuclei stained with DAPI.(**B)**Green fluorescence corresponds to anti-CD9. (**C**) Grey corresponds to Alexafluor-647 labelled anti human-anti-LAMP1 antibody. (**D**) Red fluorescence corresponds to mCherry-BLF1 (C94S). (**E**) Merged images. Slides were imaged using confocal microscopy (60 x oil objectives) using appropriate filters.

4.4 Discussion:

The aim of this chapter was to develop primitive targeted conjugates to investigate if BLF1 can be successfully targeted to model cancer cell lines using specific monoclonal antibodies. It was hoped that the use of non-covalently crosslinked conjugates would provide a means for feasibility studies before committing to the expense and effort of generating directly linked immunotoxins. Two approaches, both using secondary antibodies to cross-link BLF1 and the targeting monoclonal antibody, were used. Initially, as this had been used by another member of the group with some apparent success, secondary antibody-coated magnetic beads were used to conjugate BLF1 and targeting antibody. In a second approach, soluble non-covalently linked immunoconjugates were generated using secondary antibody alone. As described in the Introduction, the proposed target antigens were the tetraspanin proteins CD63 and CD9.

4.4.1 Binding specificity of BLF1/antibody model conjugate:

An ELISA assay was initially developed to detect BLF1 in the non-chemically linked conjugates and to ensure that the conjugates retained antigen binding ability. The assay used rat polyclonal anti-BLF1 antibodies to detect BLF1 and recombinant CD9 or CD63 protein as the target for the antibody components. These investigations revealed that all model conjugates were able to target BLF1 specifically to CD63 or CD9 antigen, with no signal detected from the isotype conjugate or non-antigen coated wells (**Fig**.4.3.3, 4.3.14, 4.3.19).

The rat anti-BLF1 antibody was also used to assess targeting of BLF1 by the model conjugates to live cells using indirect immunofluoresence. Analysis by flow cytometry demonstrated a significant, specific binding of the BLF1 component of the BLF1/anti-CD63 bead conjugate to RBL-2H3 cells transfected with human CD63, but not the wild type control cells (**Fig.**4.3.4). Subsequent analyses of the bead conjugates on A549 cell showed detection of BLF1 on the cell surface, whereas as noted in Chapter 3, the unconjugated BLF1 did not bind to these cells.

4.4.2 Studies with the RBL-2H3 rat basophilic leukaemia cell line:

As explained in the Introduction to this Chapter, our initial plan was to use the RBL-2H3 cell line as a model, since we had stable transfectants expressing the human CD63 target

antigen and the untransfected wild type cells would provide a good negative control. Flow cytometry confirmed the expression of human CD63 by these cells and as noted above, specific targeting of BLF1 to these cells was achieved using the BLF1/anti-CD63 bead conjugate. However, the BLF1/anti-CD63 beads conjugate did not show any significant toxic effect on these cells when tested using the SRB assay (**Fig**.4.3.5). High concentrations of BLF1/bead conjugates were, however, toxic to the BLF1-sensitive J774 cell line (F**ig**.4.3.8).

The effect of BLF1 alone on RBL-2H3 cells was then assessed in the presence or absence of lipofectamine (**Fig**.4.3.6) and no effect was observed even at high molar concentrations of BLF1 that were toxic to other cell lines (Chapter 3). It therefore appears that RBL2H3 cells are resistant to BLF1. Interestingly, work carried out by an MSc student under my supervision showed that the RBL2H3 cells are also resistant to the toxin saporin (**Fig**.4.3.7). The plant toxin saporin has been previously used for targeted killing of various cell types including cancer cells (Polito et al., 2013). The explanation for this is unclear, but the RBL-2H3 cell line used here is known to have a strong secretory phenotype (Bingham et al., 1994) and it is possible that the toxins were taken up and then secreted. Interestingly, later microscopy studies using soluble anti-CD63/mCherryBLF1 conjugates showed that fluorescence was present in large vesicles in RBL2H3 cells, which might correspond to secretory vesicles (**Fig.**4.10.24). Alternatively, the sequestering of the toxin into large vesicles may be a defence mechanism to overcome the stress caused by the toxin, similar to the sequestering of abrin (a type II RIPs) (Gadadhar and Karande, 2013) and viral proteins (Maroui et al., 2011).

4.4.3 Studies with A549 lung epithelial cancer cells and BLF1/antibody bead conjugates:

Since A549 cells were known to be sensitive to BLF1 and previous work in the laboratory had indicated they expressed both CD63 and CD9 as potential target antigens, further work was carried out using this cancer cell line. Significant levels of CD9 were detected on the cell surface of A549 cells with lower expression levels of CD63; this could be due the tetraspanin CD63 being mainly associated with the endosomal compartment (Rous et al., 2002, Peden et al., 2004, Janvier and Bonifacino, 2005)(**Fig.**4.3.9). In contrast, CD9 is known to localize to the plasma membrane and only partly in the endosomes of all mammalian cells (Sumiyoshi et al., 2016).

As discussed previously, antigen internalisation on antibody binding is an important property in immunotoxin therapy. **Fig**.4.3.10 shows that on anti-CD63 antibody binding at 37°C, the amount of cell surface CD63 on A549 cells decreases rapidly with >40% lost by 15 minutes and peaking at approximately 50% within 60 minutes. Thus CD63 antigen has a high rate of internalization upon anti-CD63 antibody binding on these cells, indicating that it is a suitable model target. However, on anti-CD9 binding, only 25% of CD9 was internalized by 15 minutes with little further decrease by 45 minutes. Thus CD9 antigen has a lower rate of internalization. However, as stated above, A549 cells express more CD9 on their surface than CD63 and the CD9 antigen may internalize over a longer time. As noted previously, carcinoembryonic antigen is used as tumor targeting antigen and internalizes with a half-life 10-16 hrs (Schmidt et al., 2008). Thus CD9 probably represents a potential target antigen for immunotoxin development.

The ability of BLF1/anti-CD63 and BLF1/anti-CD9 bead conjugates to target BLF1 to A549 cells was next assessed by flow cytometry. Higher levels of BLF1 were detected in bead conjugates containing the targeting antibodies compared to isotype controls (**Fig.** 4.3.11 and 4.3.15). Fluorescence microscopy of A549 cells incubated with bead conjugates constructed using mCherry BLF1 indicated that those containing targeting antibodies were internalised (**Fig.**4.3.13 and 4.3.17) whereas no internalisation was observed with conjugates containing isotype control (**Fig.**4.3.13). The targeting antibody and mCherryBLF1 also appeared to co-localise in cells.

On assessing their effect on cell growth, there appeared to be some reduction in cell growth with the highest concentration of BLF1-anti-CD63 beads, although this was not significant (**Fig**.4.3.12). No reduction was observed with lower concentrations or with the BLF/anti-CD9 beads (**Fig**.4.3.16). This indicates that the targeting conjugates were not able to deliver BLF1 effectively into the cells. It is also possible that after binding and internalization of the conjugate it was trafficked to the endosomal-lysosomal pathway leading to the deactivation of the BLF1 activity. The other possible explanation for CD63 is that since it is also found in lysosomes, the BLF1 toxin might be trafficked here and unable to escape to the cytosol to exert its effect. In the case of CD9, although the microscopy images appear to show internalisation, they may represent bead conjugates on the cell surface. As noted above, CD9 is found predominantly in the plasma membrane and internalises relatively slowly, so a

significant proportion of the BLF1/anti-CD9 bead conjugate may have remained membrane bound.

As described in Chapter 3, LF3000 was able to deliver BLF1 toxin into range of cancer cell lines (Rust et al., 2015). In the presence of lipofectamine, significant effects in cell growth were observed at the highest concentrations of the conjugates, demonstrating that they contained sufficient BLF1 to give toxicity (**Fig**.4.3.12 and 4.3.16). However, significant effects were also apparent with the isotype control beads in the presence of lipofectamine. Despite the targeting antibody beads showing some specificity in binding to A549 cells, it is likely that under the conditions of the SRB assay, isotype control beads were still able to interact with the cells (perhaps by "settling" non-specifically on the cell surface) and lipofectamine facilitated their uptake. It is also possible that lipofectamine facilitated release of the toxin into the cytosol from the endosomal compartment.

4.4.4 Studies with A549 lung epithelial cancer cells and soluble BLF1/antibody conjugates:

Soluble non-covalently crosslinked model conjugates were also developed using BLF1 and anti-CD63 and anti-CD9 antibodies. As mentioned in the Introduction to this chapter, it was reasoned that these would more closely resemble conventional immunotoxins and would perhaps be more easily taken up the cells and release the toxin into the cytosol. The binding specificity of these conjugates was assessed using the ELISA assay (with recombinant tetraspanins as antigens (**Fig.**4.3.19) and on live cells by flow cytometry (**Fig**.4.3.20) and fluorescence microscopy (**Fig**.4.3.21). All types of assay demonstrated that soluble model conjugates could specifically target BLF1 to the CD63 or CD9 antigen. In flow cytometry, significantly higher detection of BLF1 binding to cells was observed with the anti-CD63 or anti-CD9 conjugates compared to the isotype control conjugates (**Fig.**4.3.20).

Taken together, these data strongly confirms that BLF1 could be targeted specifically to the cells bearing antigen by using non-covalent coupling with antibodies that target a specific antigen expressed on cancer cells. A flow cytometry-based assay was then used to determine if the conjugates were internalised, using the anti-BLF1 antibody to detect cell surface bound BLF1. The results indicated that the percentage of internalized BLF1/anti-CD63 immunoconjugate reached approximately 60% within 15 minutes (**Fig.**4.3.22) and was relatively constant over the remaining time period tested. Hence, the majority of anti-CD63

antibody internalization occurs within minutes, which means that CD63 antigen rapidly transports BLF1/anti-CD63 conjugate from the cell membrane. Internalization of BLF1/anti-CD9 conjugate showed a fast uptake of at least 25% of the conjugates in the first 15 minutes and a slower uptake of at least another 7% of the conjugate in the subsequent 45minutes (**Fig**.4.3.22). Thus the uptake of BLF1/anti-CD63 conjugate was higher than BLF1/anti-CD9 conjugate in human lung cancer cells (A549). These results support the previous finding that the internalization of naked anti-CD63 antibody was higher than the anti-CD9 antibody (**Fig**.4.3.10).

Since the conjugates showed good binding specificity and were internalised, the cytostaticity/cytotoxicity of BLF1/anti-CD63 and BLF1/anti-CD9 immunoconjugates were tested on A549 cells. One disadvantage of the soluble conjugates is that it is not possible to purify them to remove free BLF1. For use in the SRB assay, the final concentration of BLF1 was therefore designed to be no more than 0.08 μM, since at this concentration, BLF1 alone shows no effects unless deliberately introduced into the cytoplasm (Chapter 3, **Fig.**3.3.10). Therefore, any arresting of cell growth observed should be due to successful targeting. The SRB results showed that the BLF1/anti-CD63 conjugate had no significant effect on the cell growth of A549 cells at the highest concentrations used (**Fig**.4.3.23.A, 4.2.23.C), but the BLF1/anti-CD9 conjugate did show significant inhibition of cell growth compared to untreated cells. However, at the highest concentration used (equivalent to 0.08 μM BLF1), arresting of cellular growth was also apparent with the isotype control conjugate, although at a lower level than the anti-CD9 conjugate (**Fig**. 4.3.23.B). This may have been due to non-specific binding/uptake, although the isotype control conjugate did not appear to show any significant binding by flow cytometry.

As noted above, lipofectamine combined with the BLF1/anti-CD63 and anti-CD9 bead immunoconjugates resulted in a significant reduction in cell growth (**Fig.**4.3.12, 4.3.16), but this was also evident with the isotype control conjugates. To try to improve the performance of the soluble conjugates, a different efficacy enhancer, saponin, was used, which is reported to act by enhancing endosomal escape, rather than increasing uptake of toxins. The combination of saponin (2 μg/ml) with the BLF1 model immunoconjugate augmented the effects of both immunoconjugates tremendously (**Fig**.4.3.23.C, D), with approximately 60% reduction in cell growth. However, again, similar effects were observed

with the isotype control conjugate indicating that the effect was non-specific. This is most likely correlated with saponin- mediated delivery of BLF1 into the cytosol of the cancer cells. This is consistent with work by others studying the effect of saporin- based targeted toxin in combination with saponins that triggered the release of internalized toxin molecules out of late endosomal/ lysosomal system into the cell cytosol. The synergistic effect of combination therapy (saporin targeted toxin+ saponin) was also demonstrated in tumor bearing BALB/c mice (Weng et al., 2012). Moreover, a recent study revealed that combination therapy of tiriterpenoidal saponins with Saporin-Rituximab, Saporin-anti-CD22, and Saporin-anti-CD25 resulted in enhancement factors of 700-fold, 170-fold and 25-fold, respectively in Ramos cells (Gilabert-Oriol et al., 2016).

Preliminary attempts were made to determine the trafficking routes of BLF1 (the killing domain) and the targeting domain (anti-CD63 and anti-CD9 antibodies) of the soluble immunoconjugates following incubation with live cells by fluorescence microscopy using mCherryBLF1 (C49S mutant) and directly labelled antibodies (**Fig**.4.3.24.A, 4.3.25, 4.3.27). In A549 cells, the BLF1 and antibody components of the BLF/anti-CD63 conjugate appeared identical in terms of their subcellular location, and were present mainly in small vesicles in the cytoplasm after 24 hr (**Fig**.4.3.24 and **Fig.**4.3.25). As shown by flow cytometry (**Fig**.4.3.22) and microscopy (**Fig**.4.3.21), BLF1/anti-CD63 conjugates were internalised rapidly by A549 cells. Further studies using an antibody to transferrin (a marker for early endosomes) indicated that BLF1 was localised at least partly in early endosomes after internalisation (**Fig**.4.3.26). Flow cytometry has also shown that at least some of BLF1/anti-CD9 conjugate internalised rapidly (**Fig.**4.3.22). Further studies using the lysosomal marker Lamp1 suggested partial localisation of the BLF1 in lysosomes after internalisation (**Fig.**4.3.29). Live images from confocal microscopy demonstrated that the BLF1 component of the BLF1/anti-CD9 conjugate was mainly located in the cytoplasm after 24 hr (**Fig.**4.3.27). Thus CD9 protein has the potential to internalize and can be used as a means of targeting BLF1 containing immunotoxins to antigen bearing cells. Interestingly, however, the anti-CD9 component of this conjugate was significantly present on the cell membrane at this time, suggesting that it may not have internalised or had been recycled back to the plasma membrane following internalisation.

Overall, the results reported in this Chapter demonstrate that it was possible to generate model, non-covalently linked BLF1 immunoconjugates that were useful for assessing antigen targeting and internalisation. However, using the conjugates alone, it was not really possible to demonstrate significant specific effects on cell growth. This may have been due to inefficient uptake of the toxin, problems associated with intracellular trafficking (e.g. poor endosomal escape) or instability of the conjugates.

5 Chapter 5: Construction and functional assessment of chemically linked BLF1 immunotoxin.

5.1 Introduction:

As mentioned earlier in chapter 1, a key step in the construction of chemical conjugates is the type of linker. Linking should not interfere with the binding affinity of the antibody to the target antigen, the internalization of the toxin, and the intracellular activity of the toxin. SPDP, N -succinimidyl 3-(2-pyridyldithio) propionate, is the most common heterobifunctional crosslinking reagent used for construction of immunotoxin (Fuchs and Bachran, 2009). Therefore, BLF1 was chemically cross-linked to (a) anti-CD63 (b) anti-CD9 antibody via covalent linkage introduced by SPDP as described in 2.2.24.1. Two basic strategies were used to form cleavable crosslinks between BLF1 with SPDP reagents, depending on whether or not the BLF1 used possessed a sulfhydryl group (-SH) introduced by genetic engineering. Both conjugation methods result in crosslinks that contain a disulfide bond in the spacer arm (Carlsson et al., 1978).

5.2 The role of intracellular trafficking in immunotoxin toxicity:

Many tools have become available to understand the endocytic pathway of targeted toxins as various studies have indicated that toxins can follow different intracellular pathways which is related to their cytotoxic action inside the cells (Tome-Amat et al., 2015). To follow the intracellular pathway in more detail using our model targeted conjugate, colocalization with early and late endosomal/lysosomal compartments were studied. With this purpose, early endosomes were labeled using transferrin. Lysosomes were labelled using antibodies to LAMP1, a glycoprotein specific to lysosomal membranes (Carlsson and Fukuda, 1989) or Lysotracker^{TM}green, a fluorescent dye that stains cellular compartments with a low pH in live cells. A recent pH sensitive fluorescent dye pHrododextran is used to track the conjugate as it is endocytosed into the highly acidic endosomal compartments (endosome/lysosome) (Saftig and Klumperman, 2009). Co-localization with Golgi apparatus was also investigated using wheat germ agglutinin, which is a marker for the Golgi membrane (Zhao et al., 2006).

5.3 Aims:

We aimed to prepare a variety of BLF1/IMT conjugates and estimate their specific binding compared to the non- conjugated BLF1 toxin and parental antibody using flow cytometry assay. We aimed also to determine impact on cell growth after incubating the antigen bearing cells with BLF1 targeted IMT. Furthermore, the saponins that were successful in enhancing the potency of primitive model conjugates described in the previous Chapter were again investigated with the chemically crosslinked BLF1 immunotoxin. We also assessed the effects of other reported immunotoxin efficiency enhancers, brefeldin A and bafilomycin. In addition, we attempted to investigate the intracellular co-localization of the IMTs within the endosomal compartment, since release from this compartment is required for BLF1 activity.

5.4 Results:

5.4.1 Expression and affinity purification of BLF1 6His-Cys:

As described in 2.1.8 a vector encoding BLF1 with a Cysteine in position 2 after the start codon was generated by Dr Guillaume Hautebergue, SITraN, University of Sheffield. This form of BLF1 was expressed in *E.* coli to provide protein with an N-terminal sulfhydryl group available for chemical conjugation to generate immunotoxins. As previously, the constructs was designed so that BLF1 was expressed with an N-terminal 6His tag to facilitate purification. The relevant vector (Table 2.1.5) was used to transform BL21 cells and after induction with IPTG, cultures were harvested and bacteria lysed as described in 2.2.9.1 and 2.2.9.2. The 6His tagged forms of BLF1 were purified from the lysates by affinity chromatography on Cobalt Beads as described in 2.2.9.3. Samples from each step of the purification were run on a SDS PAGE gels and subsequently stained with Coomassie blue (**Fig**.5.4.1). The His-cys-tagged BLF1 is predicted to have a molecular weight of approximately 24 kDa.The higher molecular weight band observed here after affinity purification (lane 4) at ~ 50 kDa is thought to represent dimers of BLF1 protein. BLF1 (shown in lanes 5) is the protein after gel filtration with bands being detected at the expected molecular weight as indicated by the red arrow. The concentration of purified BLF1 was quantified by measuring the absorption at 280 nm as described in 2.2.9.3.

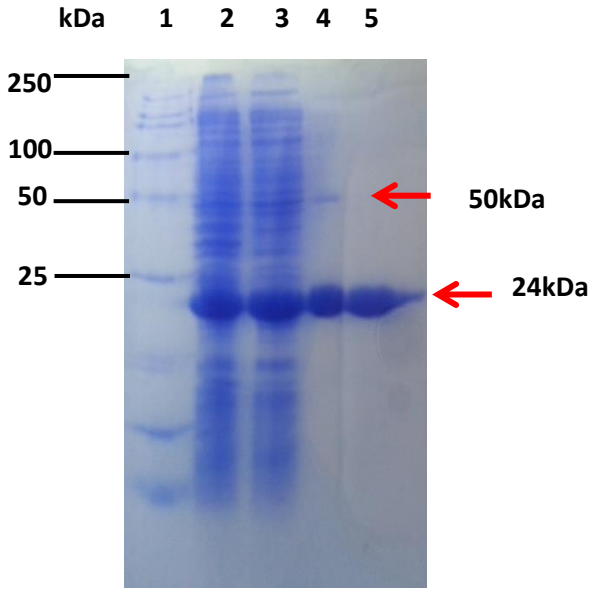

Figure 5.4.1: SDS-PAGE analysis of BLF1-6His-Cys purification from bacterial cell lysates: Lysates were prepared from *E. coli* transformed to express Cys2-6His-BLF1 as described in 2.2.9. Fractions collected after each purification step were analysed by SDS-PAGE (5-15%) under reducing conditions before Coomassie staining. Lane 1, protein markers (labelled in kDa); lane 2, cell free extract; lane 3, flow through; lane 4, elution after Cobalt column purification; lane 5, sample after gel filtration on Superdex 200.

5.4.2 Chemical conjugation of BLF1 to monoclonal antibody:

As described in section 5.1 two basic strategies were used to form cleavable crosslinks between proteins with SPDP reagents, depending on whether one or neither proteins already possesses sulfhydryl groups (-SH) in addition to primary amines.

5.4.2.1 Chemical conjugation of BLF1-6His-Cys with anti-CD63 or anti-CD9 monoclonal antibodies:

Here, we used a modified version of BLF1-6His, which has a cysteine group introduced at its N-terminus to provide a sulfhydryl group available for the conjugation with specific monoclonal antibodies (2.2.3.4.1). The NHS ester end of SPDP reacts with amine groups in the monoclonal antibody to form an amide linkage, and then the resultant 2-pyridyldithiol activated group at the other end of the antibody reacts with BLF1 that contains sulfhydryl reactive groups to form a disulfide cross linked antibody-toxin conjugate.

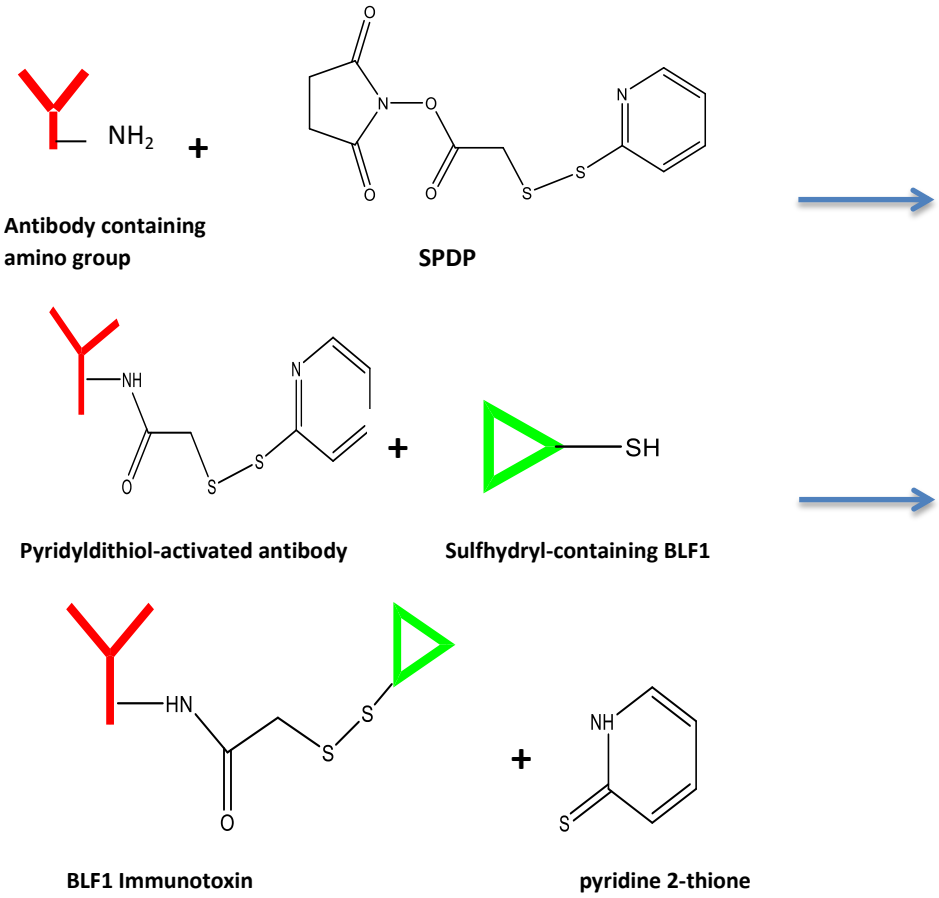

Figure 5.4.2: Coupling of BLF1 with a free (-SH) group with IgG antibody through the SPDP linker.

5.4.2.2 Chemical conjugation of un-modified mCherry tagged BLF1-6His to monoclonal antibodies:

A mCherry-tagged version of BLF1 was chemically conjugated with anti-CD63 or anti-CD9 antibody to investigate internalization and trafficking of BLF1 following binding of the immunotoxin conjugate. As no version of this protein with an N-terminal cysteine was available, a different conjugation strategy was used. For this purpose, the monoclonal antibody was modified with SPDP reagent to form pyridyldithiol-activated antibody. The resultant pyridyldithiol-activated antibody was reduced with dithiothreitol (DTT) to release pyridine 2-thione and to create a free sulfhydryl group on the monoclonal antibody. The mCherry BLF1 was then modified with SPDP and allowed to react with the thiolanated antibody to form antibody-toxin conjugate covalently linked through a disulphide bond. This crosslinking method, that involves SPDP modification of both proteins, has been used to prepare a range of IMT (Barriuso et al., 2016, Thorpe and Ross, 1982). The antibody is more

frequently thiolated in this method rather than the toxin, so as to avoid exposing the toxin to reducing conditions that could affect internal disulphide bonds of the toxin moiety. Therefore SPDP-toxin is mixed with thiolated antibody to form the final covalently linked conjugate.

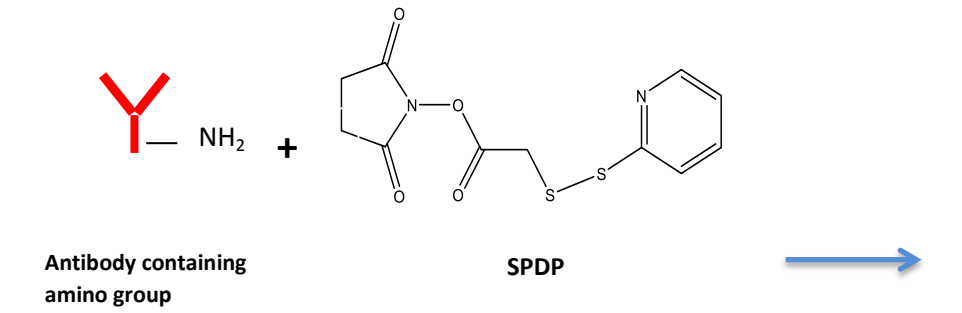

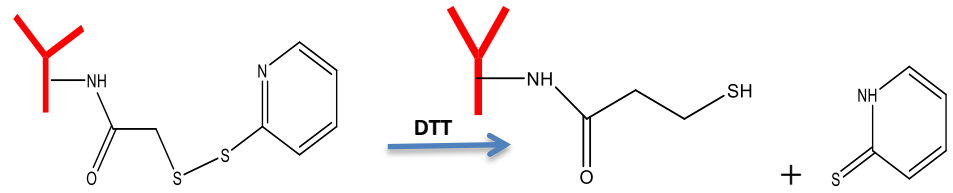

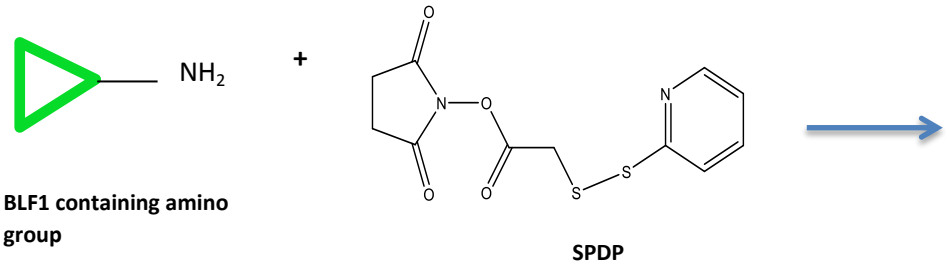

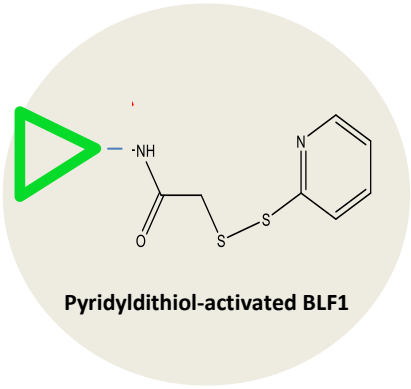

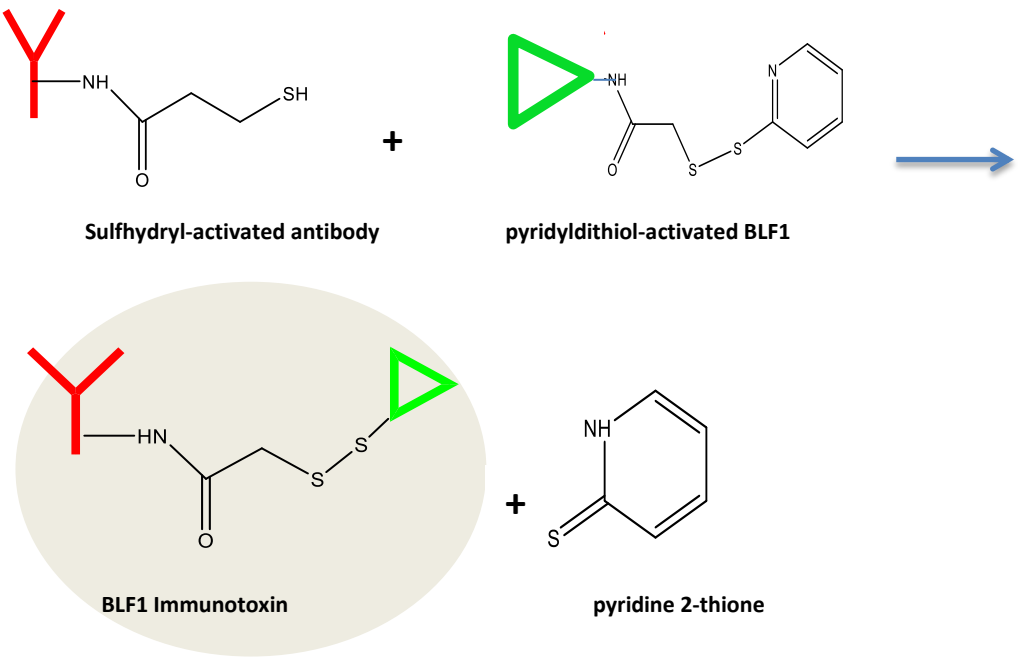

Figure 5.4.3: Coupling of BLF1 with no free (-SH) with IgG through SPDP linker.

5.4.3 Purification of (BLF1-6His-Cys/anti-CD63) immunotoxin:

Immunotoxin purification is a prerequisite for experiments in a model system *in vivo* and *in vitro*. The presence of free antibody in immunotoxin preparation may influence the results of cytotoxicity assay, for instance, by saturating the cell-surface antigen and blocking the internalization pathway (Lambert and Blattler, 1988). Initially a nickel column was used to purify the (BLF1/anti-CD63) based immunotoxin (as the BLF1 used contains a his tag) from any non-conjugated antibody. Next, gel filtration was performed to separate the immunotoxin from free BLF1, based on molecular weight. However, this strategy resulted in loss of a large amount of protein, apparently due to non-specific retention on the column. Therefore, to separate the IMT from the rest of the proteins (unconjugated BLF1 and unconjugated antibody), the reaction mixtures was subjected to purification by gel filtration only as described in 2.2.3.5. Prior to this, the reaction mixture was subjected to membrane ultrafiltration using Vivaspin devices (MW cut-off 100 kDa) to concentrate the sample and also to help remove unconjugated BLF1. The concentrated sample was applied to a Superdex 200GL column and fractions collected as shown in **Fig**.5.4.4.A. Fractions that contained protein were analysed by SDS-PAGE under non-reducing conditions, along with samples of the original conjugation mixture and those obtained after membrane

ultrafiltration. Unconjugated anti-CD63 antibody was included as a control. Only one major band (MW ~25 kDa) was identified from the flow through (lane3) after membrane ultrafiltration, presumed to correspond to free BLF1. The unconjugated antibody in lane 4 was detected at the expected molecular mass at 150 kDa. There are some additional fainter bands at lower MW, which may correspond to different glycoforms of the antibody, contaminants remaining after Protein G purification and some free heavy and light chains. As expected, in the reaction mixture after conjugation, there is a range of protein bands (Lanes 2 and 5), but very little at 150 kDa. Instead there is a range of higher molecular weight bands corresponding to antibody conjugated with different amounts of BLF1 protein. These are largely resolved by gel filtration, with fractions 8-15 (Lane 6) and fractions 16-20 (Lane 7) corresponding to immunotoxin conjugates, whereas fractions 28-32 (Lane 8) appears to contain mainly free BLF1 (MW ~25 kDa) with some appearing as dimers (50 kDa) as previously noted. The fractions 16-20 highlighted in red were used to assess the effect on the growth of a range of cancer cell lines. The total protein recovered from initial sample applied was 72%. The concentration was determined in each of the eluted fractions by Bradford assay.

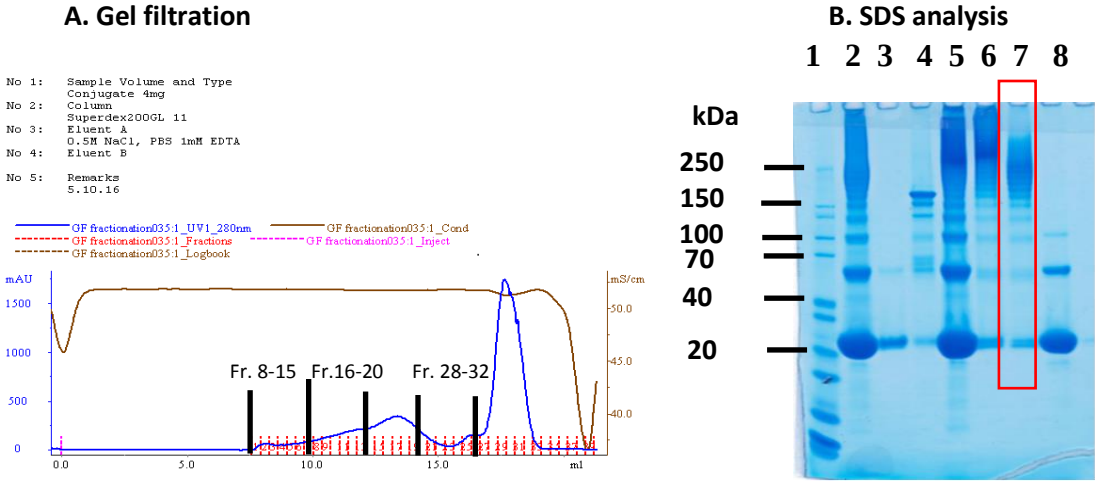

Figure 5.4.4: purification of anti-CD63 IMT:
A. Gel filtration of anti-CD63 IMT: The immunotoxin reaction mixture was applied to a 10 x 300 mm Superdex 200GL column, equilibrated with PBS-EDTA buffer. The flow rate was 0.5 ml/min. and 0.35ml fractions were collected. **B. SDS-page analysis:** Nu-PAGE 4-12% BT Novex gel was performed under non-reducing conditions before Coomassie staining. Lane 1, protein markers; lane 2, IMT before purification; lane 3, flow through after membrane ultrafiltration using Vivaspin concentrator 100 kDa; lane 4, unconjugated anti-CD63 antibody; lane 5 concentrated IMT after membrane ultrafiltration (before gel filtration); lane 6 (fr.8-15), 7 (fr.16-20) ,8 (fr.28-32), fractions after gel filtration.

5.4.4 Validation of anti-CD63 IMT purity by Western blotting:

Although successful chemical conjugation of BLF1 with anti-CD63 antibody was indicated by detection of higher molecular mass of proteins by SDS-PAGE (**Fig**.5.4.4.A, B), validation of the cross-linking reaction was confirmed again by Western blot using the primary rat antibody raised against BLF1 described previously (**Fig**.5.4.5). The unconjugated BLF1 and un-purified anti-CD63 IMT were included as controls. The exposure time in the Western blot was increased to visualise the purified anti-CD63 IMT band (fr.16-20). The results show the presence of a single band (lane 2) at the higher exposure time at ~200 kDa. This suggests that most of the immunotoxin corresponds to one antibody molecule with two BLF1 molecules attached. In the case of un-purified anti-CD63 IMT (lane 4), the BLF1 bands were specifically detected as expected at molecular mass of ~25 kDa (monomer) and 50 kDa (dimers). The results also indicate the presence of a high molecular mass band ~ more than 200 kDa in lane4 as expected to be the unpurified anti-CD63 IMT.

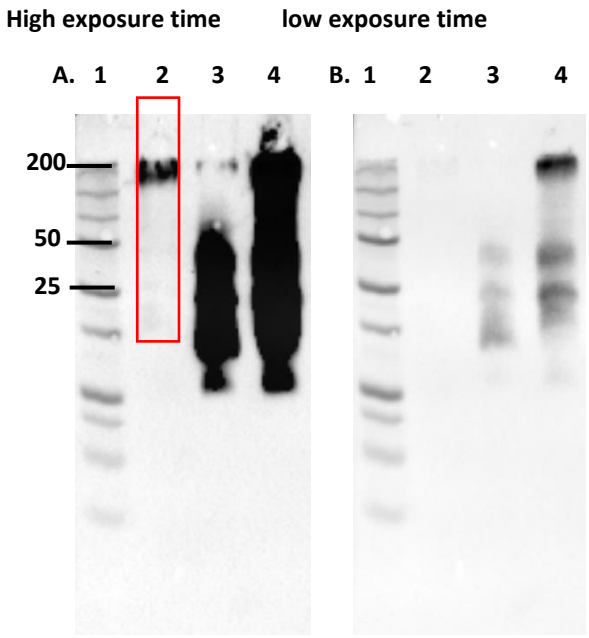

Figure 5.4.5: Western Blot of purified and un -purified anti-CD63IMT:
An aliquot of IMT after gel filtrations was separated on 12.5% SDS-PAGE and Western blotted with anti-BLF1 antibody (1/1000) followed by anti-rat HRP (1/2000) as described in 2.2.3.6. The unconjugated BLF1 and un-purified IMT were also included as a control. **A**. High exposure (10 second). **B**. Low exposure (5 second). Lane 1, protein markers; lane 2, purified IMT (fr.16-20) 5 µg; lane 3, unconjugated BLF1 (5µg); lane 4, un-purified IMT (5 µg).

5.4.5 Expression of CD63 on human melanoma cell line MeWo:

Previous work using model conjugates had been focused on the A549 lung cancer cell line as antigen positive cells; however during further study it became apparent that the level of CD63 expression on this cell line was relatively unstable and varied according to the growth status of the cells. As CD63 is a valuable antigen to target, because of its distribution on the cell surface and rapid internalization following antibody binding, another cell line expressing high levels of CD63 was sought. Therefore a human cell line derived from malignant melanoma tumors was investigated (MeWo)(Grose and Brunel, 1978), as it was expected to express high levels of CD63. Indeed, previous studies by our group had shown that this cell line expressed high levels of CD63 compared with other human melanoma cells line (Parthasarathy, PhD thesis, University of Sheffield, 2006). Flow cytometry data demonstrated high surface expression of CD63 antigen as indicated by high fluorescence intensity (**Fig.**5.4.6). Therefore the CD63 antigen could be used as potential immunotoxin target for this cancer cell line.

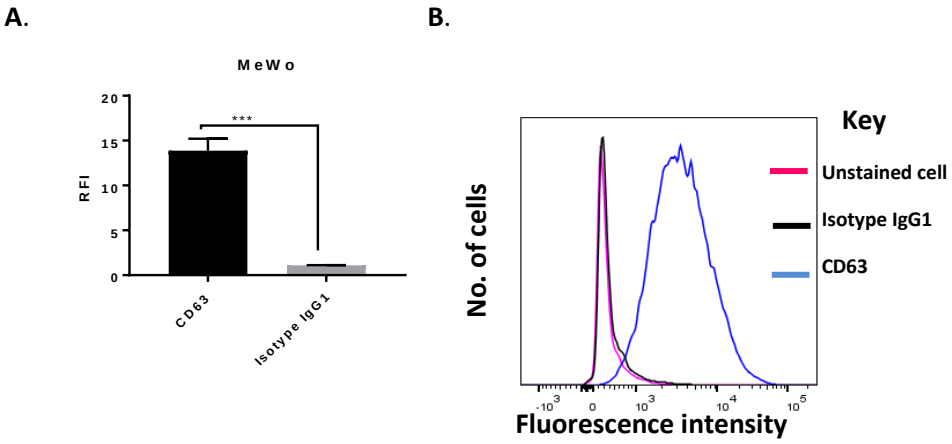

Figure 5.4.6: Surface expression of CD63 protein on human melanoma cell line (MeWo): Cells were incubated with monoclonal anti-CD63 or appropriate isotype controls followed by secondary FITC-conjugated anti-mouse IgG antibody and analysed by flow cytometry as described in (2.2.4). **A.** Bar charts represent the relative fluorescent intensity of CD63 antigen expression in MeWo (blue) as compared to isotype control (black). **B**. Overlay histograms of fluorescence intensity of anti-CD63 and its respective isotype controls in MeWo cells. Three independent experiments were performed in duplicate, with values shown as mean ± SEM. The significance of difference was determined by unpaired t- test at $p<0.0001$.

5.4.6 Functional assessment of BLF1/anti-CD63 IMT:

The chemically conjugated BLF1/anti-CD63 was assessed for target binding specificity and impact on cellular growth. Attempts were also made to determine the intracellular localisation of the IMT. As mentioned above, there were initially considerable problems in obtaining sufficient quantities of pure immunotoxin conjugate. Due to time constraints, some studies were therefore carried out using the un-purified conjugation mixture. As a high ratio of BLF1: antibody was used, it was considered that there would be relatively little free antibody. After allowing for immunotoxin binding, targeted cells were washed to remove as much free BLF1 as possible.

5.4.6.1 Assessment of binding specificity of (BLF1/anti-CD63) IMT by flow cytometry:

The cell surface binding of (BLF1/anti-CD63) IMT to MeWo cells was tested using flow cytometry. In this experiment, un-purified IMT was used. The rat anti-BLF1 antibody was used to detect the BLF1 component of the IMT as described previously. As shown in (**Fig**.5.4.7.A, B) there is high binding of the BLF1/anti-CD63 IMT compared with negligible binding of the unconjugated BLF1. The anti-mouse IgG-FITC was used to detect the monoclonal antibody component of the IMT. Again significant binding was detected, that is similar to the expression level of CD63 in MeWo cells (**Fig**.5.4.7.C).

The specificity of binding was further assessed using RBL-2H3 cells transfected with human CD63, compared with the wild type RBL-2H3 cells that only express rat CD63 (**Fig.**5.4.8). Flow cytometry data demonstrated significant binding of (BLF1/ anti-CD63) IMT to the RBL cells transfected with CD63 (hCD63) as compared the wild type (-hCD63) and unconjugated BLF1. Overall, these results confirm that the BLF1/anti-CD63 IMT targets specifically to cells expressing CD63.

A.

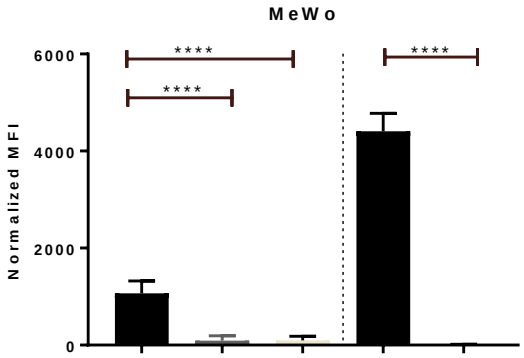

BLF1/anti-CD63 IMT	+	-	-	+	-
BLF1 alone	-	+	-	-	-
Anti-BLF1 Ab	+	+	-	-	-
Anti-CD63 Ab	-	-	-	+	+
2nd anti- rat Ab	+	+	+	-	-
2nd anti-mouse Ab	-	-	-	+	+

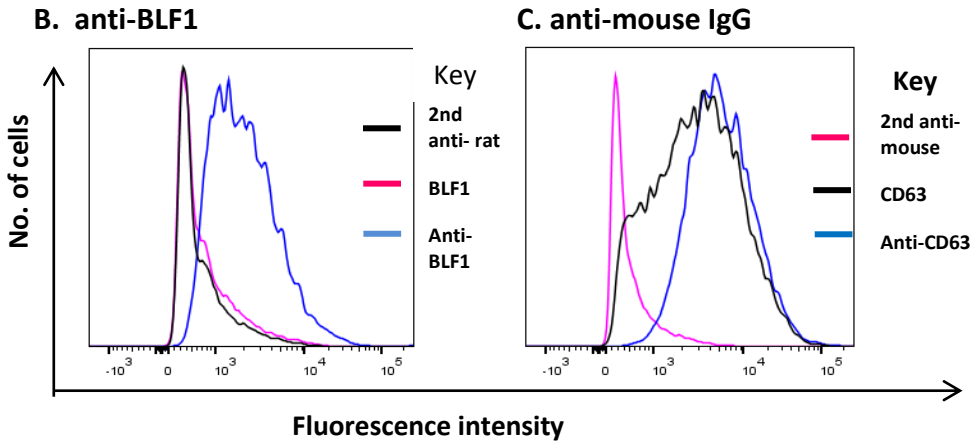

Figure 5.4.7: Assessment of binding of (BLF1/anti-CD63) IMT to MeWo cells using flow cytometry:

Cells were incubated with anti-CD63 IMT at 1:6 dilution (equivalent to 8.3 µM BLF1:0.83 µM anti-CD63), unconjugated BLF1(8.3 µM), then with rat anti-BLF1 followed by anti-rat IgG-FITC to detect BLF1 (left hand pane) or with anti-mouse IgG-FITC to detect the mouse antibodies (right hand panel) as previously described. **A.** Bar chart represents the normalised median fluorescent intensity (MFI). **B.** Overlay histogram of fluorescence intensity of anti-BLF1 (blue) of the IMT as compared to cells incubated with unconjugated BLF1 (pink). The trace in black shows the binding of secondary anti-rat antibody alone. **C.** Overlay histogram of fluorescence intensity of anti-CD63 (blue) component of the IMT as compared to cells incubated with anti-CD63 antibody alone (labelled as CD63 in black). The trace in pink shows the binding of secondary anti-mouse antibody alone. Three independent experiments performed in duplicate, with values shown as mean± SEM. Data

analysed using one way ANOVA with Sidak's multiple comparisons test where **** is significantly different at p<0.0001.

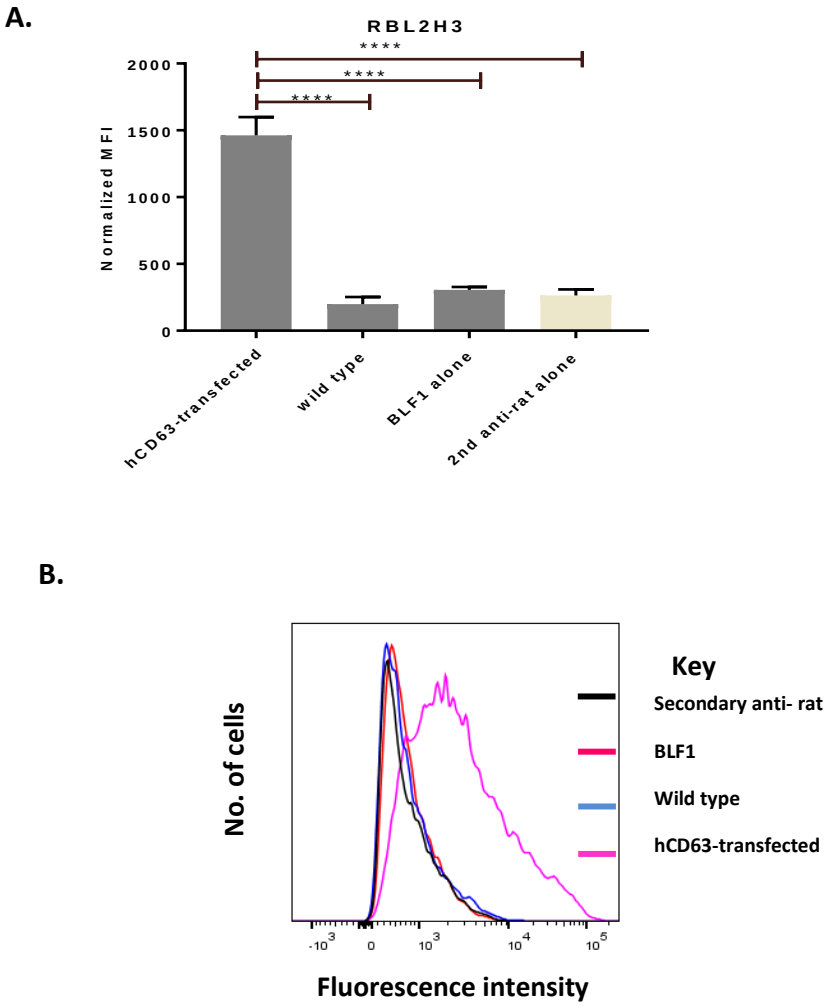

Figure 5.4.8: Assessment of binding of (BLF1/anti-CD63) IMT to RBL2H3 cells using flow cytometry:

Cells were incubated with anti-CD63 IMT (1:6 dilution, equivalent to 8.3 µM of BLF1), unconjugated BLF1 (8.3 µM), then with rat anti-BLF1 followed by anti-rat IgG-FITC to detect BLF1. **A**. Bar chart represents the median fluorescent intensity (MFI). **B.** Overlay histogram of fluorescence intensity of hCD63-transfected RBL2H3 cells incubated with IMT (pink), unconjugated BLF1 (red) or secondary rat antibody (black). The trace in blue shows the fluorescent intensity of WT RBL2H3 cells incubated with IMT. Three independent experiments performed in duplicate. Graphs represent Mean± SEM. Data were analysed as described in **Fig**.5.4.7.

5.4.6.2 Assessment of binding specificity of mCherry BLF1/anti-CD63 IMT by flow cytometry:

An immunotoxin conjugate incorporating mCherry BLF1 was developed (2.2.3.4.2) to investigate the intracellular distribution of the toxin after cell uptake as described in the following sections. Since there was no appropriate filter to efficiently detect mCherry fluorescence in the FACS machine used, binding of this IMT to MeWo cells was assessed by using anti-BLF1 antibody and anti-mouse IgG, as described in 5.4.6.1. Data from flow cytometry confirmed that the mCherry-BLF1/anti-CD63 IMT binds specifically to MeWo cells. Interestingly, the median fluorescence intensity value obtained with anti-BLF1 and anti-CD63 moieties of this conjugate were more equivalent than the conjugate prepared using cys-BLF1 described above, suggesting a higher ratio of BLF1: antibody.

A.

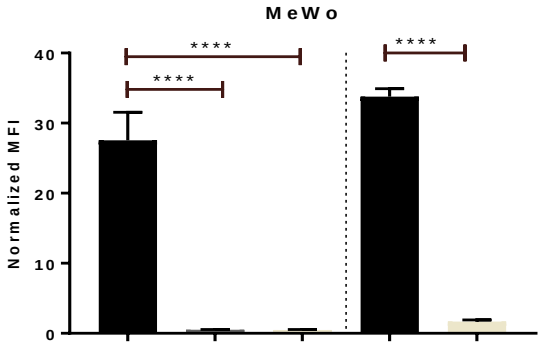

mCherry BLF1/anti-CD63 IMT	+	-	-	+	-
mCherry BLF1 alone	-	+	-	-	-
Anti-BLF1 Ab	+	+	-	-	-
Anti-CD63 Ab	-	-	-	+	+
2nd anti- rat Ab	+	+	+	-	-
2nd anti-mouse Ab	-	-	-	+	+

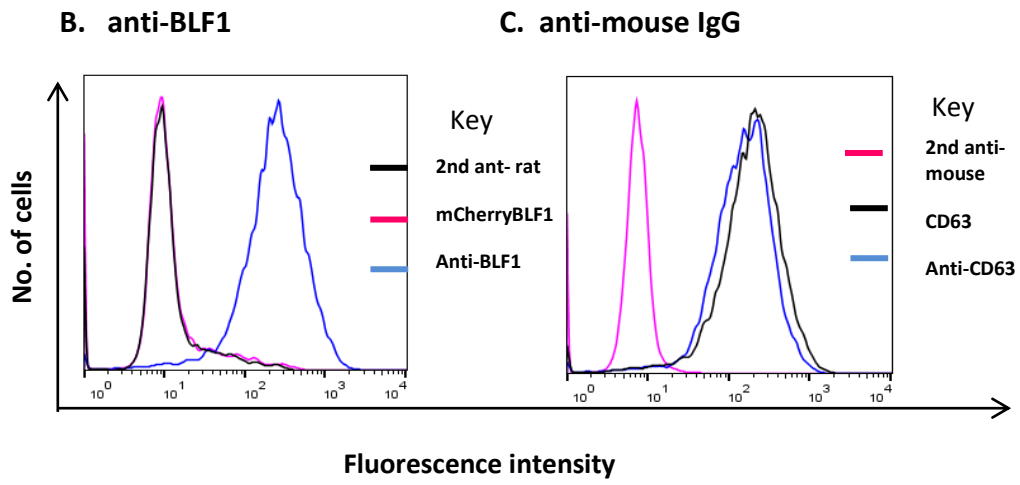

Figure 5.4.9: Assessment of binding of (mCherry BLF1/anti-CD63) IMT to MeWo cells using flow cytometry:
Cells were incubated with anti-CD63 IMT (1:6 dilution, equivalent to 8.3 µM of BLF1), unconjugated BLF1 (8.3 µM), then with rat anti-BLF1 followed by anti-rat IgG-FITC to detect BLF1 (left hand panel) or with anti-mouse IgG-FITC to detect the mouse antibodies (right hand panel). **A.** Bar chart represents the normalized median fluorescent intensity (MFI). **B.** Overlay histogram of fluorescence intensity of anti-BLF1 (blue) of the IMT as compared to cells incubated with unconjugated mCherry BLF1 (pink). The trace in black shows the binding of secondary anti-rat antibody alone. **C.** Overlay histogram of median fluorescence intensity of anti-CD63 component of the IMT (blue) as compared to cells incubated with anti-CD63 antibody alone (labeled as CD63 in black). The trace in pink shows the binding of secondary anti-mouse antibody alone. Three independent experiments performed in duplicate, with values shown as mean ± SEM. Data analysed as described in **Fig**.5.4.7.

5.4.6.3 Effect of incubation time on the toxicity of (BLF1/anti-CD63) IMT:

In order to achieve maximal killing efficiency, the cells need to internalize and process the BLF1 toxin. Therefore, we evaluated the consequence of varying exposure time of cells to BLF1/anti-CD63 IMT (unpurified) as compared to unconjugated BLF1 using the SRB assay. The BLF1/antiCD63 IMT or unconjugated BLF1 was added to the cells and incubated at 37^{o}C for 1 hr, followed by washing to remove non-cell associated protein or for 72 hr without washing. The 1 hr exposure was followed by 72 additional hours of incubation in IMT-free medium to allow time for any intoxication to become evident. As shown in **Fig**.5.4.10, there was only a slight difference in effect between cells incubated for 1 hr or 72 hr with the BLF1/anti-CD63. This indicates that the majority of IMT internalization occurs within 60 minutes time, and increasing the time exposure does not provide any advantage *in vitro*.

We conclude that the CD63 antigen rapidly transports CD63/IMT complex from the cell membrane.

However, there was a marked difference in the effects observed for cells incubated with unconjugated BLF1; although some reduction in cell growth was apparent with the 1 hr incubation time, this was relatively modest compared to effects with the IMT over the same time. This suggests that the uptake and cytotoxic effect of the IMT is specific to cells expressing CD63. As described previously the uptake of unconjugated BLF1 is likely due to non-specific macropinocytosis which may require longer exposure times to permit internalization of sufficient quantities of the toxin. It is likely that the effects seen with BLF1 alone are due to this non-specific uptake mechanism, and a much greater effect was observed for cells incubated with BLF1 for 72 hr. This is consistent with the effect of a similar concentration of BLF1 on MeWo cells described in Chapter 3 (**Fig.**3.3.10). Since it has been shown previously in 3.3.4.1 that there is significant level of dextran uptake by MeWo cells after 1 hr at 37°C compared to control cells incubated on ice, this indicates that these cells are capable of taking up BLF1 by macropinocytosis.

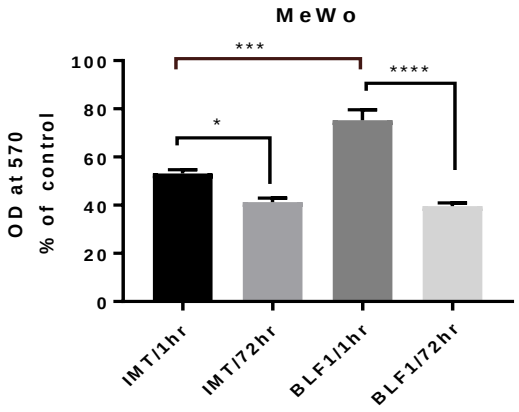

Figure 5.4.10: Effect of (BLF1/anti-CD63) IMT on MeWo cells after 1hr or 72hr incubation: Cells were seeded in 96-well plates and after 24 hr of proliferation, cells were treated with BLF1/anti-CD63 (1:10 dilution, equivalent to 5 µM of BLF1) or unconjugated BLF1 (5 µM) and incubated for 1 hr or 72 hr. The 1 hr treated cells were washed, supplemented with fresh medium and incubated for a further 72 hr (whereas the cells labeled 72 hr were not washed after treatment). The cell growth was then assessed by SRB assay as previously described in 2.2.2. Three independent experiments were performed in quadruplicate, with values shown as mean ± SEM. The significance of difference between treated and untreated cells was determined as described in **Fig.**5.4.7.

5.4.6.4 Assessing the effect of BLF1/anti-CD63 IMT on the growth of MeWo cells in absence or presence of saponin:

The experiments described above show that the BLF1/anti-CD63 IMT can target the toxin to the MeWo melanoma cell line and that incubation of the cells with the IMT for just 1 hr delivers sufficient toxin to the cells to have marked effect on cell growth in the ensuing 72 hr. Hereafter, therefore, cells were washed following treatment with BLF1 or IMTs for 1 hr. The effect of different concentrations of purified and un-purified (BLF1/anti-CD63) IMT on the growth of MeWo cells were assessed using the SRB assay. Additionally, saponin was tested for its ability to further improve the effect of purified and un-purified (BLF1/anti-CD63) IMT by enhancing endosomal escape and release of toxin in the cytosol. Measurement of cellular growth after 72 hours revealed that there is approximately 50% reduction in cell growth, in the presence of 1:10 dilution of neat un-purified IMT (equivalent to 5 μM of BLF1 prior to washing). A further reduction in cell growth was observed in combination with nontoxic concentrations of saponin (2 μg/ml) although it was not statistically significant (**Fig**.5.4.11.A). Anti-CD63 antibody on its own displayed no impact on cell growth at the concentration tested (0.5 μM). Although some reduction in cell growth was apparent with unconjugated BLF1 (at a concentration of 5 μM prior to washing), this was relatively modest compared to effects with the IMT, in line with the results described in the previous section.

The column purified IMT (see section 5.4.3, fr.16-20) also induced an approximately 30% reduction in cell growth at the indicated concentration of purified IMT (total protein 0.2 μg/ml~0.001 μM). Again, a further significant arrest in cell growth was observed in combination with a nontoxic concentration of saponin (2 μg/ml) (**Fig.**5.4.11.B). As expected, unconjugated BLF1 on its own displayed no significant effect at the concentration tested (0.2 μg/ml ~0.001 μM) as shown previously in 3.3.2.3.3.

A.

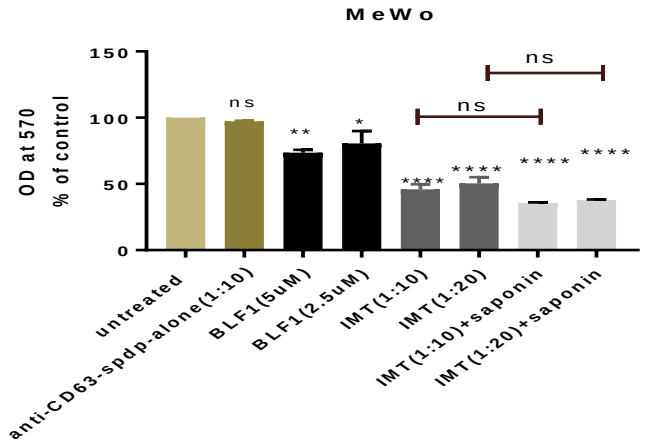

B.

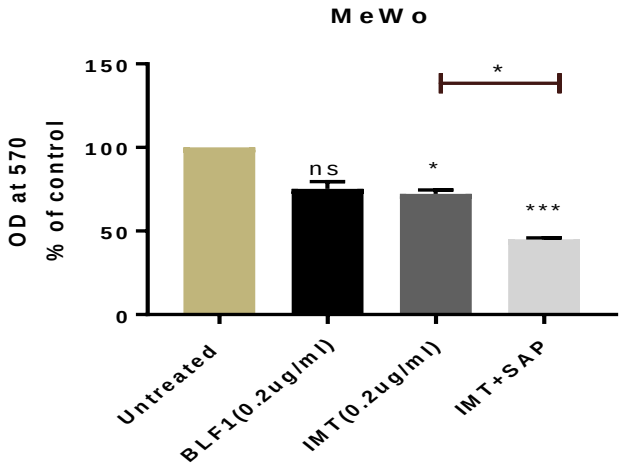

Figure 5.4.11: Effect of (BLF1/anti-CD63) IMT on the growth of MeWo cells:
Cells were seeded in 96-well plate and allowed to proliferate for 24 hr. **A.** Cells were then treated with doubling dilution of unpurified BLF1/anti-CD63 IMT (starting with 1:10 dilution of neat IMT, corresponds to 5 µM of BLF1) in absence or presence of 2 µg/ml of saponin. Some cells were treated with thiolnated anti-CD63 antibody (1:10 dilution, equivalent to 0.5 µM) and BLF1 (5 and 2.5 µM). **B.** Cells were treated with 0.2 µg/ml of purified BLF1/anti-CD63 IMT in the absence or presence of saponin. Some cells were incubated with 0.2 µg/ml of unconjugated BLF1. After 1 hr the cells were washed, re-supplemented with fresh medium as described in 2.2.2.4 and incubated for a further 72 hr before analysis using the SRB assay. Three independent experiments were performed in quadruplicate, with values shown as mean ±SEM. The significance of difference between treated and untreated cells was determined by one way ANOVA with Dunnett's and Sidak's multiple comparisons test where **** is significantly different at $p<0.0001$, ** is significantly different at $p<0.01$ and * is significantly different at $p< 0.05$.

5.4.6.5 Assessing the effect of (mCherryBLF1/anti-CD63) IMT on human melanoma cell line in absence or presence of saponin:

The mCherryBLF1/anti-CD63 IMT appeared to show higher levels of BLF1 targeting to MeWo cells, as shown in (**Fig.**5.4.9). Therefore the effect of different concentrations of unpurified mCherryBLF1/anti-CD63 IMT on the growth of MeWo cells was assessed in the absence or presence of saponin. The measurement of cell growth after 72 hr shows that the mCherryBLF1/anti-CD63 IMT had similar activity to the unlabelled BLF1/anti-CD63 IMT with approximately 50% reduction in cellular growth (**Fig**.5.4.12). A further significant reduction in cell growth was observed in combination with a nontoxic concentration of saponin (2 µg/ml). Unconjugated mCherry BLF1 appeared to be non- toxic to the cells at the indicated concentration.

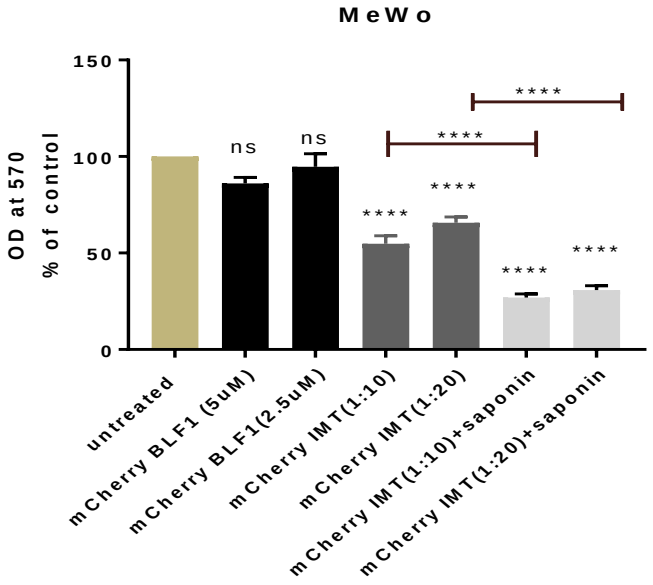

Figure 5.4.12: Effect of (mCherryBLF1/anti-CD63) IMT on the growth of MeWo cells:
Cells were seeded in 96-well plate and after 24 hr of proliferation, cells were treated with doubling dilution of mCherry BLF1/anti-CD63 IMT (starting with 1:10 dilution of neat IMT, corresponds to 5 µM of mCherry BLF1) in presence/absence of saponin (2 µg/ml). Some cells were treated with unconjugated mCherry BLF1 (5 and 2.5 µM). After 1 hr the cells were washed and then re-supplemented with pre-warmed medium as described in 2.2.2.4 and incubated for a further 72 hr before analysis using SRB assay. Three independent experiments were performed in quadruplicate, with values shown as mean ± SEM. The significance of difference between treated and untreated cells was determined as described in **Fig**.5.4.12.

5.4.6.6 Assessing the effect of (mCherryBLF1/anti-CD63) IMT on human melanoma cell line in absence or presence of brefeldin A:

After binding of mCherry BLF1/anti-CD63 IMT to MeWo (**Fig**.5.4.9), the IMT is endocytosed and processed through the vesicular system in a poorly understood way, prior to translocation to the cytosol. Thus the role of Golgi apparatus in toxin processing was studied by investigating the effect of (mCherryBLF1/anti-CD63) IMT in combination with brefeldin A. As described previously (1.1.3.3.4) brefeldin A blocks the function of the Golgi and has been reported to enhance/reduce the potency of some toxins. The results from the SRB assay revealed that the impact of (mCherryBLF1/anti-CD63) IMT on the cellular growth of MeWo cells was markedly potentiated in presence of Brefeldin A (**Fig**.5.4.13) in a dose-dependent manner at concentrations of brefeldin A that were themselves non-toxic.

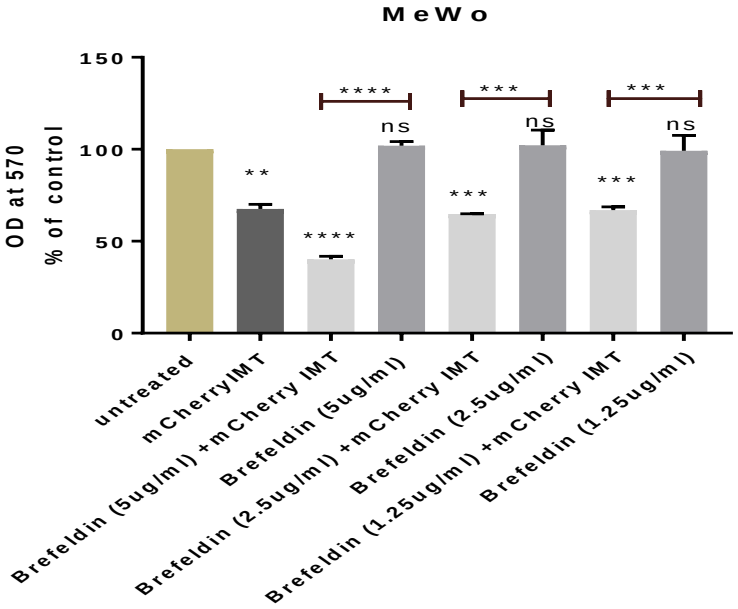

Figure 5.4.13: Effect of brefeldin A on the toxicity of (mCherryBLF1/anti-CD63) IMT to MeWo cells:

Cells were seeded in 96-well plates and after 24 hr of proliferation, cells were either incubated with the indicated concentration of brefeldin A in absence/presence of mCherry BLF1/anti-CD63 IMT at 1:10 dilution (equivalent to 5 µM BLF1), or with medium containing the mCherry BLF1/anti-CD63 IMT only (control). After 1 hr the cells were washed and then re-supplemented with pre-warmed medium as described in 2.2.2.4. After 72 hr the cellular growth was assessed by SRB assay. Three independent experiments were performed in quadruplicate, with values shown as mean ± SEM. The significance of difference between treated and untreated cells was determined as described in **Fig**.5.4.11.

5.4.6.7 Assessing the effect of (mCherryBLF1/anti-CD63) IMT on MeWo cell in absence or presence of bafilomycin A_1:

As mentioned previously (1.1.3.3.3) bafilomycin A_1 prevents acidification and thereby inactivates lysosomal proteases in addition to preventing cellular trafficking from early endosome to the late endosomes and lysosomes (Bowman et al., 1988). To determine whether the sensitivity to the BLF1/anti-CD63 IMT could be affected by preventing intracellular toxin transport, MeWo cells were pre-incubated with this inhibitor prior to treatment with the IMT. Assessment of cellular growth after 72 hours revealed a decrease in the effect of mCherry BLF1/anti-CD63 IMT in combination with bafilomycin A_1 compared to cells incubated with IMT only (**Fig.**5.4.14). At the concentrations tested (5 ng/ml, 0.25 ng/ml), bafIlomycin A_1 had no effect on cell growth. Impairment of cell growth was observed at 5 ng/ml bafilomycin A1, but was not significant at the lower concentration.

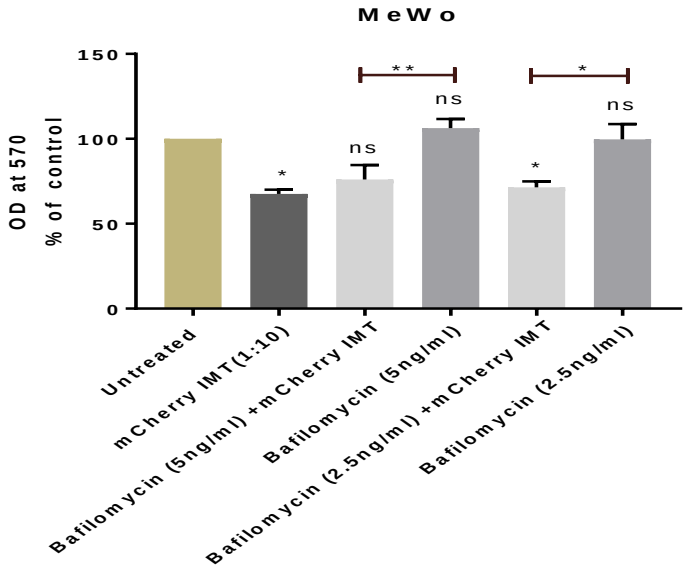

Figure 5.4.14: Effect of bafilomycin A1 on the toxicity of (mCherryBLF1/anti-CD63) IMT to MeWo cells:
Cells were seeded in 96-well plate and after 24 hr of cell proliferation, cells were either incubated with the indicated concentration of bafilomycin A_1 in absence/presence of mCherry BLF1/anti-CD63 IMT at 1:10 dilution (equivalent to 5 µM BLF1), or with medium containing mCherry BLF1/anti-CD63 IMT only (control). After 1 hr the cells were washed and then re-supplemented with pre-warmed medium as described in 2.2.2.4. After 72 hr the cells growth were assessed by SRB assay. Three independent experiments were performed in quadruplicate, with values shown as mean ± SEM. The significance of difference between treated and untreated cells was determined as described in **Fig.5**.4.11.

5.4.6.8 Assessing the effect of unconjugated BLF1 on MeWo cells in absence or presence of brefeldin A, bafilomycin A_1 or saponin:

Previously, the effects of agents that affect intracellular trafficking on the activity of the IMTs were investigated. Brefeldin A was shown to enhance the effect of the anti-CD63 IMT (5.4.6.6), whereas bafilomycin had a slightly protective effect (5.4.6.7). To try to determine if the intracellular trafficking route and cytostatic/cytotoxic efficiency of unconjugated BLF1 was similarly related, the effects of these agents on the toxin alone were investigated. The combination of BLF1 with inhibitor of Golgi function brefeldin A was found to increase the sensitivity of MeWo cells to BLF1 toxin (**Fig**.5.4.15.A). However, the combination of BLF1 with bafilomycin A_1, an inhibitor of lysosomal function, had no effect on BLF1 activity (**Fig**.5.4.15.B).

The effect of saponin on BLF1 toxicty towards MeWo cells was similarly investigated using the SRB assay. The arresting of cell growth effect of BLF1 was significantly enhanced when combined with saponin (**Fig.**5.4.15.C).

A.

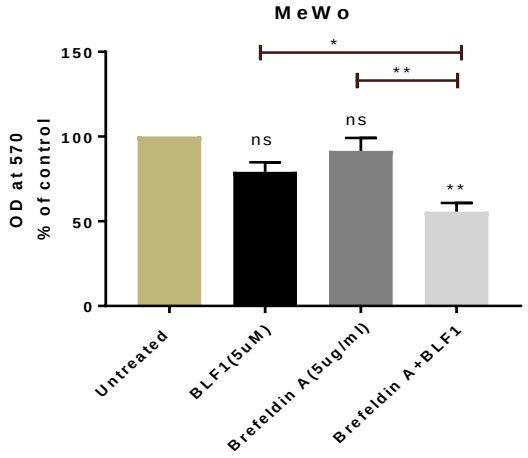

B.

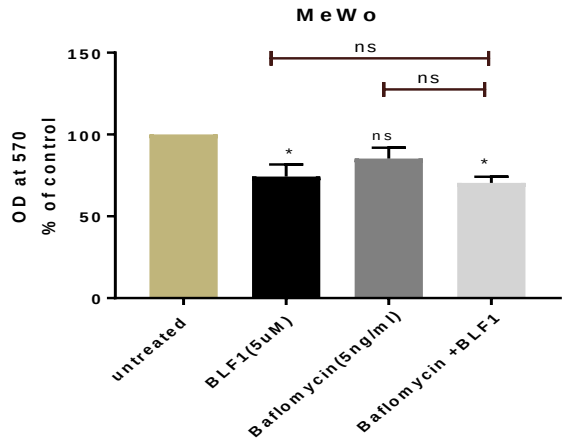

C.

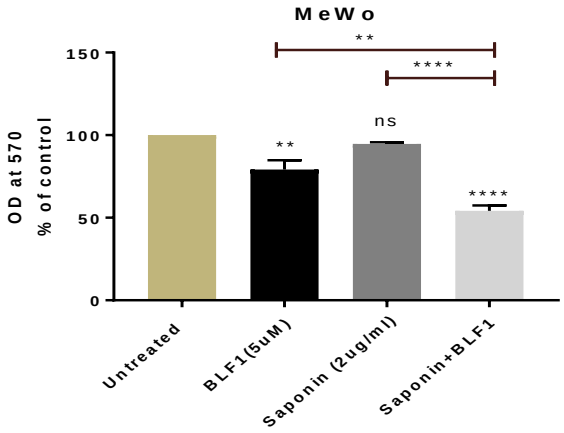

Figure 5.4.15: Effect of brefeldin A, bafilomycin A_1 and saponin on the toxicity of unconjugated BLF1 to MeWo cells:
Cells were seeded in 96-well plate and after 24 hr of cell proliferation, cells were either incubated with the indicated concentration of brefeldin A (**A**), bafilomycin A_1 (**B**) or saponin (**C**) in absence/presence of BLF1, or with medium containing BLF1 only (control). After 1 hr the cells were washed and then re-supplemented with pre-warmed medium as described in 2.2.2.4. After 72 hr the cells growth was assessed by SRB assay. Three independent experiments were performed in quadruplicate, with values shown as mean ± SEM. The significance of difference between treated and untreated cells was determined as described in **Fig**.5.4.11.

5.4.6.9 Intracellular trafficking of BLF1 in absence/presence of saponin:

In order to try to identify the intracellular compartment in which the unconjugated BLF1 accumulated after internalization in MeWo cells, the co-localisation of BLF1 (chemically

labelled with Alexa Fluor 488) and the endosomal marker pHrodo™Red dextran was examined after incubation for 4 hr in absence /presence of saponin. The images obtained (**Fig**.5.4.16) showed that fluorescently labelled BLF1 accumulated in acidic vesicles around the nucleus as shown by colocalization with pHrodo dextran. Interestingly when BLF1 was cultured in presence of non-toxic concentrations of saponin, diffuse green fluorescent staining was observed within the cytoplasm, suggesting enhanced escape from the endosomal compartment.

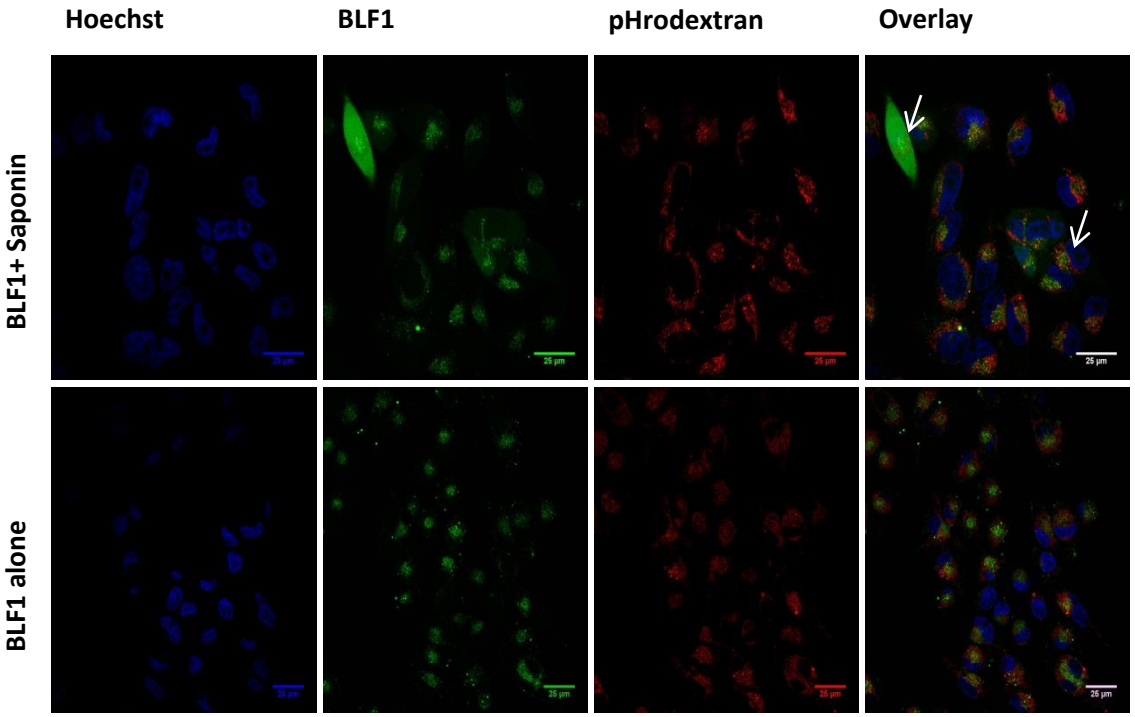

Figure 5.4.16: Effect of saponin on the intracellular trafficking of fluorescently labelled BLF1:
Cells were grown overnight in a glass-bottomed FluoroDish™, then incubated with medium containing Alexa Fluor 488 labelled BLF1 (1 µM) in absence/presence of saponin (2 µg/ml) for 1 hr. After 1 hr the cells were washed and re-supplemented with pre-warmed medium and incubated for further 3 hr. Cells were then washed 3 times with HBSS, and stained with pHrodo® Red Dextran for 30 minutes. Cells were washed again and re-suspended with phenol red free medium containing Hoechst stain as described in 2.2.8.3. Blue fluorescence corresponds to Hoechst nuclear stain. Green fluorescence corresponds to BLF1 toxin. Red fluorescence corresponds to pHrodo red dextran. Live cells were imaged imaged using confocal microscopy (60 x oil objective).

5.4.7 Functional assessment of BLF1/anti-CD9 IMT:

Although CD63 represents a good model target antigen because it internalises rapidly, it was of interest to also investigate IMTs directed at CD9, which has previously been studied as described in chapter 4. However, due to problems with purifying IMT and time constraints the non-purified IMT was tested for binding specificity, cytostaticity/cytotoxicity, and intracellular co-localization.

5.4.7.1 Assessment of binding specificity of (BLF1/anti-CD9) IMT using flow cytometry:

The cell surface binding of (BLF1/anti-CD9) IMT to A549 cells was tested using flow cytometry. The rat anti-BLF1 antibody was used to detect the BLF1 component of the IMT as described previously. As shown in (**Fig.**5.4.17) there is high binding of the BLF1/anti-CD9 IMT compared with negligible binding of the unconjugated BLF1. The anti-mouse IgG-FITC was used to detect the monoclonal antibody component of the IMT. Again significant binding was detected with the anti-CD9 containing IMT.

A.

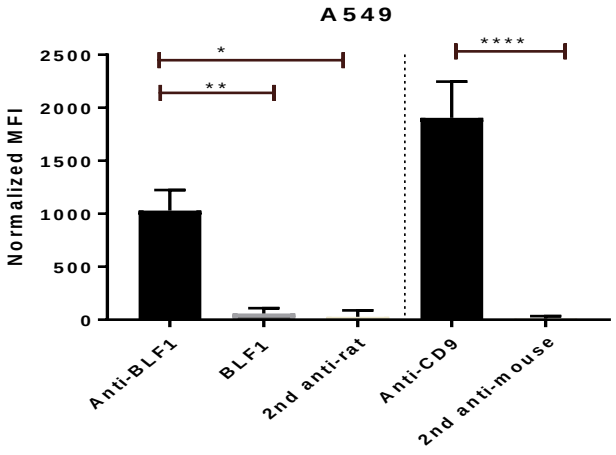

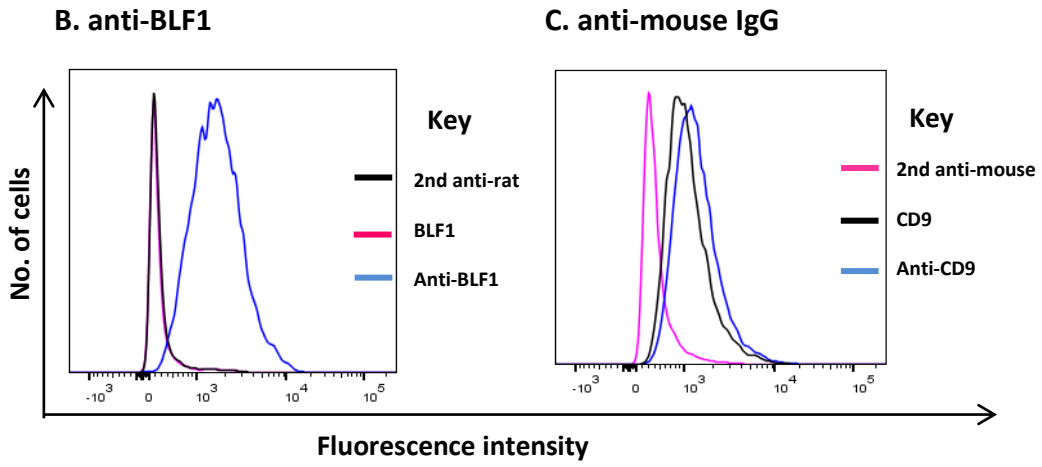

Figure 5.4.17: Assessment of binding of (BLF1/anti-CD9) IMT to A549 cells using flow cytometry:
Cells were incubated with anti-CD9 IMT (1:6 dilution, equivalent to 8.3 µM BLF1:0.83 µM anti-CD9), unconjugated BLF1 (8.3 µM), then with rat anti-BLF1 followed by anti-rat IgG-FITC to detect BLF1 (left hand pane) or with anti-mouse IgG-FITC to detect the mouse antibodies (right hand panel). **A**. Bar chart represents the normalised median fluorescent intensity (MFI). **B.** Overlay histogram of fluorescence intensity of anti-BLF1 (blue) of the IMT as compared to unconjugated BLF1 (pink). The trace showed in black shows the binding of secondary anti-rat antibody alone. **C.** Overlay histogram of median fluorescence intensity of the anti-CD63 antibody component of the IMT (blue) as compared to cells incubated with anti-CD9 antibody alone (labelled as CD9 in black). The trace in pink shows the binding of secondary anti-mouse antibody alone. Three independent experiments performed in duplicate, with values shown as mean ± SEM. Data analysed as described in **Fig**.5.4.7.

5.4.7.2 Assessing the effect of BLF1/anti-CD9 IMT on the growth of A549 cells in absence or presence of saponin:

The effect of different concentration of (BLF1/anti-CD9) IMT on the growth of A549 cells was assessed using the SRB assay. Moreover, saponin was tested for its ability to further improve the cytotoxic effect of (BLF1/anti-CD9) IMT. Measurement of cellular growth after 72 hours revealed that there is approximately 50% reduction in cell growth for cells incubated with unpurified IMT containing 5 µM BLF1 (prior to washing) compared with a negligible effect for unconjugated BLF1. A further significant reduction in cell growth was observed in combination with nontoxic concentrations of saponin (2 µg/ml) (**Fig**.5.4.18). Anti-CD9 antibody on its own displayed no toxic effect at the concentration tested (0.5 µM).

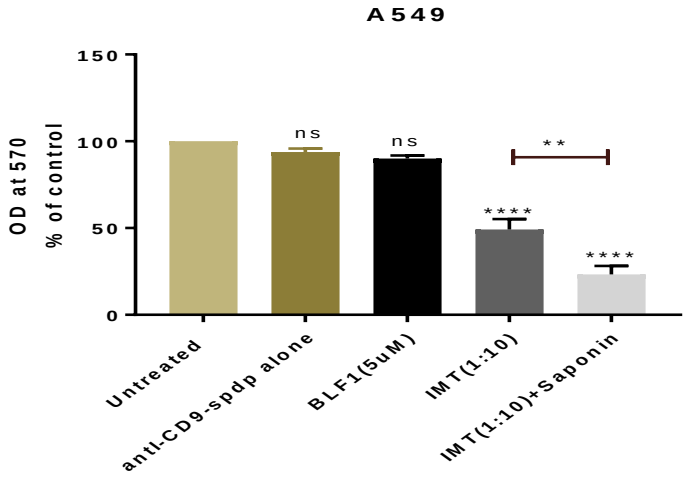

Figure 5.4.18: Effect of (BLF1/anti-CD9) IMT on the growth of A549 cells:
Cells were seeded in 96-well plates and after 24 hr of proliferation, cells were treated with BLF1/anti-CD9 IMT at 1:10 dilution (equivalent to 5 µM BLF1) in absence/presence of saponin (2 µg/ml). Some cells were treated with unconjugated anti-CD9 antibody (0.5 µM) and BLF1 (5 µM). After 1hr the cells were washed, re-supplemented with fresh medium as described in 2.2.2.4 and incubated for a further 72 hr before analysis using the SRB assay. Three independent experiments were performed in quadruplicate, with values shown as mean ± SEM. Data analysed as described in **Fig**.5.4.11.

5.4.7.3 Assessing the effect of BLF1/anti-CD9 IMT on A549 cells line in the absence or presence of Brefeldin A:

As in section 5.4.6.6, the possible role of the Golgi apparatus in toxin processing was also studied by investigating the effect of brefeldin A on the cytostacitiy/cytotoxicity of (BLF1/anti-CD9) IMT. The results from the SRB assay revealed that the effect of BLF1/anti-CD9 against A549 cells was not enhanced by brefeldin A (**Fig**.5.4.19) at a concentration (5 µg/ml) that was not toxic to the target cells, but which was previously shown to enhance the effect of mCherry BLF1/anti-CD63 IMT (see **Fig.**5.4.13).

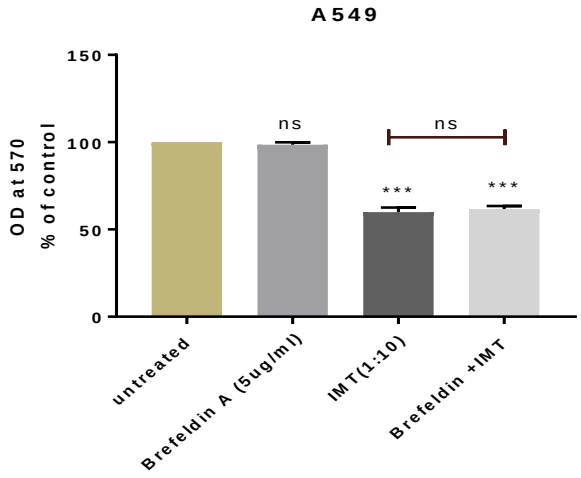

Figure 5.4.19: Effect of brefeldin A on the toxicity of (BLF1/anti-CD9) IMT to A549 cells: Cells were seeded in 96-well plates and after 24 hr of proliferation, cells were either incubated with the indicated concentration of brefeldin A in absence/presence of BLF1/anti-CD9 IMT at 1:10 dilution (equivalent to 5 µM BLF1) or with medium containing the BLF1/anti-CD9 IMT only (control). After 1 hr the cells were washed and then re-supplemented with pre-warmed medium as described in 2.2.2.4. After 72 hr the cellular growth was assessed by SRB assay. Three independent experiments were performed in quadruplicate, with values shown as mean ±SEM. The significance of difference between treated and untreated cells was determined as described in **Fig**.5.4.11.

5.4.7.4 Assessing the effect of BLF1/anti-CD9 IMT on A549 cell in presence of bafilomycin A_1:

The experiment described in 5.4.6.7 showed that the sensitivity of MeWo cells to BLF1/anti-CD63 IMT was reduced in presence of bafilomycin A_1.Therefore A549 cells were pre-incubated with the same reagent prior to treatment with the BLF1/anti-CD9 IMT. Assessment of cell growth after 72 hours revealed a slight decrease in the cytotoxic effect of BLF1/anti-CD9 IMT in combination with bafilomycin A_1 compared to cells incubated with IMT only (**Fig**.5.4.20). At the concentration tested (5 ng/ml), bafilomycin A_1 alone had no effect on cell growth. Therefore, the protective effect of bafilomycin A_1 was not observed in this IMT.

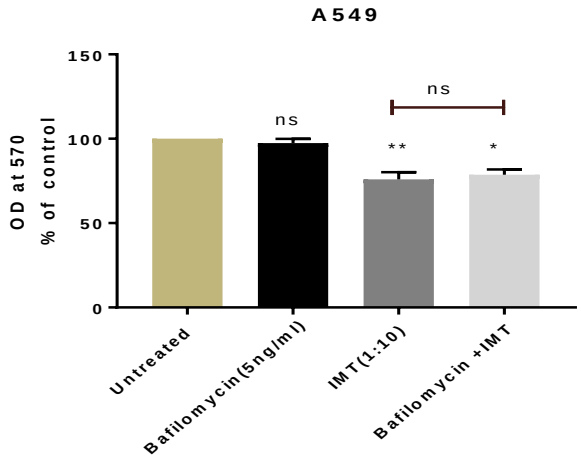

Figure 5.4.20: Effect of bafilomycin A1 on the toxicity of (BLF1/anti-CD9) IMT to A549 cells:

Cells were seeded in 96-well plate and after 24 hr of cell proliferation; cells were either incubated with the indicated concentration of bafilomycin A_1 in absence/presence of BLF1/anti-CD9 IMT at 1:10 dilution (equivalent to 5 µM BLF1), or with medium containing BLF1/anti-CD9 IMT only (control). After 1 hr the cells were washed and then re-supplemented with pre-warmed medium as described in 2.2.2.4. After 72 hr the cells growth was assessed by SRB assay. Three independent experiments were performed in quadruplicate, with values shown as mean ± SEM. The significance of difference between treated and untreated cells was determined as described in **Fig**.5.4.7.

5.4.8 Combined effect of un-purified BLF1/anti-CD63 IMT and BLF1/anti-CD9 IMT on human lung cancer cell line (A549):

Having constructed immunotoxins targeting CD63 and CD9 that are both expressed by A549 cells, it was of interest to look at their combined effect. In our study, we did not observe a significantly higher impact on cellular growth when using two immunotoxins (**Fig**.5.4.21). Moreover, the anti-CD63 and anti-CD9 IMTs have very similar effects on A549 cells despite targeting different antigens with different rates of internalization.

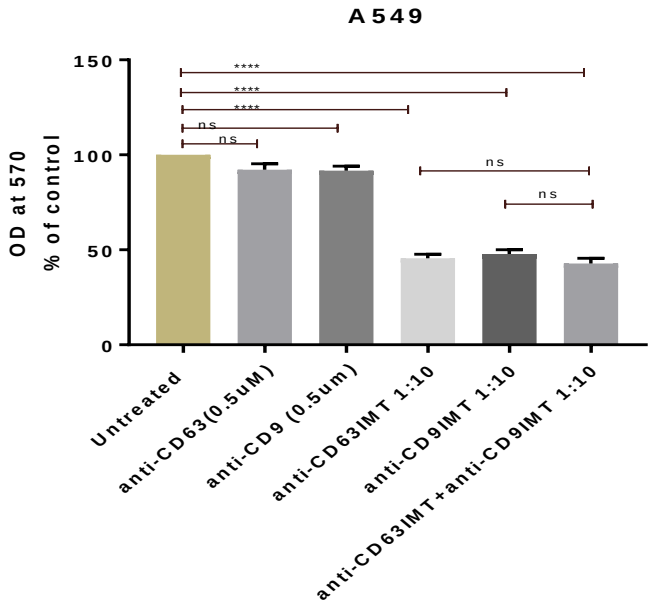

Figure 5.4.21: Effect of combinational BLF1 targeted IMT on human lung cancer cell line (A549):

Cells were seeded in 96-well plate and after 24 hr of proliferation; cells were either incubated with anti-CD63 IMT at 1:10 dilution (equivalent to 5 µM BLF1), anti-CD9 IMT at 1:10 dilution (equivalent to 5 µM BLF1), or combination of both IMTs. Cells were also incubated with medium containing anti-CD63 or antiCD9 antibodies alone (control). After 1 hr the cells were washed and then re-supplemented with pre-warmed medium as described in 2.2.2.4. After 72 hr the cell growth was assessed by SRB assay. Three independent experiments were performed in quadruplicate, with values shown as mean ±SEM. Significant of difference was analysed as described in **Fig**.5.4.7.

5.4.9 Specificity of targeted BLF1 immunotoxins:

In attempts to validate the specificity of the immunotoxins for their corresponding target antigen (CD63 or CD9), the effects of excess free unconjugated antibodies (0.5 µM) on the toxicity of the IMTs for the relevant target cell line was assessed using the SRB assay. For both IMTs, there was a significant reduction in the effects of the IMTs on the cells when they were treated with free unconjugated antibody compared with IMT alone. In addition, it was shown that incubation with 0.5 µM of unconjugated anti-CD63 and anti-CD9 antibody by itself did not inhibit the proliferation of the tested cell lines.

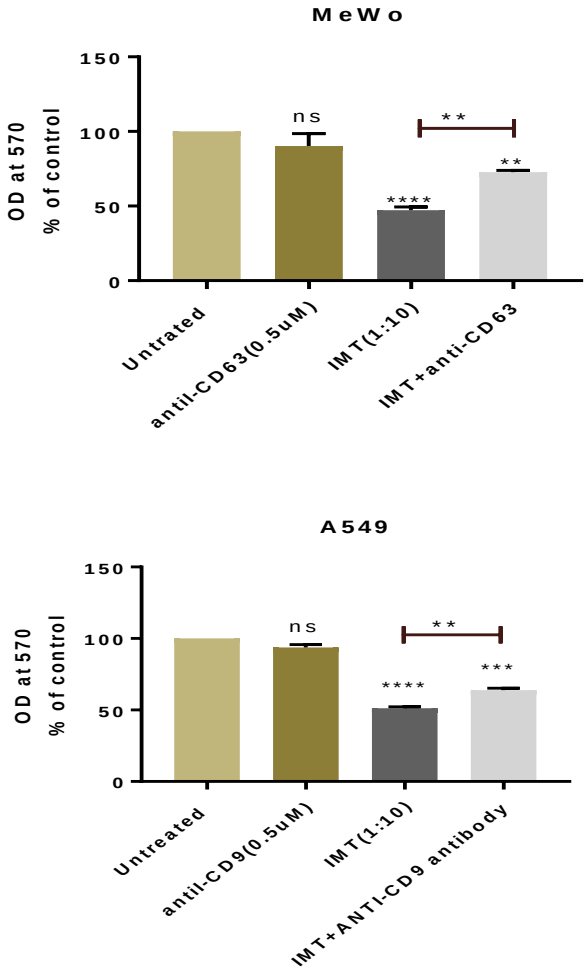

Figure 5.4.22: specificity of targeted BLF1 IMT:
A549 or MeWo cells were seeded in 96 well plates and allowed to proliferate for 24 hr. Subsequently, cells were pre- incubated with 0.5 µM of free unconjugated anti-CD63 or CD9 antibody or buffer for 1 hr before adding the immunotoxin at 1:10 dilution (equivalent to 5 µM BLF1:0.5 µM targeting antibody) for an additional 1 hr. Cells were then washed and cell growth was assessed after 72 hr using the SRB assay as described in 2.2 Significant of difference was analyzed by One way ANOVA test. Bar chart represent three independent experiments were performed in quadruplicate. Graphs represent Mean ± SEM.

5.4.10 Effect of BLF1 IMT on the growth of human chemo resistant uterine sarcoma cells:

As discussed previously in 1.1.4.2 one possible application for immunotoxins is for treating cancers that have developed resistance to conventional chemotherapy reagents. The MES-SA/Dx-5 cell line is a multi-drug resistant cell line derived from human uterine sarcoma cells

(Harker and Sikic, 1985). It was therefore of interest to investigate the effects of the IMTs on this cell line.

We initially screened the cell line to determine the levels of CD63 and CD9 expression in order to choose the most suitable IMT to use. Data from flow cytometry as shown in (**Fig.**5.4.23.A, B) indicated high levels of CD63 antigen on the cell surface, but low levels of CD9, therefore (BLF1/anti-CD63) IMT was investigated. In these experiments, both purified and un-purified BLF1/anti-CD63 IMT, and unconjugated BLF1 were investigated. After 72 hr, the SRB assay demonstrated a significant reduction in the growth of cells treated with targeted IMT as compared to untreated (control), the unconjugated BLF1 toxin also had a significant toxic effect on the growth of cells (**Fig**.5.4.24). Incubation of chemo-resistant cells in the absence or presence of various concentrations of BLF1 for 72 hr showed that significant effects were observed down to 0.5 µM compared to the control (no toxin) (**Fig.**5.4.25). Thus, this cell line could be sensitive to BLF1 and may have high rates of macropinocytosis.

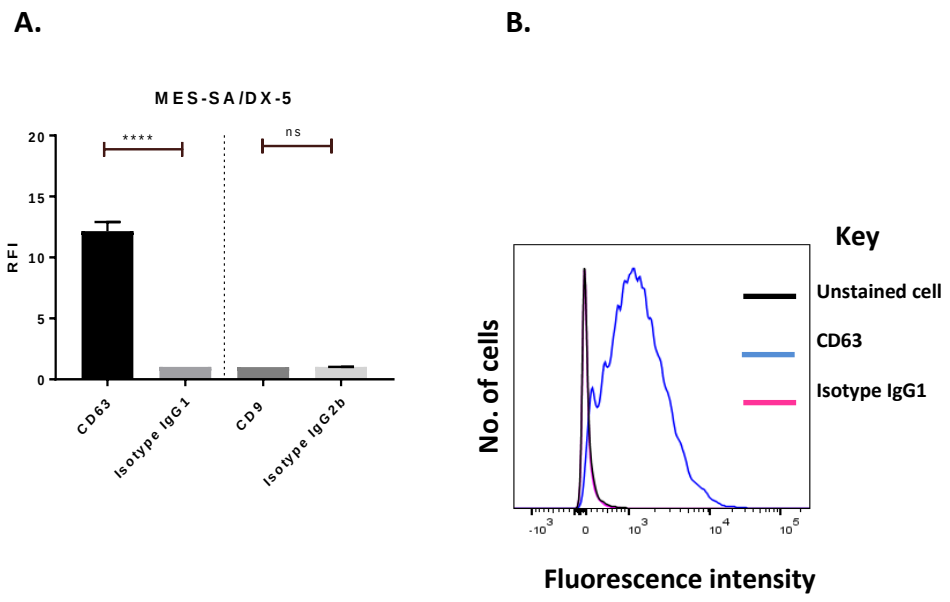

Figure 5.4.23: Surface expression of CD63 and CD9 protein on chemo-resistant uterine sarcoma cell line (MES-SA/DX-5 cell line):
Cells were incubated with anti-CD63 antibody, anti-CD9 antibody or their isotype controls. The secondary antibody was FITC-conjugated anti-mouse antibody as described in (2.2.4). Stained cells were analysed with flow cytometry. Three independent experiments were performed in duplicate; with values shown as mean ± SEM. **A.** Bar charts represent the relative fluorescent intensity of CD63 and CD9 antigens expression in MES-SA/Dx-5 cells as compared to isotype control. The significance of difference was determined by unpaired t-

test at p<0.001. **B.** Overlay histogram of fluorescence intensity of anti-CD63 and their isotype in chemo-resistant cells.

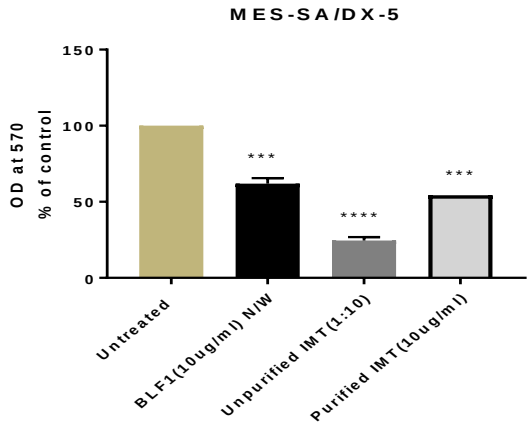

Figure 5.4.24: Effect of (BLF1/anti-CD63) IMT on chemo-resistance uterine sarcoma cell line (MES-SA/DX-5 cell line):

Cells were seeded in a 96-well plate and after 24 hr of proliferation; cells were either treated with purified BLF1/anti-CD63 IMT at 2 µg/ml (corresponds to total protein as determined by Bradford assay), un-purified BLF1/anti-CD63 IMT at 1:10 dilution (equivalent to 5 µM BLF1), or unconjugated BLF1 (10 µg/ml equivalent to 0.4 µM). After 1 hr the cells were washed and then re-supplemented with pre-warmed medium as described in 2.2.2.4. After 72hr the cell growth was assessed by SRB assay. Three independent experiments were performed in quadruplicate, with values shown as mean ± SEM. Significant of difference was analysed as described in **Fig**.5.4.11.

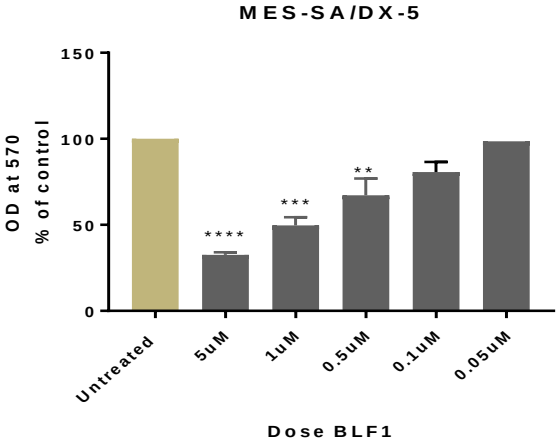

Figure 5.4.25: Effect of BLF1 on human chemo-resistant uterine sarcoma cell line (MES-SA/DX-5 cell line):

Cells were cultured in the presence or absence of various concentration of BLF1 toxin for 72 hours and cell growth assessed using the SRB as described in **Fig**.3.3.4.Three independent experiments were performed in quadruplicate, with values shown as mean ±SEM. The

significance of difference between treated and untreated cells was determined as described in **Fig**.3.3.4.

5.4.11 Binding characterisation of BLF1/anti-CD63IMT and BLF1/anti-CD9 IMT to the antigen positive cells using confocal microscopy:

The targeting of BLF1 by the IMTs to the appropriate cell type (MeWo for anti-CD63 IMT, A549 for anti-CD9 IMT) was visualised by confocal microsocopy, detected using the rat anti-BLF1 antibody and anti-rat IgG-FITC as in flow cytometry. The images showed that both IMTs bound to the membrane of CD63 and CD9 positive cells (**Fig**.5.4.26), consistent with the flow cytometry assays.

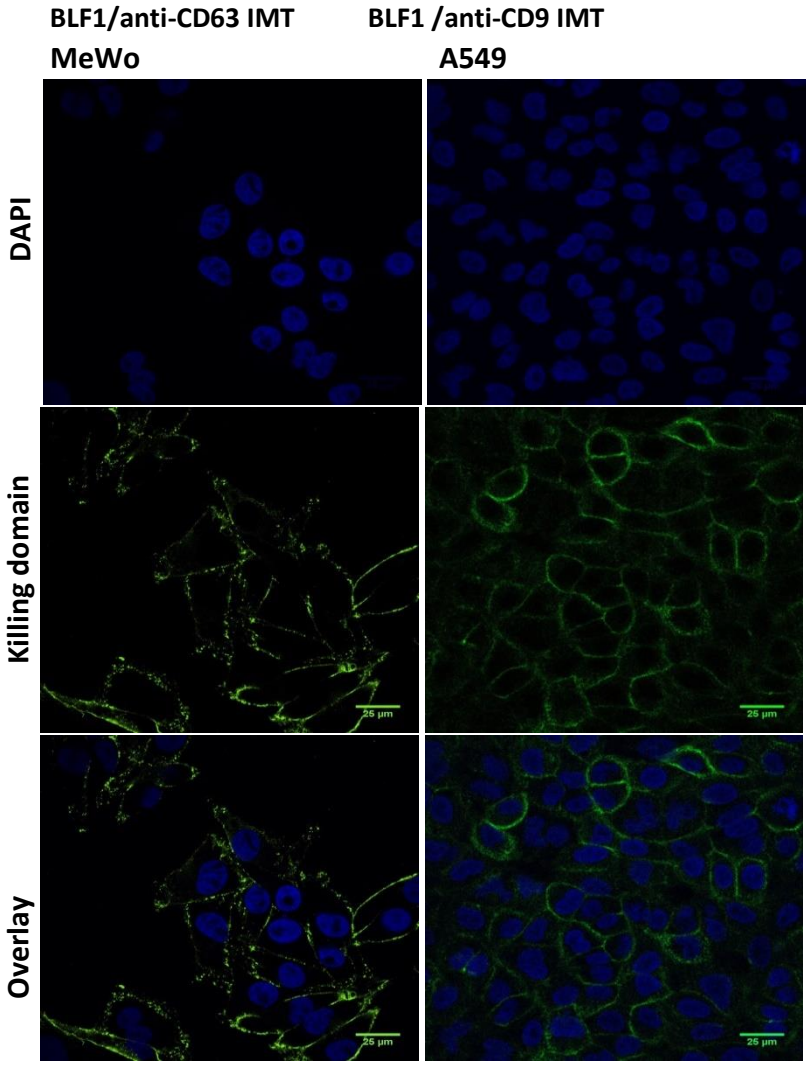

Figure 5.4.26: Binding of unlabelled BLF1/anti-CD63 IMT to MeWo cells and BLF1/anti-CD9 IMT to A549 cells:
Cells were cultured overnight on a coverslip placed in 24 well plates. Cells were then incubated with unpurified BLF1/anti-CD63 IMT or BLF1/anti-CD9 IMT at 1:100 dilution (equivalent to 0.5 μM) after being fixed as described in (2.2.7.1). The cells were then incubated with anti-BLF1 followed by anti-rat IgG-FITC as described in 2.2.7.1. Blue fluorescence corresponds to DAPI nuclear stain. Green fluorescence corresponds to the killing domain (BLF1). Slides were imaged using confocal microscope (60x oil objective).

5.4.12 Visualizing the internalization of BLF1/anti-CD63 IMT:

Internalization of the IMT by MeWo cells after cell surface binding was monitored essentially as described previously for the model immunoconjugates (4.3.3.6.1) i.e. cells were incubated with the IMT on ice for 1 hr to allow binding and then moved to 37^{o}C to induce internalization. BLF1 was detected using anti-BLF1 antibody followed by the appropriate secondary antibody, as described above. Binding was observed immediately after the cells were transferred to 37^{o}C (time 0), where the majority of the stain intensity was on the cell surface. After 1hr, the anti-CD63 IMT was observed around the nucleus. This indicates that the IMT internalizes rapidly after binding to cell surface CD63 antigen.

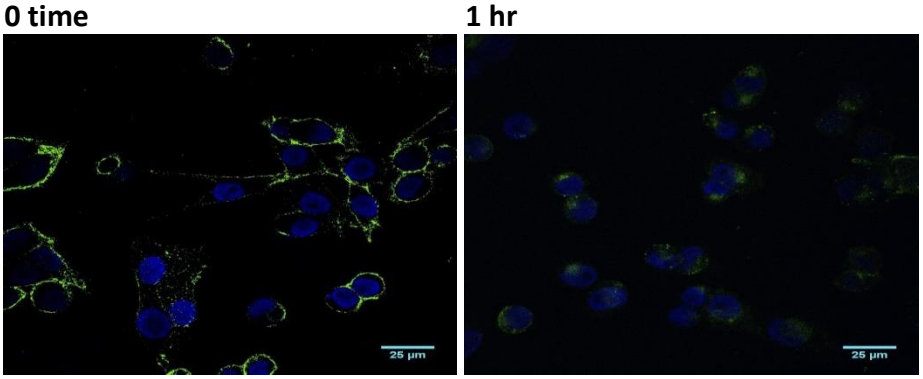

Figure 5.4.27: Binding and internalization of BLF1/anti-CD63 IMT into human melanoma cell line MeWo:
Cells were cultured overnight on a coverslip placed in a 24 well plates, then incubated with medium containing anti-CD63 IMT on ice. After 1 hr, the cells were transferred to 37^{o}C (0 time) and monitored for IMT internalization for an additional 1 hour (1 hr time). The cells at (0 and 1 hr) time were fixed and incubated with BLF1 specific antibody followed by an appropriate secondary antibody. Blue fluorescence corresponds to DAPI nuclear stain. Green fluorescence corresponds to BLF1. Detection of internalized conjugate was performed by confocal microscope with 60x oil objective.

We next examined the internalization of IMTs containing the mCherry tagged BLF1 by live MeWo cells. Confocal images again showed internalization of the mCherry BLF1 component to the cytoplasm.

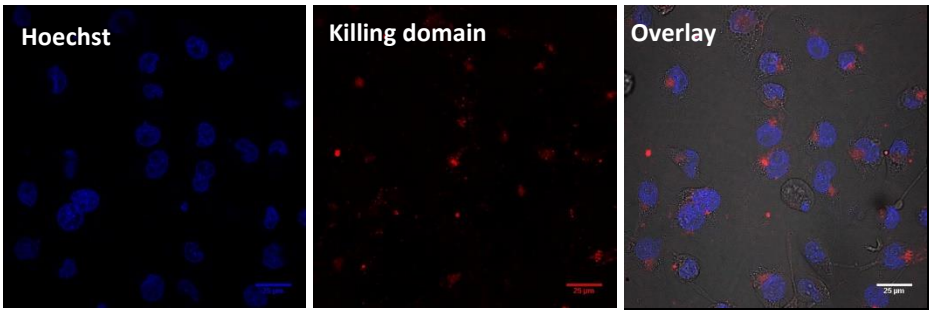

Figure 5.4.28: Immunofluorescence live images of MeWo cells incubated for 24 hours with mCherry BLF1/anti-CD63 IMT:
Cells were cultured overnight in glass bottom FluoroDish™ plate and then incubated with mCherry BLF1/anti-CD63 IMT at 1:100 dilution (corresponds to 0.5 µM BLF1) for 1 hr. After 1 hr the cells were washed and then re-supplemented with pre-warmed medium and incubated for 24hr as described in 2.2.6. Blue fluorescence corresponds to Hoechst nuclear stain. Red fluorescence corresponds to mCherry BLF1 (killing domain) in the IMT. Slides were imaged by confocal microscopy (60 x oil objectives) using appropriate filters.

5.4.13 Intracellular trafficking of mCherry BLF1/anti-CD63 IMT in MeWo cells:

Attempts were made to identify the organelles in which the mCherry BLF1 accumulates after internalization of the IMT in MeWo cells. Co-localization with early endosomes was investigated using transferrin as a marker and visualized 2hrs after the addition of IMT (**Fig.**5.4.29.A). Images from confocal microscopy indicated a partial co-localization between the immunotoxin and early endosomes.

Co-localization with lysosomes and the Golgi apparatus, two of the main pathways that toxins are usually directed to after endosomes (Tome-Amat et al., 2015), was also investigated. The co-localization of BLF1 with lysosomes was studied after 4hr and 16 hr incubation with IMT, using Lyostracker®-Green. Images from the confocal microscopy revealed a high degree of co-localization between the mCherry BLF1 and lysosomes. The fluorescence signal was more intense for the latter time point as shown in (**Fig.5**.4.29.C). A similar experiment was performed using wheat germ agglutinin, which is a Golgi-specific probe; no co-localization with m-Cherry-BLF1 was observed (**Fig**.5.4.29.D). To determine if the toxin and antibody component of the IMT co-localised after internalisation, cells were

fixed and stained using anti-mouse IgG-FITC. Co-localisation of these components in the cytoplasm was observed after 4hr (**Fig**.5.4.29.E).

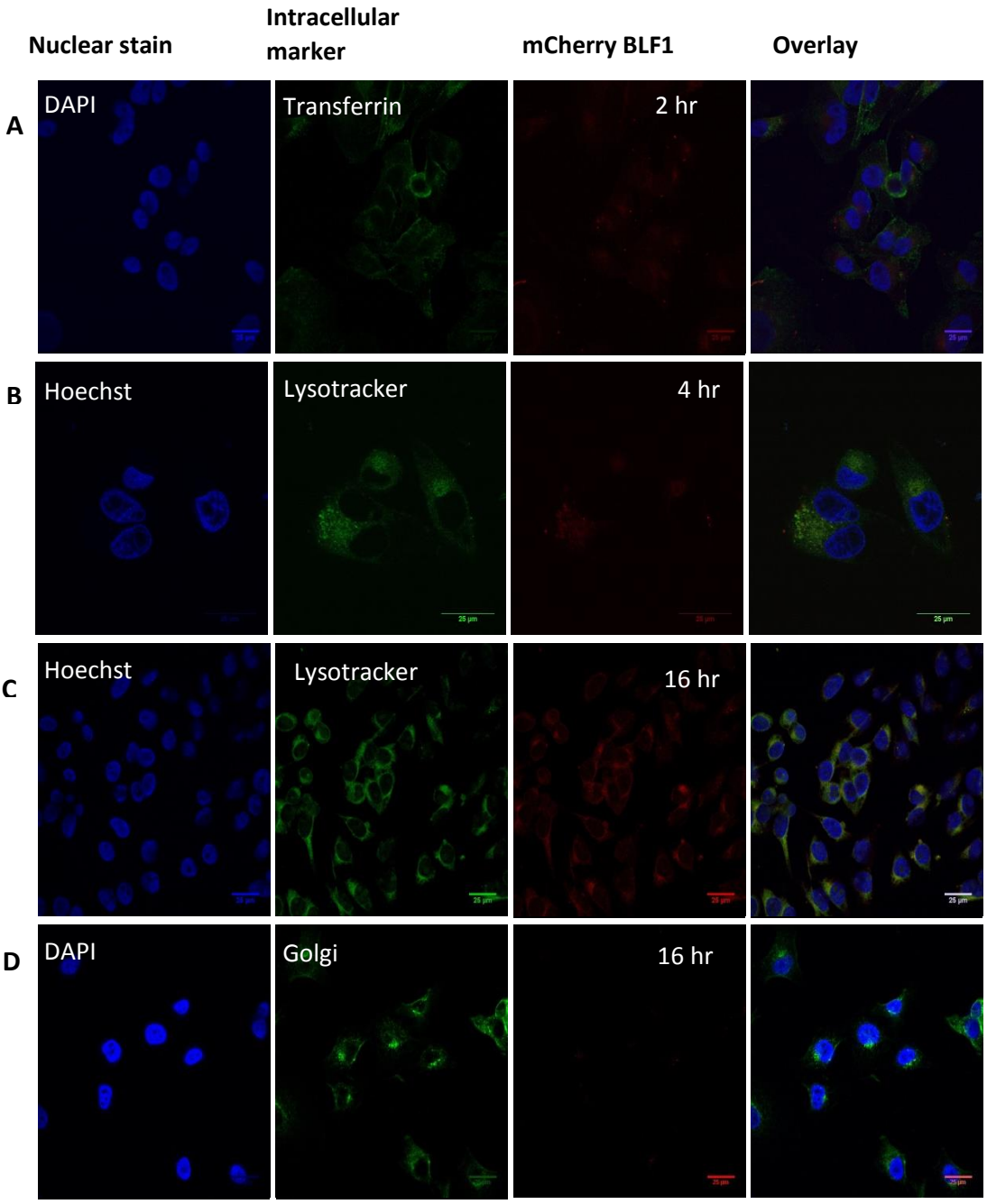

E

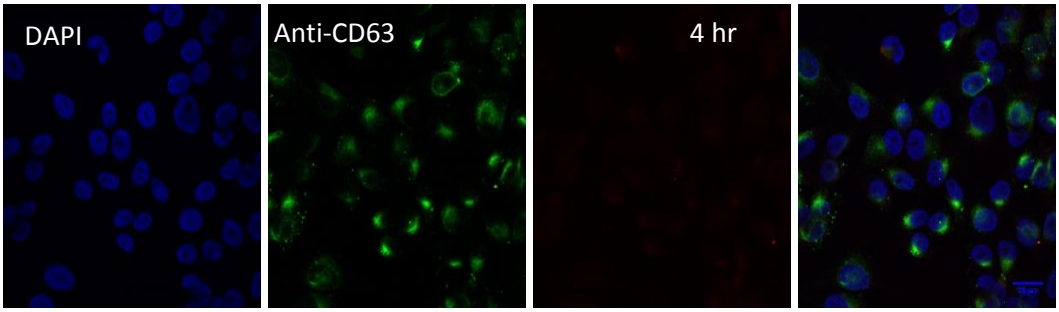

Figure 5.4.29: Intracellular trafficking of mCherry BLF1/anti-CD63IMT in MeWo cells: Cells were grown overnight and then incubated with medium containing mCherry BLF1/anti-CD63 IMT for 1 hr. After 1 hr the cells were washed and re-supplemented with pre-warmed medium and incubated for the indicated time. (**B, C**) The cells were washed and stained with Lyostracker®-Green and nuclei stained using the Hoechst stain, as described in 2.2.8.4.2. (**A, D, E**) The cells were fixed and stained with Golgi specific probe (WGA-FITC) or FITC-labelled anti-mouse antibody to detect anti-CD63 antibody in the conjugate as described in 2.2.8.4.1. Slides were imaged using confocal microscopy (60 x oil objectives) using appropriate filters.

Similar experiments were performed for the mCherry BLF1/anti-CD9 IMT in A549 cells. Confocal images showed some accumulation of BLF1 in lysosomes after 4 hr incubation with the IMT as shown by co-localization with Lysotracker®, but again the fluorescence signal is more intense for the 16 hr incubation time. In this case, some diffuse red fluorescence was also observed in the cytoplasm, which presumably corresponds to the release of the mCherry-BLF1 from acidic vesicles into the cytosol. Interestingly, in this case, when a similar experiment was performed using the Golgi-specific probe (WGA), some co-localization was found with BLF1 (**Fig**.5.4.30).

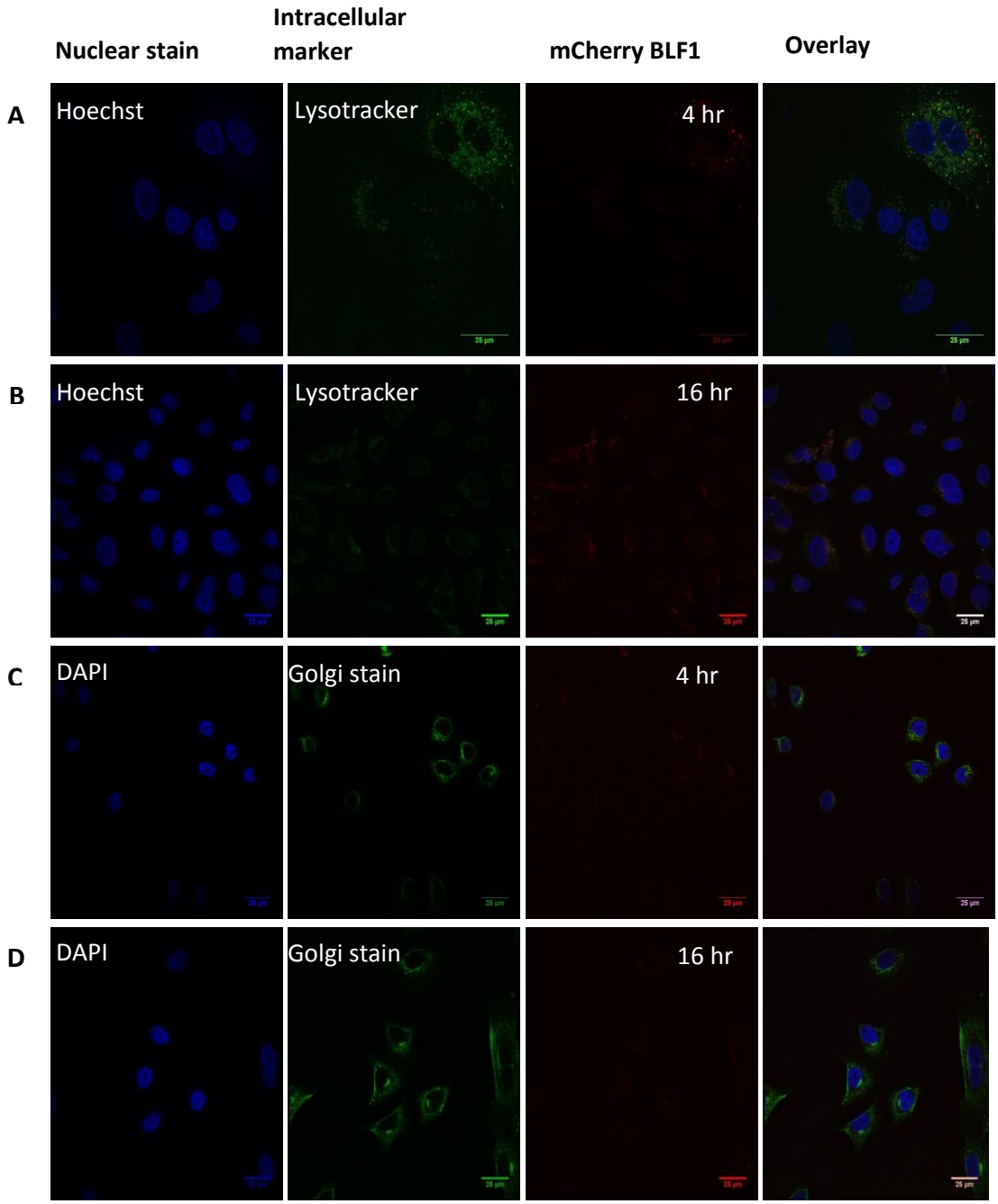

Figure 5.4.30: Intracellular trafficking of mCherry BLF1/anti-CD9IMT in A549 cells:
Cells were grown overnight and then incubated with medium containing mCherry BLF1/anti-CD9 IMT for 1 hr. After 1 hr the cells were washed and re-supplemented with pre-warmed medium and incubated for the indicated time. (**A, B**) The cells were washed and stained with Lyostracker®-Green and nuclei stained using the Hoechst stain, as described in 2.2.8.4.2. (**C, D**) The cells were fixed and stained with Golgi specific probe (WGA-FITC) as described in 2.2.8.4.1. Slides were imaged using confocal microscopy (60 x oil objectives) using appropriate filters.

5.5 Discussion:

We used murine anti-CD63 and anti-CD9 antibodies to generate a chemical conjugate with BLF1 toxin using the heterobifunctional cross-linker SPDP as described in (2.2.3.4). The anti-CD63/BLF1 IMT was purified and the final product was found to contain no free BLF1 as evident from western blotting (**Fig.**5.4.5). The shift in the apparent electrophoretic mobility to ~200 kDa in comparison to BLF1 (25 kDa) and CD63 antibody (150 kDa) confirmed successful conjugation. The low proportion of non-conjugated antibodies present (**Fig**.5.4.4) in the anti-CD63 IMT preparation are unlikely to affect the outcomes of cytotoxicity assay, particularly at sub-saturating levels of antibodies. However, the range of bands indicates a range of IMTs containing different ratios of BLF1: antibody. Indeed, the main drawback of a chemical conjugation method through native residues in monoclonal antibodies is the heterogeneous product and batch-to-batch variation (Acchione et al., 2012).

Indirect flow cytometry demonstrated a significant binding of the killing domain (BLF1 toxin) of the anti-CD63 IMT preparation to MeWo and RBL cells transfected with hCD63 as compared the unconjugated BLF1 or wild type (**Fig**.5.4.7, 5.4.8, 5.4.9). Additionally, analysis of the targeting domain (anti-CD63) component of the IMT binding by flow cytometry revealed that this is significantly detected on the surface of the tested cell line and its specificity is retained after chemical conjugation, since binding was similar for the IMT and anti-CD63 antibody alone. Interestingly, the binding profile of the unmodified mCherry BLF1/anti-CD63 IMT was higher than cys- modified BLF1/anti-CD63 IMT (**Fig**.5.4.7, 5.4.9). Since two basic strategies were used to crosslink BLF1 with SPDP reagents (depending on whether or not the BLF1 used possessed a sulfhydryl group (-SH)), our data suggested that by modifying BLF1 with SPDP, more (-SH) groups are introduced that are available for cross linking and therefore higher ratios of BLF1: antibody are achieved. However, there is only one cysteine in the modified BLF1 (cysteine tag) available for interaction with the thiolated antibody. Ideally, purification and an SDS-PAGE analysis should be carried out to further investigate the mCherry BLF1/antibody IMT. Furthermore, testing of anti-CD9 IMT binding to A549 cells showed a similar binding profile to the modified anti-CD63 IMT (**Fig.**5.4.17). In addition, confocal microscope images indicated that BLF1 (as a component of the IMT) is significantly detected on the cell surface (**Fig.**5.4.26). Taken together, these data strongly confirms our previous finding with the model conjugates that BLF1 could be delivered to the

cell by chemically coupling with antibodies that target a specific antigen expressed on cancer cells.

As expected, anti-CD63 and anti-CD9 IMTs retained specific activity against CD63 and CD9 antigen positive MeWo and A549 cells, respectively (**Fig**.5.4.11, 5.4.12, 5.4.18) with the same pattern as the model conjugate described previously (4.3.1, 4.3.2). In addition, the anti-CD63 and anti-CD9 antibodies alone showed no impact on cell growth, because this ability resides in the toxin domain of the immunotoxin. It has been previously reported that gelonin immunotoxin targeting two different antigens with different binding affinity exhibit the same cytotoxic potency regardless of the pathway followed to drive its internalization. This was attributed to endosomal escape being the rate limiting step (Pirie et al., 2011).

In addition, the anti-CD63 and anti-CD9 IMT were evaluated for cytostatic/cytotoxic activity in presence of non-toxic concentrations of saponin (**Fig.**5.4.11, 5.4.12, 5.4.18). For all IMTs, the effects on cell growth was increased ~2 fold in the presence of saponin. Saponin has been previously shown to have tremendous potential in enhancing the effectiveness of targeted toxins, mainly type I ribosomal inactivating plant saporin and dianthin, where it enhanced the endosomal escape without affecting membrane integrity (Gilabert-Oriol et al., 2014). The results demonstrate that the endosomal escape is the rate limiting step for efficient intoxication.

Furthermore, the anti-CD63 and anti-CD9 IMT were evaluated for cytotoxic activity in presence of brefeldin A that blocks Golgi function. For mCherry BLF1/anti-CD63 IMT, the cytostatic/cytotoxic activity was significantly enhanced in the presence of brefeldin A (**Fig**.5.4.13). Our data suggest that in MeWo cells, brefeldin A has no effect on immunotoxin processing but could enhance the immunotoxin translocation step. In this regards, confocal images showed no colocalization of mCherry BLF1/anti-CD63 IMT with a Golgi specific probe (WGA-FITC) (**Fig**.5.4.29.D). In contrast to ricin toxin that follows a pathway through Golgi apparatus (Yoshida et al., 1991), BLF1 was not hampered in its effects in brefeldin A treated MeWo cells (**Fig.**5.4.15.A). A similar result was seen with agrostin toxin, where its cytotoxicity was enhanced in the presence of brefeldin A (Hebestreit et al., 2006). Thus it is probable that BLF1 activity is independent on a functioning Golgi apparatus in MeWo cells. However, for BLF1/anti-CD9 IMT, the cytostatic/cytotoxic activity was not affected in the presence of brefeldin A (**Fig.**5.4.19) and interestingly, partial colocalization with the Golgi

apparatus was observed for this IMT (**Fig.**5.4.30). The results could suggest different internalization routing may be involved in the uptake of IMT for a specific cell type or targeting antigen.

We also investigated the effect of bafilomycin A at concentrations which inhibited intracellular trafficking in other cell types (Hebestreit et al., 2006). The mCherry BLF1/anti-CD63 and BLF1/anti-CD9 IMT were hampered in their toxicity in bafilomycin A_1 treated MeWo and A549 cells (**Fig**.5.4.14, 5.4.20). This indicates that the translocation of BLF1 to the cytosol does not occur so efficiently from early endosomes and therefore the cytostatic/cytotoxic potency of the IMT is reduced in the presence of bafilomycin. Bafilomycin inhibits acidification of endosomes, which could be required for the release of BLF1 from the IMT by reduction of disulphide bond. However, the effect of unconjugated BLF1 was not reduced in bafilomycin A_1 treated MeWo cells (**Fig.**5.4.15.B).

In addition, the unconjugated BLF1 was also evaluated for cytostatic/cytotoxic activity in presence of brefeldin A, and saponin in MeWo cells. The cytostatic/cytotoxic activity was significantly enhanced in presence of brefeldin A and saponin (**Fig**.5.4.15.A, 5.4.15.B). Our data suggest that in MeWo cells, brefeldin A and saponin could have enhanced the BLF1 translocation to the cytosol.

Images from confocal microscopy (**Fig**.5.4.16) elucidated that BLF1 toxin is internalized into the MeWo cells and accumulates in acidic vesicles (late endosome, lysosomes) as evident by the colocalization with red fluorescent signal from dextran conjugate (pHrododextran). However, when saponin is added, a diffuse green fluorescent signal was observed indicating the escape of the labelled BLF1 from acidic vesicle into the cytosol.

As tumour cells tend to mutate, the target antigen may be absent or expressed at levels that are too low for effective killing by the immunotoxin. Accordingly mutant cancer cells could be eradicated using cocktails of two or more immunotoxins recognising different target antigens (Ghetie et al., 1992). However, when both anti-CD63 IMT and anti-CD9 IMT added to antigen bearing A549 (**Fig**.5.4.21), no significant higher toxic effect was observed. This suggests that targeting two different antigens may not significantly increase the amount of BLF1 delivered to the cell and we may already be seeing a maximal effect with the IMTs.

The specificity of uptake and toxicity of un-purified IMT by cancer cells was confirmed by initially treating CD63 and CD9 bearing cells with excess concentration of either unconjugated anti-CD63 or anti-CD9 antibody prior treating with targeted IMT (**Fig**.5.4.22). This lead to significant reduction in the toxicity of IMT, although not 100%. There is possibly some free BLF1 toxin in the un-purified IMT preparation that would possibly internalize by the non-specific macropinocytosis pathway. This demonstrates, however, that surface antigen recognition contributes to initiate the cytotoxic effect of the IMT.

The results also indicated that BLF1/anti-CD63 IMT markedly suppressed the growth of the chemo resistant cell line, MES-SA/DX5 (**Fig**.5.4.24). However, the unconjugated BLF1 also had a significant effect on cell growth in a dose-dependent manner down to 0.5 µM (**Fig.**5.4.25). As described previously the uptake of unconjugated BLF1 is likely due to non-specific macropinocytosis. It would have been interesting to investigate the macropinocytosis activity of this cell line using fluorescent dextran as described in chapter 3. This also demonstrates that MES-SA/DX5 cell are highly dependent on eIF4A activity for cell survival and suggests that BLF1 based IMTs could be ideal for treating cancers that have become resistant to conventional chemotherapy drugs.

As shown in **Fig.**5.4.27 there was a strong binding of BLF1/anti-CD63 IMT to MeWo cell surface on ice, a temperature, which prevents metabolic activity including internalization of the IMT. However, under normal physiological conditions (37°C, humidified atmosphere of 5% CO_2) internalized immunotoxin was observed inside the cells. Furthermore, confocal live images in (**Fig**.5.4.28) showed that mCherry BLF1 component of anti-CD63 IMT is internalized to the cells.

Confocal microscopy images in (**Fig.**5.4.29.E) show that both targeting domain (anti-CD63) and killing domain (BLF1) of the mCherry BLF1/anti-CD63 IMT show considerable co-localization to the same intracellular compartment in MeWo cells after 4 hr.

The toxin release to the cytosol can follow different intracellular pathway that usually involves the Golgi apparatus or the lysosomes (Tome-Amat et al., 2015). In our study the co-localization of mCherry BLF1/anti-CD63IMT was observed with early endosomes, and lysosomes in MeWo cells (**Fig**.5.4.29.A, B, and C). However, the co-localization of mCherry BLF1/anti-CD9 IMT was observed with both lysosomes and the Golgi specific probe in A549

cells (**Fig**.5.4.30.A, B, C, and D). The data reported here indicate that different pathways are followed by mCherryBLF1/anti-CD63 and mCherryBLF1/anti-CD9 IMT.

6 Chapter 6: General discussion

BLF1 is a potent and irreversible translation initiation inhibitor that kills rapidly dividing and not non-dividing cells. Initially, as described in chapter 3, it has been found that 72 hr incubation is the optimum time required for the toxin to be endocytosed, reach the endosomal compartment, and subsequently release into the cytosol to exert its effect. However, it is possible that any toxic effects of the BLF1 may fade after periods longer than 3 days, due to either toxin exclusion from cells or lysosomal degradation. Therefore it would be of interest to perform longer time course assays to examine BLF1 effect on cell growth.

The catalytic activity of BLF1 was not uniform across different cellular models, as it is most likely dependent on the cells reliance on eIF4A activity as well as toxin uptake. We have recently reported that BLF1 had a significant effect on cells that take up dextran more efficiently as shown with the mouse macrophage cell lines J774 and RAW, a lower effect with A549 and HeLa cells and no effect with normal kidney cells (HEK293), and human monocytic cell lines (HL60,U937, andTHP1).

In the study described here, we have also characterized the binding and internalization properties of mCherry tagged BLF1 to the surface of J774.2 by flow cytometry. This showed no evidence of interaction with any type of receptor; this was also confirmed for untagged BLF1 using an anti-BLF1 antibody. This confirms that there is no receptor for BLF1 on J774.2 and A549 cells and the uptake of the toxin by these cells is through nonspecific uptake involving macropinocytosis. This pathway of BLF1 uptake was also confirmed by pre-incubation of J774.2 cells with a known inhibitor of macropinocytosis (amiloride) and also confirmed by fluorescent microscopy studies carried out in cooperation with Professor Bazbek Davletov's laboratory for mCherry C94S BLF1 (Rust et al., 2015). Flow cytometry analysis in mouse macrophage and a human epithelial cell line over 1 and 24 hr (**Fig.**3.3.20**,** 3.3.21) again indicated a non-specific fluid phase uptake of mCherry-tagged BLF1 by macropinocytosis. Its low toxicity and unique activity against rapidly diving cells may allow the use of intact BLF1 for development as a therapeutic agent for cancer.

In chapter 4, initial studies were carried out using non-chemically linked reagents to couple BLF1 to specific monoclonal antibodies. BLF1 was linked to anti-CD63 and anti-CD9 monoclonal antibodies by either antibody coated magnetic beads or secondary antibodies.

Previous attempts used magnetic particles for controlled drug targeting with the aid of a magnetic field to concentrate the drug at the site of action (Gallo and Hafeli, 1997, Lubbe et al., 2001). The resulting non-covalently linked BLF1 conjugates demonstrated a strong binding to CD63 and CD9 positive cells, and appeared to internalise, whereas the isotype conjugates did not bind or internalise.

We investigated the cytotoxic properties of the model BLF1/anti-CD63 bead conjugates directed against the hCD63 transfected RBL-2H3 cell line as a model system. Our results indicated that this model cell line was not sensitive to loss of eIF4A activity caused by BLF1. As RBL-2H3 is known to have a strong secretory phenotype (Bingham et al., 1994), it is possible that the toxins were taken up and then secreted. Further work carried out by an MSc student under my supervision has shown that the RBL-2H3 cells are also resistant to the toxin saporin. It was also interesting to note that RBL-2H3, having comparatively high levels of CD63 expression, showed resistance to BLF1 toxin, as it is been reported that the intoxication process is more dependent on the internalization pathway and intracellular processing of IMT rather than binding of IMT on the cell membrane (Azemar et al., 2000).

Similarly the BLF1/anti-CD63 and BLF1/anti-CD9 bead conjugates were tested on a human epithelial cell line (A549) that expresses high levels of CD9 and moderate levels of CD63. The results revealed that the targeted conjugate had only a very slight effect on cellular growth as compared to untreated cells and isotype control conjugate. It is possibly that after binding and internalization of these conjugates, BLF1 will be trafficked to the endosomal-lysosomal compartments where the toxin was deactivated. Another possible explanation considered was that since CD63 is also found in lysosomes, the BLF1 toxin might not be able to escape to the cytosol to exert its effect. This was subsequently shown to unlikely as the chemically conjugated anti-CD63 IMT retained activity. Furthermore, we tested lipofectamine, for its ability to deliver BLF1/antibody conjugate into A549 cells; this showed that LF3000 increased the sensitivity of cells to both conjugates, but this effect was also observed with the isotype controls. This result suggests that the model immunoconjugates contained sufficient BLF1 to mediate cytotoxic effects, but that the toxin was not delivered efficiently into the cytosol by the specific antibody component. In the case of the anti-CD9 bead conjugate, although immunfluorecsence images showed their association with cells, it is possible that these remained bound to the cell surface.

Binding studies showed that the soluble immunoconjugates made with BLF1 and anti-CD63 and anti-CD9 antibodies similarly bound specifically to antigen-bearing cells. Flow cytometry and microscopy studies also showed that BLF1/anti-CD63 immunoconjugates were internalised more rapidly than BLF1/anti-CD9 immunoconjugates by A549 cells.
Cytostaticity/cytotoxicity experiments showed that BLF1/anti-CD9 immunoconjugates had a significant toxic effect at the highest concentrations used (0.08 μM), but the BLF1/anti-CD63 immunoconjugate conjugate did not show significant inhibition of cell growth. Furthermore, non- toxic concentrations of saponin in combination with BLF1/anti-CD63 and anti-CD9 immunoconjugates dramatically improved the effect of both immunoconjugate on cells; however, similar results were again observed for the isotype controls.

Labelled endocytic probes for transferrin and LAMP1 were used to try to define the cellular association and fate of the BLF1 component of the model conjugates inside the cells. Confocal images indicated that BLF1 was localised at least partly in early endosomes and lysosomes after internalisation and no internalisation was observed with conjugates containing isotype control. The targeting antibody and mCherry BLF1 also appeared to co-localise in cells. Interestingly, the anti-CD9 component of the both model conjugates was significantly present on the cell membrane, suggesting that it may not have internalised or had been recycled back to the plasma membrane following internalisation. By contrast, the BLF1 and anti-CD63 antibody components of model conjugate were present mainly in small vesicles in the cytoplasm. Different targeting antigens may follow different routes inside the cells, particularly as CD63 is a known lysosomal trafficking protein(Takino et al., 2003) ; indeed, one of its former names was lysosomal associated membrane protein 3 (LAMP3). It would have been interesting to complete more microscopy work examining exactly what happens to the BLF1/conjugate within early time periods (internalisation within 0-15 minutes), as well as later periods to examine the degradation and potential secretion from cells within 1-3 days and even later.

Overall, the model immunoconjugates were useful in assessing the ability of different antibodies to target BLF1 to cells, but could not be used to predict cytostatic/cytotoxic efficiency.

The final results Chapter describe the chemical conjugation of BLF1 to antibodies using a heterobifunctional cross-linker, SPDP. Difficulties were encountered in purifications of

BLF1/anti-CD63 IMT after conjugation. Initially a nickel column was used to purify the IMT (as the BLF1 used contains 6xhis tag) from any non-reacted antibody. Next, gel filtration (GF) was performed to separate the immunotoxin from free BLF1, based on molecular weight. However, this strategy resulted in loss of a large amount of protein especially after nickel column purification. In addition purified IMT contained free BLF1; this is probably due to nonspecific binding of BLF1 to the targeting antibodies. Another approach was applied by performing gel filtration first followed by nickel column purification; there was higher yield but for example starting with 900 µg of the IMT, only 160 µg was obtained and after nickel column purification only 25 µg. It was suggested that the retention of material on the column could be due to hydrophobic interactions of free SPDP to the column material or it could be due unreacted groups on the antibodies. Therefore the conjugated sample was incubated with 1mM cysteine for 30 minutes before application on a Superdex200 GL column, as free SPDP would link to cysteine (to block any potential binding site). The yield remained suboptimal, even when trying gel fitration using a small column of Superdex75. Further attempts were performed by concentrating the conjugate through 100 kDa MWCO vivaspin and washing with PBS-EDTA buffer intensively to remove free BLF1. One step purification was then performed by application to a Superdex200 gel filtration column in the presence of 0.5 M NaCl. This was suitable for purification of BLF1/anti-CD63 IMT and the pure IMT collected contained less than 10% unconjugated antibody as shown in SDS-PAGE analysis (**Fig**.5.4.4). The pure BLF1/anti-CD63 IMT was recognized via western blotting using anti-BLF1 antibodies, with band being detected at ~ 200 kDa under non-reducing conditions (**Fig.**5.4.5).

The results presented in chapter 5 show the successful production of functional BLF1/anti-CD63 and antI-CD9 IMT. Flow cytometry demonstrated specific binding of the IMTs to cell lines expressing the target antigen, with no discernible loss of antibody recognition.

The IMTs showed significant effects on cell lines expressing the target antigen (30-50% reduction in cell growth). The cytotoxic activity of anti-CD63 and anti-CD9 IMT has clearly shown target- specific cell killing, as it was inhibited by free (unconjugated) antibodies. It would have been interesting to test a higher concentration of free antibody and a range of dilutions of IMT to observe stronger competitive inhibition.

Both MeWo and the uterine sarcoma multi-drug chemoresistant cell line MES-SA/Dx-5 showed high sensitivity to BLF1/ anti-CD63 IMT, whereas the unconjugated antibody was not toxic to the cells. The ability of BLF1/anti-CD63 IMT to control the growth of chemo resistant cells makes this immunotoxin a potential alternative for targeted therapy in chemo-relapsed patients.

The release of the toxin into the cytosol is a rate- limiting step in targeted therapy (Olsnes et al., 1989, Pirker et al., 1985, Ravel et al., 1992). Therefore, the high potency of toxin component is undermined by the requirement of high doses of the toxin to achieve the desired rate of cytosolic uptake. Thus it is obvious that efficacy enhancers are important tools to improve the endosomal escape and accordingly decrease the dose of toxin (Fuchs et al., 2016). From the earliest days, immunotoxins have been administered in combination with enhancer agents in the hopes of making better reagents (Kreitman et al., 2001, Schindler et al., 2011). These findings encouraged us to investigate the potential augmentation properties of saponin with BLF1 targeted conjugates. BLF1 toxin is a monomeric protein similar to type 1 RIP that does not have a binding domain and its cytotoxicity was greatly enhanced in the presence of lipfectamine (LF3000) reagent that aids delivery of the toxin into the cell cytosol as shown in previous chapters. The results here confirmed that the anti-proliferative effect of the IMTs can be improved by combination with saponin. Build-up of such a significant cytostatic/cytotoxic effect of BLF1 IMT in the presence of saponin, suggests that not only the binding and internalization of the immunotoxin are vital perquisites but also the endosomal escape is the rate- limiting step for efficient intoxication.

Determination of the intracellular trafficking of BLF1 is important for its optimal use as an anticancer drug, as the active toxin target, eIF4A, resides preferentially in the cytoplasm. Confocal images indicated that the internalization of mCherry BLF1/anti-CD63 IMT in MeWo cells took place leading to localisation in the lysosome. Surprisingly, the internalization of mCherry BLF1/anti-CD9 IMT in A549 via endocytosis apparently resulted in some trafficking to the Golgi complex. Additionally, anti-CD63 IMT toxicity is significantly enhanced upon the addition of brefeldin A, whereas the toxicity of BLF1/anti-CD9 IMT was not affected by brefeldin A. The results could suggest different internalization routing may be involved in the uptake of IMT for a specific cell type or targeting antigen. Our results for the anti-CD63

IMT are consistent with the function of the CD63 antigen, where the tyrosine-based internalization motif is present, and has been shown to enhance the internalization of partner proteins that interact with CD63 on the cell surface and facilitate their targeting to late endocytic compartments (Pols and Klumperman, 2009).

Suggestions for future work:

Further progress and improved in vitro and in vivo responses of targeted BLF1 IMT against cancer depends on the identification of new tumor target to enhance its antitumor efficacy and specificity with minimal side effects on normal tissues. There are several limitations to the use of the targeted BLF1 IMTs that was used in the previous mentioned experiments.

Firstly, the anti-human CD63 antibodies were used as a model to direct BLF1 to the CD63 expressing cells. As the CD63 antigen is widely expressed in the human body, this conjugate is not suitable for direct use in humans. Instead, this strategy could be applied clinically with the use of antibodies that target a specific protein, sugar chain, lipid and other molecule expressed on the surface of cancer cells derived extracellular vesicles (Nishida-Aoki, Tominaga et al. 2017). These specific cancer molecules have been recognised as cancer biomarkers (Czernek and Duchler, 2017) for instance CD24 and EpCAM in ovarian cancer (Rupp et al., 2011), CD147 in colon cancer (Luz et al., 2017). Furthermore, HER2 is an example of another ideal antigen that could be targeted, as this antigen internalizes fairly quickly, and is present in millions of copies on HER2 positive cancer cells with low expression levels on other tissues. Importantly this antigen does not get down regulated (Hughes, 2010).

In addition, the use of bispecific antibodies and bispecific antibody fragments, that binds to two different antigens or epitopes on the same antigen, is considered as a promising means of targeting molecules (Spiess et al., 2015). A recent in vitro study reported that the bispecific immunotoxin $VEGF_{165}$-ephrin A1-PE38KDEL delivered by human mesenchymal stem cells significantly inhibited the growth of mouse malignant gliomas (Zhang et al., 2015).

Secondly, it is important to reduce the heterogeneity of the generated targeted BLF1 IMT. This means different toxin loads due to the presence of several binding sites on the mAbs. Various toxin-loaded forms of targeted BLF1 IMT may have variations in pharmacokinetic

properties *in vivo* and may differ in clinical effect. Nowadays, a number of strategies are applied in the field of site-specific conjugation to produce more homogenous IMT. One approach is by introducing a reactive cysteine residue at a specific position on the monoclonal antibody that does not interfere with the antigen binding site and antibody function (Sochaj et al., 2015).

In addition, the coupling of single chain antibody fragment (scFv) as a targeting moiety in the construction of targeted BLF1 IMT could further improve its penetration into tumor cells. This approach has been applied previously to construct several scFv based IMTs using a modified Pseudomonas exotoxin A (Klimka et al., 1999).

Further successes in generating targeted BLF1 IMT could be achieved by using human or humanized antibody as a targeting moiety, to reduce the immunogenicity of the targeted part of the IMT. A similar strategy was used to construct a humanized anti-EGFR immunotoxin that was generated by genetic fusing of a humanized anti-EGFR single-chain variable fragment with a modified *Pseudomonas aeruginosa* exotoxin A. This IMT has been shown to have anti-proliferative activity against EGFR-overexpressing A431 cells (Akbari et al., 2017)

As previously indicated, at least some of the targeted BLF1 IMT remain trapped inside the endocytic organelles and are not efficiently delivered to the cytosol. The toxin component needs to reach the cytosol to display it biological activity on its cytosolic eIF4A target. There is previous evidence that cell penetrating peptides (CPP) mediate endosomal escape of various cargos such as DNA, siRNA, proteins, fluorophores, and drugs both *in vivo* and *in vitro.* These CPP were suggested to disrupt the lipid bilayer of endocytic organelles (Erazo-Oliveras et al., 2012).

Furthermore, targeted BLF1 IMT could be co-administered with other therapeutic reagents that may work synergistically to enhance the potency as a combinatorial therapy. Zhang and co-workers showed that mesothelin-targeted immunotoxin RG7787 has a synergistic anti-tumor efficacy when used in combination with Nab-Paclitaxel against human mesothelioma cell lines and tumor xenografts (Zhang et al., 2017).

In summary, we have developed novel immunotoxins that are designed to have a wider therapeutic window, and the next step would be to test these in animal to address the value of BLF1 for promised immunotoxin therapy.

The future perspectives of this work are two fold: first, reformation of the antibodies with covalently conjugated toxin payloads for in vivo experiments on animal models; second, determination of the therapeutic properties, including pharmacokinetics and antitumor efficacy of the designed BLF1 IMT.

7 Appendix

Conjugate	Stock conc. BLF1:Ab µM	Dilution	Assay
BLF1/anti-CD63 BLF1/anti-CD9 bead conjugate	0.8:0.3 (20µg/ml:40µg/ml)	1:6	Binding assay
		1:10	SRB
		1:10	Confocal images
BLF1/anti-CD63 BLF1/anti-CD9 immunoconjugate	0.8:0.3 (20µg/ml:40µg/ml)	1:6	Binding assay
		1:10	SRB
		1:10	Confocal images
Un-purified mCherryBLF1/antiCD63 BLF1/anti-CD63 BLF1/anti-CD9 IMT	50:5 (1.2mg/ml:0.75mg/ml)	1:6	Binding assay
		1:10	SRB
		1:100	Confocal images
		1:10	Titration

Table A: Model conjugates and BLF1/ IMT working concentration

MCSHHHHHHSMPNSLEAQIRQAMKTGSTLTIEFDQALNQKSPGTLNVFLHPANGGVRIDL
DSGNQGEPAKILWLPWKQGELQTLQPGSISTVDMLFFTYYLSGCKVFAGDGGPVWHIDAP
VEANQFWRRMSSDEWMEDWEVGTDRQVAYLHRAGQSDSLWNLSAYLEGAAPSTYGRDNLG
QAVVGGIVTGRQQMSLYQYATTSSGSSAWSPLTYTLQQRKQ

Figure A: pET24b vector encodes modified BLF1 containing a cysteine residue at position 2 from the N-terminus.

MGSSHHHHHHSSGLVPRGSHMPNSLEAQIRQAMKTGSTLTIEFDQALNQKSPGTLNVFLH
PANGGVRIDDSGNQGEPAKILWLPWKQGELQTLQPGSISTVDMLFFTYYLSGCKVFAGDG
GPVWHIDAPVEANQFWRRMSSDEWMEDWEVGTDRQVAYLHRAGQSDSLWNLSAYLEGAAP
STYGRDNLGQAVVGGIVTGRQQMSLYQYATTSSGSSAWSPLTYTLQQRKQ

Figure B: pET14b vector encodes BLF1 containing 6 HIS at the N-terminal.

MGSSHHHHHHSSGLVPRGSHMVSKGEEDNMAIIKEFMRFKVHMEGSVNGHEFEIEGEGEG
RPYEGTQTAKLKVTKGGPLPFAWDILSPQFMYGSKAYVKHPADIPDYLKLSFPEGFKWER
VMNFEDGGVVTVTQDSSLQDGEFIYKVKLRGTNFPSDGPVMQKKTMGWEASSERMYPEDG
ALKGEIKQRLKLKDGGHYDAEVKTTYKAKKPVQLPGAYNVNIKLDITSHNEDYTIVEQYE
RAEGRHSTGGMDELYKGILDMPNSLEAQIRQAMKTGSTLTIEFDQALNQKSPGTLNVFLH

PANGGVRIDLDSGNQGEPAKILWLPWKQGELQTLQPGSISTVDMLFFTYYLSGCKVFAGD
GGPVWHIDAPVEANQFWRRMSSDEWMEDWEVGTDRQVAYLHRAGQSDSLWNLSAYLEGAA
PSTYGRDNLGQAVVGGIVTGRQQMSLYQYATTSSGSSAWSPLTYTLQQRKQ

Figure C: pET14b vector encodes mCherry tagged BLF1 containing 6 HIS at the N-terminal

MGSSHHHHHHSSGLVPRGSHMVSKGEEDNMAIIKEFMRFKVHMEGSVNGHEFEIEGEGEG
RPYEGTQTAKLKVTKGGPLPFAWDILSPQFMYGSKAYVKHPADIPDYLKLSFPEGFKWER
VMNFEDGGVVTVTQDSSLQDGEFIYKVKLRGTNFPSDGPVMQKKTMGWEASSERMYPEDG
ALKGEIKQRLKLKDGGHYDAEVKTTYKAKKPVQLPGAYNVNIKLDITSHNEDYTIVEQYE
RAEGRHSTGGMDELYKGILDMPNSLEAQIRQAMKTGSTLTIEFDQALNQKSPGTLNVFLH
PANGGVRIDLDSGNQGEPAKILWLPWKQGELQTLQPGSISTVDMLFFTYYLSGSKVFAGD
GGPVWHIDAPVEANQFWRRMSSDEWMEDWEVGTDRQVAYLHRAGQSDSLWNLSAYLEGAA
PSTYGRDNLGQAVVGGIVTGRQQMSLYQYATTSSGSSAWSPLTYTLQQRKQ

Figure D: pET14b vector encodes mCherry tagged C94S containing 6 HIS at the N-terminal and with a cysteine at position 94 changed to serine.

8 Bibliography

ACCHIONE, M., KWON, H., JOCHHEIM, C. M. & ATKINS, W. M. 2012. Impact of linker and conjugation chemistry on antigen binding, Fc receptor binding and thermal stability of model antibody-drug conjugates. *MAbs,* 4**,** 362-72.

ADKINS, I., HOLUBOVA, J., KOSOVA, M. & SADILKOVA, L. 2012. Bacteria and their toxins tamed for immunotherapy. *Curr Pharm Biotechnol,* 13**,** 1446-73.

AKBARI, B., FARAJNIA, S., ZARGHAMI, N., MAHDIEH, N., RAHMATI, M., KHOSROSHAHI, S. A., BARZEGAR, A. & RAHBARNIA, L. 2017. Construction, expression, and activity of a novel immunotoxin comprising a humanized antiepidermal growth factor receptor scFv and modified Pseudomonas aeruginosa exotoxin A. *Anticancer Drugs,* 28**,** 263-270.

ALACHKAR, H., SANTHANAM, R., HARB, J. G., LUCAS, D. M., OAKS, J. J., HICKEY, C. J., PAN, L., KINGHORN, A. D., CALIGIURI, M. A., PERROTTI, D., BYRD, J. C., GARZON, R., GREVER, M. R. & MARCUCCI, G. 2013. Silvestrol exhibits significant in vivo and in vitro antileukemic activities and inhibits FLT3 and miR-155 expressions in acute myeloid leukemia. *J Hematol Oncol,* 6**,** 21.

ALEWINE, C., HASSAN, R. & PASTAN, I. 2015. Advances in anticancer immunotoxin therapy. *Oncologist,* 20**,** 176-85.

ALPUCHE-ARANDA, C. M., RACOOSIN, E. L., SWANSON, J. A. & MILLER, S. I. 1994. Salmonella stimulate macrophage macropinocytosis and persist within spacious phagosomes. *J Exp Med,* 179**,** 601-8.

AMYERE, M., METTLEN, M., VAN DER SMISSEN, P., PLATEK, A., PAYRASTRE, B., VEITHEN, A. & COURTOY, P. J. 2002. Origin, originality, functions, subversions and molecular signalling of macropinocytosis. *Int J Med Microbiol,* 291**,** 487-94.

ANDREWS, P. W., KNOWLES, B. B. & GOODFELLOW, P. N. 1981. A human cell-surface antigen defined by a monoclonal antibody and controlled by a gene on chromosome 12. *Somatic Cell Genet,* 7**,** 435-43.

ANTIGNANI, A. & FITZGERALD, D. 2013. Immunotoxins: the role of the toxin. *Toxins (Basel),* 5**,** 1486-502.

ANTIGNANI, A., MATHEWS GRINER, L., GUHA, R., SIMON, N., PASETTO, M., KELLER, J., HUANG, M., ANGELUS, E., PASTAN, I., FERRER, M., FITZGERALD, D. J. & THOMAS, C. J. 2016. Chemical Screens Identify Drugs that Enhance or Mitigate Cellular Responses to Antibody-Toxin Fusion Proteins. *PLOS ONE,* 11**,** e0161415.

ARSENAULT, J., CUIJPERS, S. A., FERRARI, E., NIRANJAN, D., RUST, A., LEESE, C., O'BRIEN, J. A., BINZ, T. & DAVLETOV, B. 2014. Botulinum protease-cleaved SNARE fragments induce cytotoxicity in neuroblastoma cells. *J Neurochem,* 129**,** 781-91.

AUDRAN, R., DRENOU, B., WITTKE, F., GAUDIN, A., LESIMPLE, T. & TOUJAS, L. 1995. Internalization of human macrophage surface antigens induced by monoclonal antibodies. *J Immunol Methods,* 188**,** 147-54.

AUTENRIETH, S. E. & AUTENRIETH, I. B. 2009. Variable antigen uptake due to different expression of the macrophage mannose receptor by dendritic cells in various inbred mouse strains. *Immunology,* 127**,** 523-9.

AZEMAR, M., SCHMIDT, M., ARLT, F., KENNEL, P., BRANDT, B., PAPADIMITRIOU, A., GRONER, B. & WELS, W. 2000. Recombinant antibody toxins specific for ErbB2 and EGF receptor inhibit the in vitro growth of human head and neck cancer cells and cause rapid tumor regression in vivo. *Int J Cancer,* 86**,** 269-75.

AZORSA, D. O., HYMAN, J. A. & HILDRETH, J. E. 1991. CD63/Pltgp40: a platelet activation antigen identical to the stage-specific, melanoma-associated antigen ME491. *Blood,* 78**,** 280-4.

BACHANOVA, V., FRANKEL, A. E., CAO, Q., LEWIS, D., GRZYWACZ, B., VERNERIS, M. R., USTUN, C., LAZARYAN, A., MCCLUNE, B., WARLICK, E. D., KANTARJIAN, H., WEISDORF, D. J., MILLER, J. S. & VALLERA, D. A. 2015. Phase I study of a bispecific ligand-directed toxin targeting CD22 and CD19 (DT2219) for refractory B-cell malignancies. *Clin Cancer Res,* 21**,** 1267-72.

BACHRAN, C., DURKOP, H., SUTHERLAND, M., BACHRAN, D., MULLER, C., WENG, A., MELZIG, M. F. & FUCHS, H. 2009. Inhibition of tumor growth by targeted toxins in mice is dramatically improved by saponinum album in a synergistic way. *J Immunother,* 32**,** 713-25.

BARRIUSO, B., ANTOLIN, P., ARIAS, F. J., GIROTTI, A., JIMENEZ, P., CORDOBA-DIAZ, M., CORDOBA-DIAZ, D. & GIRBES, T. 2016. Anti-Human Endoglin (hCD105) Immunotoxin-Containing Recombinant Single Chain Ribosome-Inactivating Protein Musarmin 1. *Toxins (Basel),* 8.

BARSUMIAN, E. L., ISERSKY, C., PETRINO, M. G. & SIRAGANIAN, R. P. 1981. IgE-induced histamine release from rat basophilic leukemia cell lines: isolation of releasing and nonreleasing clones. *Eur J Immunol,* 11**,** 317-23.

BATTELLI, M. G., CITORES, L., BUONAMICI, L., FERRERAS, J. M., DE BENITO, F. M., STIRPE, F. & GIRBES, T. 1997. Toxicity and cytotoxicity of nigrin b, a two-chain ribosome-inactivating protein from Sambucus nigra: comparison with ricin. *Arch Toxicol,* 71**,** 360-4.

BAYER, N., SCHOBER, D., PRCHLA, E., MURPHY, R. F., BLAAS, D. & FUCHS, R. 1998. Effect of bafilomycin A1 and nocodazole on endocytic transport in HeLa cells: implications for viral uncoating and infection. *J Virol,* 72**,** 9645-55.

BECK, A., SENTER, P. & CHARI, R. 2011. World Antibody Drug Conjugate Summit Europe: February 21-23, 2011; Frankfurt, Germany. *MAbs,* 3**,** 331-7.

BHAT, M., ROBICHAUD, N., HULEA, L., SONENBERG, N., PELLETIER, J. & TOPISIROVIC, I. 2015. Targeting the translation machinery in cancer. *Nat Rev Drug Discov,* 14**,** 261-78.

BINGHAM, B. R., MONK, P. N. & HELM, B. A. 1994. Defective protein phosphorylation and Ca2+ mobilization in a low secreting variant of the rat basophilic leukemia cell line. *J Biol Chem,* 269**,** 19300-6.

BLAKEY, D. C., WATSON, G. J., KNOWLES, P. P. & THORPE, P. E. 1987. Effect of chemical deglycosylation of ricin A chain on the in vivo fate and cytotoxic activity of an immunotoxin composed of ricin A chain and anti-Thy 1.1 antibody. *Cancer Res,* 47**,** 947-52.

BLAKKISRUD, J., LONDALEN, A., MARTINSEN, A. C., DAHLE, J., HOLTEDAHL, J. E., BACH-GANSMO, T., HOLTE, H., KOLSTAD, A. & STOKKE, C. 2017. Tumor-Absorbed Dose for Non-Hodgkin Lymphoma Patients Treated with the Anti-CD37 Antibody Radionuclide Conjugate 177Lu-Lilotomab Satetraxetan. *J Nucl Med,* 58**,** 48-54.

BOLOGNESI, A., POLITO, L., TAZZARI, P. L., LEMOLI, R. M., LUBELLI, C., FOGLI, M., BOON, L., DE BOER, M. & STIRPE, F. 2000. In vitro anti-tumour activity of anti-CD80 and anti-CD86 immunotoxins containing type 1 ribosome-inactivating proteins. *Br J Haematol,* 110**,** 351-61.

BOQUET, P., SILVERMAN, M. S. & PAPPENHEIMER, A. M., JR. 1977. Interaction of diphtheria toxin with mammalian cell membranes. *Prog Clin Biol Res,* 17**,** 501-9.

BORDELEAU, M. E., ROBERT, F., GERARD, B., LINDQVIST, L., CHEN, S. M., WENDEL, H. G., BREM, B., GREGER, H., LOWE, S. W., PORCO, J. A., JR. & PELLETIER, J. 2008. Therapeutic suppression of translation initiation modulates chemosensitivity in a mouse lymphoma model. *J Clin Invest,* 118**,** 2651-60.

BOROWIEC, M., GORZKIEWICZ, M., GRZESIK, J., WALCZAK-DRZEWIECKA, A., SALKOWSKA, A., RODAKOWSKA, E., STECZKIEWICZ, K., RYCHLEWSKI, L., DASTYCH, J. & GINALSKI, K. 2016.

Towards Engineering Novel PE-Based Immunotoxins by Targeting Them to the Nucleus. *Toxins (Basel),* 8.

BOUCHARD, H., VISKOV, C. & GARCIA-ECHEVERRIA, C. 2014. Antibody-drug conjugates-a new wave of cancer drugs. *Bioorg Med Chem Lett,* 24**,** 5357-63.

BOUKAMP, P., PETRUSSEVSKA, R. T., BREITKREUTZ, D., HORNUNG, J., MARKHAM, A. & FUSENIG, N. E. 1988. Normal keratinization in a spontaneously immortalized aneuploid human keratinocyte cell line. *J Cell Biol,* 106**,** 761-71.

BOWMAN, E. J., SIEBERS, A. & ALTENDORF, K. 1988. Bafilomycins: a class of inhibitors of membrane ATPases from microorganisms, animal cells, and plant cells. *Proc Natl Acad Sci U S A,* 85**,** 7972-6.

BRIGOTTI, M., ALFIERI, R., SESTILI, P., BONELLI, M., PETRONINI, P. G., GUIDARELLI, A., BARBIERI, L., STIRPE, F. & SPERTI, S. 2002. Damage to nuclear DNA induced by Shiga toxin 1 and ricin in human endothelial cells. *FASEB J,* 16**,** 365-72.

BROSS, P. F., BEITZ, J., CHEN, G., CHEN, X. H., DUFFY, E., KIEFFER, L., ROY, S., SRIDHARA, R., RAHMAN, A., WILLIAMS, G. & PAZDUR, R. 2001. Approval summary: gemtuzumab ozogamicin in relapsed acute myeloid leukemia. *Clin Cancer Res,* 7**,** 1490-6.

BROWNE, G. J. & PROUD, C. G. 2002. Regulation of peptide-chain elongation in mammalian cells. *Eur J Biochem,* 269**,** 5360-8.

BUSS, N. A., HENDERSON, S. J., MCFARLANE, M., SHENTON, J. M. & DE HAAN, L. 2012. Monoclonal antibody therapeutics: history and future. *Curr Opin Pharmacol,* 12**,** 615-22.

BUTTGEREIT, F. & BRAND, M. D. 1995. A hierarchy of ATP-consuming processes in mammalian cells. *Biochem J,* 312 (Pt 1)**,** 163-7.

CARLSSON, J., DREVIN, H. & AXEN, R. 1978. Protein thiolation and reversible protein-protein conjugation. N-Succinimidyl 3-(2-pyridyldithio)propionate, a new heterobifunctional reagent. *Biochem J,* 173**,** 723-37.

CARLSSON, S. R. & FUKUDA, M. 1989. Structure of human lysosomal membrane glycoprotein 1. Assignment of disulfide bonds and visualization of its domain arrangement. *J Biol Chem,* 264**,** 20526-31.

CAVALLARO, U., NYKJAER, A., NIELSEN, M. & SORIA, M. R. 1995. Alpha 2-macroglobulin receptor mediates binding and cytotoxicity of plant ribosome-inactivating proteins. *Eur J Biochem,* 232**,** 165-71.

CENCIC, R., CARRIER, M., GALICIA-VAZQUEZ, G., BORDELEAU, M. E., SUKARIEH, R., BOURDEAU, A., BREM, B., TEODORO, J. G., GREGER, H., TREMBLAY, M. L., PORCO, J. A., JR. & PELLETIER, J. 2009. Antitumor activity and mechanism of action of the cyclopenta[b]benzofuran, silvestrol. *PLoS One,* 4**,** e5223.

CENCIC, R., ROBERT, F., GALICIA-VAZQUEZ, G., MALINA, A., RAVINDAR, K., SOMAIAH, R., PIERRE, P., TANAKA, J., DESLONGCHAMPS, P. & PELLETIER, J. 2013. Modifying chemotherapy response by targeted inhibition of eukaryotic initiation factor 4A. *Blood Cancer J,* 3**,** e128.

CHANDRAMOHAN, V., PEGRAM, C. N., PIAO, H., SZAFRANSKI, S. E., KUAN, C. T., PASTAN, I. H. & BIGNER, D. D. 2017. Production and quality control assessment of a GLP-grade immunotoxin, D2C7-(scdsFv)-PE38KDEL, for a phase I/II clinical trial. *Appl Microbiol Biotechnol,* 101**,** 2747-2766.

CHANDRAMOHAN, V., SAMPSON, J. H., PASTAN, I. & BIGNER, D. D. 2012. Toxin-based targeted therapy for malignant brain tumors. *Clin Dev Immunol,* 2012**,** 480429.

CHARI, R. V. 2008. Targeted cancer therapy: conferring specificity to cytotoxic drugs. *Acc Chem Res,* 41**,** 98-107.

CHARRIN, S., JOUANNET, S., BOUCHEIX, C. & RUBINSTEIN, E. 2014. Tetraspanins at a glance. *J Cell Sci,* 127**,** 3641-8.

CHOUDHARY, S., MATHEW, M. & VERMA, R. S. 2011. Therapeutic potential of anticancer immunotoxins. *Drug Discov Today,* 16**,** 495-503.

CHU, J. & PELLETIER, J. 2015. Targeting the eIF4A RNA helicase as an anti-neoplastic approach. *Biochim Biophys Acta,* 1849**,** 781-91.

COLLINS, S. J., GALLO, R. C. & GALLAGHER, R. E. 1977. Continuous growth and differentiation of human myeloid leukaemic cells in suspension culture. *Nature,* 270**,** 347-9.

COMMISSO, C., FLINN, R. J. & BAR-SAGI, D. 2014. Determining the macropinocytic index of cells through a quantitative image-based assay. *Nat Protoc,* 9**,** 182-92.

CREGG, J. M., CEREGHINO, J. L., SHI, J. & HIGGINS, D. R. 2000. Recombinant protein expression in Pichia pastoris. *Mol Biotechnol,* 16**,** 23-52.

CRUZ-MIGONI, A., HAUTBERGUE, G. M., ARTYMIUK, P. J., BAKER, P. J., BOKORI-BROWN, M., CHANG, C. T., DICKMAN, M. J., ESSEX-LOPRESTI, A., HARDING, S. V., MAHADI, N. M., MARSHALL, L. E., MOBBS, G. W., MOHAMED, R., NATHAN, S., NGUGI, S. A., ONG, C., OOI, W. F., PARTRIDGE, L. J., PHILLIPS, H. L., RAIH, M. F., RUZHEINIKOV, S., SARKAR-TYSON, M., SEDELNIKOVA, S. E., SMITHER, S. J., TAN, P., TITBALL, R. W., WILSON, S. A. & RICE, D. W. 2011. A Burkholderia pseudomallei toxin inhibits helicase activity of translation factor eIF4A. *Science,* 334**,** 821-4.

CURRIE, B. J. 2015. Melioidosis: evolving concepts in epidemiology, pathogenesis, and treatment. *Semin Respir Crit Care Med,* 36**,** 111-25.

CZERNEK, L. & DUCHLER, M. 2017. Functions of Cancer-Derived Extracellular Vesicles in Immunosuppression. *Arch Immunol Ther Exp (Warsz)*.

DALBY, B., CATES, S., HARRIS, A., OHKI, E. C., TILKINS, M. L., PRICE, P. J. & CICCARONE, V. C. 2004. Advanced transfection with Lipofectamine 2000 reagent: primary neurons, siRNA, and high-throughput applications. *Methods,* 33**,** 95-103.

DANG, N. H., PRO, B., HAGEMEISTER, F. B., SAMANIEGO, F., JONES, D., SAMUELS, B. I., RODRIGUEZ, M. A., GOY, A., ROMAGUERA, J. E., MCLAUGHLIN, P., TONG, A. T., TURTURRO, F., WALKER, P. L. & FAYAD, L. 2007. Phase II trial of denileukin diftitox for relapsed/refractory T-cell non-Hodgkin lymphoma. *Br J Haematol,* 136**,** 439-47.

DAS, M. K., SHARMA, R. S. & MISHRA, V. 2012. Induction of apoptosis by ribosome inactivating proteins: importance of N-glycosidase activity. *Appl Biochem Biotechnol,* 166**,** 1552-61.

DAVIDS, M. S. & LETAI, A. 2012. Targeting the B-cell lymphoma/leukemia 2 family in cancer. *J Clin Oncol,* 30**,** 3127-35.

DAVIS, B. H., MCCABE, E. & LANGWEILER, M. 1986. Characterization of f-Met-Leu-Phe-stimulated fluid pinocytosis in human polymorphonuclear leukocytes by flow cytometry. *Cytometry,* 7**,** 251-62.

DE ZOYSA, A., EFSTRATIOU, A. & HAWKEY, P. M. 2005. Molecular characterization of diphtheria toxin repressor (dtxR) genes present in nontoxigenic Corynebacterium diphtheriae strains isolated in the United Kingdom. *J Clin Microbiol,* 43**,** 223-8.

DIAMANTIS, N. & BANERJI, U. 2016. Antibody-drug conjugates--an emerging class of cancer treatment. *Br J Cancer,* 114**,** 362-7.

DOSIO, F., BRUSA, P. & CATTEL, L. 2011. Immunotoxins and anticancer drug conjugate assemblies: the role of the linkage between components. *Toxins (Basel),* 3**,** 848-83.

DOSIO, F., STELLA, B., CERIONI, S., GASTALDI, D. & ARPICCO, S. 2014. Advances in anticancer antibody-drug conjugates and immunotoxins. *Recent Pat Anticancer Drug Discov,* 9**,** 35-65.

DOUDNA, J. A. & RATH, V. L. 2002. Structure and function of the eukaryotic ribosome: the next frontier. *Cell,* 109**,** 153-6.

DUCRY, L. 2013. Antibody-Drug Conjugates.

DUFFIELD, A., KAMSTEEG, E. J., BROWN, A. N., PAGEL, P. & CAPLAN, M. J. 2003. The tetraspanin CD63 enhances the internalization of the H,K-ATPase beta-subunit. *Proc Natl Acad Sci U S A,* 100**,** 15560-5.

EBERLE, J., KRASAGAKIS, K. & ORFANOS, C. E. 1997. Translation initiation factor eIF-4A1 mRNA is consistently overexpressed in human melanoma cells in vitro. *Int J Cancer,* 71**,** 396-401.

ECKER, D. M., JONES, S. D. & LEVINE, H. L. 2015. The therapeutic monoclonal antibody market. *MAbs,* 7**,** 9-14.

ERAZO-OLIVERAS, A., MUTHUKRISHNAN, N., BAKER, R., WANG, T. Y. & PELLOIS, J. P. 2012. Improving the endosomal escape of cell-penetrating peptides and their cargos: strategies and challenges. *Pharmaceuticals (Basel),* 5**,** 1177-209.

ERAZO-OLIVERAS, A., NAJJAR, K., DAYANI, L., WANG, T. Y., JOHNSON, G. A. & PELLOIS, J. P. 2014. Protein delivery into live cells by incubation with an endosomolytic agent. *Nat Methods,* 11**,** 861-7.

FELGNER, J. H., KUMAR, R., SRIDHAR, C. N., WHEELER, C. J., TSAI, Y. J., BORDER, R., RAMSEY, P., MARTIN, M. & FELGNER, P. L. 1994. Enhanced gene delivery and mechanism studies with a novel series of cationic lipid formulations. *J Biol Chem,* 269**,** 2550-61.

FITZGERALD, D., IDZIOREK, T., BATRA, J. K., WILLINGHAM, M. & PASTAN, I. 1990. Antitumor activity of a thioether-linked immunotoxin: OVB3-PE. *Bioconjug Chem,* 1**,** 264-8.

FITZGERALD, D. J., WAYNE, A. S., KREITMAN, R. J. & PASTAN, I. 2011. Treatment of hematologic malignancies with immunotoxins and antibody-drug conjugates. *Cancer Res,* 71**,** 6300-9.

FLATAU, G., LEMICHEZ, E., GAUTHIER, M., CHARDIN, P., PARIS, S., FIORENTINI, C. & BOQUET, P. 1997. Toxin-induced activation of the G protein p21 Rho by deamidation of glutamine. *Nature,* 387**,** 729-33.

FLYGARE, J. A., PILLOW, T. H. & ARISTOFF, P. 2013. Antibody-drug conjugates for the treatment of cancer. *Chem Biol Drug Des,* 81**,** 113-21.

FRANKEL, A. E., POWELL, B. L., HALL, P. D., CASE, L. D. & KREITMAN, R. J. 2002. Phase I trial of a novel diphtheria toxin/granulocyte macrophage colony-stimulating factor fusion protein (DT388GMCSF) for refractory or relapsed acute myeloid leukemia. *Clin Cancer Res,* 8**,** 1004-13.

FROYSNES, I. S., ANDERSSON, Y., LARSEN, S. G., DAVIDSON, B., OIEN, J. T., OLSEN, K. H., GIERCKSKY, K. E., JULSRUD, L., FODSTAD, O., DUELAND, S. & FLATMARK, K. 2017. Novel Treatment with Intraperitoneal MOC31PE Immunotoxin in Colorectal Peritoneal Metastasis: Results From the ImmunoPeCa Phase 1 Trial. *Ann Surg Oncol*.

FUCHS, H. & BACHRAN, C. 2009. Targeted tumor therapies at a glance. *Curr Drug Targets,* 10**,** 89-93.

FUCHS, H., WENG, A. & GILABERT-ORIOL, R. 2016. Augmenting the Efficacy of Immunotoxins and Other Targeted Protein Toxins by Endosomal Escape Enhancers. *Toxins (Basel),* 8.

FURUYA, M., KATO, H., NISHIMURA, N., ISHIWATA, I., IKEDA, H., ITO, R., YOSHIKI, T. & ISHIKURA, H. 2005. Down-regulation of CD9 in human ovarian carcinoma cell might contribute to peritoneal dissemination: morphologic alteration and reduced expression of beta1 integrin subsets. *Cancer Res,* 65**,** 2617-25.

GADADHAR, S. & KARANDE, A. A. 2013. Abrin immunotoxin: targeted cytotoxicity and intracellular trafficking pathway. *PLoS One,* 8**,** e58304.

GALLO, J. M. & HAFELI, U. 1997. A.S. Lubbe et al., Preclinical experiences with magnetic drug targeting: tolerance and efficacy. Cancer Res., 56: 4694-4701, 1996; and Clinical experiences with magnetic drug targeting: a phase I study with 4'-epidoxorubicin in 14 patients with advanced solid tumors. Cancer Res., 56: 4686-4693, 1996. *Cancer Res,* 57**,** 3063-5.

GHETIE, M. A., TUCKER, K., RICHARDSON, J., UHR, J. W. & VITETTA, E. S. 1992. The antitumor activity of an anti-CD22 immunotoxin in SCID mice with disseminated Daudi lymphoma is enhanced by either an anti-CD19 antibody or an anti-CD19 immunotoxin. *Blood,* 80**,** 2315-20.

GHETIE, V. & VITETTA, E. S. 2001. Chemical construction of immunotoxins. *Mol Biotechnol,* 18**,** 251-68.

GIARD, D. J., AARONSON, S. A., TODARO, G. J., ARNSTEIN, P., KERSEY, J. H., DOSIK, H. & PARKS, W. P. 1973. In vitro cultivation of human tumors: establishment of cell lines derived from a series of solid tumors. *J Natl Cancer Inst,* 51**,** 1417-23.

GILABERT-ORIOL, R., THAKUR, M., HAUSSMANN, K., NIESLER, N., BHARGAVA, C., GORICK, C., FUCHS, H. & WENG, A. 2016. Saponins from Saponaria officinalis L. Augment the Efficacy of a Rituximab-Immunotoxin. *Planta Med,* 82**,** 1525-1531.

GILABERT-ORIOL, R., WENG, A., MALLINCKRODT, B., MELZIG, M. F., FUCHS, H. & THAKUR, M. 2014. Immunotoxins constructed with ribosome-inactivating proteins and their enhancers: a lethal cocktail with tumor specific efficacy. *Curr Pharm Des,* 20**,** 6584-643.

GRAHAM, F. L., SMILEY, J., RUSSELL, W. C. & NAIRN, R. 1977. Characteristics of a human cell line transformed by DNA from human adenovirus type 5. *J Gen Virol,* 36**,** 59-74.

GROSE, C. & BRUNEL, P. A. 1978. Varicella-zoster virus: isolation and propagation in human melanoma cells at 36 and 32 degrees C. *Infect Immun,* 19**,** 199-203.

GRZMIL, M. & HEMMINGS, B. A. 2012. Translation regulation as a therapeutic target in cancer. *Cancer Res,* 72**,** 3891-900.

HA, C. T., WATERHOUSE, R., WESSELLS, J., WU, J. A. & DVEKSLER, G. S. 2005. Binding of pregnancy-specific glycoprotein 17 to CD9 on macrophages induces secretion of IL-10, IL-6, PGE2, and TGF-beta1. *J Leukoc Biol,* 77**,** 948-57.

HAMBLETT, K. J., SENTER, P. D., CHACE, D. F., SUN, M. M., LENOX, J., CERVENY, C. G., KISSLER, K. M., BERNHARDT, S. X., KOPCHA, A. K., ZABINSKI, R. F., MEYER, D. L. & FRANCISCO, J. A. 2004. Effects of drug loading on the antitumor activity of a monoclonal antibody drug conjugate. *Clin Cancer Res,* 10**,** 7063-70.

HASSAN, R., ALEWINE, C. & PASTAN, I. 2016. New Life for Immunotoxin Cancer Therapy. *Clin Cancer Res,* 22**,** 1055-8.

HASSAN, R., BERA, T. & PASTAN, I. 2004. Mesothelin: a new target for immunotherapy. *Clin Cancer Res,* 10**,** 3937-42.

HASSAN, R., LERNER, M. R., BENBROOK, D., LIGHTFOOT, S. A., BRACKETT, D. J., WANG, Q. C. & PASTAN, I. 2002. Antitumor activity of SS(dsFv)PE38 and SS1(dsFv)PE38, recombinant antimesothelin immunotoxins against human gynecologic cancers grown in organotypic culture in vitro. *Clin Cancer Res,* 8**,** 3520-6.

HASSAN, R., SHARON, E., THOMAS, A., ZHANG, J., LING, A., MIETTINEN, M., KREITMAN, R. J., STEINBERG, S. M., HOLLEVOET, K. & PASTAN, I. 2014. Phase 1 study of the antimesothelin immunotoxin SS1P in combination with pemetrexed and cisplatin for front-line therapy of pleural mesothelioma and correlation of tumor response with serum mesothelin, megakaryocyte potentiating factor, and cancer antigen 125. *Cancer,* 120**,** 3311-9.

HAUTBERGUE, G. M. & WILSON, S. A. 2012. BLF1, the first Burkholderia pseudomallei toxin, connects inhibition of host protein synthesis with melioidosis. *Biochem Soc Trans,* 40**,** 842-5.

HEBESTREIT, P. & MELZIG, M. F. 2003. Cytotoxic activity of the seeds from Agrostemma githago var. githago. *Planta Med,* 69**,** 921-5.

HEBESTREIT, P., WENG, A., BACHRAN, C., FUCHS, H. & MELZIG, M. F. 2006. Enhancement of cytotoxicity of lectins by Saponinum album. *Toxicon,* 47**,** 330-5.

HEISLER, I., SUTHERLAND, M., BACHRAN, C., HEBESTREIT, P., SCHNITGER, A., MELZIG, M. F. & FUCHS, H. 2005. Combined application of saponin and chimeric toxins drastically enhances the targeted cytotoxicity on tumor cells. *J Control Release,* 106**,** 123-37.

HEMLER, M. E. 2005. Tetraspanin functions and associated microdomains. *Nat Rev Mol Cell Biol,* 6**,** 801-11.

HEXHAM, J. M., DUDAS, D., HUGO, R., THOMPSON, J., KING, V., DOWLING, C., NEVILLE, D. M., JR., DIGAN, M. E. & LAKE, P. 2001. Influence of relative binding affinity on efficacy in a panel of anti-CD3 scFv immunotoxins. *Mol Immunol,* 38**,** 397-408.

HIGASHIYAMA, M., DOI, O., KODAMA, K., YOKOUCHI, H., ADACHI, M., HUANG, C. L., TAKI, T., KASUGAI, T., ISHIGURO, S., NAKAMORI, S. & MIYAKE, M. 1997. Immunohistochemically detected expression of motility-related protein-1 (MRP-1/CD9) in lung adenocarcinoma and its relation to prognosis. *Int J Cancer,* 74**,** 205-11.

HIGGINBOTTOM, A., WILKINSON, I., MCCULLOUGH, B., LANZA, F., AZORSA, D. O., PARTRIDGE, L. J. & MONK, P. N. 2000. Antibody cross-linking of human CD9 and the high-affinity immunoglobulin E receptor stimulates secretion from transfected rat basophilic leukaemia cells. *Immunology,* 99**,** 546-52.

HO, M., BERA, T. K., WILLINGHAM, M. C., ONDA, M., HASSAN, R., FITZGERALD, D. & PASTAN, I. 2007. Mesothelin expression in human lung cancer. *Clin Cancer Res,* 13**,** 1571-5.

HOLLIGER, P. & HUDSON, P. J. 2005. Engineered antibody fragments and the rise of single domains. *Nat Biotechnol,* 23**,** 1126-36.

HOTTA, H., ROSS, A. H., HUEBNER, K., ISOBE, M., WENDEBORN, S., CHAO, M. V., RICCIARDI, R. P., TSUJIMOTO, Y., CROCE, C. M. & KOPROWSKI, H. 1988. Molecular cloning and characterization of an antigen associated with early stages of melanoma tumor progression. *Cancer Res,* 48**,** 2955-62.

HUDSON, T. H. & GRILLO, F. G. 1991. Brefeldin-A enhancement of ricin A-chain immunotoxins and blockade of intact ricin, modeccin, and abrin. *J Biol Chem,* 266**,** 18586-92.

HUGHES, B. 2010. Antibody-drug conjugates for cancer: poised to deliver? *Nat Rev Drug Discov,* 9**,** 665-7.

HUNZIKER, W. & GEUZE, H. J. 1996. Intracellular trafficking of lysosomal membrane proteins. *Bioessays,* 18**,** 379-89.

IGLESIAS, R., PEREZ, Y., DE TORRE, C., FERRERAS, J. M., ANTOLIN, P., JIMENEZ, P., ROJO, M. A., MENDEZ, E. & GIRBES, T. 2005. Molecular characterization and systemic induction of single-chain ribosome-inactivating proteins (RIPs) in sugar beet (Beta vulgaris) leaves. *J Exp Bot,* 56**,** 1675-84.

JACKSON, R. J., HELLEN, C. U. & PESTOVA, T. V. 2010. The mechanism of eukaryotic translation initiation and principles of its regulation. *Nat Rev Mol Cell Biol,* 11**,** 113-27.

JANG, H. I. & LEE, H. 2003. A decrease in the expression of CD63 tetraspanin protein elevates invasive potential of human melanoma cells. *Exp Mol Med,* 35**,** 317-23.

JANTHUR, W. D., CANTONI, N. & MAMOT, C. 2012. Drug Conjugates Such as Antibody Drug Conjugates (ADCs), Immunotoxins and Immunoliposomes Challenge Daily Clinical Practice. *Int J Mol Sci,* 13**,** 16020-45.

JANVIER, K. & BONIFACINO, J. S. 2005. Role of the endocytic machinery in the sorting of lysosome-associated membrane proteins. *Mol Biol Cell,* 16**,** 4231-42.

KALIN, S., AMSTUTZ, B., GASTALDELLI, M., WOLFRUM, N., BOUCKE, K., HAVENGA, M., DIGENNARO, F., LISKA, N., HEMMI, S. & GREBER, U. F. 2010. Macropinocytotic uptake and infection of human epithelial cells with species B2 adenovirus type 35. *J Virol,* 84**,** 5336-50.

KATZ, J., JANIK, J. E. & YOUNES, A. 2011. Brentuximab Vedotin (SGN-35). *Clin Cancer Res,* 17**,** 6428-36.

KITSON, S. L., QUINN, D. J., MOODY, T. S., SPEED, D., WATTERS, W. & ROZZELL, D. 2013. Antibody-Drug Conjugates (ADCs) - Biotherapeutic bullets. *Chimica Oggi-Chemistry Today,* 31**,** 29-35.

KLIMKA, A., BARTH, S., MATTHEY, B., ROOVERS, R. C., LEMKE, H., HANSEN, H., ARENDS, J. W., DIEHL, V., HOOGENBOOM, H. R. & ENGERT, A. 1999. An anti-CD30 single-chain Fv selected by phage display and fused to Pseudomonas exotoxin A (Ki-4(scFv)-ETA') is a potent immunotoxin against a Hodgkin-derived cell line. *Br J Cancer,* 80**,** 1214-22.

KOGURE, T., KINGHORN, A. D., YAN, I., BOLON, B., LUCAS, D. M., GREVER, M. R. & PATEL, T. 2013. Therapeutic potential of the translation inhibitor silvestrol in hepatocellular cancer. *PLoS One,* 8**,** e76136.

KOHLER, G. & MILSTEIN, C. 1975. Continuous cultures of fused cells secreting antibody of predefined specificity. *Nature,* 256**,** 495-7.

KOIVUSALO, M., WELCH, C., HAYASHI, H., SCOTT, C. C., KIM, M., ALEXANDER, T., TOURET, N., HAHN, K. M. & GRINSTEIN, S. 2010. Amiloride inhibits macropinocytosis by lowering submembranous pH and preventing Rac1 and Cdc42 signaling. *J Cell Biol,* 188**,** 547-63.

KOVTUN, Y. V., AUDETTE, C. A., YE, Y., XIE, H., RUBERTI, M. F., PHINNEY, S. J., LEECE, B. A., CHITTENDEN, T., BLATTLER, W. A. & GOLDMACHER, V. S. 2006. Antibody-drug conjugates designed to eradicate tumors with homogeneous and heterogeneous expression of the target antigen. *Cancer Res,* 66**,** 3214-21.

KREITMAN, R. J. 2006. Immunotoxins for targeted cancer therapy. *AAPS J,* 8**,** E532-51.

KREITMAN, R. J., HASSAN, R., FITZGERALD, D. J. & PASTAN, I. 2009a. Phase I trial of continuous infusion anti-mesothelin recombinant immunotoxin SS1P. *Clin Cancer Res,* 15**,** 5274-9.

KREITMAN, R. J., STETLER-STEVENSON, M., JAFFE, E. S., CONLON, K. C., STEINBERG, S. M., WILSON, W., WALDMANN, T. A. & PASTAN, I. 2016. Complete Remissions of Adult T-cell Leukemia with Anti-CD25 Recombinant Immunotoxin LMB-2 and Chemotherapy to Block Immunogenicity. *Clinical Cancer Research,* 22**,** 310-318.

KREITMAN, R. J., STETLER-STEVENSON, M., MARGULIES, I., NOEL, P., FITZGERALD, D. J. P., WILSON, W. H. & PASTAN, I. 2009b. Phase II Trial of Recombinant Immunotoxin RFB4(dsFv)-PE38 (BL22) in Patients With Hairy Cell Leukemia. *Journal of Clinical Oncology,* 27**,** 2983-2990.

KREITMAN, R. J., WILSON, W. H., BERGERON, K., RAGGIO, M., STETLER-STEVENSON, M., FITZGERALD, D. J. & PASTAN, I. 2001. Efficacy of the anti-CD22 recombinant immunotoxin BL22 in chemotherapy-resistant hairy-cell leukemia. *N Engl J Med,* 345**,** 241-7.

KUO, S. R., ALFANO, R. W., FRANKEL, A. E. & LIU, J. S. 2009. Antibody internalization after cell surface antigen binding is critical for immunotoxin development. *Bioconjug Chem,* 20**,** 1975-82.

KUPCHAN, S. M., KOMODA, Y., COURT, W. A., THOMAS, G. J., SMITH, R. M., KARIM, A., GILMORE, C. J., HALTIWANGER, R. C. & BRYAN, R. F. 1972. Maytansine, a novel antileukemic ansa macrolide from Maytenus ovatus. *J Am Chem Soc,* 94**,** 1354-6.

KWON, M. S., SHIN, S. H., YIM, S. H., LEE, K. Y., KANG, H. M., KIM, T. M. & CHUNG, Y. J. 2007. CD63 as a biomarker for predicting the clinical outcomes in adenocarcinoma of lung. *Lung Cancer,* 57**,** 46-53.

LA-BECK, N. M., JEAN, G. W., HUYNH, C., ALZGHARI, S. K. & LOWE, D. B. 2015. Immune Checkpoint Inhibitors: New Insights and Current Place in Cancer Therapy. *Pharmacotherapy,* 35**,** 963-76.

LAMBERT, J. M. & BLATTLER, W. A. 1988. Purification and biochemical characterization of immunotoxins. *Cancer Treat Res,* 37**,** 323-48.

LI, Y. M., VALLERA, D. A. & HALL, W. A. 2013. Diphtheria toxin-based targeted toxin therapy for brain tumors. *J Neurooncol,* 114**,** 155-64.

LIM, J. P. & GLEESON, P. A. 2011. Macropinocytosis: an endocytic pathway for internalising large gulps. *Immunol Cell Biol,* 89**,** 836-43.

LIPPINCOTT-SCHWARTZ, J., YUAN, L., TIPPER, C., AMHERDT, M., ORCI, L. & KLAUSNER, R. D. 1991. Brefeldin A's effects on endosomes, lysosomes, and the TGN suggest a general mechanism for regulating organelle structure and membrane traffic. *Cell,* 67**,** 601-16.

LOMAKIN, I. B. & STEITZ, T. A. 2013. The initiation of mammalian protein synthesis and mRNA scanning mechanism. *Nature,* 500**,** 307-11.

LORD, J. M. & ROBERTS, L. M. 1998. Retrograde transport: going against the flow. *Curr Biol,* 8**,** R56-8.

LUBBE, A. S., ALEXIOU, C. & BERGEMANN, C. 2001. Clinical applications of magnetic drug targeting. *J Surg Res,* 95**,** 200-6.

LUCAS, D. M., EDWARDS, R. B., LOZANSKI, G., WEST, D. A., SHIN, J. D., VARGO, M. A., DAVIS, M. E., ROZEWSKI, D. M., JOHNSON, A. J., SU, B. N., GOETTL, V. M., HEEREMA, N. A., LIN, T. S., LEHMAN, A., ZHANG, X., JARJOURA, D., NEWMAN, D. J., BYRD, J. C., KINGHORN, A. D. & GREVER, M. R. 2009. The novel plant-derived agent silvestrol has B-cell selective activity in chronic lymphocytic leukemia and acute lymphoblastic leukemia in vitro and in vivo. *Blood,* 113**,** 4656-66.

LUZ, M. C., PEREZ, M. M., AZZALIS, L. A., SOUSA, L. V., ADAMI, F., FONSECA, F. L. & ALVES, B. D. 2017. Evaluation of MCT1, MCT4 and CD147 Genes in Peripheral Blood Cells of Breast Cancer Patients and Their Potential Use as Diagnostic and Prognostic Markers. *Int J Mol Sci,* 18.

MALINA, A., MILLS, J. R. & PELLETIER, J. 2012. Emerging therapeutics targeting mRNA translation. *Cold Spring Harb Perspect Biol,* 4**,** a012377.

MAROUI, M. A., PAMPIN, M. & CHELBI-ALIX, M. K. 2011. Promyelocytic leukemia isoform IV confers resistance to encephalomyocarditis virus via the sequestration of 3D polymerase in nuclear bodies. *J Virol,* 85**,** 13164-73.

MATHEW, M. & VERMA, R. S. 2009. Humanized immunotoxins: a new generation of immunotoxins for targeted cancer therapy. *Cancer Sci,* 100**,** 1359-65.

MCCANN, S., AKILOV, O. E. & GESKIN, L. 2012. Adverse effects of denileukin diftitox and their management in patients with cutaneous T-cell lymphoma. *Clin J Oncol Nurs,* 16**,** E164-72.

MCGRATH, M. S., ROSENBLUM, M. G., PHILIPS, M. R. & SCHEINBERG, D. A. 2003. Immunotoxin resistance in multidrug resistant cells. *Cancer Res,* 63**,** 72-9.

MERRICK, W. C. 1992. Mechanism and regulation of eukaryotic protein synthesis. *Microbiol Rev,* 56**,** 291-315.

MOHLER, J. L. & SHARIEF, Y. 1993. Flow cytometric assay of pinocytosis: correlation with membrane ruffling and metastatic potential in the Dunning R-3327 rat prostatic adenocarcinoma model. *Cytometry,* 14**,** 826-31.

MOLDENHAUER, G., SALNIKOV, A. V., LUTTGAU, S., HERR, I., ANDERL, J. & FAULSTICH, H. 2012. Therapeutic potential of amanitin-conjugated anti-epithelial cell adhesion molecule monoclonal antibody against pancreatic carcinoma. *J Natl Cancer Inst,* 104**,** 622-34.

MURANOVA, T. A., RUZHEINIKOV, S. N., HIGGINBOTTOM, A., CLIPSON, J. A., BLACKBURN, G. M., WENTWORTH, P., DATTA, A., RICE, D. W. & PARTRIDGE, L. J. 2004. Crystallization of a carbamatase catalytic antibody Fab fragment and its complex with a transition-state analogue. *Acta Crystallogr D Biol Crystallogr,* 60**,** 172-4.

MURAYAMA, Y., ORITANI, K. & TSUTSUI, S. 2015. Novel CD9-targeted therapies in gastric cancer. *World J Gastroenterol,* 21**,** 3206-13.

NAGLICH, J. G., METHERALL, J. E., RUSSELL, D. W. & EIDELS, L. 1992. Expression cloning of a diphtheria toxin receptor: identity with a heparin-binding EGF-like growth factor precursor. *Cell,* 69**,** 1051-61.

NORBURY, C. C., HEWLETT, L. J., PRESCOTT, A. R., SHASTRI, N. & WATTS, C. 1995. Class I MHC presentation of exogenous soluble antigen via macropinocytosis in bone marrow macrophages. *Immunity,* 3**,** 783-91.

OHKUMA, S., SHIMIZU, S., NOTO, M., SAI, Y., KINOSHITA, K. & TAMURA, H. 1993. Inhibition of cell growth by bafilomycin A1, a selective inhibitor of vacuolar H(+)-ATPase. *In Vitro Cell Dev Biol Anim,* 29A**,** 862-6.

OLAFSEN, T. & WU, A. M. 2010. Antibody vectors for imaging. *Semin Nucl Med,* 40**,** 167-81.

OLSEN, E., DUVIC, M., FRANKEL, A., KIM, Y., MARTIN, A., VONDERHEID, E., JEGASOTHY, B., WOOD, G., GORDON, M., HEALD, P., OSEROFF, A., PINTER-BROWN, L., BOWEN, G., KUZEL, T., FIVENSON, D., FOSS, F., GLODE, M., MOLINA, A., KNOBLER, E., STEWART, S., COOPER, K., STEVENS, S., CRAIG, F., REUBEN, J., BACHA, P. & NICHOLS, J. 2001. Pivotal phase III trial of two dose levels of denileukin diftitox for the treatment of cutaneous T-cell lymphoma. *J Clin Oncol,* 19**,** 376-88.

OLSNES, S., SANDVIG, K., PETERSEN, O. W. & VAN DEURS, B. 1989. Immunotoxins--entry into cells and mechanisms of action. *Immunol Today,* 10**,** 291-5.

PAMELA A. TRAIL AUTH., G. L. P. E. 2013. Antibody-Drug Conjugates and Immunotoxins From Pre-Clinical Development to Therapeutic Applications South San Francisco, CA, USA.

PARTHASARATHY, V., MARTIN, F., HIGGINBOTTOM, A., MURRAY, H., MOSELEY, G. W., READ, R. C., MAL, G., HULME, R., MONK, P. N. & PARTRIDGE, L. J. 2009. Distinct roles for tetraspanins CD9, CD63 and CD81 in the formation of multinucleated giant cells. *Immunology,* 127**,** 237-48.

PASTAN, I., HASSAN, R., FITZGERALD, D. J. & KREITMAN, R. J. 2006. Immunotoxin therapy of cancer. *Nat Rev Cancer,* 6**,** 559-65.

PEDEN, A. A., OORSCHOT, V., HESSER, B. A., AUSTIN, C. D., SCHELLER, R. H. & KLUMPERMAN, J. 2004. Localization of the AP-3 adaptor complex defines a novel endosomal exit site for lysosomal membrane proteins. *J Cell Biol,* 164**,** 1065-76.

PETERSDORF, S. H., KOPECKY, K. J., SLOVAK, M., WILLMAN, C., NEVILL, T., BRANDWEIN, J., LARSON, R. A., ERBA, H. P., STIFF, P. J., STUART, R. K., WALTER, R. B., TALLMAN, M. S., STENKE, L. & APPELBAUM, F. R. 2013. A phase 3 study of gemtuzumab ozogamicin during induction and postconsolidation therapy in younger patients with acute myeloid leukemia. *Blood,* 121**,** 4854-60.

PHILLIPS, G. L. 2013. *Antibody-drug conjugates and immunotoxins: from pre-clinical development to therapeutic applications,* New York, Springer.

PIRIE, C. M., HACKEL, B. J., ROSENBLUM, M. G. & WITTRUP, K. D. 2011. Convergent potency of internalized gelonin immunotoxins across varied cell lines, antigens, and targeting moieties. *J Biol Chem,* 286**,** 4165-72.

PIRKER, R., FITZGERALD, D. J., HAMILTON, T. C., OZOLS, R. F., LAIRD, W., FRANKEL, A. E., WILLINGHAM, M. C. & PASTAN, I. 1985. Characterization of immunotoxins active against ovarian cancer cell lines. *J Clin Invest,* 76**,** 1261-7.

POLITO, L., BORTOLOTTI, M., MERCATELLI, D., BATTELLI, M. G. & BOLOGNESI, A. 2013. Saporin-S6: a useful tool in cancer therapy. *Toxins (Basel),* 5**,** 1698-722.

POLS, M. S. & KLUMPERMAN, J. 2009. Trafficking and function of the tetraspanin CD63. *Exp Cell Res,* 315**,** 1584-92.

POSEY, J. A., KHAZAELI, M. B., BOOKMAN, M. A., NOWROUZI, A., GRIZZLE, W. E., THORNTON, J., CAREY, D. E., LORENZ, J. M., SING, A. P., SIEGALL, C. B., LOBUGLIO, A. F. & SALEH, M. N.

2002. A phase I trial of the single-chain immunotoxin SGN-10 (BR96 sFv-PE40) in patients with advanced solid tumors. *Clin Cancer Res,* 8**,** 3092-9.

PRINCE, H. M., DUVIC, M., MARTIN, A., STERRY, W., ASSAF, C., SUN, Y., STRAUS, D., ACOSTA, M. & NEGRO-VILAR, A. 2010. Phase III Placebo-Controlled Trial of Denileukin Diftitox for Patients With Cutaneous T-Cell Lymphoma. *Journal of Clinical Oncology,* 28**,** 1870-1877.

PURI, M., KAUR, I., PERUGINI, M. A. & GUPTA, R. C. 2012. Ribosome-inactivating proteins: current status and biomedical applications. *Drug Discov Today,* 17**,** 774-83.

RALPH, P. & NAKOINZ, I. 1975. Phagocytosis and cytolysis by a macrophage tumour and its cloned cell line. *Nature,* 257**,** 393-4.

RALPH, P. & NAKOINZ, I. 1977a. Antibody-dependent killing of erythrocyte and tumor targets by macrophage-related cell lines: enhancement by PPD and LPS. *J Immunol,* 119**,** 950-54.

RALPH, P. & NAKOINZ, I. 1977b. Direct toxic effects of immunopotentiators on monocytic, myelomonocytic, and histiocytic or macrophage tumor cells in culture. *Cancer Res,* 37**,** 546-50.

RANA, S. & ZOLLER, M. 2011. Exosome target cell selection and the importance of exosomal tetraspanins: a hypothesis. *Biochem Soc Trans,* 39**,** 559-62.

RAVEL, S., COLOMBATTI, M. & CASELLAS, P. 1992. Internalization and intracellular fate of anti-CD5 monoclonal antibody and anti-CD5 ricin A-chain immunotoxin in human leukemic T cells. *Blood,* 79**,** 1511-7.

RAVINDAR, K., REDDY, M. S., LINDQVIST, L., PELLETIER, J. & DESLONGCHAMPS, P. 2011. Synthesis of the antiproliferative agent hippuristanol and its analogues via Suarez cyclizations and Hg(II)-catalyzed spiroketalizations. *J Org Chem,* 76**,** 1269-84.

REICHERT, J. M., ROSENSWEIG, C. J., FADEN, L. B. & DEWITZ, M. C. 2005. Monoclonal antibody successes in the clinic. *Nat Biotechnol,* 23**,** 1073-8.

RICART, A. D. & TOLCHER, A. W. 2007. Technology insight: cytotoxic drug immunoconjugates for cancer therapy. *Nat Clin Pract Oncol,* 4**,** 245-55.

ROBERTS, L. M. & LORD, J. M. 2004. Ribosome-inactivating proteins: entry into mammalian cells and intracellular routing. *Mini Rev Med Chem,* 4**,** 505-12.

ROGERS, G. W., JR., KOMAR, A. A. & MERRICK, W. C. 2002. eIF4A: the godfather of the DEAD box helicases. *Prog Nucleic Acid Res Mol Biol,* 72**,** 307-31.

ROUS, B. A., REAVES, B. J., IHRKE, G., BRIGGS, J. A., GRAY, S. R., STEPHENS, D. J., BANTING, G. & LUZIO, J. P. 2002. Role of adaptor complex AP-3 in targeting wild-type and mutated CD63 to lysosomes. *Mol Biol Cell,* 13**,** 1071-82.

RUPP, A. K., RUPP, C., KELLER, S., BRASE, J. C., EHEHALT, R., FOGEL, M., MOLDENHAUER, G., MARME, F., SULTMANN, H. & ALTEVOGT, P. 2011. Loss of EpCAM expression in breast cancer derived serum exosomes: role of proteolytic cleavage. *Gynecol Oncol,* 122**,** 437-46.

RUST, A., HASSAN, H. H., SEDELNIKOVA, S., NIRANJAN, D., HAUTBERGUE, G., ABBAS, S. A., PARTRIDGE, L., RICE, D., BINZ, T. & DAVLETOV, B. 2015. Two complementary approaches for intracellular delivery of exogenous enzymes. *Sci Rep,* 5**,** 12444.

SAFAVY, A., BONNER, J. A., WAKSAL, H. W., BUCHSBAUM, D. J., GILLESPIE, G. Y., KHAZAELI, M. B., ARANI, R., CHEN, D. T., CARPENTER, M. & RAISCH, K. P. 2003. Synthesis and biological evaluation of paclitaxel-C225 conjugate as a model for targeted drug delivery. *Bioconjug Chem,* 14**,** 302-10.

SAFTIG, P. & KLUMPERMAN, J. 2009. Lysosome biogenesis and lysosomal membrane proteins: trafficking meets function. *Nat Rev Mol Cell Biol,* 10**,** 623-35.

SALLUSTO, F., CELLA, M., DANIELI, C. & LANZAVECCHIA, A. 1995. Dendritic cells use macropinocytosis and the mannose receptor to concentrate macromolecules in the major

histocompatibility complex class II compartment: downregulation by cytokines and bacterial products. *J Exp Med,* 182**,** 389-400.

SAMPSON, J. H., AKABANI, G., ARCHER, G. E., BIGNER, D. D., BERGER, M. S., FRIEDMAN, A. H., FRIEDMAN, H. S., HERNDON, J. E., 2ND, KUNWAR, S., MARCUS, S., MCLENDON, R. E., PAOLINO, A., PENNE, K., PROVENZALE, J., QUINN, J., REARDON, D. A., RICH, J., STENZEL, T., TOURT-UHLIG, S., WIKSTRAND, C., WONG, T., WILLIAMS, R., YUAN, F., ZALUTSKY, M. R. & PASTAN, I. 2003. Progress report of a Phase I study of the intracerebral microinfusion of a recombinant chimeric protein composed of transforming growth factor (TGF)-alpha and a mutated form of the Pseudomonas exotoxin termed PE-38 (TP-38) for the treatment of malignant brain tumors. *J Neurooncol,* 65**,** 27-35.

SANDERSON, R. J., HERING, M. A., JAMES, S. F., SUN, M. M., DORONINA, S. O., SIADAK, A. W., SENTER, P. D. & WAHL, A. F. 2005. In vivo drug-linker stability of an anti-CD30 dipeptide-linked auristatin immunoconjugate. *Clin Cancer Res,* 11**,** 843-52.

SANDVIG, K. & OLSNES, S. 1981. Rapid entry of nicked diphtheria toxin into cells at low pH. Characterization of the entry process and effects of low pH on the toxin molecule. *J Biol Chem,* 256**,** 9068-76.

SANDVIG, K., PRYDZ, K., HANSEN, S. H. & VAN DEURS, B. 1991. Ricin transport in brefeldin A-treated cells: correlation between Golgi structure and toxic effect. *J Cell Biol,* 115**,** 971-81.

SANDVIG, K. & VAN DEURS, B. 1996. Endocytosis, intracellular transport, and cytotoxic action of Shiga toxin and ricin. *Physiol Rev,* 76**,** 949-66.

SANDVIG, K. & VAN DEURS, B. 2000. Entry of ricin and Shiga toxin into cells: molecular mechanisms and medical perspectives. *EMBO J,* 19**,** 5943-50.

SAUER, G., KURZEDER, C., GRUNDMANN, R., KREIENBERG, R., ZEILLINGER, R. & DEISSLER, H. 2003. Expression of tetraspanin adaptor proteins below defined threshold values is associated with in vitro invasiveness of mammary carcinoma cells. *Oncol Rep,* 10**,** 405-10.

SCHELHAAS, M., SHAH, B., HOLZER, M., BLATTMANN, P., KUHLING, L., DAY, P. M., SCHILLER, J. T. & HELENIUS, A. 2012. Entry of human papillomavirus type 16 by actin-dependent, clathrin- and lipid raft-independent endocytosis. *PLoS Pathog,* 8**,** e1002657.

SCHERER, W. F., SYVERTON, J. T. & GEY, G. O. 1953. Studies on the propagation in vitro of poliomyelitis viruses. IV. Viral multiplication in a stable strain of human malignant epithelial cells (strain HeLa) derived from an epidermoid carcinoma of the cervix. *J Exp Med,* 97**,** 695-710.

SCHINDLER, J., GAJAVELLI, S., RAVANDI, F., SHEN, Y., PAREKH, S., BRAUNCHWEIG, I., BARTA, S., GHETIE, V., VITETTA, E. & VERMA, A. 2011. A phase I study of a combination of anti-CD19 and anti-CD22 immunotoxins (Combotox) in adult patients with refractory B-lineage acute lymphoblastic leukaemia. *Br J Haematol,* 154**,** 471-6.

SCHMIDT, M. M., THURBER, G. M. & WITTRUP, K. D. 2008. Kinetics of anti-carcinoembryonic antigen antibody internalization: effects of affinity, bivalency, and stability. *Cancer Immunol Immunother,* 57**,** 1879-90.

SCHROEDER, H. W., JR. & CAVACINI, L. 2010. Structure and function of immunoglobulins. *J Allergy Clin Immunol,* 125**,** S41-52.

SCHROT, J., WENG, A. & MELZIG, M. F. 2015. Ribosome-inactivating and related proteins. *Toxins (Basel),* 7**,** 1556-615.

SENTER, P. D. 2009. Potent antibody drug conjugates for cancer therapy. *Curr Opin Chem Biol,* 13**,** 235-44.

SENTER, P. D. & SIEVERS, E. L. 2012. The discovery and development of brentuximab vedotin for use in relapsed Hodgkin lymphoma and systemic anaplastic large cell lymphoma. *Nat Biotechnol,* 30**,** 631-7.

SHAN, L., LIU, Y. & WANG, P. 2013. Recombinant Immunotoxin Therapy of Solid Tumors: Challenges and Strategies. *J Basic Clin Med,* 2**,** 1-6.

SHEFET-CARASSO, L. & BENHAR, I. 2015. Antibody-targeted drugs and drug resistance--challenges and solutions. *Drug Resist Updat,* 18**,** 36-46.

SIEGALL, C. B. 1994. Targeted toxins as anticancer agents. *Cancer,* 74**,** 1006-12.

SIEVERS, E. L. & SENTER, P. D. 2013. Antibody-drug conjugates in cancer therapy. *Annu Rev Med,* 64**,** 15-29.

SKEHAN, P., STORENG, R., SCUDIERO, D., MONKS, A., MCMAHON, J., VISTICA, D., WARREN, J. T., BOKESCH, H., KENNEY, S. & BOYD, M. R. 1990. New colorimetric cytotoxicity assay for anticancer-drug screening. *J Natl Cancer Inst,* 82**,** 1107-12.

SMITH, D. A., MONK, P. N. & PARTRIDGE, L. J. 1995. Antibodies against human CD63 activate transfected rat basophilic leukemia (RBL-2H3) cells. *Mol Immunol,* 32**,** 1339-44.

SOCHAJ, A. M., SWIDERSKA, K. W. & OTLEWSKI, J. 2015. Current methods for the synthesis of homogeneous antibody-drug conjugates. *Biotechnol Adv,* 33**,** 775-84.

SONENBERG, N. & HINNEBUSCH, A. G. 2009. Regulation of translation initiation in eukaryotes: mechanisms and biological targets. *Cell,* 136**,** 731-45.

SORDAT, I., DECRAENE, C., SILVESTRE, T., PETERMANN, O., AUFFRAY, C., PIETU, G. & SORDAT, B. 2002. Complementary DNA arrays identify CD63 tetraspanin and alpha3 integrin chain as differentially expressed in low and high metastatic human colon carcinoma cells. *Lab Invest,* 82**,** 1715-24.

SPIESS, C., ZHAI, Q. & CARTER, P. J. 2015. Alternative molecular formats and therapeutic applications for bispecific antibodies. *Mol Immunol,* 67**,** 95-106.

SPRIGGS, K. A., BUSHELL, M. & WILLIS, A. E. 2010. Translational regulation of gene expression during conditions of cell stress. *Mol Cell,* 40**,** 228-37.

SRINIVASAN, A. R., LAKSHMIKUTTYAMMA, A. & SHOYELE, S. A. 2013. Investigation of the stability and cellular uptake of self-associated monoclonal antibody (MAb) nanoparticles by non-small lung cancer cells. *Mol Pharm,* 10**,** 3275-84.

STIRPE, F. 2004. Ribosome-inactivating proteins. *Toxicon,* 44**,** 371-83.

STIRPE, F. & BATTELLI, M. G. 2006. Ribosome-inactivating proteins: progress and problems. *Cell Mol Life Sci,* 63**,** 1850-66.

STIRPE, F., GASPERI-CAMPANI, A., BARBIERI, L., FALASCA, A., ABBONDANZA, A. & STEVENS, W. A. 1983. Ribosome-inactivating proteins from the seeds of Saponaria officinalis L. (soapwort), of Agrostemma githago L. (corn cockle) and of Asparagus officinalis L. (asparagus), and from the latex of Hura crepitans L. (sandbox tree). *Biochem J,* 216**,** 617-25.

SUMIYOSHI, N., ISHITOBI, H., MIYAKI, S., MIYADO, K., ADACHI, N. & OCHI, M. 2016. The role of tetraspanin CD9 in osteoarthritis using three different mouse models. *Biomed Res,* 37**,** 283-291.

SUNDSTROM, C. & NILSSON, K. 1976. Establishment and characterization of a human histiocytic lymphoma cell line (U-937). *Int J Cancer,* 17**,** 565-77.

SWANSON, J. A. 1989. Phorbol esters stimulate macropinocytosis and solute flow through macrophages. *J Cell Sci,* 94 (Pt 1)**,** 135-42.

SWANSON, J. A. & WATTS, C. 1995. Macropinocytosis. *Trends Cell Biol,* 5**,** 424-8.

TAKINO, T., MIYAMORI, H., KAWAGUCHI, N., UEKITA, T., SEIKI, M. & SATO, H. 2003. Tetraspanin CD63 promotes targeting and lysosomal proteolysis of membrane-type 1 matrix metalloproteinase. *Biochem Biophys Res Commun,* 304**,** 160-6.

TAZZYMAN, S., HAUTBERGUE, G., KHURRAM, A., BRYAN, M., CHANTRY, A. & FRAGIADAKI, M. 2015. The application of antibotoxsome, a novel cytotoxic conjugate, in cell death in in

vitro models of pancreatic, liver, breast, cervical cancer, and myeloma. *Journal of Clinical Oncology,* 33**,** e12018-e12018.

TEICHER, B. A. & CHARI, R. V. 2011. Antibody conjugate therapeutics: challenges and potential. *Clin Cancer Res,* 17**,** 6389-97.

TELANG, S., RASKU, M. A., CLEM, A. L., CARTER, K., KLARER, A. C., BADGER, W. R., MILAM, R. A., RAI, S. N., PAN, J., GRAGG, H., CLEM, B. F., MCMASTERS, K. M., MILLER, D. M. & CHESNEY, J. 2011. Phase II trial of the regulatory T cell-depleting agent, denileukin diftitox, in patients with unresectable stage IV melanoma. *BMC Cancer,* 11**,** 515.

TEN CATE, B., BREMER, E., DE BRUYN, M., BIJMA, T., SAMPLONIUS, D., SCHWEMMLEIN, M., HULS, G., FEY, G. & HELFRICH, W. 2009. A novel AML-selective TRAIL fusion protein that is superior to Gemtuzumab Ozogamicin in terms of in vitro selectivity, activity and stability. *Leukemia,* 23**,** 1389-97.

TERWISSCHA VAN SCHELTINGA, A. G., OGASAWARA, A., PACHECO, G., VANDERBILT, A. N., TINIANOW, J. N., GUPTA, N., LI, D., FIRESTEIN, R., MARIK, J., SCALES, S. J. & WILLIAMS, S. P. 2017. Preclinical Efficacy of an Antibody-Drug Conjugate Targeting Mesothelin Correlates with Quantitative 89Zr-ImmunoPET. *Mol Cancer Ther,* 16**,** 134-142.

THORPE, P. E. & ROSS, W. C. 1982. The preparation and cytotoxic properties of antibody-toxin conjugates. *Immunol Rev,* 62**,** 119-58.

THORPE, P. E., WALLACE, P. M., KNOWLES, P. P., RELF, M. G., BROWN, A. N., WATSON, G. J., BLAKEY, D. C. & NEWELL, D. R. 1988. Improved antitumor effects of immunotoxins prepared with deglycosylated ricin A-chain and hindered disulfide linkages. *Cancer Res,* 48**,** 6396-403.

TOME-AMAT, J., RUIZ-DE-LA-HERRAN, J., MARTINEZ-DEL-POZO, A., GAVILANES, J. G. & LACADENA, J. 2015. alpha-sarcin and RNase T1 based immunoconjugates: the role of intracellular trafficking in cytotoxic efficiency. *FEBS J,* 282**,** 673-84.

TORCHILIN, V. P. 2006. Recent approaches to intracellular delivery of drugs and DNA and organelle targeting. *Annu Rev Biomed Eng,* 8**,** 343-75.

TSUCHIYA, S., KOBAYASHI, Y., GOTO, Y., OKUMURA, H., NAKAE, S., KONNO, T. & TADA, K. 1982. Induction of maturation in cultured human monocytic leukemia cells by a phorbol diester. *Cancer Res,* 42**,** 1530-6.

TSUCHIYA, S., YAMABE, M., YAMAGUCHI, Y., KOBAYASHI, Y., KONNO, T. & TADA, K. 1980. Establishment and characterization of a human acute monocytic leukemia cell line (THP-1). *Int J Cancer,* 26**,** 171-6.

VAGO, R., MARSDEN, C. J., LORD, J. M., IPPOLITI, R., FLAVELL, D. J., FLAVELL, S. U., CERIOTTI, A. & FABBRINI, M. S. 2005. Saporin and ricin A chain follow different intracellular routes to enter the cytosol of intoxicated cells. *FEBS J,* 272**,** 4983-95.

VITETTA, E. S. 2000. Immunotoxins and vascular leak syndrome. *Cancer J,* 6 Suppl 3**,** S218-24.

VITETTA, E. S. & THORPE, P. E. 1991. Immunotoxins containing ricin or its A chain. *Semin Cell Biol,* 2**,** 47-58.

VOGEL, C. & MARCOTTE, E. M. 2012. Insights into the regulation of protein abundance from proteomic and transcriptomic analyses. *Nat Rev Genet,* 13**,** 227-32.

VOGELZANG, N. J., RUSTHOVEN, J. J., SYMANOWSKI, J., DENHAM, C., KAUKEL, E., RUFFIE, P., GATZEMEIER, U., BOYER, M., EMRI, S., MANEGOLD, C., NIYIKIZA, C. & PAOLETTI, P. 2003. Phase III study of pemetrexed in combination with cisplatin versus cisplatin alone in patients with malignant pleural mesothelioma. *J Clin Oncol,* 21**,** 2636-44.

WANG, J. C., BEGIN, L. R., BERUBE, N. G., CHEVALIER, S., APRIKIAN, A. G., GOURDEAU, H. & CHEVRETTE, M. 2007. Down-regulation of CD9 expression during prostate carcinoma progression is associated with CD9 mRNA modifications. *Clin Cancer Res,* 13**,** 2354-61.

WAYNE, A. S., FITZGERALD, D. J., KREITMAN, R. J. & PASTAN, I. 2014a. Immunotoxins for leukemia. *Blood*.

WAYNE, A. S., FITZGERALD, D. J., KREITMAN, R. J. & PASTAN, I. 2014b. Immunotoxins for leukemia. *Blood,* 123**,** 2470-7.

WELDON, J. E. & PASTAN, I. 2011. A guide to taming a toxin--recombinant immunotoxins constructed from Pseudomonas exotoxin A for the treatment of cancer. *FEBS J,* 278**,** 4683-700.

WELDON, J. E., SKARZYNSKI, M., THERRES, J. A., OSTOVITZ, J. R., ZHOU, H., KREITMAN, R. J. & PASTAN, I. 2015. Designing the furin-cleavable linker in recombinant immunotoxins based on Pseudomonas exotoxin A. *Bioconjug Chem,* 26**,** 1120-8.

WELDON, J. E., XIANG, L., CHERTOV, O., MARGULIES, I., KREITMAN, R. J., FITZGERALD, D. J. & PASTAN, I. 2009. A protease-resistant immunotoxin against CD22 with greatly increased activity against CLL and diminished animal toxicity. *Blood,* 113**,** 3792-800.

WENG, A., JENETT-SIEMS, K., SCHMIEDER, P., BACHRAN, D., BACHRAN, C., GORICK, C., THAKUR, M., FUCHS, H. & MELZIG, M. F. 2010. A convenient method for saponin isolation in tumour therapy. *J Chromatogr B Analyt Technol Biomed Life Sci,* 878**,** 713-8.

WENG, A., THAKUR, M., VON MALLINCKRODT, B., BECEREN-BRAUN, F., GILABERT-ORIOL, R., WIESNER, B., EICHHORST, J., BOTTGER, S., MELZIG, M. F. & FUCHS, H. 2012. Saponins modulate the intracellular trafficking of protein toxins. *J Control Release,* 164**,** 74-86.

WIERSINGA, W. J., VAN DER POLL, T., WHITE, N. J., DAY, N. P. & PEACOCK, S. J. 2006. Melioidosis: insights into the pathogenicity of Burkholderia pseudomallei. *Nat Rev Micro,* 4**,** 272-282.

WILLCOCKS, S. J., DENMAN, C. C., ATKINS, H. S. & WREN, B. W. 2016. Intracellular replication of the well-armed pathogen Burkholderia pseudomallei. *Curr Opin Microbiol,* 29**,** 94-103.

WOLFE, A. L., SINGH, K., ZHONG, Y., DREWE, P., RAJASEKHAR, V. K., SANGHVI, V. R., MAVRAKIS, K. J., JIANG, M., RODERICK, J. E., VAN DER MEULEN, J., SCHATZ, J. H., RODRIGO, C. M., ZHAO, C., RONDOU, P., DE STANCHINA, E., TERUYA-FELDSTEIN, J., KELLIHER, M. A., SPELEMAN, F., PORCO, J. A., JR., PELLETIER, J., RATSCH, G. & WENDEL, H. G. 2014. RNA G-quadruplexes cause eIF4A-dependent oncogene translation in cancer. *Nature,* 513**,** 65-70.

XIE, L. Y., PIAO, H. L., FAN, M., ZHANG, Z., WANG, C., BIGNER, D. D. & BAO, X. H. 2017. Immunotoxin Therapy for Lung Cancer. *Chin Med J (Engl),* 130**,** 607-612.

YANEZ-MO, M., BARREIRO, O., GORDON-ALONSO, M., SALA-VALDES, M. & SANCHEZ-MADRID, F. 2009. Tetraspanin-enriched microdomains: a functional unit in cell plasma membranes. *Trends Cell Biol,* 19**,** 434-46.

YIN, J., LI, G., REN, X. & HERRLER, G. 2007. Select what you need: a comparative evaluation of the advantages and limitations of frequently used expression systems for foreign genes. *J Biotechnol,* 127**,** 335-47.

YOON, S. O., ZHANG, X., FREEDMAN, A. S., ZAHRIEH, D., LOSSOS, I. S., LI, L. & CHOI, Y. S. 2010. Down-regulation of CD9 expression and its correlation to tumor progression in B lymphomas. *Am J Pathol,* 177**,** 377-86.

YOSHIDA, T., CHEN, C. C., ZHANG, M. S. & WU, H. C. 1991. Disruption of the Golgi apparatus by brefeldin A inhibits the cytotoxicity of ricin, modeccin, and Pseudomonas toxin. *Exp Cell Res,* 192**,** 389-95.

YOSHIMORI, T., YAMAMOTO, A., MORIYAMA, Y., FUTAI, M. & TASHIRO, Y. 1991. Bafilomycin A1, a specific inhibitor of vacuolar-type H(+)-ATPase, inhibits acidification and protein degradation in lysosomes of cultured cells. *J Biol Chem,* 266**,** 17707-12.

YOULE, R. J. & COLOMBATTI, M. 1987. Hybridoma cells containing intracellular anti-ricin antibodies show ricin meets secretory antibody before entering the cytosol. *J Biol Chem,* 262**,** 4676-82.

ZHAN, H., CHOE, S., HUYNH, P. D., FINKELSTEIN, A., EISENBERG, D. & COLLIER, R. J. 1994. Dynamic transitions of the transmembrane domain of diphtheria toxin: disulfide trapping and fluorescence proximity studies. *Biochemistry,* 33**,** 11254-63.

ZHANG, J., KHANNA, S., JIANG, Q., ALEWINE, C., MIETTINEN, M., PASTAN, I. & HASSAN, R. 2017. Efficacy of Anti-mesothelin Immunotoxin RG7787 plus Nab-Paclitaxel against Mesothelioma Patient-Derived Xenografts and Mesothelin as a Biomarker of Tumor Response. *Clin Cancer Res,* 23**,** 1564-1574.

ZHANG, Y., SUN, X., HUANG, M., KE, Y., WANG, J. & LIU, X. 2015. A novel bispecific immunotoxin delivered by human bone marrow-derived mesenchymal stem cells to target blood vessels and vasculogenic mimicry of malignant gliomas. *Drug Des Devel Ther,* 9**,** 2947-59.

ZHAO, G. & LONDON, E. 2005. Behavior of diphtheria toxin T domain containing substitutions that block normal membrane insertion at Pro345 and Leu307: control of deep membrane insertion and coupling between deep insertion of hydrophobic subdomains. *Biochemistry,* 44**,** 4488-98.

ZHAO, W., CHEN, T. L., VERTEL, B. M. & COLLEY, K. J. 2006. The CMP-sialic acid transporter is localized in the medial-trans Golgi and possesses two specific endoplasmic reticulum export motifs in its carboxyl-terminal cytoplasmic tail. *J Biol Chem,* 281**,** 31106-18.

ZHIJUN, X., SHULAN, Z. & ZHUO, Z. 2007. Expression and significance of the protein and mRNA of metastasis suppressor gene ME491/CD63 and integrin alpha5 in ovarian cancer tissues. *Eur J Gynaecol Oncol,* 28**,** 179-83.

ZHOU, J. & ROSSI, J. J. 2014. Cell-type-specific, Aptamer-functionalized Agents for Targeted Disease Therapy. *Mol Ther Nucleic Acids,* 3**,** e169.

ZHOU, X., QIU, J., WANG, Z., HUANG, N., LI, X., LI, Q., ZHANG, Y., ZHAO, C., LUO, C., ZHANG, N., TENG, X., CHEN, Z., LIU, X., YU, X., WU, W., WEI, Y. Q. & LI, J. 2012. In vitro and in vivo anti-tumor activities of anti-EGFR single-chain variable fragment fused with recombinant gelonin toxin. *J Cancer Res Clin Oncol,* 138**,** 1081-90.

ZIMMERMANN, S., WELS, W., FROESCH, B. A., GERSTMAYER, B., STAHEL, R. A. & ZANGEMEISTER-WITTKE, U. 1997. A novel immunotoxin recognising the epithelial glycoprotein-2 has potent antitumoural activity on chemotherapy-resistant lung cancer. *Cancer Immunol Immunother,* 44**,** 1-9.

ZOVICKIAN, J., JOHNSON, V. G. & YOULE, R. J. 1987. Potent and specific killing of human malignant brain tumor cells by an anti-transferrin receptor antibody-ricin immunotoxin. *J Neurosurg,* 66**,** 850-61.